Seismic Response of Multi-Storey Cross-Laminated Timber Buildings

Cagatay Demirci
Department of Civil and Environmental Engineering
Imperial College London

A thesis submitted for
the degree of Doctor of Philosophy
and the Diploma of Imperial College London
January 2019

“In the name of Allah, most Gracious, most Compassionate.”

They said, ”Exalted are You; we have no knowledge except what You have taught us. Indeed, it is You who is the Knowing, the Wise.”

Surat Al-Baqarah [verse 32]

Abstract

Multi-storey building construction with cross-laminated timber (CLT) is growing around the globe. This increased interest in CLT construction is driven by the numerous benefits it offers over conventional materials in terms of minimum environmental cost, outstanding structural performance, and reduced construction time and cost. Besides, CLT multi-storey construction is an attractive and environmentally-responsive building option to optimise the use of the scarce area in emerging metropolitan cities where an influx of over 2.5 billion people is expected in the following three decades. Furthermore, CLT construction is an appealing building alternative in seismically prone areas due to its in-plane stiffness and potentially ductile structural joinery design. For these reasons, the dynamic response of CLT buildings under earthquake loading has been subject of numerous experimental and numerical research efforts during the last 2 decades. Surprisingly, however, most of past research has been circumscribed to strength estimations and, no comprehensive assessment has been conducted with regards to the expected level of inelastic demands in CLT buildings. In particular, the influence of the ground-motion frequency content, which has long been recognized as determinant on the seismic response, has been usually neglected in studies on CLT structures. This thesis aims to provide a detailed characterization of seismic demands in multi-storey CLT buildings and their dependency on the frequency content of the ground-motion. Attention is given to the evolution of inelastic deformations, base and inter-storey shear forces, and peak floor accelerations and their relationship with salient building and ground-motion characteristics.

A comprehensive building database including 60 multi-storey CLT buildings representative of a wide range of structural configurations is constructed. To study the influence of ground-motion frequency content on peculiar design practices, a suite of 1656 real ground-motion records is used. Subsequently, a parametric study is conducted by means of a probabilistic demand assessment and non-linear regression models are proposed for the estimation of seismic demands in multi-storey CLT buildings. In addition, the use of multiple sliding sections as a potential means of mitigating the large peak accelerations observed in taller CLT buildings is also investigated. Finally, practical implications of the findings on available seismic design and assessment provisions are highlighted throughout the thesis and recommendations on future work are summarized at the end.

To Aysel and Memet Alp
for always giving me strength, inspiration and joie de vivre...

Declaration of Originality

I confirm that this thesis and the work presented in it are my own and has been generated by me as the result of my own original research. I give references and citations whenever I consulted the published or unpublished work of others.

Cagatay Demirci

Copyright Declaration

The copyright of this thesis rests with the author. Unless otherwise indicated, its contents are licensed under a Creative Commons Attribution-Non Commercial 4.0 International Licence (CC BY-NC).

Under this licence, you may copy and redistribute the material in any medium or format. You may also create and distribute modified versions of the work. This is on the condition that: you credit the author and do not use it, or any derivative works, for a commercial purpose.

When reusing or sharing this work, ensure you make the licence terms clear to others by naming the licence and linking to the licence text. Where a work has been adapted, you should indicate that the work has been changed and describe those changes.

Please seek permission from the copyright holder for uses of this work that are not included in this licence or permitted under UK Copyright Law.

Acknowledgements

The work presented in this thesis was carried out under the supervision of Dr Christian Málaga-Chuquitaype. I owe special thanks to Dr Málaga-Chuquitaype for being an outstanding advisor to me, for his endless support and encouragement throughout the completion of this study. Besides, I can never thank him enough for believing in me and supporting all my funding applications when my scholarship was taken away from me right after the half way of this journey. I would have never accomplished this research without his very kind cooperation during the last years. I also thank to my second supervisor Dr Lorenzo Macorini for his invaluable support, guidance and involvement throughout the completion of my research.

The first half of this work was funded by the Ministry of Education of Turkey. Their financial support was gratefully acknowledged. The second half of this work was funded by Old Centralians' Trust, Faculty of Engineering Deans' Fund, Student Support Fund, and Student Global Relief Fund schemes of Imperial College London. I owe special thanks to Prof. Catherine O'Sullivan and Prof. Dennis Wright at Imperial College London, Prof. Robert C. Schroter and Mr. Chris Lumb in Old Centralians' Trust for their kind acceptance and generous help to obtain funds to be able to complete this research. Besides, essential assistance from the staff of Department of Civil and Environmental Engineering, especially Fionnuala Ni Dhonnabhain, and Sarah Willis is wholeheartedly appreciated.

I would also like to thank my parents for their love, blessings and prayers all throughout my life. Finally, I am thankful to my wonderful wife, Aysel, for always giving me strength, inspiration, hope, and joie de vivre. The last 2 years, when we were left without any support, were extremely difficult in different aspects of life. However, your encouragement, unconditional love and knowing that you are always there with me, made this dream come true. Above everything else, bringing our lovely son, Memet Alp, into our life was the most beautiful present I could ever have. My love and prayers are for ever with you.

Contents

Abstract **5**

Declaration of Originality **9**

Copyright Declaration **11**

Acknowledgements **13**

List of Tables **22**

List of Figures **27**

Notations **29**

1 Introduction **33**

1.1 Background 33

1.2 Motivation and objectives 34

1.3 Outline of the thesis 35

2 Literature Review **37**

2.1 Introduction 37

2.2 Timber as a construction material 37

2.3 Multi-storey timber building projects 38

2.4 Research on seismic response of cross-laminated timber buildings 44

2.4.1 Experimental research on CLT walls 44

2.4.2 Full-scale experimental studies on CLT buildings 46

2.4.3 Numerical research on the seismic response of CLT walls 48

2.4.4 Seismic response of multi-storey CLT buildings 49

2.5 Summary 53

3 Seismic Design and Building Database **55**
3.1 Introduction . . . 55
3.2 Seismic Design . . . 55
3.2.1 Seismic base shear . . . 60
3.2.2 Lateral load distribution . . . 62
3.2.3 Lateral load distribution into load bearing walls . . . 63
3.2.4 Load bearing wall thickness . . . 63
3.2.5 Floor slab thickness . . . 64
3.2.6 Design of CLT connections . . . 64
3.3 Concluding remarks . . . 65

4 Numerical Modelling, Analysis and Parameters Investigated **67**
4.1 Introduction . . . 67
4.2 Numerical modelling . . . 67
4.2.1 Hysteretic material definition . . . 69
4.2.2 Joint types . . . 70
4.2.3 Vertical joints between adjacent wall panels . . . 70
4.2.4 CLT panel stiffness . . . 72
4.3 Numerical validation . . . 77
4.3.1 Connection hysteresis calibration . . . 77
4.3.2 Cyclic behaviour of a single CLT wall . . . 78
4.3.3 Cyclic behaviour of a coupled CLT wall . . . 79
4.3.4 Response of 7-storey SOFIE building . . . 80
4.4 Non-linear response history analyses and parameters investigated . . . 84
4.4.1 Ground-motion characteristics . . . 85
4.4.2 Structural parameters . . . 86
4.5 Concluding remarks . . . 88

5 Assessment of Seismic Drift Demands **90**
5.1 Introduction . . . 90
5.2 Assessment of seismic drift demands . . . 91
5.2.1 Assessment procedure . . . 91
5.2.2 Global drift demands . . . 91
5.2.3 Maximum inter-storey drift demands . . . 94
5.3 Regression analyses . . . 96
5.3.1 Global drift modification factor . . . 96
5.3.2 Maximum drift modification factor . . . 98

5.4 Comparative studies . . . 99
5.5 Concluding remarks . . . 103

6 Assessment of Seismic Force Demands 106
6.1 Introduction . . . 106
6.2 Structural response parameters . . . 107
6.3 Assessment of peak forces . . . 107
6.3.1 Base shear demands . . . 108
6.3.2 Inter-storey shear demands . . . 111
6.4 Regression analyses . . . 112
6.4.1 Base shear modification factor . . . 113
6.4.2 Inter-storey shear modification factor . . . 114
6.5 Model simplification . . . 115
6.5.1 Building height index . . . 116
6.5.2 Storey shear modification factor . . . 117
6.6 Concluding remarks . . . 118

7 Assessment of Seismic Acceleration Demands 120
7.1 Introduction . . . 120
7.2 Assessment of peak floor accelerations . . . 121
7.2.1 Peak floor accelerations . . . 121
7.3 Regression analysis . . . 126
7.3.1 Prediction model for acceleration amplification factor γ . . . 126
7.3.2 Prediction model for acceleration amplification factor γ° . . . 127
7.3.3 Model simplification . . . 128
7.4 Concluding remarks . . . 130

8 CLT Buildings Equipped with Flat Sliding Bearings 132
8.1 Introduction . . . 132
8.2 Design and numerical modelling formulation . . . 133
8.2.1 PTFE slide bearing design . . . 133
8.2.2 Numerical modelling . . . 134
8.2.3 Static and Dynamic Response of CLT buildings with sliding sections . . . 137
8.3 Assessment of seismic drift demands . . . 139
8.3.1 Inter-storey drift demands . . . 140
8.3.2 Regression analysis . . . 142
8.4 Assessment of seismic shear demands . . . 143
8.4.1 Base shear demands . . . 143

8.4.2 Regression analysis . . . 145
8.5 Assessment of acceleration demands . . . 146
8.5.1 Acceleration amplification factor . . . 146
8.5.2 Seismic acceleration demands . . . 146
8.5.3 Regression analysis . . . 148
8.6 Seismic demand comparison . . . 148
8.7 Concluding remarks . . . 151

9 Closure **153**
9.1 Preamble . . . 153
9.2 Summary of main findings . . . 153
9.2.1 Drift demands . . . 154
9.2.2 Shear force demands . . . 155
9.2.3 Acceleration demands . . . 156
9.2.4 Seismic demands in CLT buildings equipped with flat sliding bearings 157
9.3 Future work . . . 159
9.4 Dissemination . . . 160

Appendices **171**

A Summary of Design Values **173**
A.1 Design values for 6-storey CLT building . . . 173

B Panel thickness verifications in CLT designer **182**

C Design of Connections **209**

D Response of other building heights **224**
D.1 Drift response . . . 224
D.2 Shear response . . . 224
D.3 Acceleration response . . . 224

List of Tables

2.1 Multi-storey mass timber building projects around the world, as of 2018. . . . 38
2.1 Multi-storey mass timber building projects around the world, as of 2018. . . . 39
2.1 Multi-storey mass timber building projects around the world, as of 2018. . . . 40

3.1 Building configuration database developed herein this research. 57
3.2 Imposed loads for residential buildings. 58
3.3 Corresponding building weight and seismic mass for taller buildings. 58
3.4 Spectral parameters for areas of high seismicity [29]. 60
3.5 Fundamental period and seismic base shear forces for taller buildings. 62
3.6 CLT panel thickness values along the building height in 6-storey CLT building. 64
3.7 Variation of the type and number of structural connections in building configuration A1. 66

4.1 Hysteretic material properties of metal connectors. 71
4.2 CLT panel stiffness. 72
4.3 Orthotropic material properties. 76
4.4 Comparison of 2 material modelling approach of CLT wall panels in A1 building. 77
4.5 Calibration of mean values obtained from experimental results on CLT connections. 78
4.6 Experimental [75] and numerical comparison of fundamental period of 7-storey SOFIE building. 82
4.7 Ground motion catalogue employed for non-linear response history analysis of buildings. 89

5.1 Regression coefficients for the global drift modification factor (δ_{mod}). 98
5.2 Regression coefficients for the maximum drift modification factor (θ_{mod}). . . . 99
5.3 Computation of building aspect ratio (λ) and joint density parameter ($\beta = P_o/P$). 101
5.4 Computation of q values using the proposed Equation 5.7 for building configurations. 102

List of Tables

6.1 Computation of building height indexes, ξ_1. 114
6.2 Regression coefficients for the base shear modification factor (V_{mod}). 114
6.3 Regression coefficients for the storey shear modification factor ($V_{st,mod}$). 115
6.4 Comparison of building height indexes, ξ. 116
6.5 Regression coefficients for the storey shear modification factor ($V_{st,mod}$), obtained using the simplified model. 117

7.1 Regression coefficients for the peak floor acceleration (γ) in Equation 7.3. . . . 127
7.2 Regression coefficients for the peak floor acceleration (γ°) in Equation 7.4. . . 128
7.3 Regression coefficients for the simplified peak floor acceleration amplification model (γ°). 129

8.1 Structural response comparison of multi-storey CLT buildings equipped with and without flat slide bearings. 139
8.2 Regression coefficients for the non-linear displacement demands ($\ln(\theta_{max})$) in Equation 8.1. 142
8.3 Regression coefficients for the non-linear shear demands (V_b/W) in Equation 8.2. 145
8.4 Regression coefficients for the non-linear acceleration demands ($\ln(\gamma^{\circ})$) associated with Equation 8.4. 148

A.1 Floor-slab components. 173
A.2 Roof components. 174
A.3 External wall components. 174
A.4 Internal wall components. 174
A.5 Permanent action due to ceiling. 175
A.6 Permanent action due to flat roof. 175
A.7 Permanent action due to external load bearing wall. 175
A.8 Permanent action due to internal load bearing wall. 176
A.9 Calculation of permanent loads. 176
A.10 Calculation of superimposed loads. 176
A.11 Calculation of superimposed loads for 6-storey CLT building 177
A.12 Lateral load distribution for the 6-storey CLT building 177
A.13 Storey shear and bending moment distribution for the 6-storey CLT building . 177
A.14 Distributed lateral forces to each 8.5 m length walls for the 6-storey CLT building. 178
A.15 Lateral load distribution for the 8-storey CLT building 179
A.16 Lateral load distribution for the 12-storey CLT building 179
A.17 Lateral load distribution for the 16-storey CLT building 180

A.18 Lateral load distribution for the 20-storey CLT building 181
A.19 Design values for PTFE slide bearings in taller buildings 181

C.1 Number of connections for 6-storey A2 building. 209
C.2 Number of connectors for 6-storey A3 building. 210
C.3 Number of connectors for 8-storey B1 building. 210
C.4 Number of metal connectors determined for 8-storey B2 building. 211
C.5 Number of metal connectors for 8-storey B3 building. 212
C.6 Number of metal connectors for 12-storey C1 building. 213
C.7 Number of metal connectors for 12-storey C2 building. 214
C.8 Number of metal connectors for 12-storey C3 building. 215
C.9 Number of metal connectors for 16-storey D1 building. 216
C.10 Number of metal connectors for 16-storey D2 building. 217
C.11 Number of metal connectors for 16-storey D3 building. 218
C.12 Number of metal connectors for 20-storey E1 building. 218
C.13 Number of metal connectors for 20-storey E2 building. 220
C.14 Number of metal connectors for 20-storey E3 building. 221

List of Figures

2.1 Structural timber products. 41
2.2 Multi-storey CLT building projects. 43

3.1 Plan view and elevation of the 6-storey CLT building. Units in [m]. 56
3.2 Design response spectrum (soil class C, $\alpha_g = 3.0\ m/s^2$). 61
3.3 Schematic of load distribution in coupled CLT panels. Adapted from [52]. . . . 65

4.1 Schematic of numerical modelling approach for CLT buildings. 68
4.2 Hysteretic material definition available in OpenSees [59]. 69
4.3 TTF200 angle bracket and WHT hold-down connectors. 70
4.4 Hysteretic response and backbone curve of metal connectors employed in the study. 71
4.5 Composition factors k_i for solid wood panels with cross layers [9]. 73
4.6 Comparison of panel stiffness values with fundamental period of buildings. . . 74
4.7 Principal axes definition of CLT wall panel [31]. 75
4.8 Comparison of the results of non-linear static analyses using two different CLT material models. 77
4.9 Comparison of numerical and experimental hysteresis [38, 39] of metal connectors. 78
4.10 Schematic of single CLT wall panel, Specimen 1.2 [36]. 79
4.11 Experimental and numerical response comparison of a single panel CLT wall, (Specimen 1.2 from [36]). 80
4.12 Schematic of a coupled CLT wall panel, Specimen 1.2 [36]. 80
4.13 Experimental and numerical response comparison of a coupled CLT wall panel, Specimen 2.1 [36]. 81
4.14 North-East and South-West views of the 7-storey SOFIE building [25]. 82
4.15 Placement of structural joinery elements at each floor level [25]. 83
4.16 Plan view and the elevation of SOFIE building. 84

4.17 Experimental [76] and numerical response comparison of 7-storey SOFIE building. 85
4.18 Distribution of mean periods (T_m) employed in the study. 86
4.19 Distribution of key structural parameters. 87
4.20 Scatterplot matrix of the key structural characteristics. 88

5.1 Mean logarithmic global drift modification factor ($\ln(\delta_{mod})$), against period ratio (T_1/T_m) for a response modification factor of q = 3. 92
5.2 Relationship between $\ln(\delta_{mod})$ and T_1/T_m for various response modification (q) factors, level of panel fragmentation (m), and number of storeys (n). 94
5.3 Mean logarithmic maximum drift modification factor ($\ln(\theta_{mod})$), against period ratio (T_1/T_m) for a response modification factor of q = 3. 95
5.4 Relationship between $\ln(\theta_{mod})$ and T_1/T_m for various response modification (q) factors, level of panel fragmentation (m), and number of storeys (n). 97
5.5 Residual plots for the global drift modification factor (δ_{mod}) prediction model. 98
5.6 Residual plots for the maximum drift modification factor (θ_{mod}) prediction model. 99
5.7 Computation of indexes for the actual and reference configurations. 100
5.8 Comparison of mean logarithmic global drift modification factors ($\ln(\delta_{mod})$) obtained using the prediction model developed in this study with the proposal by Pozza and Trutalli [71] as well as Eurocode 8 [29] approximations. 103

6.1 Mean logarithmic base shear modification factor ($\ln(V_{mod})$) against period ratio (T_1/T_m) for a response modification factor of q = 3. 109
6.2 Relationship between $\ln(V_{mod})$ and T_1/T_m for various response modification (q) factors, level of panel fragmentation (m), and number of storeys (n). 110
6.3 Mean logarithmic storey shear modification factor ($\ln(V_{st,mod})$), against period ratio (T_1/T_m) for a response modification factor of q = 3. 111
6.4 Relationship between $\ln(V_{st,mod})$ and T_1/T_m for various response modification (q) factors, and level of panel fragmentation (m), and number of storeys (n). . . 113
6.5 Residual plots of the parameters used in the base shear modification factor V_{mod} prediction model. 115
6.6 Residual plots for the storey shear modification factor $V_{st,mod}$ prediction model. 116
6.7 Mean storey shear modification ($V_{st,mod}$) against period ratios (T_1/T_m), obtained using the simplified prediction model of Equation 6.7, for a response modification factor of q = 3. 117
6.8 Comparison between the results of mean storey shear modification ($V_{st,mod}$) against period ratios (T_1/T_m), obtained by means of the full and simplified models for a response modification factor of q = 3. 118

7.1 Mean peak floor acceleration amplification factor (γ) against period ratios (T_1/T_m), q = 3. 122
7.2 Mean peak floor acceleration amplification factor (γ) against period ratios (T_1/T_m), for different key structural parameters. 123
7.3 Mean peak floor acceleration amplification factor (γ°) against period ratios (T_1/T_m), q = 3. 124
7.4 Mean peak floor acceleration amplification factor (γ°) against period ratios (T_1/T_m), for different key structural parameters. 125
7.5 Residual plots for the amplification of peak floor acceleration (γ) prediction model. 127
7.6 Residual plots for the amplification of peak floor acceleration (γ°) prediction model. 128
7.7 Mean peak floor acceleration amplification factor (γ°) against period ratios (T_1/T_m), q = 3. 129
7.8 Comparison of full and simplified prediction models for mean peak floor acceleration amplification factor (γ°) against period ratios (T_1/T_m), q = 3. 130

8.1 A typical configuration of PTFE Slide bearings [72]. 134
8.2 Location of flat sliding bearing elements in building models (6, 8, 12 and 16 storeys). 135
8.3 A possible connection detail of a PTFE slide bearing. 135
8.4 Hysteretic material behaviour of isolation bearing element and stopper in shear. 136
8.5 Non-linear pushover curves of 6-storey buildings with and without flat sliding bearing elements. 136
8.6 Fundamental period comparison of CLT buildings equipped with and without multiple sliding sections. 137
8.7 Seismic response comparison of 6-storey (A1) CLT buildings with and without flat sliding bearing elements. 138
8.8 Seismic response comparison of 16-storey (D1) CLT buildings with and without flat sliding bearing elements. 139
8.9 Comparison of peak floor accelerations (α_{max}), base shear forces (V_b), and inter-storey drifts (θ_{max}) obtained from extensive non-linear response history analyses on the 6-storey A1 buildings with and without slide bearings. 140
8.10 Maximum inter-storey drift ($\ln(\theta_{max})$) against period ratio (T_1/T_m) when there is no contact between the isolation bearing and the stopper. 141
8.11 Maximum inter-storey drift ($\ln(\theta_{max})$) against period ratio (T_1/T_m) when there is contact between the isolation bearing and the stopper. 142

8.12 Residual plots for the maximum inter-storey drift ($\ln(\theta_{max})$) prediction model. 143
8.13 Mean normalized base shear forces (V_b/W) against period ratio (T_1/T_m) when there is no contact between the isolation bearing and the stopper. 144
8.14 Mean normalized base shear forces (V_b/W) against period ratio (T_1/T_m) when there is contact between the isolation bearing and the stopper. 145
8.15 Residual plots for the normalized base shear (V_b/W) prediction model. 146
8.16 Relationship between acceleration amplification factor ($\ln(\gamma^\circ)$) and period ratio (T_1/T_m) when there is no contact between the isolation bearing and the stopper. 147
8.17 Relationship between acceleration amplification factor ($\ln(\gamma^\circ)$) and period ratio (T_1/T_m) when there is contact between the isolation bearing and the stopper. . 147
8.18 Residual plots for the acceleration amplification factor (γ°) prediction model. . 149
8.19 Acceleration amplification factor (γ°) comparison between the conventional and buildings with multiple sliding sections. 150
8.20 Inter-storey drift demand (θ_{max}) comparison between the conventional and buildings with multiple sliding sections. 150

A.1 Cantilever wall model with actions and internal forces. 178

D.1 Mean global drift modification factor ($\ln(\delta_{mod})$) against period ratios (T_1/T_m), for different structural heights. 225
D.2 Mean maximum drift modification factor ($\ln(\theta_{mod})$) against period ratios (T_1/T_m), for different structural heights. 226
D.3 Mean base shear modification factor ($\ln(V_{mod})$) against period ratios (T_1/T_m), for different structural heights. 227
D.4 Mean storey shear modification factor ($\ln(V_{st,mod})$) against period ratios (T_1/T_m), for different structural heights. 228
D.5 Mean acceleration amplification factor (γ) associated with $S_a(T_1)$ against period ratios (T_1/T_m), for different structural heights. 229
D.6 Mean acceleration amplification factor (γ°) associated with PGA against period ratios (T_1/T_m), for different structural heights. 230

Notations

α	plasticity resistance ratio
α_g	design ground acceleration
α_{gR}	reference peak ground acceleration
α_{max}	peak storey acceleration
A_s	effective shear cross section
β	joint density parameter
C_i	Fourier amplitude corresponding to i^th frequency
d	layer thickness
δ	accidental torsional effect
δ_{mod}	global drift modification factor
Δ_{max}	maximum roof displacement
$\Delta_{1,roof}$	yield roof displacement
$E_{0,mean}$	modulus of elasticity in the grain direction
$E_{90,mean}$	modulus of elasticity in perpendicular to the direction of the grain
$E_{0,eq}$	equivalent elastic moduli associated with the vertical direction of the outer layers
$E_{90,eq}$	equivalent elastic moduli in the perpendicular direction to the outer layers
$E_{0,T}$	elastic moduli parallel to grain of transversal layers
$E_{0,L}$	elastic moduli parallel to grain in the longitudinal layers
$E_{90,L}$	elastic moduli perpendicular to the grain of the longitudinal layers
$E_{90,T}$	elastic moduli of transversal layers
E_x	elastic moduli associated with x direction
E_y	elastic moduli associated with y direction
E_z	elastic moduli associated with z direction
$f_{c,CLT,d}$	design compressive strength in grain direction
$f_{c,CLT,k}$	characteristic compressive strength in grain direction
$f_{c,CLT,90,d}$	design compressive strength perpendicular to grain direction
$f_{c,CLT,90,k}$	characteristic compressive strength perpendicular to grain direction
$f_{v,CLT,d}$	design in-plane shear strength
$f_{v,CLT,k}$	characteristic in-plane shear strength

$f_{tor,CLT,k}$	characteristic in-plane torsional strength
$f_{tor,CLT,d}$	design in-plane torsional strength
F_b	seismic base shear force
F_{eq}	force equilibrium in the vertical connection
F_i	horizontal seismic base shear force at the i^{th} level
k_{panel}	CLT panel stiffness
I_{eff}	effective radius of gyration
γ	acceleration amplification factor associated with S_aT_1
γ°	acceleration amplification factor associated with PGA
γ_i	building importance factor
γ_m	partial safety factor for accidental combinations
Γ_s	the centre of the stiffness
G_{xy}	shear moduli associated with xy plane
G_{xz}	shear moduli associated with xz plane
G_{yz}	shear moduli associated with yz plane
G_T	shear moduli associated with transversal layer direction
G_L	shear moduli associated with longitudinal layer direction
$G_{0,mean}$	shear modulus
$G_{90,mean}$	rolling shear modulus
G	dead load
H	height of the building in m
k_{mod}	strength modification factor
λ	building aspect ratio
λ_{Ei}	reduction factor
m	level of panel fragmentation
n	number of storey
ν_{xy}	poisson's ratio associated with xy plane
ν_{xz}	poisson's ratio associated with xz plane
ν_{yz}	poisson's ratio associated with yz plane
q	response modification factor
q_k	live load
Q	superimposed load
P_0	all fastening lines in the wall
P	wall perimeter
PGA	peak ground acceleration
R_d	design load carrying capacity
R_k	characteristic load carrying capacity

S_aT_1	spectral acceleration
$S_d(T_1)$	ordinate of the design spectrum at the fundamental period
t_{tot}	total thickness of the wall panel
t_i	layer thickness associated with longitudinal layers
t_j	layer thickness associated with transversal layers
θ_{mod}	maximum inter-storey drift modification factor
θ_{max}	maximum inter-storey drift
$\theta_{1,max}$	maximum inter-storey drift at first yield
T_1	fundamental period
T_m	mean period of ground-motion
T_s	geometric centre of the building
v_{eq}	equilibrium of displacement in the vertical connection
V_{max}	maximum base shear force
$V_{i,max}$	maximum shear force at the i^{th} storey
$V_{st,max}$	maximum inter-storey shear force
V_b/W	normalized base shear
V_1	shear force at the first yield of an element
$V_{i,1}$	total shear force at the i^{th} storey, at the formation of first yield in the structure
V_{mod}	base shear modification factor
$V_{st,mod}$	storey shear modification factor
V_u	ultimate base shear force
ξ	building height index

Chapter 1

Introduction

1.1 Background

The global population has increased from 1 billion to 6.9 billion in the last two hundred years and it is expected to reach 9 billion in four decades [81]. The demands of infrastructure imposed by this rapid growth have to be attended in the context of a deteriorating environment with two-thirds of the global carbon emissions being emitted by the construction industry. Therefore, the future of our planet is tied to the way we build cities.

An efficient way to respond to the challenges described above is through the American invention of the tall building [81]. Most current tall buildings are built in steel and concrete which are materials associated with very high energy consumption and very high greenhouse gas emissions. Steel causes approximately 3% of global greenhouse gas emissions and concrete beyond 5%. This means that 8% of mans contribution to greenhouse gases is provided only by the production of steel and concrete [40]. On the other hand, wood is a material that stores carbon. One cubic meter of wood can store one tonne of carbon dioxide.

The number of storeys necessary to consider a timber building as tall has remained at around 10 due to the limits imposed by lateral load demands that increase with building height [32]. However, the field of timber engineering has made a valuable progress with the recent introduction of new engineered timber products such as Cross-Laminated-Timber (CLT) which has the potential to make the wooden skyscraper dream come true. Accordingly, the utilization of CLT is becoming very common in high-rise timber construction throughout the world [15, 49].

The issue of the seismic performance of CLT buildings has been subject of numerous past experimental and numerical research. Past investigations have generally focused on the calibration of finite element models, the reproduction of test results, and the identification of adequate

force reduction factors for low- and mid-rise CLT structures [25, 33, 60, 70, 71, 76]. However, no thoroughly generalizable outcomes have been derived regarding their inelastic seismic demands. Furthermore, the influence of the ground-motion frequency content, which has long been recognized as determinant on the seismic response, [17, 58, 78, 88] has been usually neglected in studies on CLT structures and needs to be explicitly accounted for. Therefore, the aim of this thesis is to provide a detailed characterization of the seismic demands in multi-storey CLT buildings.

1.2 Motivation and objectives

As outlined in the previous section, there is a need to evaluate the seismic response of multi-storey CLT buildings and the influence of frequency content measures on the inelastic demands of these structures. Therefore, the fundamental purpose of this research is to gain a comprehensive understanding of the influence of structural parameters as well as the ground-motion frequency content on the seismic response of multi-storey cross-laminated timber buildings. In doing so, rigorous non-linear regression models to estimate seismic drift, force, and acceleration demands are proposed. To this end, a total of 60 CLT buildings are designed in accordance with available national, international guiding principles, and past research studies.

The mean period, T_m [74], is selected as a scalar frequency content indicator in this research given its demonstrated efficiency for predicting seismic demands in other types of generic structures [19, 20, 54, 55]. The influence of ground-motion mean period and structural characteristics on the seismic demands of multi-storey CLT buildings is then explored. Global drift, maximum inter-storey drift, base shear, maximum inter-storey shear, and maximum acceleration demands on conventional CLT buildings are examined. The parameters that are found to have significant influence on the seismic demands are identified and employed to perform regression analyses. The results of prediction models are then compared with recent assessment proposals and current design provisions wherever relevant.

Finally, the potential of a new configuration of CLT structures equipped with multiple sliding segments to mitigate large accelerations is studied. The proposed system incorporates PTFE sliding bearing elements at critical locations along the height of the building, hence imposing a limit on the amount of shear forces transferred between different sliding blocks. The significant improvements brought about by this innovative solution in comparison with conventional CLT configurations is demonstrated through the results of extensive non-linear analyses.

1.3 Outline of the thesis

A detailed literature review is represented in Chapter 2. This chapter ends with a summary of gaps identified in previous research on CLT buildings and sets the context for the investigations presented in the next chapters of this thesis.

Chapter 3 presents a detailed account of the seismic design of multi-storey CLT buildings in accordance with available national and international design guidance and previous research efforts. A detailed description of the structural configurations considered to represent a wide variety of practical design assumptions is presented. Subsequently, the numerical modelling approach developed in this research is described in Chapter 4. To validate the numerical modelling approach adopted, a series of comparisons between numerical and experimental predictions are conducted and described in this chapter.

Chapter 5 investigates the influence of ground-motion characteristics and structural parameters such as building height, level of panel fragmentation, and design response modification factor on the global and maximum drift demands in multi-storey CLT buildings. Extensive non-linear response history analyses are performed using a suite of 1656 real strong ground-motion records. On the basis of these investigations, the structural characteristics that have influence on the seismic drift demands in multi-storey CLT buildings are identified and employed in the formulation of prediction models.

Following a similar approach, Chapter 6 examines the influence of ground-motion frequency content and structural characteristics on the seismic base shear and inter-storey shear force demands in multi-storey CLT buildings and prediction models are proposed for the estimation of force demands in multi-storey CLT buildings.

Chapter 7 deals with the seismic acceleration demands in multi-storey CLT buildings. To this end, two acceleration demand parameters are evaluated: i) the ratio of the peak floor acceleration to the spectral acceleration of the ground-motion at the buildings' fundamental period, and ii) the ratio of the peak floor acceleration to the peak ground acceleration. As in the other cases, prediction models for the estimation of seismic acceleration demands are proposed, by taking into account of the parameters that have greatest influence on acceleration demands.

The available experimental evidence as well as the findings of this thesis underline the significant levels of floor acceleration demands experienced in tall CLT buildings. This has led to the proposals of various new configurations and devices designed to enhance the performance

of CLT buildings. However, these attempts have mostly neglected the influence of ground-motion characteristics and have been limited to very few selected cases. Therefore, Chapter 8 discusses the design and seismic response of multi-storey CLT buildings equipped with flat sliding bearing elements located at different levels of the buildings. The assessment is performed with due account for the earthquake frequency content, and comparison between the new and conventional systems are presented. A summary of main conclusions drawn from this research together with recommendations for future research on the possible issues addressed in this thesis, is presented in the final chapter.

Chapter 2

Literature Review

2.1 Introduction

This chapter reviews the technical literature relevant to this thesis. It starts by setting the context and highlighting the importance of timber as a construction material. It continues with the presentation of a number of multi-storey timber buildings made of cross-laminated timber (CLT) including completed and ongoing projects around the world. Subsequently, the extensive research efforts carried out in the last years, both experimental and numerical on CLT structures together with three-dimensional full-scale CLT buildings are summarized. The chapter ends by pointing out the lack of research on inelastic seismic demands in multi-storey CLT buildings from a coherent performance based perspective.

2.2 Timber as a construction material

Structural timber is one of the oldest materials used in construction. The most basic structural timber component, as shown in Figure 2.1a, is obtained by sawing the log parallel to grain and forming prismatic elements of mostly rectangular cross-section. These elements are typically used as load bearing columns, beams, floor joists and stud-work.

Glued-laminated timber, shown in Figure 2.1b, also known as Glulam, is an engineered timber product which consists of individual wood laminations bonded together with durable, moisture-resistant structural adhesives. Structural members made of Glulam are used as beams and columns as well as in curved and arched shapes. Given the high strength and stiffness of laminated timber, glulam beams and arches can span large distances without intermediate supports which allows for a greater design flexibility than that offered by other more conventional timber products.

Cross-laminated timber, also referred to as CLT or X-Lam, is a relatively new timber product typically made of 3, 5, or 7 layers of fast growing and industrially dried spruce planks, oriented at 90 degrees one to another and glued together with waterproof adhesives to constitute massive solid wood panels. Figure 2.1c shows a CLT panel and orientation of timber layers. Massive panels of CLT elements with standard panel thicknesses ranging from 57 to 320 mm can be employed as lateral resisting elements in tall timber buildings. At present, CLT panels are used to form multi-storey building structures also in earthquake prone areas due to their large in-plane stiffness, the lightweight nature of timber, and the possibility to use ductile joints.

The history of nail-laminated timber dates back to a century ago when it was used for walls, floors, and roof structures. The formation of nail-laminated timber enables a very straightforward manufacturing by fastening individual laminations using structural nails or screws. The strength and durability of nail-laminated timber is influenced by the strength characteristics of the nails that connect individual lumbers into a single mass timber element. Figure 2.1d shows an example of nail-laminated timber.

Dowel-laminated timber, displayed in Figure 2.1e, is an engineered wood product which is mainly common in Europe and is gaining popularity in the US due to its ease of construction assisted by computer numerical control (CNC) machinery. It is very similar to nail-laminated timber. However, it replaces the structural nails and screws with wooden dowels to join the laminations.

2.3 Multi-storey timber building projects

The number of timber towers around the world has been increasing rapidly and the idea of timber skyscraper dream is coming true. A list of completed, ongoing, and proposed multi-storey timber building projects are presented in Table 2.1 and some of the most important structures made of CLT panels are discussed subsequently.

Table 2.1: Multi-storey mass timber building projects around the world, as of 2018.

Project	Location	Storey	Typology	Status
E3	Berlin	7	Composite	Completed - 2008
Kingsgate House	London	7	Timber	Completed - 2014

Table 2.1: Multi-storey mass timber building projects around the world, as of 2018.

Project	Location	Storey	Typology	Status
Maison De L'Inde	Paris	7	Timber	Completed - 2013
Panorama Giustinelli	Trieste	7	Composite	Completed - 2013
Sanctuary	Yoker	7	Timber	Under construction
T3 Building	Minneapolis	7	Timber	Completed - 2016
Tamedia	Zurich	7	Timber	Completed - 2013
UEA Blackdale Student Residence	Norwich	7	Timber	Completed - 2016
Wagramerstrae	Vienna	7	Composite	Completed - 2013
The Wood Innovation and Design Centre	Prince George	7	Timber	Completed - 2014
Standparken	Stockholm	8	Timber	Completed - 2014
St. Di-des-Vosges	St. Di des Vosges	8	Timber	Completed - 2014
Puukuokka	Jyvaskyla	8	Timber	Completed - 2015
Life Cycle Tower	Dornbirn	8	Composite	Completed - 2012
Carbon 12	Portland	8	Composite	Completed - 2018
Arbora	Montreal	8	Timber	Completed - 2016
Limnologen	Vaxjo	8	Timber	Completed - 2009
Bridport House	London	8	Timber	Completed - 2011
Holz8	Bad Aibling	8	Timber	Completed - 2011
Murrey Grove	London	9	Timber	Completed - 2009
Moholt 50—50	Trondheim	9	Timber	Completed - 2016
Cenni di Cambiamento	Milan	9	Timber	Completed - 2013
Forte	Melbourne	10	Timber	Completed - 2012
Dalston Lane	London	10	Timber	Completed - 2017
The Cube Building	London	10	Composite	Completed - 2015
Trafalgar Place	London	10	Timber	Completed - 2015
Lagerhuset	Eslov	10	Timber	Completed - 2008

Table 2.1: Multi-storey mass timber building projects around the world, as of 2018.

Project	Location	Storey	Typology	Status
25 King	Brisbane	10	Timber	Completed - 2017
Framework	Portland	12	Timber	Completed - 2018
Origine	Quebec	13	Timber	Completed - 2017
The Treet	Bergen	14	Timber	Completed - 2015
Kulturhus Skellefte	Skelleftea	16	Composite	Under construction
55 Southbank	Melbourne	16	Composite	Proposed
Canopia	Bordeaux	17	Timber	Proposed
Hyperion	Bordeaux	18	Timber	Under construction
Tallwood House	Vancouver	18	Composite	Completed - 2017
Silva	Bordeaux	18	Composite	Under construction
Mjsa Tower	Brumunddal	18	Timber	Under construction
Terrace House	Vancouver	19	Composite	Under construction
De Karel Doorman	Rotterdam	23	Composite	Completed - 2012
Barentshus Tower	Kirkenes	20	Timber	Proposed
Haut	Amsterdam	20	Timber	Completed - 2018
Hoho	Vienna	24	Composite	Completed - 2017
Abebe Court Tower	Lagos	26	Composite	Proposed
Baobab	Paris	35	Timber	Proposed

Limnologen project, Vaxjo (Figure 2.2a) is the first multi-storey cross-laminated timber building complex in Sweeden which was completed in 2009. The project involves 4-building blocks of 8-storeys each. CLT was employed for the load bearing system of the structure, walls, and floor elements. This building blocks comprise 134 apartments with a total area of 10.700 m^2.

The Stadthaus (Figure 2.2b) is the first cross-laminated timber tower of London located in the Murray Grove area. It is a 9-storey, 29 m tall CLT building which comprises 29 apartments. The building was completed in 2009 by Waugh Thistleton Architects and Techniker structural engineers in collaboration with KLH UK. The project has proved, for the first time, that CLT



(a) Structural timber [48].



(b) Glued-laminated timber [27].



(c) Cross-laminated timber [93].



(d) Nail-laminated timber [87].



(e) Dowel-laminated timber [5].

Figure 2.1: Structural timber products.

has the potential to be an environmentally-responsive, affordable, and efficient replacement for reinforced-concrete and steel in high-density housing.

Forte (Figure 2.2c) was the tallest timber building made of CLT in the world in its time (completed in 2012). The structure is a 32.2 m tall 10-storey apartment in Melbourne, Australia.

The construction employed 759 CLT panels shipped from Europe to Australia in 25 shipping containers and 5,500 angle brackets together with 34,550 structural screws for its erection.

Dalston Lane (Figure 2.2d) is the most recent multi-storey timber building construction in London. The project is considered as the world's largest CLT building and is the winner of the 2017 Solid Wood Housing award. The 10-storey building was completed in 2017. A 121-unit development made entirely from CLT, weighs only a fifth of a reinforced-concrete building of the same size reducing the amount of deliveries by %80 during the course of construction.

The Treet (Figure 2.2e) is the tallest timber frame building in the world. The 14-storey luxury apartment block in central Bergen was completed in 2015 offering 11 one-bedroom and 51 two-bedroom apartments. Cross-laminated timber panels were used for wall and floor elements while all frame elements are made of glued-laminated timber. To construct such a high-rise building, 49-meters tall and 1-meters thick large glulam columns were employed.

Brock Commons Tallwood house (Figure 2.2f) is one of the tallest innovative hybrid mass-timber building around the world serving occupiers since July 2017. The 18-storey hybrid building consists of cross-laminated timber floors supported by columns made of glued-laminated timber on top of a concrete base together with two concrete cores to place stairs and lifts. Tallwood house is a university resident located in University of British Columbia providing students 33 4-bed suites together with 272 en-suite studio flats, and is home to over 400 students. The building was completed in 9 weeks with only 9 crew after the prefabricated components arrived, saving approximately two months of construction time in comparison with a typical project of similar size.

It is important to note that among all multi-storey CLT building projects, only Tallwood house, which is the tallest timber building today, is located on a mid-risk seismic zone and another tall timber building is underway in Chile. Although most of the projects have been completed in non-seismic zones so far, the multi-storey CLT buildings are now becoming an attractive option in areas that are seismically active. To this end, the research on the seismic response of CLT buildings is outlined in the following section.



(a) Limnologen Project - Vaxjo, Sweden [57].



(b) Murrey Grove - London, UK [47].



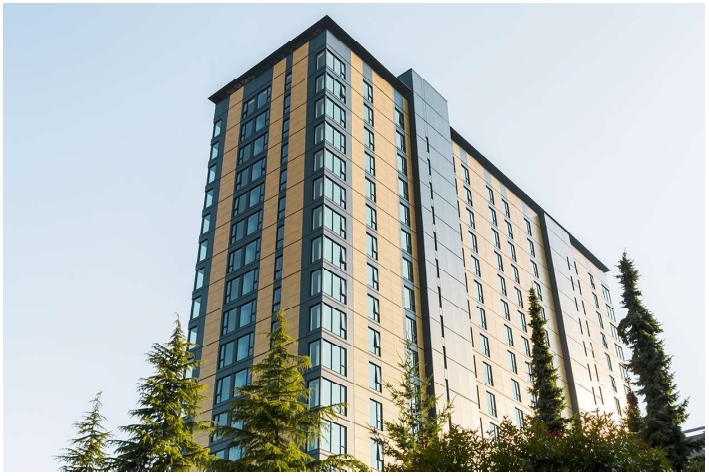
(c) Forte - Melbourne, Australia [89].



(d) Dalston Lane - London, UK [92].



(e) 14-storey timber building, Treet - Bergen, Norway [90, 91].



(f) 18-storey Brock Commons, Tallwood House - Vancouver, British Columbia [86].

Figure 2.2: Multi-storey CLT building projects.

2.4 Research on seismic response of cross-laminated timber buildings

As highlighted in the previous section, the multi-storey construction with cross-laminated timber buildings in seismically prone areas is now becoming an appealing option given the notable in-plane stiffness coupled with a ductile structural joinery design. Therefore, it is important to conduct research studies to fully understand the inelastic response of multi-storey CLT buildings subjected to earthquake ground-motions. To this end, a comprehensive literature is outlined with regards to experimental and numerical research studies on CLT buildings and building sub-assemblies in this section.

2.4.1 Experimental research on CLT walls

One of the earliest experimental research efforts on the lateral response of cross-laminated timber wall panels was conducted by Dujic et al. [23] at the University of Ljubljana, Slovenia. The CLT panels employed in the study were produced by KLH Massiveholz GmbH from Austria. A total of 15 CLT wall panels with different connection and level of vertical load arrangements were tested under monotonic and reversed cyclic loading. Two main conclusions can be drawn from these tests: i) concentrated local failure of the wood is the main failure mechanism observed and ii) the connection stiffness limits the load-bearing capacity of the CLT wall panels. Furthermore, the level of vertical loads play an essential role in increasing the lateral resistance of the panel, particularly when the strength of the connections is insufficient.

Another set of experiments was performed by Dujic and Zarnic [24] on the influence of boundary conditions and the level of vertical loads on the CLT wall panel lateral resistance. Three different boundary conditions were examined. The top of the CLT wall panel was free to translate and rotate in Case A, the wall was free to translate but no rotation was allowed in Case B, and neither translation nor rotation were allowed in Case C. The test results showed that the ultimate strength of the wall component in Case A was half of the observed ultimate strength under Case C boundary conditions. Therefore, the study indicated that the lateral resistance of CLT shear-wall panels is significantly affected by the boundary conditions.

A study on the influence of openings in CLT wall panels was carried out by Dujic et al. [25]. Four different panel configuration including two solid CLT panels and two CLT panels with openings. Besides, the mechanical characteristics of CLT panels and the hysteretic behaviour of CLT joints were investigated. In parallel, numerical models of 36 CLT wall panels with different arrangements were developed in SAP2000 [80]. It was found that the shear resistance of

CLT wall panels is not influenced significantly when the openings in the wall panel are less than %30 of the total CLT panel area. Additionally, it was confirmed that the shear wall strength of the CLT wall panels is remarkably influenced by the shear capacity of CLT connections and anchors.

A series of experiments on the seismic response of CLT systems was performed by Gavric et al. [36]. As part of the experimental programme, reversed cyclic tests were carried out on full-scale single as well as coupled CLT wall panels covering different configurations and structural joint details. An advanced non-linear hysteretic spring element was defined and incorporated subsequently in ABAQUS [1] FE package that captures the cyclic response of structural joinery elements accurately. The structural model employing these spring elements was used for the reproduction of the experimental behaviour of CLT shear-wall panels. Based on these comparative studies, the numerical model developed in the study was found to be suitable for the estimation of dissipated energy and seismic performance of CLT structures.

Joyce et al. [45] carried out an experimental study on the effect of vertical connections of two adjacent wall panels. The performance of traditional spline nails and angled screw connections was examined. Four different arrangements were investigated under quasi-static monotonic and cyclic loading conditions. As a result of the investigation, the angle screw connections were found to have remarkably stiffer and less ductile response compared to spline nails due to their combined axial and shear resistance. Therefore, spline nails were recommended to be utilized in the vertical connections of CLT wall panels in seismic areas.

FPInnovations, in British Columbia, carried out a number of research projects on the seismic behaviour and design of CLT systems. Popovski et al. [67] performed an experimental study on 32 shear-wall panels with different panel arrangements, wall openings, and several aspect ratios as part of the FPInnovations programme. Different type of timber connectors and different connection arrangements were examined. A valuable data set was obtained on the seismic response of CLT panels in North America. The main results on the inter-panel connections and metal connectors showed that a good level of the overall ductility of the system was provided by these connections and as such they were recommended to be employed in CLT building construction in seismically prone areas.

Shen et al. [83] carried out an experimental campaign on a series of CLT connections and shear wall panels to develop a comprehensive understanding of structural properties by means of quasi-static monotonic and reversed cyclic loading protocols at FPInnovations in Canada. Based on the tests results, they implemented two hysteretic models namely a 16-parameter

Pinching4 model and 10-parameter SAWS model in OpenSees. Pinching behaviour, strength and stiffness degradation were considered for both material models. Numerical outcomes were compared to experimental results of CLT shear wall panels under monotonic and cyclic loading protocols. According to comparisons, the authors concluded that Pinching4 model guarantees a better performance than SAWS model in terms of rapid degradation of reloading and unloading stiffness of the bracket connection.

A recent research study on the analytical and experimental lateral-load response of self-centering post-tensioned CLT walls was conducted by Akbas et al [3]. A number of self-centering CLT wall panels with different configurations were tested under cyclic loading and their structural limit states were identified. To estimate SC-CLT wall panel response two analytical models were proposed, namely, a design-oriented model based on simple mathematical expressions, and a fiber-based-element numerical model. Comparative studies between analytical models and experimental results indicated both models can provide accurate lateral-load response estimates for SC-CLT wall panels subjected to cyclic loading.

2.4.2 Full-scale experimental studies on CLT buildings

Following the set of CLT connector and shear wall tests described in the previous sections, Dujic et al. [26, 44] tested two full-scale single-storey shear wall buildings on the shaking table of the Dynamic Testing Laboratory of the Institute of Earthquake Engineering and Engineering Seismology (IZIIS) in Skopje, Macedonia. A computational software developed by IZIIS was used. Zero-length elements were employed to simulate timber connections and friction to model the specimen responses. The displacement and acceleration estimations from the numerical model were found to be in good agreement with the shaking table test measurements. The authors concluded that CLT wall panels, under dynamic loading, exhibited a rigid body response, and a notable level of ductility was provided by inter-panel connections.

Popovski et al. [68] tested a two-storey full-scale CLT-walled structure to investigate the three-dimensional response of the building by means of quasi-static monotonic and cyclic loading at FPInnovations. The building was 4.9 m in height and 6.0x4.8 m^2 in plan. Different number of tie-down connectors, structural screws between two adjacent wall panels, and different level of loading were employed in each case. Based on these experiments, the structure performed in accordance with the initial design objectives. Perpendicular walls provided remarkable enhancement of the load bearing capacity of the system and vertical structural joinery elements between adjacent wall panels offered a relative resistance to slip during rocking of CLT wall

panels, as expected. An important observation from this study was that the rocking behaviour of CLT wall panels is not fully restricted by the rigid floor diaphragms above the walls. Besides, a negligible slip between floor panels in the diaphragm provided evidence that structural connections were properly designed. Based on the kinematic behaviour of the structure, connection type, resistance and positioning were found to play a crucial role in the design of CLT buildings. However, the research was limited only to static loadings and requires more evaluation under dynamic loads.

A three-storey CLT building was designed and tested on a shaking table at the National Research Institute for Earthquake Science and Disaster Prevention (NIED) in Tsukuba, Japan by Ceccotti [13]. The building was 7x7 m^2 in plan with a storey height of 3 m. The main objective of the experimental campaign was to identify an approximate value for the behaviour (q) factor, for CLT shear wall buildings which should be applied in accordance with the Eurocode 8 [29] provisions. The building was subjected to 15 real ground-motion excitations with PGAs ranging from 0.5 to 1.2 g. The building was able to remain standing without significant damage and with minor repair works in terms of tightening and connection replacement after the tests. In addition to the experimental study, a numerical model was constructed using Drain-3DX to perform non-linear response history analyses and simulate the seismic response of the structure. CLT wall and floor panels were modelled using rigid braced frame elements and non-linear spring elements were used to model structural connections. Numerical results showed a very good agreement with the experiments in terms of uplift deformation and maximum lateral displacements for most of the earthquake records. A value of q = 3 was proposed for the design of CLT shear-walled buildings in consistency with Eurocode 8 [29] provisions. During the shaking table tests, most of the CLT wall and floor panels remained stable, while ground floor anchorage elements experienced very high uplift reactions.

Finally, the largest shaking table experiment on the seismic performance of CLT systems performed to date was carried out as part of the SOFIE project. The experimental campaign included structural timber connection tests, CLT shear wall panel tests, and full-scale 3- and 7-storey shaking table tests [13, 14, 15, 25, 34, 36, 37, 76]. As part of this project, Gavric et al. [34] performed various connection tests in 20 different panel configurations. In-plane screwed connections as well as connections between perpendicular wall panels were also tested. Based on the test results, the authors recommended a range of connector over-strength factors between 1.2 and 1.9 with an average value of 1.74. In addition, a full-scale 7-storey CLT building was tested on a shake table at Japan's E-Defence laboratory. The building was designed in accordance with Eurocode 8 [29] provisions, with a response modification factor of q = 3. The building dimensions were 7.5x13.5 m^2 in plan and 23.5 m in height. The total weight of the building

was 284 tonnes. A total of 10 real ground-motion records were applied to the building with increasing intensity levels and a maximum peak ground acceleration of 0.82 g for JMA Kobe ground-motion record. After all ground-motions were applied to the building, the 7-storey structure showed only limited damage without any residual plastic deformation. Nonetheless, damage was concentrated at the tie-down connectors at lower levels of the building due to high over-turning demands. Furthermore, considerable high floor accelerations around 3.8 g were observed at the top storey levels of the buildings. Thus, it was recommended to introduce more ductility to the structure by the researchers. The major finding of the full-scale CLT building testing was the verification that high-rise CLT buildings can be designed with current available force-based procedures, employing a behaviour factor of q = 3. However, the use of current design approach is expected to lead to the development of damage at the tie-down connections at the lower levels. Moreover, the high level of floor accelerations at top levels of the building is an important issue and requires further attention.

2.4.3 Numerical research on the seismic response of CLT walls

A research project was conducted by Fragiacomo et al. [33] aiming to identify an appropriate value for the design over-strength factor of CLT-walled structures. Based on a series of quasi-static tests on nailed and screwed connections, the authors recommended an over-strength value of 1.3 for metal connectors. In addition, a four-storey CLT building was designed using a non-linear static analysis approach. The numerical model of the building was developed employing shell elements for the CLT wall panels and non-linear springs for the connections in SAP2000 [80]. The analysis concluded that the fundamental mode of vibration of the building and the peak structural deformations are underestimated in the case that rigid links are employed and ductility is ignored. Besides, the peak base shear reactions can be over-predicted. It was also observed that the non-existence of inter-panel friction may cause over-estimation of the natural period of the CLT structures. To this end, the benefits of ductile connections on the system ductility and enhanced seismic performance was proved.

Following shaking table tests of the 7-storey SOFIE building [15], a numerical research was carried out by Dujic et al. [25] in order to analyse the seismic response of the building. A numerical model was developed in SAP2000 [80] using shell elements for CLT wall and floor panels, and non-linear springs for the tie-down and angle bracket connectors. A convergence problem of numerical integration was reported caused by the descending branch in the envelope of non-linear springs. To overcome this issue, equivalent linear springs were defined in the model in order to capture the secant stiffness of the connections with %15 viscous damping and reasonable prediction were attained.

The influence of the level of vertical loads and friction on the dynamic behaviour of CLT panel systems were investigated by Sustersic et al. [85] by means of a parametric assessment. A numerical model was developed in SAP2000 [80] employing shell elements for walls and rigid floor diaphragms, and gap elements for the non-linear springs at the connections. A friction element with a friction coefficient value of 0.4 was employed between CLT panels. In addition, a simplified model that relied on diagonal truss elements instead of shells, was also built and evaluated. Non-linear two-node link elements were employed to simulate friction elements in this model. Non-linear response history analysis were performed on the developed numerical models employing different arrangements and friction coefficients. In conclusion, dynamic response of CLT wall panels was remarkably influenced by the level of vertical load and friction.

A numerical model was built in ABAQUS by Rinaldin et al.[75] in order to estimate the dissipation capacity of CLT structures taking into account of an element calibration approach. The main focus of this research was on the calibration of non-linear hysteretic and pinching behaviour of CLT connectors. After a comprehensive comparative study comparing numerical simulations against wall tests and one-storey building experiments, the numerical model developed in the study was shown to accurately estimate the dissipated energy under reversed-cyclic loading.

2.4.4 Seismic response of multi-storey CLT buildings

Pozza and Trutalli [71] studied the seismic response of CLT buildings aiming to assess the relationship between the behaviour (q) factor, panel assembling methodologies and geometrical characteristics of mid-rise CLT buildings up to seven storeys. A parametric study was conducted via incremental dynamic analyses on building configurations with varying levels of vertical connection layers and different building aspect ratios. The numerical simulation results were used to identify parameters that are representative of the geometry of the building configuration and assembling methodology. Then a correlation function was developed to compute the most-appropriate behaviour factor as a function of the previously mentioned parameters. Finally, the proposed correlation equation was validated with reference to available case studies of multi-storey CLT buildings.

A brief account of the seismic design and performance of CLT structures is presented in Popovski et al. [69] as part of the FPInnovations' CLT Design Handbook, Canadian edition. The handbook provided an initial guidance in the design and construction of CLT building

projects in North America. After the publication of Canadian edition of CLT handbook, The U.S. edition of the handbook was prepared through a collaborative work of American Wood Council, APA, FPInnovations, WoodWorks U.S., and USFPL [46]. The project was funded by Forestry Innovation Investment (BC FII), USFPL, Binational Softwood Council, and three CLT manufacturers. The information provided in the handbook addresses several aspects of CLT as a product, structural system, design approaches, fire performance, etc. It also provides a chapter on the lateral load design of CLT structures together with recommended design assumptions.

One of the earliest innovative concept on seismic resilient CLT systems was proposed by Pei et al. [60]. The authors designed a 10-storey CLT building replacing rigid long shear wall panels with short panel components at different floor levels in order introduce ductility to the structure. The building was designed using an R factor of 2.0 based on the equivalent force procedure outlined in ASCE 7 [6]. A series of non-linear response history analyses were performed on numerical models developed using SAPWood [64] software. Based on the analyses results, the proposed configuration proved that lateral deformations were concentrated at ductile floor levels and accelerations at the upper levels were reduced remarkably.

To increase their structural resiliency against large ground-motions, Dolan et al. [21] proposed introducing ductile elements in multi-storey CLT platform buildings. A 10-storey CLT building with floor diaphragms allowing in-plane deformation by means of passive damping elements was modelled and analysed under real strong ground-motion records. Based on the numerical simulations, the authors concluded that the incorporation of passive damping elements at floor layers can improve the seismic response of multi-storey CLT buildings reducing high floor accelerations and strength demands on structural joinery.

Previous observations in full-scale shaking table tests on CLT buildings made evident that these buildings are susceptible to damage due to overturning when subjected to lateral seismic actions [15]. Thus, an innovative floor panel connection technique was proposed by Pei et al. [65] to resist overturning effectively. The new floor panel connection engages CLT panels as coupling elements for CLT shear-wall stacks in the building floor plan. The seismic design of 12-storey CLT building located in Los Angeles is used as a case study. A numerical model of 12-storey CLT building was developed in AxisVm [7] analysis software. The authors concluded that the proposed load-transferring mechanism had a good potential to be implemented in CLT platform buildings. However, the analysis was limited to only static loading conditions, and the simulated demands exceeded simplified calculations in a few cases. Therefore, it is required to study the dynamic response of multi-storey CLT buildings equipped with innovative response modification mechanisms.

Scotta et al. [82] proposed an innovative connection, X-bracket, for cross-laminated timber wall panels aiming to introduce a dissipative connection developed for CLT structures that helps improve the intrinsic ductility and cyclic response of CLT wall panels. Different panel and connection configurations were tested under reversed cyclic loading conditions. Two-dimensional numerical models of experimental configurations were developed using the FE package ANSYS Workbench [4]. A comparative study was conducted with experimental results of CLT panels with typical hold-down and shear bracket connections. It was found that the proposed innovative X-bracket connection provided improved ductility and higher energy dissipation capacity.

Hashemi et al. [42] developed a new slip friction device which replaces traditional structural connections, hold-down and shear bracket, to construct a low-damage panelised CLT system. The study was limited only to numerical simulations. A low-rise building incorporating the new connection concept was modelled in ABAQUS [1] and subjected to reversed cyclic loading in order to investigate the seismic performance of the building. The numerical outcomes demonstrated that the initial strength of the system remained the same during numerous quasi-static analyses. Furthermore, the concept proved that a significant amount of energy was absorbed. The authors concluded that based on the preliminary numerical investigations, the proposed system has the potential to provide a low-damage seismic design for CLT platform structures. However, it is necessary to perform further experimental investigations to confirm the numerical outcomes.

A novel friction joint called a resilient slip friction (RSF) was proposed by Hashemi et al. [43] in order to provide energy dissipation and self-centering behaviour to CLT shear wall panels. Traditional hold-down connections were replaced with RSF joint elements and a large-scale experimental research was conducted on rocking CLT wall panels. After several displacement-control quasi-static tests on the specimen, no damage was observed both in the CLT panel and in the RSF joints. The experimental results showed that the proposed friction joint can provide an increased performance when a seismic resilient design is desired. In addition, the authors proposed a series of analytical formulations to design CLT rocking walls equipped with RSF joints. Subsequently, the analytical results were compared to experimental outcomes and they were found to accurately estimate the lateral strength of the system. Furthermore, a numerical model was built using SAP2000 [80] and validated against experimental results. Finally, the authors concluded that the proposed system demonstrated an excellent performance suggesting the potential application in seismic-resilient CLT structures when no damage design (NDD) philosophy together with no post-event maintenance is desired.

The potential use of elastoplastic behaviour on CLT structures was studied based on experimental investigations on a 2.44x2.44 m rigid timber shear wall panel incorporating slip-friction connectors [50]. A new set of connectors were proposed to replace traditional tie-down steel brackets. In a latter research effort, a numerical study was performed on rocking CLT structures constructed with slip friction devices by Loo et al. [51]. A direct displacement design procedure was proposed for a multi-storey CLT wall panel with slip-friction elements at the edges of the wall. The seismic behaviour of the proposed system was compared to an idealized structure incorporating a plastically deformable hinge at the base. In light of these comparisons, no difference was found between the wall assembly with slip friction connectors and the idealized structure with plastic hinges when the gravity effects were excluded. On the other hand, the inclusion of gravity effects lead to an improved seismic performance of the assembly with remarkable reduction of maximum drifts. Furthermore, the use of slip-friction connectors significantly decreased the maximum accelerations experienced in the structure. Overall, despite the very limited results with only one wall panel and a few ground-motion records employed, the concept of CLT rocking wall with slip-friction connectors appears as a promising system.

A numerical investigation on the effectiveness of tuned mass dampers employed in a high-rise CLT building was performed by Poh'sie et al. [66]. The full-scale 7-storey CLT building tested by Ceccotti et al. [15] was equipped with different tuned mass damper options to investigate buildings' seismic performance. A number of configurations were considered in the study (e.g. (i) a single bilinearized tuned mass damper at 6th floor (BTMD), (ii) single BMTDs at floor levels 4, 5, and 6 (MS-BTMD), (iii) multiple BTMDs at 6th floor (MBTMD), and (iv) multiple BTMDs at floor levels 4, 5, and 6 (MS-MBTMD)). The design of a simplified MDOF model consisting of linear bi-directional spring elements and dampers together with storey masses to represent the floor levels was presented. Based on the results from numerical simulations, the proposed BTMD configurations experienced up to 40% reduction in the horizontal floor accelerations. The analysis results from the simplified model with masses at each floor level (seven-mass model) demonstrated that the seismic performance of the building slightly improved when multiple devices were considered in the building. Besides, TMDs remained mainly ineffective at lower levels. A detailed model with elastic shell elements to simulate CLT wall panels and linear springs corresponding to structural connections was employed with to study the detailed model response under Kobe earthquake. As before, MS-BTMDs slightly improved the structural response (41% reduction in floor acceleration), however, the overall mass of the TMDs and its cost increased, whereas reduction of up to 37% in floor accelerations were observed when the BTMD was placed at the 6th floor. Although the seismic performance of CLT buildings was improved using tuned mass dampers, an efficient and innovative solution

is still required to incorporate into multi-storey CLT buildings.

One of the most recent study on the seismic resilience of CLT buildings was conducted by Bolvardi et al. [10] on the direct displacement design of tall cross-laminated timber platform buildings incorporating inter-storey isolation layers. The fundamental objective of their study was to explore the potential application of inter-storey isolation systems to improve seismic resiliency of high-rise CLT platform buildings. In order to achieve pre-defined displacement targets, a generalized Direct Displacement-based Design was employed. Two design cases of a 12-storey CLT building with a flexible diaphragm at levels 4 and 6. Numerical non-linear response history analyses with a suite of 22 ground-motion records on 12-storey CLT building were performed using SAPWood [64]. Based on the numerical analyses results the buildings with isolation layers were able to meet pre-selected non-linear deformation targets for all hazard levels with the required non-exceedance probability. Following the proposed DDD method, the performance of the design was found to be effective to control the isolation-layer and remaining storey drifts under pre-defined boundary conditions. For comparison purposes, the analyses of 12-storey CLT building without inter-storey isolation layers were also performed. The comparative investigations demonstrated that in the case of large seismic events, additional inter-storey isolation layers can remarkably reduce the level of non-linear deformations as well as damage in multi-storey CLT buildings. However, this study was limited with only a few building configurations and very limited number of ground-motion records employed. These limitations point towards the importance of a comprehensive assessment of inelastic seismic demands in multi-storey CLT buildings equipped with inter-storey isolation systems with a large building and ground-motion database.

2.5 Summary

A complete literature review has been presented in this chapter. The aim of this literature survey was to identify outstanding research needs in the area of seismic design and assessment of CLT buildings. In the light of the above review, a set of conclusions, which set out the context for the corresponding contributions highlighted in later chapters of this thesis, are listed below.

- Drift estimations have a paramount importance in modern seismic design and assessment of buildings. This is because there is a strong relationship between drift and damage, both structural and non-structural. The extensive experimental and numerical research on CLT systems conducted to date seems to overlook this fact and no comprehensive assessment on the expected level of inelastic deformation demands in multi-storey CLT buildings has been performed. Moreover, no research has considered the influence of

ground-motion characteristics such as frequency content that have been widely accepted as determinant on the seismic response of buildings. Therefore, Chapter 5 is devoted to a detailed characterisation of inelastic deformation demands in multi-storey CLT building configurations and their dependency on the frequency content of the ground-motion.

- Even though global and storey drifts have primary consideration in performance-based design philosophies due to their strong correlation with damage, it is imperative that a structure meets capacity design requirements in order to ensure predictability of response and failure mode control. Therefore, it is important to investigate the evolution of strength demands and their correlation with frequency content of the ground-motion. A comprehensive evaluation of strength demands in multi-storey CLT buildings is thus addressed in Chapter 6.

- A relatively good seismic performance of low to mid-rise multi-storey CLT buildings has been documented by means of full-scale shaking table experiments. However, studies have shown that multi-storey CLT buildings might experience high levels of floor accelerations [2, 15, 16, 76] which can affect building content and cause harm to its occupants leading to significant losses. A detailed characterisation of acceleration demands incorporating the frequency dependency on the acceleration response of multi-storey CLT buildings is performed in Chapter 7.

- The literature review has also highlighted a number of novel CLT systems with several innovative configurations aimed at increasing the resiliency of CLT buildings. These includes short CLT panel configurations at some floor levels instead of traditionally employed long CLT panels [60, 61, 62, 63], innovative slip-friction devices [42, 43, 50] and floor panel connections [65] to replace traditional hold-down connections, flexible diapgrahm configuration [10], and new connections to replace traditional angle bracket and tie-down connectors [82]. Among these, the provision of inter-storey isolation layers appears to be an attractive solution to limit storey shears and accelerations in tall CLT structures. However, previous assessments have relied on a limited number of ground-motions and neglected the effects of frequency variations. To this end, Chapter 8 is dedicated to the evaluation of the seismic response of multi-storey CLT buildings equipped with flat sliding bearing elements at particular floor levels, taken into account frequency content of the ground-motion.

Chapter 3

Seismic Design and Building Database

3.1 Introduction

As identified in the literature review presented in the preceding section, there is an urgent need to evaluate the seismic demands in conventional multi-storey cross-laminated timber (CLT) buildings and to identify the salient structural parameters that have a determinant influence on the response of such buildings. In this context, a series of prototype CLT buildings are designed in accordance with available national, international standards, and previous research efforts in order to build an extensive database of structures that covers a wide range of building configurations.

The following sections of this chapter describe the structural design procedure followed for the seismic design of multi-storey CLT buildings and analysed later in this thesis as well as the database of buildings generated.

3.2 Seismic Design

A number of buildings designed based on different assumptions and structural characteristics were considered to investigate their influence on the seismic response of buildings. To this end, different number of storeys (i.e. n = 6, 8, 12, 16, 20), level of panel fragmentation (i.e. m = 1, 2, 3), and different behaviour factors (i.e. q = 2, 2.5, 3, 4) were employed. Table 3.1 presents the building configurations considered in this study.

To illustrate the design steps followed, the seismic design of a 6-storey CLT building (A1 in Table 3.1) for a response modification factor of q = 3 is described in this section. Figure 3.1 presents a typical plan view and elevation of the 6-storey CLT building under consideration.

The building represents a hotel with a single-storey podium and a 6-storey tower block [52].

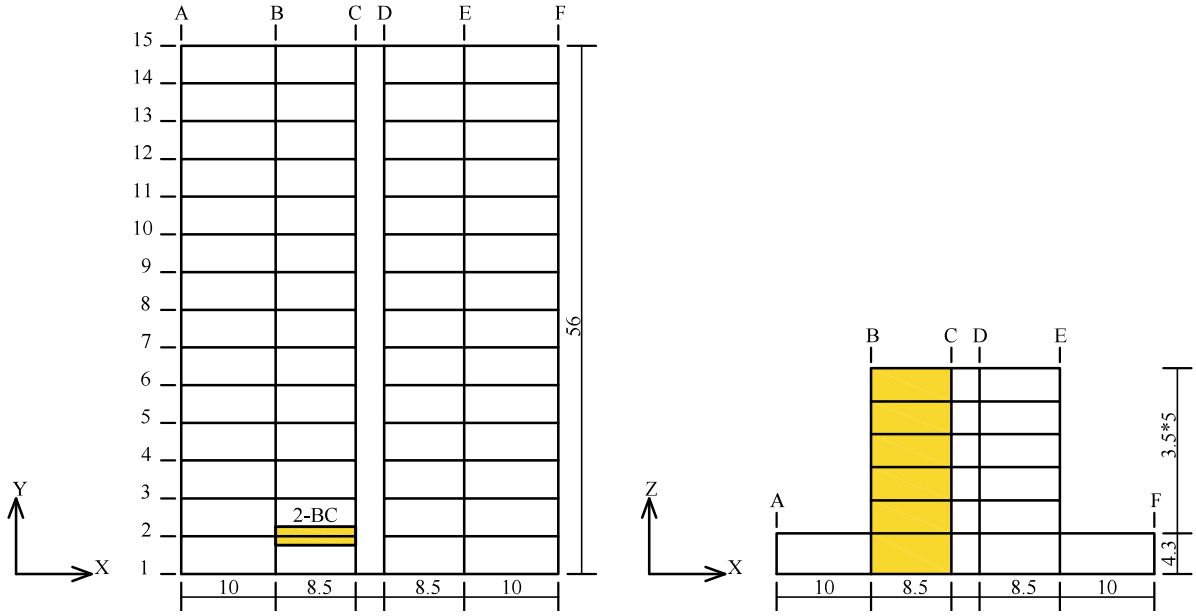


Figure 3.1: Plan view and elevation of the 6-storey CLT building. Units in [m].

Permanent action

An overview of the assemblies utilised to calculate in the building is provided in this section. The building components such as floor slab, roof, internal and external wall panels employed for the building assemblage are shown in Tables A.1 to A.4 while Tables A.5 to A.8 summarize the calculation of permanent actions considered. To this end, the initial wall and floor panel thickness values are determined as follows: 402 mm thick floor panels, 677 mm thick roof panels, 158 mm thick internal wall panels, and 358 mm thick external wall panels.

Variable action

To determine variable action in the buildings, the following loads defined in BS EN 1991-1 [28] for a residential building (Service Class A) were assumed (Table 3.2).

Table 3.1: Building configuration database developed herein this research.

Storeys	n = 6			n = 8			n = 12			n = 16			n = 20		
ID	A1	A2	A3	B1	B2	B3	C1	C2	C3	D1	D2	D3	E1	E2	E3
Vertical joints/ width	m = 1	m = 2	m = 3	m = 1	m = 2	m = 3	m = 1	m = 2	m = 3	m = 1	m = 2	m = 3	m = 1	m = 2	m = 3
Typical CLT wall considered (2-BC in Figure 3.1)															

Table 3.2: Imposed loads for residential buildings.

Category		q_k [kN/m^2]	Q_k [kN]
A	Floors	2.0	2.0
	Staircases	3.0	3.0
	Balconies	4.0	3.0

Total building weight

Based on the assumptions in the previous section the total dead load for the 6-storey building is shown in Table A.9 while Table A.10 reports the live load calculations. To this end, the total dead load for the 6-storey CLT building is 34,497.98 kN and the live load is 20,620.00 kN.

Seismic mass

The seismic mass was calculated with the load combination in Cl. 3.2.4.:

$$M = G + \lambda_{Ei}.Q \tag{3.1}$$

where G is the total dead load, Q is the total superimposed load, and λ_{Ei} is the reduction factor taken as 0.3. Therefore, the corresponding building weight is 40,683.98 kN and the seismic mass is 4,148.59 tonne. The corresponding building weights and seismic masses of taller buildings are also summarized in Table 3.3.

Table 3.3: Corresponding building weight and seismic mass for taller buildings.

Building	Building weight [kN]	Seismic mass [tonne]
8 storey	52,978.88	5,402.31
12 storey	77,568.68	7,909.83
16 storey	102,158.48	10,417.29
20 storey	126,748.28	12,924.76

Material properties

The material used for the load bearing walls is cross-laminated timber made of C24 wood. The Service Class 1 conditions were assumed. According to EN 1995-1-1 [28] Table 3.1 the modification factor for glued laminated timber under instantaneous action is:

$$k_{mod} = 1.1 \tag{3.2}$$

The following equation was employed to calculate the design resistance value R_d of a strength property according to EN 1995-1-1: 2004 - 2.4.1:

$$R_d = k_{mod} * \frac{R_k}{\gamma_m} \tag{3.3}$$

where k_{mod} is the strength modification factor, R_k is the characteristic load carrying capacity, and γ_m is the partial safety factor. The partial safety factor γ_m for accidental combinations "instantaneous load case" assumed as:

$$\gamma_m = 1.0 \tag{3.4}$$

in accordance with Table 2.3 in EN 1995-1-1. Similarly, the strength and stiffness properties of cross-laminated timber were determined by means of following expressions;

* **Strength**
  - ◇ Compressive strength in the grain direction:

$$f_{c,CLT,d} = k_{mod} * \frac{f_{c,CLT,k}}{\gamma_m} \tag{3.5}$$

  - ◇ Compressive strength perpendicular to grain direction:

$$f_{c,CLT,90,d} = k_{mod} * \frac{f_{c,CLT,90,k}}{\gamma_m} \tag{3.6}$$

  - ◇ In-plane shear strength:

$$f_{v,CLT,d} = k_{mod} * \frac{f_{v,CLT,k}}{\gamma_m} \tag{3.7}$$

  - ◇ In-plane torsional strength:

$$f_{tor,CLT,d} = k_{mod} * \frac{f_{tor,CLT,k}}{\gamma_m} \tag{3.8}$$

* **Stiffness**
  - ◇ Modulus of elasticity in the grain direction:

$$E_{0,mean} = 11,000 \ \text{N/mm}^2 \tag{3.9}$$

  - ◇ Modulus of elasticity in perpendicular to the direction of the grain:

$$E_{90,mean} = 370 \ \text{N/mm}^2 \tag{3.10}$$

◇ Shear modulus:

$$G_{0,mean} = 690 \ \ N/mm^2 \tag{3.11}$$

◇ Rolling shear modulus:

$$G_{90,mean} = 69 \ \ N/mm^2 \tag{3.12}$$

It is important to note that all relevant material properties for C24 product class have been obtained from "KLH" [47] which is one of the earliest CLT suppliers in Europe.

3.2.1 Seismic base shear

To determine seismic base shear, the Eurocode 8 [29] Type 1 Response Spectrum (for high seismicity areas) is adopted along with soil type C conditions. To this end, the following spectral parameters are obtained from Table 3.2. of Eurocode 8 [29]:

Table 3.4: Spectral parameters for areas of high seismicity [29].

S	T_B [s]	T_C [s]	T_D [s]
1.15	0.3	0.6	2.0

The reference peak ground acceleration employed is:

$$\alpha_{gR} = 3.0 \ \ m/s^2 \tag{3.13}$$

and the building importance factor is:

$$\gamma_I = 1.0 \ \ m/s^2 \tag{3.14}$$

Therefore, the design ground acceleration can be calculated as:

$$\alpha_g = \alpha_{gR} * \gamma_I = 3.0 \ \ m/s^2 \tag{3.15}$$

It should be noted that a design behaviour factor of q = 3 was employed following recommendations from numerous research studies. However, to investigate the influence of other design assumptions on the seismic response of CLT buildings, additional q factors of q = {2, 2.5, 3 and 4} have also been employed in later chapters of this thesis.

Design response spectrum

The seismic design response spectrum for calculating the seismic base shear force F_b is the result of the previously defined parameters in combination with the following equations taken from EN 1998-1:2004 [29] section 3.2.2.5(4):

$$0 \le T \le T_B: \qquad S_d(T) = \alpha_g * S * \left[\frac{2}{3} + \frac{T}{T_B} * \left(\frac{2.5}{q} - \frac{2}{3}\right)\right] \tag{3.16}$$

$$T_B \le T \le T_C: \qquad S_d(T) = \alpha_g * S * \frac{2.5}{q} \tag{3.17}$$

$$T_C \le T \le T_D: \qquad S_d(T) \begin{cases} = & \alpha_g * S * \frac{2.5}{q} * \left[\frac{T_C}{T}\right] \\ \ge & \beta * \alpha_g \end{cases} \tag{3.18}$$

$$T_D \le T: \qquad S_d(T) \begin{cases} = & \alpha_g * S * \frac{2.5}{q} * \left[\frac{T_C T_D}{T^2}\right] \\ \ge & \beta * \alpha_g \end{cases} \tag{3.19}$$

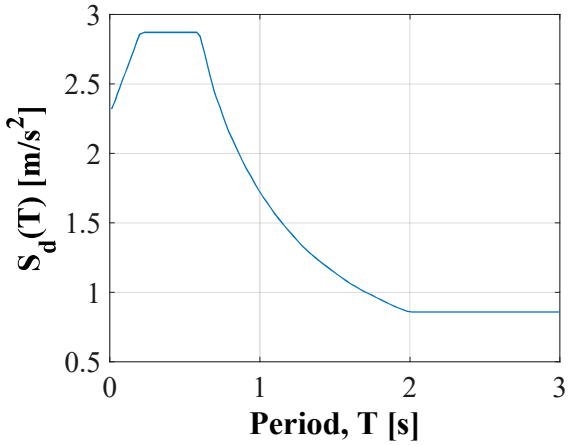


Figure 3.2: Design response spectrum (soil class C, $\alpha_g = 3.0\ m/s^2$).

Base shear force

The seismic base shear force F_b employed in the design of these buildings was determined by using the following equation as described in EC8 [29]:

$$F_b = S_d(T_1) * m * \lambda \tag{3.20}$$

where $S_d(T_1)$ is the ordinate of the design spectrum at the fundamental period (T_1); T_1 is the period associated with the first mode of vibration; m is the total building mass above the foun-

dation; and λ is the correction factor. The following criteria has been followed to determine the factor λ:

$\lambda = 0.85$ if $T_1 < 2 * T_C$ and the building has more than 2 storeys, or $\lambda = 1.0$ in other cases.

Fundamental period

According to the expression 4.3.3.2.2 of Eurocode 8 [29], the value of the natural period for timber structures up to 40 m height can be determined as follows:

$$T_1 = C_t * H^{0.75} \tag{3.21}$$

where C_t is 0.05 for tall buildings, and H is the height of the building above the rigid basement, in m. Therefore, the structural period associated with the first mode of vibration for the 6-storey CLT building is $T_1 = 0.05 * 21.8^{0.75} = 0.50$ s. The corresponding fundamental periods for taller buildings are summarized in Table 3.5.

In the particular case of the 6-storey CLT building since $T_B < T_1 < T_C$, Equation 3.17 applies and $S_d(T_1) = 3.0 * 1.15 * 2.5/3.0 = 2.875$ m/s^2.

Under these conditions, the seismic base shear force can be determined as $F_b = 2.875 * 4148.60 * 0.85 = 10,138.14$ kN. Table 3.5 summarizes the calculation of base shear forces for other building heights designed in this thesis.

Table 3.5: Fundamental period and seismic base shear forces for taller buildings.

Building	Fundamental period, T_1 [s]	Base shear F_b [kN]
8-storey	0.62	12,765.66
12-storey	0.82	14,320.75
16-storey	1.00	15,274.35
20-storey	1.18	16,039.63

3.2.2 Lateral load distribution

The distribution of the horizontal seismic base shear force F_i between floors follows an inverse relationship with the height and mass that can be calculated with the following expression:

$$F_i = F_b * \frac{z_i * m_i}{\sum(z_j * m_j)} \tag{3.22}$$

Figure A.1 and Table A.12 indicate the lateral load distribution and bending moments determined for the core-wall model of the 6-storey CLT building described before, while the distribution of storey shear forces can be seen in Table A.13.

3.2.3 Lateral load distribution into load bearing walls

All buildings considered have a perfectly symmetrical configuration. Therefore, the geometric centre of the building, T_s, the centre of stiffness as well as, Γ_s, centre of mass all coincide at the same point in plan. Since only seismic forces in x- direction are taken into account in the design and given that all dimensions of load bearing walls in x- direction are equal, their relative stiffness values are also the same. Therefore, the storey shear forces for each level is distributed on the grounds of this equality.

However, it is important to note that despite buildings' perfectly symmetrical configuration, the action effects on the load bearing wall elements should be increased to allow for accidental torsion such that Section 4.3.3.2.4 of EC8 [29]:

$$\delta = 1 + 0.6\frac{x}{L_e} \tag{3.23}$$

where x is the distance of the element under consideration from the centre of mass of the building in plan, measured perpendicularly to the direction of the seismic action considered, and L_e is the distance between the two outermost lateral load resisting elements, measured perpendicularly to the direction of the seismic action being considered.

In the case of the core section 2-BC in Figure 3.1, the value of δ is determined as $\delta = 1.25$. Therefore, the action forces previously calculated will be increased by a factor of 1.25 to account for the accidental torsional effects. Table A.14 shows the final design lateral forces including additional torsional effects.

3.2.4 Load bearing wall thickness

It is important to verify the resistance of load bearing walls against vertical and horizontal actions. To this end, a simple yet robust research tool, CLT designer [18], is employed. The initial wall thickness of 128 mm was assigned to both internal and external walls. To verify the thickness of CLT wall panels to withstand the seismic shear and torsion, the previously calculated lateral forces are applied to the wall panels in CLT designer [18]. In order to ensure a ductile failure mechanism, the distributed lateral forces were multiplied by an over-strength factor of $\gamma_{ov} = 1.6$ as recommended in [36]. The final wall thickness values for the 6-storey CLT

building obtained for this design process are summarised in Table 3.6. A detailed information for CLT wall panel thickness verification can be found in Appendix B.

Table 3.6: CLT panel thickness values along the building height in 6-storey CLT building.

Floor level	Ground	1	2	3	4	5
Wall thickness [mm]	120	120	100	100	100	100

3.2.5 Floor slab thickness

To verify the floor slab thickness of the different building configurations, the same research tool CLT designer [18] is used. As a preliminary assumption, 182 mm and 200 mm thick 5-layered CLT panels were examined under dead and superimposed loads for floor slabs. It was found that vibration verifications are not satisfied when the 182 mm thick panel is used but the 200 mm thick panel is able to fulfil all serviceability verifications. Therefore, 200 mm thick CLT panels are used for all floor slabs in the building dataset. A detailed verification procedure can be found in Appendix B.

3.2.6 Design of CLT connections

This section summarizes the design of CLT wall panel connections employed in this study. Due to the lack of codified design provisions for CLT wall and floor panel connections, previous research efforts [13, 35, 52] have been followed. To determine the resistance of a CLT wall panel under lateral loads, the most common approach defined in Europe and North American practice is followed. In order to ensure an energy dissipation mechanism through controlled yielding only at the metal connectors, an over-strength factor should be employed for the design of other non-dissipative joints. These joints are: horizontal joints between floor panels to form a rigid diaphragm, connections between floor and the wall panels underneath, and connections between corner wall panels to ensure a box-like behaviour [52].

The lateral loads applied on a CLT wall panel were uniformly distributed to all connection elements at the bottom of the wall panel. Similarly, uplift forces were shared among tie-down connectors, based on their relative position with respect to the pivoting point of the wall following a triangular distribution of forces and in proportion to the connection stiffness ratios [13]. Finally, to ensure the segmented panels rock separately, the following inequality was satisfied [52]:

$$R_s \leq R_v + \sum R_{B,y,i} \frac{x_i}{b_i} \tag{3.24}$$

where R_v is the design resistance of the tie-down connector; $R_{B,y,i}$ is the vertical resistance of the shear brackets; x_i is the lateral distance between the centre of the shear bracket and the corner of the wall panel; and b_i is the length of an individual panel [52].

Figure 3.3 depicts the analytical model used to determine the lateral resistance of CLT shear walls used currently in Europe [13]. The number and type of the connection elements in the 6-storey A1 CLT building is summarised in Table 3.7. The corresponding design values of other building configurations with additional response modification factors (i.e. q = 2, 2.5, and 4) are reported in Appendix C.

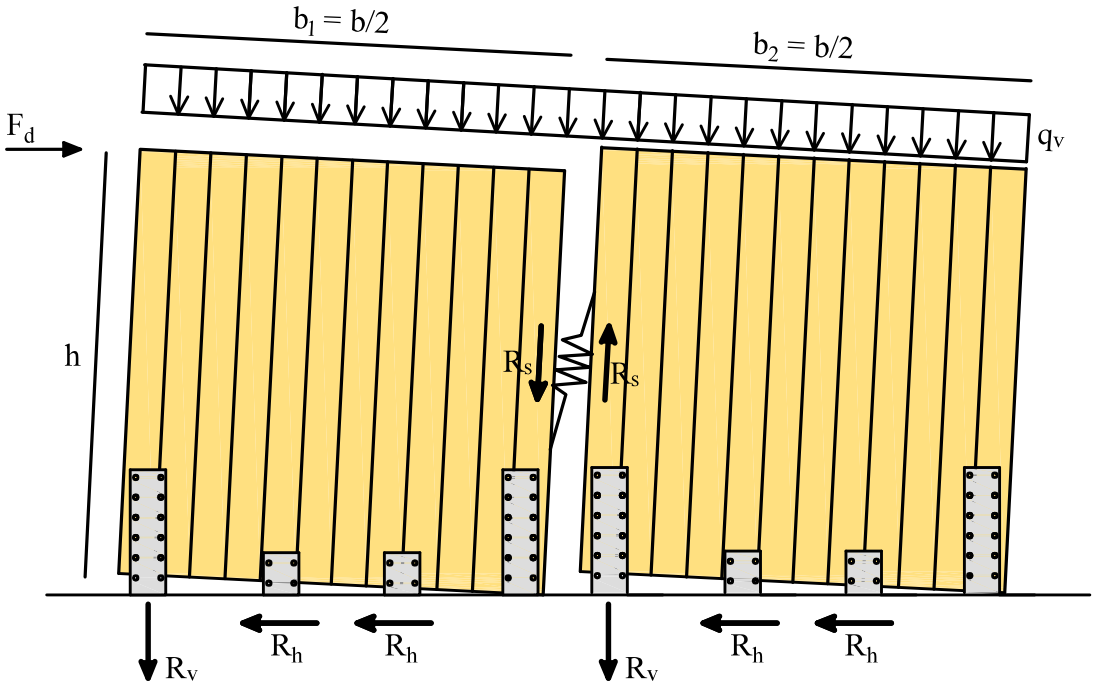


Figure 3.3: Schematic of load distribution in coupled CLT panels. Adapted from [52].

3.3 Concluding remarks

This chapter has presented a detail account of the seismic design of the CLT buildings. The design follows available national and international seismic design principles as well as findings

Table 3.7: Variation of the type and number of structural connections in building configuration A1.

Floor level	q = 2	q = 2.5	q = 3	q = 4
1	9 TTF200 4 WHT620	8 TTF200 4 WHT620	6 TTF200 4 WHT620	5 TTF200 2 WHT620
2	9 TTF200 4 WHT620	7 TTF200 4 WHT620	6 TTF200 2 WHT620	5 TTF200 2 WHT620
3	8 TTF200 4 WHT540	6 TTF200 4 WHT540	5 TTF200 2 WHT540	4 TTF200 2 WHT540
4	6 TTF200 4 WHT440	5 TTF200 4 WHT440	4 TTF200 2 WHT440	3 TTF200 2 WHT440
5	5 TTF200 4 WHT440	4 TTF200 2 WHT440	3 TTF200 2 WHT440	3 TTF200 2 WHT440
6	3 TTF200 2 WHT340	3 TTF200 2 WHT340	3 TTF200 2 WHT340	3 TTF200 2 WHT340

* TTF stands for the type of angle bracket and WHT stands for the type of tie-down connector.

from previous research on CLT structures. A good building database was developed considering different number of storeys (n), employing different design practices characterised herein by the behaviour factor (q), and the level of panel fragmentation (m). To this end, the next chapter introduces the numerical modelling strategy adopted as well as numerous validation studies. Moreover, it presents the building and ground-motion characteristics of interest which are considered in the parametric investigations later in this thesis.

Chapter 4

Numerical Modelling, Analysis and Parameters Investigated

4.1 Introduction

It is required to develop numerical models to study the seismic response of multi-storey CLT buildings. To this end, a detailed account of the numerical modelling strategy adopted in this thesis together with the parameters of interest are described in this chapter.

This chapter is divided into 4 sections. The first section presents a description of the numerical modelling approach. This includes the modelling strategy, materials employed, and a detailed investigation on CLT panel stiffness. Extensive numerical validation studies consist of connection hysteresis response, cyclic response of single and coupled CLT wall panels, and the response of full-scale CLT building are demonstrated in the second section. Subsequently, the third section provides information on the non-linear response history analyses conducted to study the inelastic demands in multi-storey CLT buildings. The section ends with the introduction of structural parameters and ground-motion characteristics investigated. Finally, concluding remarks are outlined in the last section of this chapter.

4.2 Numerical modelling

Numerical models of representative core sections of the CLT building configurations were developed in the open-source research oriented finite element framework OpenSees [59]. The model takes into account material and geometric non-linearities. Figure 4.1 depicts the modelling approach adopted in this research. It is widely accepted that non-linear behaviour is mostly concentrated at the joints in CLT structures. Thus, linear elastic 4-node Quad elements,

available in OpenSees [59], were employed to simulate CLT shear-wall panels. On the other hand, zero-length and two-node link elements were used for the structural connections. Equivalent isotropic wood material characteristics were assumed for CLT wall panels and tri-linear hysteretic rules were calibrated to experimental results and assigned to the structural joints.

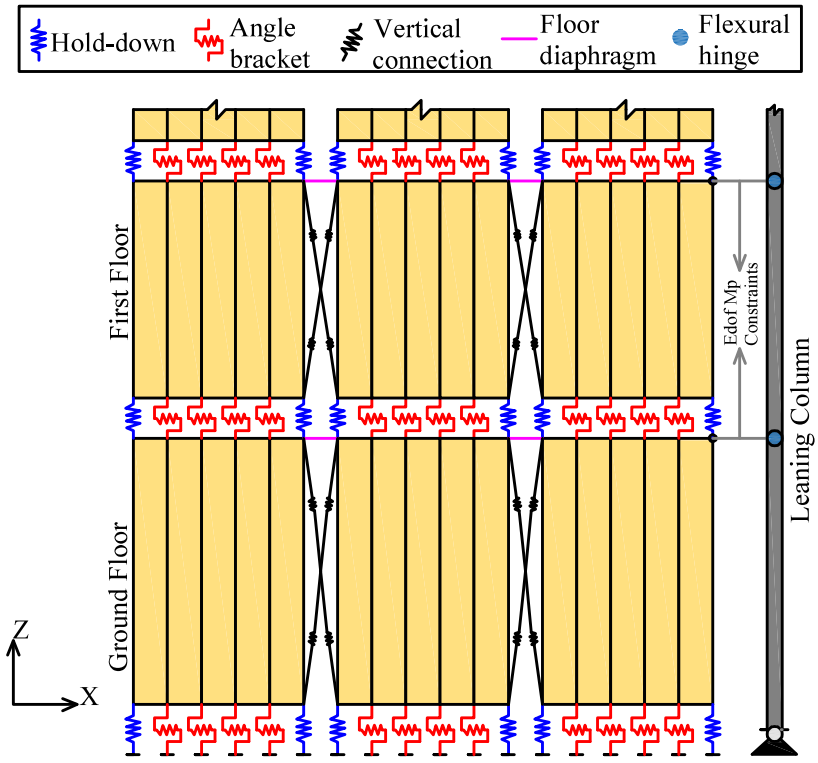


Figure 4.1: Schematic of numerical modelling approach for CLT buildings.

It is important to note that Quad elements in OpenSees [59] rely on a 2-degree of freedom per-node idealization and allow only a linear geometric transformation. Therefore, a leaning column was constructed using 3-degrees-of-freedom per-node idealized beam-column elements to account for P-delta second order effects. Subsequently, the corresponding vertical loads were applied at each floor level of the leaning column and an Equal-degree-of-freedom multi-point constraint (EdofMP) was defined to connect the two model domains. A parametric investigation was performed to determine the degradation parameters employed in the non-linear links on the basis of previous experimental studies [38]. To this end, values between 0.2 and 0.8 achieved the closest estimation of the hysteretic behaviour of structural connections. Finally, structural joinery elements between two adjacent CLT wall panels were simulated with experimentally calibrated non-linear spring elements [39].

4.2.1 Hysteretic material definition

A bilinear uni-axial hysteretic material model was employed to simulate structural connections based on the available material definition in OpenSees [59]. This model requires the specification of a minimum of two and a maximum of there positive and negative points in the stress-strain (force-displacement) domain as well as pinching factors to fully define the stress-strain relationship. Figure 4.2 demonstrates the model domain in detail. The command line used to construct a uniaxial bilinear hysteretic material object in OpenSees [59] can be found in Appendix A.

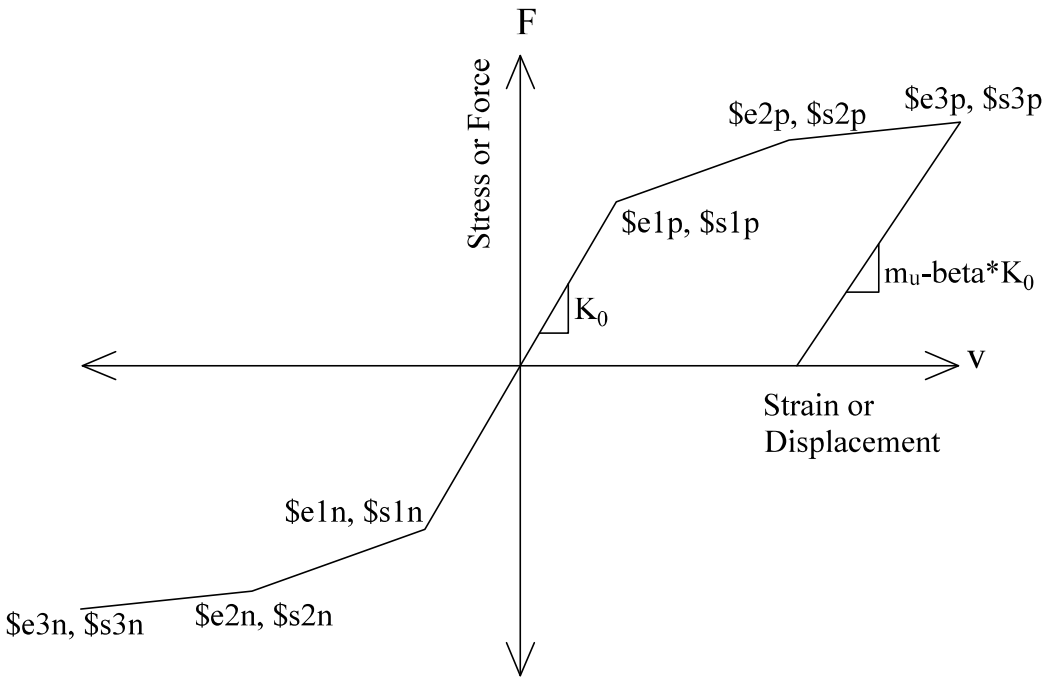


Figure 4.2: Hysteretic material definition available in OpenSees [59].

Where "matTag" is the material tag identifier; "e1p s1p" are the stress and strain (force and deformation) at the first point of the envelope in the positive direction; "e2p s2p" are stress and strain (force and deformation) at the second point of the envelope in the positive direction; "e3p s3p" are stress and strain (force and deformation) at the third point of the envelope in the positive direction (optional); while "e1n s1n", "e2n s2n", and "e3n s3n" are the corresponding negative values; "pinching x" is the pinching factor for strain (deformation) during reloading; "pinching y" is the pinching factor for stress (force) reloading; "damage1" is damage due to ductility: D1($m_u - 1$); "damage2" is damage due to energy: D2($E_{ii} - E_{ult}$); "beta" is power used to determine the degraded unloading stiffness based on ductility, m_u – beta (optional, default = 0.0).

4.2.2 Joint types

The type of joints employed in the design and modelling of the multi-storey CLT buildings under consideration are:

- Angle brackets made of pre-galvanised mild steel as shear connectors to fasten the above-grade walls, and lower walls to floor panels. The type TTF200 angle bracket seen in Figure 4.3, fastened with 30 CNA annular ring-shank nails 4.0x60 mm for each flange were generally employed [77].
- Rothoblaas hold-downs of types WHT340, WHT440, WHT540 and WHT620 shown in Figure 4.3 were employed as tension anchors at wall corners. This connectors were fastened with a number of 4.0x60 mm anchor nails and with 16.0x190 mm bolds [77].



(a) TTF200 angle bracket. (b) WHT hold-down connectors.

Figure 4.3: TTF200 angle bracket and WHT hold-down connectors.

The hysteretic material properties of angle bracket and hold-down connectors are presented in Table 4.1. Figure 4.4 depicts the hysteretic behaviour of typical angle bracket and tie-down connectors employed.

4.2.3 Vertical joints between adjacent wall panels

The modelling of vertical connections between two adjacent wall panels is defined by assuming all the screws behave as springs in parallel. Thus, the equivalent hysteretic material properties of the vertical connections were determined in accordance with the Equations 4.1 and 4.2.

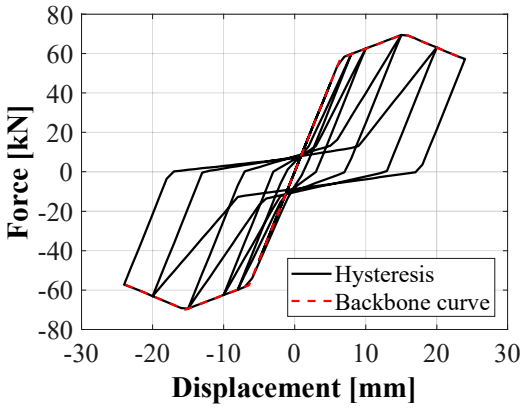
$$v_{eq} = v_1 = v_2 = v_n \tag{4.1}$$

$$F_{eq} = F_1 + F_2 + F_n \tag{4.2}$$

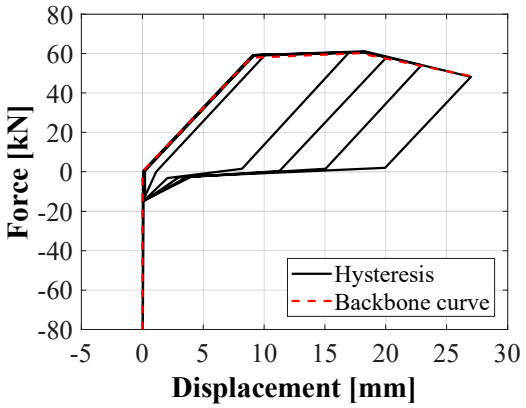
where v_{eq} is the equivalent displacement of vertical connection elements and F_{eq} is the sum of forces for all individual springs.

Table 4.1: Hysteretic material properties of metal connectors.

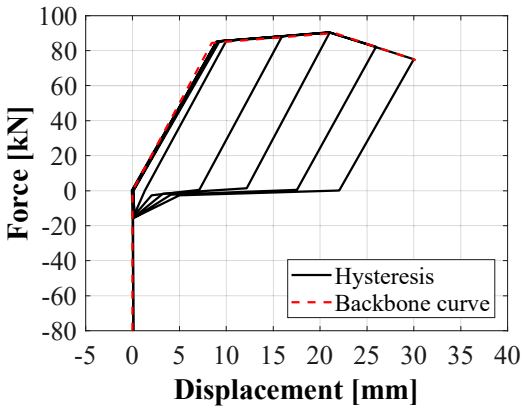
Angle bracket	F_u [kN]	v_u [mm]	F_{max} [kN]	v_{max} [mm]	F_y [kN]	v_y [mm]	K_{ser} [N/mm]
TTF200	57.24	23.85	70.04	15.42	57.69	6.45	8945
Hold-down	F_u [kN]	v_u [mm]	F_{max} [kN]	v_{max} [mm]	F_y [kN]	v_y [mm]	K_{ser} [N/mm]
WHT340	48.15	27.31	60.19	17.84	50.89	8.92	5,705
WHT440	62.72	36.81	78.14	25.46	61.33	9.28	6,609
WHT540	74.46	22.99	90.08	21.52	84.32	8.46	9,967
WHT620	85.86	27.39	107.32	19.28	84.51	6.38	13,247



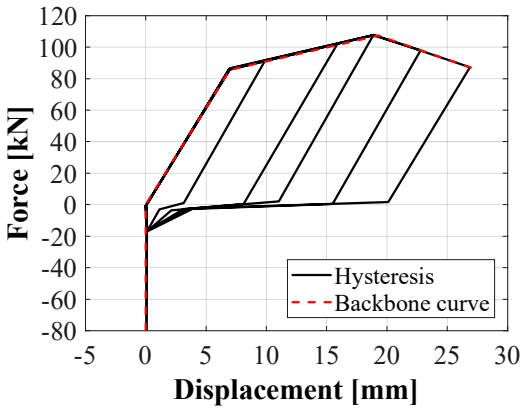
(a) Angle bracket type TTF200.



(b) Hold-down type WHT340.



(c) Hold-down type WHT540.



(d) Hold-down type WHT620.

Figure 4.4: Hysteretic response and backbone curve of metal connectors employed in the study.

4.2.4 CLT panel stiffness

The approximation of CLT panel stiffness proposed by Blass and Fellmoser [9] was employed. Therefore:

$$k_{panel} = \frac{3 \cdot E \cdot Ieff \cdot 0.8 \cdot G \cdot A_s}{3 \cdot E \cdot Ieff \cdot H + 0.8 \cdot G \cdot A_s \cdot H^3} \tag{4.3}$$

where E is the elastic modulus of timber parallel to grain; I_{eff} is the effective radius of gyration for a given cross section; G is the shear modulus of timber; A_s is the effective shear cross section; and H is the height of the wall panel.

The effective radius of gyration (I_{eff}) for a given cross section is determined in accordance with a method proposed by Blass and Fellmoser [9]. On the other hand, the effective bending and axial stiffness can be directly determined using the modulus of elasticity.

To this end, the bending stiffness perpendicular to the plane and parallel (perpendicular) to the grain of outer skins is:

$$(EI)_{ef} = E_0 \cdot \frac{b \cdot a_m^3}{12} \cdot k_{1(2)} \tag{4.4}$$

where b is the width of the solid wood panel when loading perpendicular to the plane.

Similarly, the bending stiffness in the tension and compression in plane and parallel (perpendicular) to the grain of outer skin is:

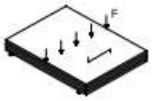
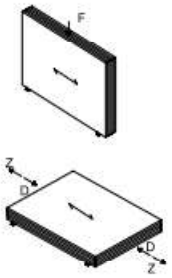
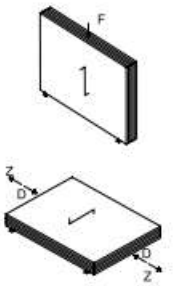
$$(EI)_{ef} = E_0 \cdot \frac{h^3 \cdot a_m}{12} \cdot k_{3(4)} \tag{4.5}$$

$$(EA)_{ef} = E_0 \cdot h \cdot a_m \cdot k_{3(4)} \tag{4.6}$$

Therefore, CLT panel stiffness for three different thickness values (i.e. 85 mm, 125 mm, and 142 mm) can be determined with reference to Table 4.5. To this end, the stiffness values for three different wall panel thickness are summarized in Table 4.2.

Table 4.2: CLT panel stiffness.

Panel thickness [mm]	Stiffness [N/mm]
85	46,277.90
125	62,169.12
142	69,534.13

	k_i
	$k_1 = 1 - \left(1 - \frac{E_{90}}{E_0}\right) \cdot \frac{a_{m-2}^3 - a_{m-4}^3 + \ldots \pm a_1^3}{a_m^3}$
	$k_2 = \frac{E_{90}}{E_0} + \left(1 - \frac{E_{90}}{E_0}\right) \cdot \frac{a_{m-2}^3 - a_{m-4}^3 + \ldots \pm a_1^3}{a_m^3}$
	$k_3 = 1 - \left(1 - \frac{E_{90}}{E_0}\right) \cdot \frac{a_{m-2} - a_{m-4} + \ldots \pm a_1}{a_m}$
	$k_4 = \frac{E_{90}}{E_0} + \left(1 - \frac{E_{90}}{E_0}\right) \cdot \frac{a_{m-2} - a_{m-4} + \ldots \pm a_1}{a_m}$

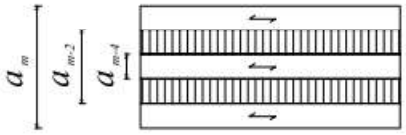


Figure 4.5: Composition factors k_i for solid wood panels with cross layers [9].

A sensitivity study was conducted to investigate the influence of the elastic and shear modulus of timber on the panel stiffness and on the corresponding fundamental period of the CLT buildings under consideration. To this end, a range of elastic and shear modulus values were employed. The result of the parametric study informed the determination of panel stiffness for numerical modelling of conventional multi-storey CLT buildings. Figure 4.6 presents the influence of CLT panel stiffness on structural periods associated with the first elastic mode of the structures. This figure shows that a panel stiffness of 10^8 N/mm (nearly rigid) for CLT corresponds to the closest estimation of fundamental period of the 7-storey SOFIE building (e.g. T = 0.46 s) considered as part of the experimental study in [33].

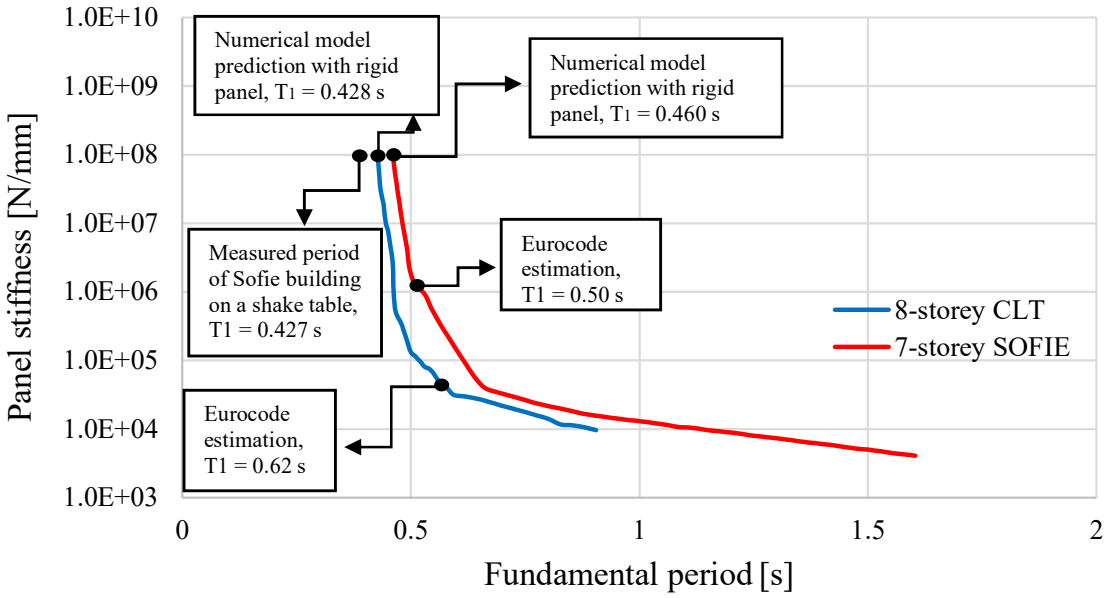


Figure 4.6: Comparison of panel stiffness values with fundamental period of buildings.

Despite the absence of a codified guidance on the estimation of panel stiffness of CLT, most of the research studies conducted to date, considered the panel stiffness of CLT as rigid in comparison with the connectors. The sensitivity study performed in this thesis also confirms that a nearly rigid panel stiffness value for CLT can be employed for practical purposes.

In addition, a full consideration of the influence of vertical and horizontal stiffness of CLT wall panels on the building models response was carried out. Based on two different criteria, the orthotropic material properties of wood are defined [31] as (i) the orthotropic properties of the wood strength class, (ii) the orthotropic properties calculated on the basis of the number, thickness, and grain direction of CLT layers.

To use an orthotropic material in Opensees [59], nine values need to be defined, such as three elastic moduli associated with perpendicular directions, (i.e. E_x, E_y, E_z), three Poisson's ratio (i.e. ν_{xy}, ν_{xz}, ν_{yz}), and three shear moduli (i.e. G_{xy}, G_{xz}, G_{yz}). Figure 4.7 depicts the principal axes defined to determine orthotropic material properties employed in the numerical models developed in this thesis.

$E_z = E_{0,eq}$ is the equivalent elastic modulus associated with the vertical direction to the outer

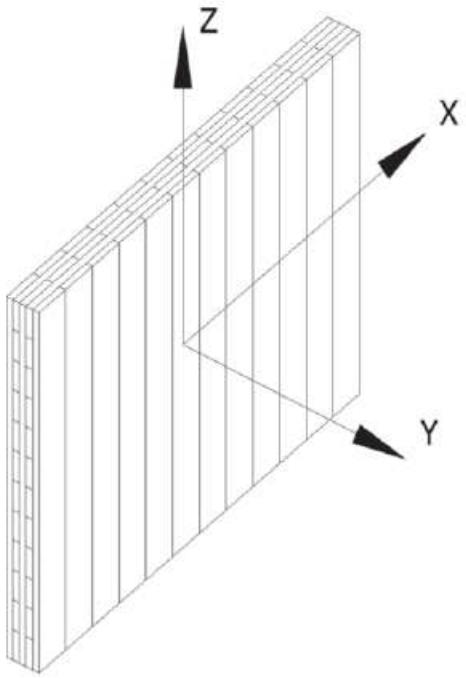


Figure 4.7: Principal axes definition of CLT wall panel [31].

layers. For 5-layer CLT wall panels, it can be estimated from Equation 4.7 as suggested in [9]:

$$E_{0,eq} = \left[1 - \left(1 - \frac{E_{90,T}}{E_{0,T}}\right)\left(\frac{a_3 - a_1}{a_5}\right)\right] \cdot E_{0,L} \tag{4.7}$$

where $E_{0,L}$ is the elastic modulus parallel to grain in the longitudinal direction; $E_{90,T}$ is the elastic modulus of transversal layers; a_1, a_3, a_5 are the layer thickness of the 1st, 3rd, and the 5th layers, respectively.

$E_x = E_{90,eq}$ is the equivalent elastic modulus in the perpendicular direction to the outer layers. It can be determined with the following equation:

$$E_{90,eq} = \left[\frac{E_{90,L}}{E_{0,T}} - \left(1 - \frac{E_{90,L}}{E_{0,T}}\right)\left(\frac{a_3 - a_1}{a_5}\right)\right] \cdot E_{0,L} \tag{4.8}$$

where $E_{0,T}$ is the elastic modulus parallel to grain of transversal layers; and $E_{90,L}$ is the elastic moduli perpendicular to the grain of longitudinal layers.

The equivalent elastic modulus to be employed as E_y, can be calculated with the following

expression:

$$E_y = t_{tot} \cdot \left(\sum_{i=1,3,5...n} t_i/E_{90,L,i} + \sum_{j=2,4,6...n-1} t_j/E_{90,T,j} \right)^{-1} \tag{4.9}$$

where t_{tot} is the total thickness of the wall panel; t_i and t_j are the layer thickness associated with transversal and longitudinal directions; n is the number of layers.

Finally, Equation 4.10 represents the shear moduli, G, of CLT wall panels as:

$$G = t_{tot} \cdot \left(\sum_{i=1,3,5...n} t_i/G_{L,i} + \sum_{j=2,4,6...n-1} t_j/G_{T,j} \right)^{-1} \tag{4.10}$$

where G_T and G_L are the shear moduli associated with transversal and longitudinal layer directions, respectively.

The orthotropic material properties of CLT wall panels to be employed in numerical models were determined using above expressions together with given elastic and shear moduli of CLT panels and presented in Table 4.3.

Table 4.3: Orthotropic material properties.

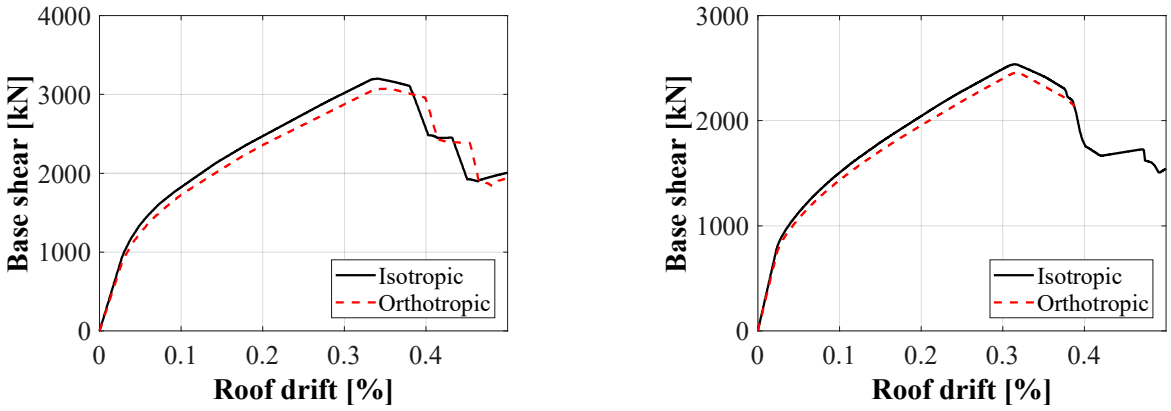
E_x	E_y	E_z	G_{xy}	G_{xz}	G_{yz}	ν_{xy}	ν_{xz}	ν_{yz}
4594	370	6776	690	690	690	0.42	0.42	0.42

A comparative study was conducted to assess the effects of the material modelling approach in the dynamic response of CLT building numerical models. To this end, the results of Eigen-value analysis using an Elastic-Isotropic material model with rigid panel stiffness and an Elastic-Orthotropic material model employing the orthotropic material properties of CLT wall panels calculated as described above. Table 4.4 shows the first 5 fundamental vibration periods of the multi-storey CLT A1 building have been compared.

It can be seen from Table 4.4 that no significant difference is expected between the two material modelling approaches. Furthermore, non-linear static analyses of the 8-storey B2 and 20-storey E2 CLT buildings adopting the two material modelling alternatives were also performed and compared in Figure 4.8. A good level of approximation between two modelling approaches is evident from Figure 4.8. Therefore, both modelling approaches for CLT panel stiffness are expected to provide similar results and the rigid panel approximation is deemed preferable on practical grounds.

Table 4.4: Comparison of 2 material modelling approach of CLT wall panels in A1 building.

Modal period	Isotropic model	Orthotropic model	Error [%]
T_1	0.363 s	0.366 s	0.82
T_2	0.258 s	0.261 s	1.15
T_3	0.152 s	0.154 s	1.29
T_4	0.047 s	0.049 s	4.08
T_5	0.045 s	0.045 s	0.00



(a) 8-storey CLT.

(b) 20-storey CLT.

Figure 4.8: Comparison of the results of non-linear static analyses using two different CLT material models.

4.3 Numerical validation

In order to gain confidence on the numerical modelling approach described above, extensive validation studies were performed focusing on connection hysteretic response calibration, seismic response of single and coupled CLT wall panels, and by comparing the response of the models with that of a multi-storey CLT building tested under seismic actions.

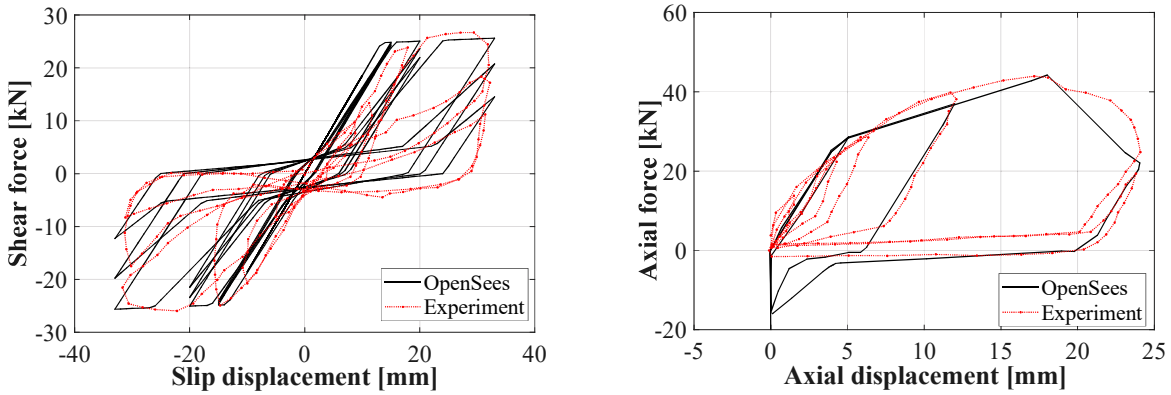
4.3.1 Connection hysteresis calibration

The first series of validation studies was concerned with the hysteretic response of structural connections. Figure 4.9 presents the test results of an angle bracket type BMF 90x116x48x3 mm with 11 annular ringed nails 4x60 mm, and a hold-down connector type WHT540 with

12 annular ringed nails 4x60 mm as obtained from Gavric et al. [36]. Table 4.5 presents the mechanical properties of the structural connectors in shear and tension. A reversed cyclic loading protocol was employed and the numerical predictions are also presented in Figure 4.9. It is evident from this figure that the adopted hysteretic numerical model is able to reproduce all main aspects of the hysteretic response of CLT metal connectors.

Table 4.5: Calibration of mean values obtained from experimental results on CLT connections.

Parameter description	Angle bracket in shear	Angle bracket in tension	Hold-down in tension	Hold-down in shear
Elastic stiffness k_{el} [kN/mm]	1.78	2.76	4.82	0.99
1st inelastic stiffness k_{pl} [kN/mm]	0.22	0.41	0.69	0.12
Yield force F_y [kN]	23.77	19.23	40.3	9.79
Maximum force F_{max} [kN]	27.71	23.51	48.33	13.88



(a) Angle bracket in shear.

(b) Hold-down in tension.

Figure 4.9: Comparison of numerical and experimental hysteresis [38, 39] of metal connectors.

4.3.2 Cyclic behaviour of a single CLT wall

The cyclic response of a single panel CLT shear-wall tested by Gavric et al. [36] is presented in Figure 4.11. Four angle (shear) brackets and two tie-down (uplift) connectors at both ends of the wall panel were employed to connect the wall panel to the foundation. BMF 90x48x3x116

mm angle brackets with 11 ϕ4x60 mm nails and ϕ12 bolts as well as HTT22 hold-downs with 12 ϕ4x60 nails and ϕ16 bolts were connected to the foundation. The CLT wall panel was formed by five 17-mm thick planks with a total thickness of 85 mm and dimensions of 2.95x2.95 m in hight and length, respectively. A reverse cyclic loading protocol was employed as described in EN12512 [30]. Besides, the panel was subjected to an additional vertical load of 18.5 kN/m at its top. All connection elements were calibrated using the experimental outcomes reported in Gavric et al. [37]. Figure 4.10 depicts a schematic of the single CLT wall panel, Specimen 1.2 from [36], whereas Figure 4.11 presents the hysteretic response of the wall panel and cumulative dissipated energy during loading and reloading. The very good agreement between numerical and experimental curves in Figure 4.11 confirms the ability of the numerical models developed in this thesis to provide accurate prediction of the response of single CLT panels subjected to in-plane cyclic loading.

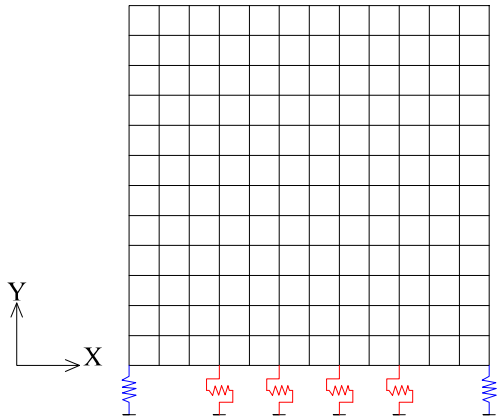
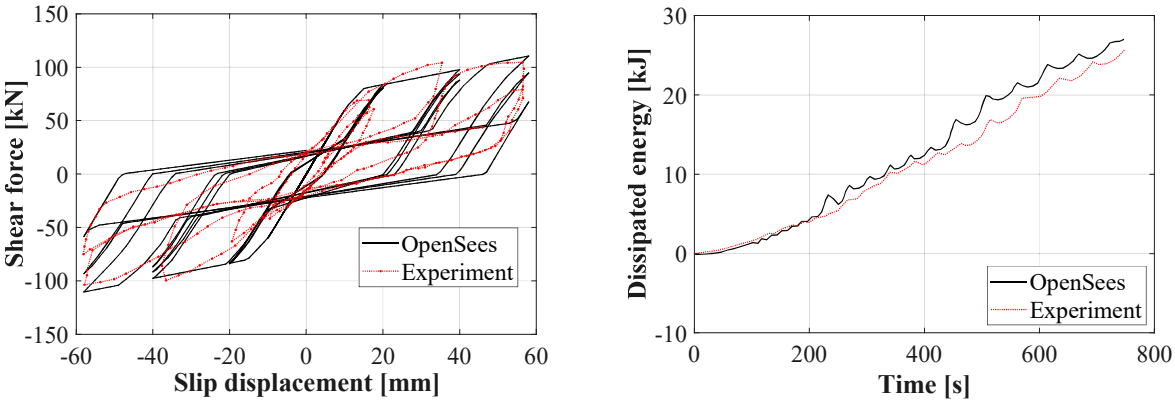


Figure 4.10: Schematic of single CLT wall panel, Specimen 1.2 [36].

4.3.3 Cyclic behaviour of a coupled CLT wall

The cyclic behaviour of a coupled wall panel with a half-lap joint connection using self-threaded screws of type HBS ϕ8x80 mm was analysed following the modelling approach employed for tall buildings described in the previous sections. Vertical connections were provided using 2 diagonal spring elements. The numerical model of coupled wall concept is depicted in Figure 4.12. A reverse cyclic non-linear push-over analysis was performed in OpenSees [59] and the experimental outcomes from Gavric et al. [36] were compared to the resulting numerical simulations. Figure 4.13 shows a relatively good approximation of the experimental response of the coupled CLT wall specimen and its numerical prediction.



(a) Hysteretic response of a single CLT wall panel, Specimen 1.2 [36].

(b) Cumulative energy dissipation of a single CLT wall panel, Specimen 1.2 [36].

Figure 4.11: Experimental and numerical response comparison of a single panel CLT wall, (Specimen 1.2 from [36]).

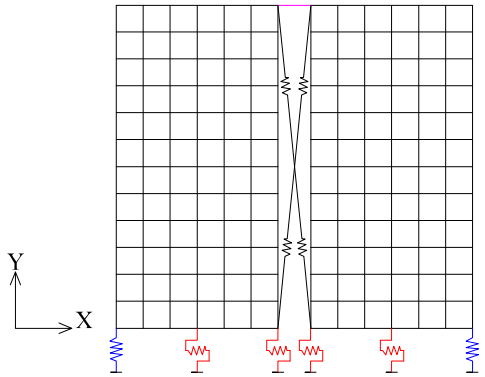
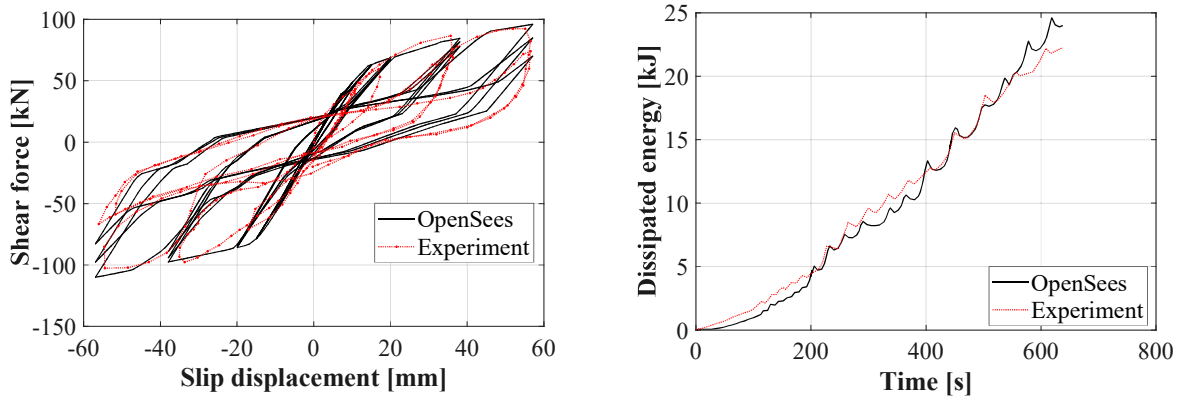


Figure 4.12: Schematic of a coupled CLT wall panel, Specimen 1.2 [36].

4.3.4 Response of 7-storey SOFIE building

As described in Chapter 2, SOFIE (Construction System Fiemme) was an experimental research effort ending in the full-scale test of a multi-storey CLT building conducted by the Italian National Research Council, Trees and Timber Institute and supported by the Trento Province. A full-scale 7-storey CLT building was subjected to a series of ground-motion records, on a shaking table at the (NIED) E-Defence laboratory in the Japanese National Research Institute for Earth Science and Disaster Prevention. In particular, and due to availability of data, the building response to the Kobe JMA 1995 earthquake record is studied in the following section.



(a) Hysteresic response of a coupled CLT wall panel, Specimen 2.1 [36].

(b) Cumulative energy dissipation of a coupled CLT wall panel, Specimen 2.1 [36].

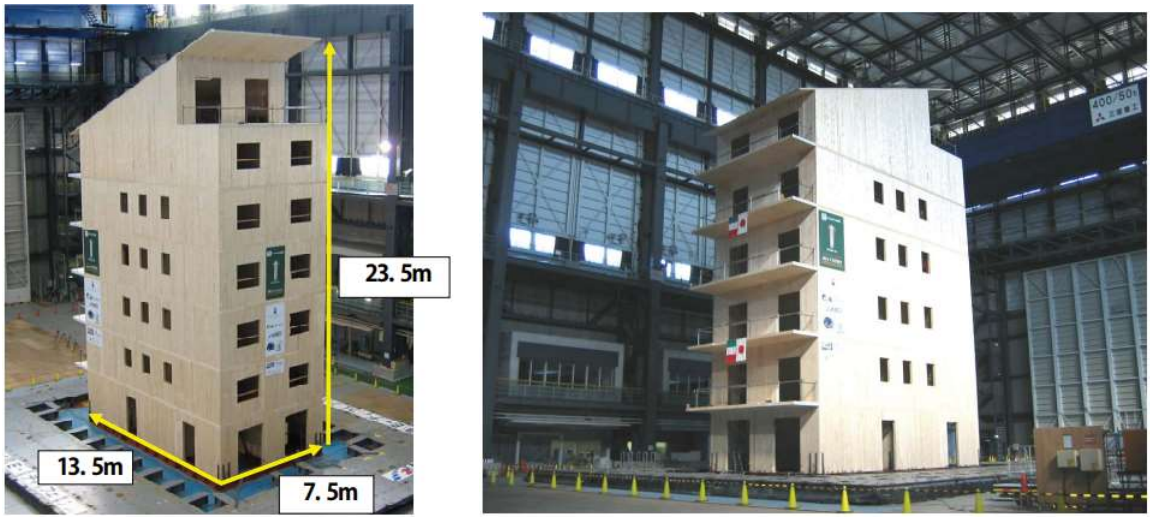
Figure 4.13: Experimental and numerical response comparison of a coupled CLT wall panel, Specimen 2.1 [36].

Structural details

Figure 4.14 shows the North-East and South-West views of the 7-storey CLT building [25] under consideration. As indicated in Figure 4.14, the 7-storey building constructed for the full-scale shaking table experiment has plan dimensions of 7.5 m by 13.5 m and a total height of 23.5 m. The position, dimension, type and number of structural joinery elements between two adjacent wall panels, and between wall panels and floor slabs were determined following capacity design principles. HTT22 tie-down connectors with maximum 32 nails and BMF 90x48x3x116 shear brackets with maximum 18 nails were used to connect the CLT panels. 5-layered CLT panels with varying thickness were employed. As the lateral seismic forces decrease along the building height, the CLT wall panel thickness is also reduced in upper storeys [25]. Figure 4.15 indicates (with colour notation) the placement of structural joinery elements at each floor level of the building.

Numerical analyses

To investigate the seismic behaviour of the 7-storey SOFIE building, a numerical model was constructed in OpenSees [59] following the modelling approach described previously in Section 4.2. A modal analysis and a non-linear response history analysis using the Kobe Japan JMA earthquake record were performed and the numerical outcomes were compared to their corresponding experimental results as reported in [75]. Following the previously described modelling strategy, 4-node quad elements were used to simulate CLT panels incorporating a very high stiffness value hence assuming wall panels behave rigidly, and Zero-length and 2-



(a) North-East. (b) South-West.

Figure 4.14: North-East and South-West views of the 7-storey SOFIE building [25].

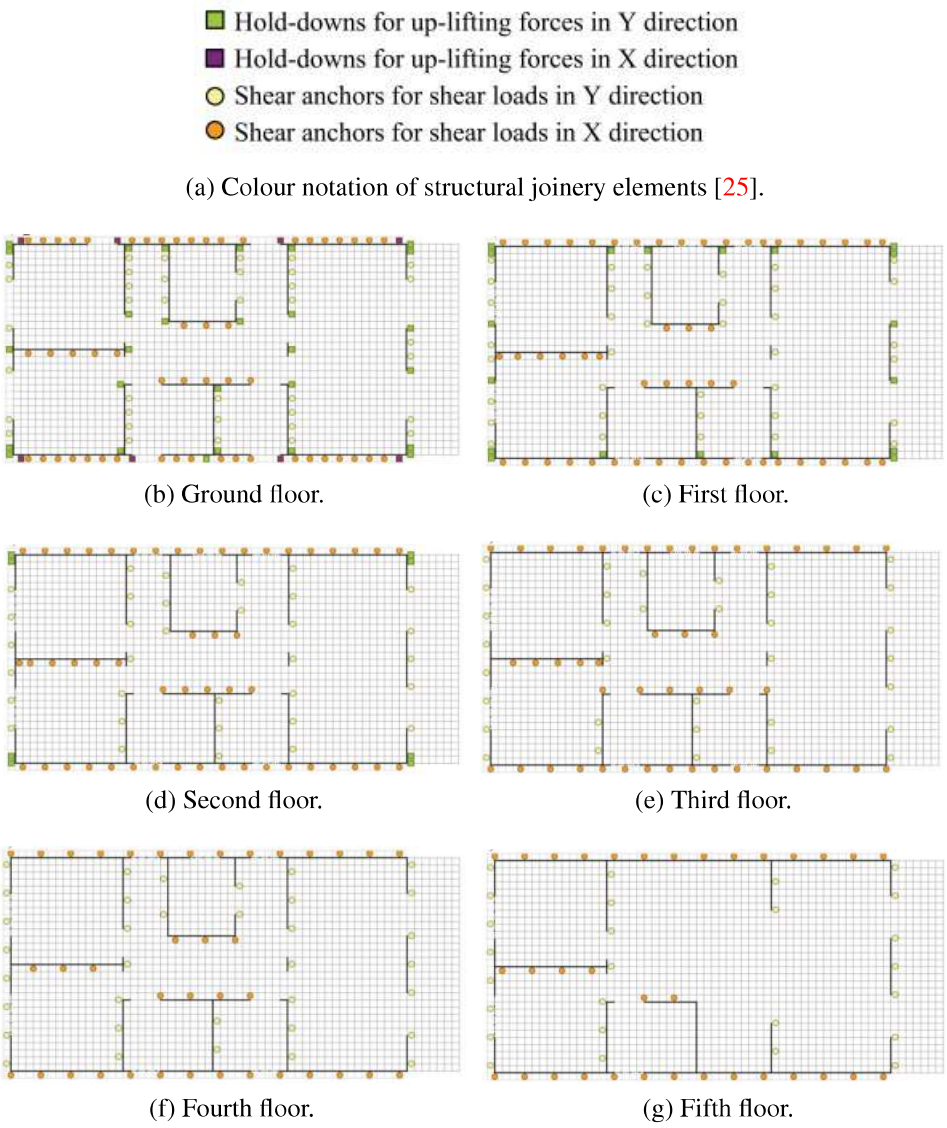
node link spring elements were used to simulate structural connections with 3-linear hysteretic material properties.

Table 4.6 shows the measured structural period corresponding to the first and second elastic modes of the 7-storey CLT building. The numerical outcomes are also presented in Table 4.6. A good agreement was obtained between the measurements and the OpenSees [59] numerical model. Furthermore, the fundamental period of the 7-storey CLT building was also obtained using the k_{panel} stiffness equation proposed in [9] and a period of 0.73 s was observed. Since this value does not correspond to the field measurement, it is concluded that using a rigid body stiffness approximation is also a good modelling assumption.

Table 4.6: Experimental [75] and numerical comparison of fundamental period of 7-storey SOFIE building.

Structural period	Shake table measurement	OpenSees simulation	Error [%]
T_1	0.427	0.463	8.43
T_2	0.301	0.313	3.98

In addition, results of shake table dynamic tests on the 7-storey building reported in [76] were also used for numerical validations. A typical comparison between the measured displacement and acceleration response histories and the finite element estimations can be seen in Figure 4.17. The displacement histories of the first and top floor levels of the building are presented in



(a) Colour notation of structural joinery elements [25].

(b) Ground floor.

(c) First floor.

(d) Second floor.

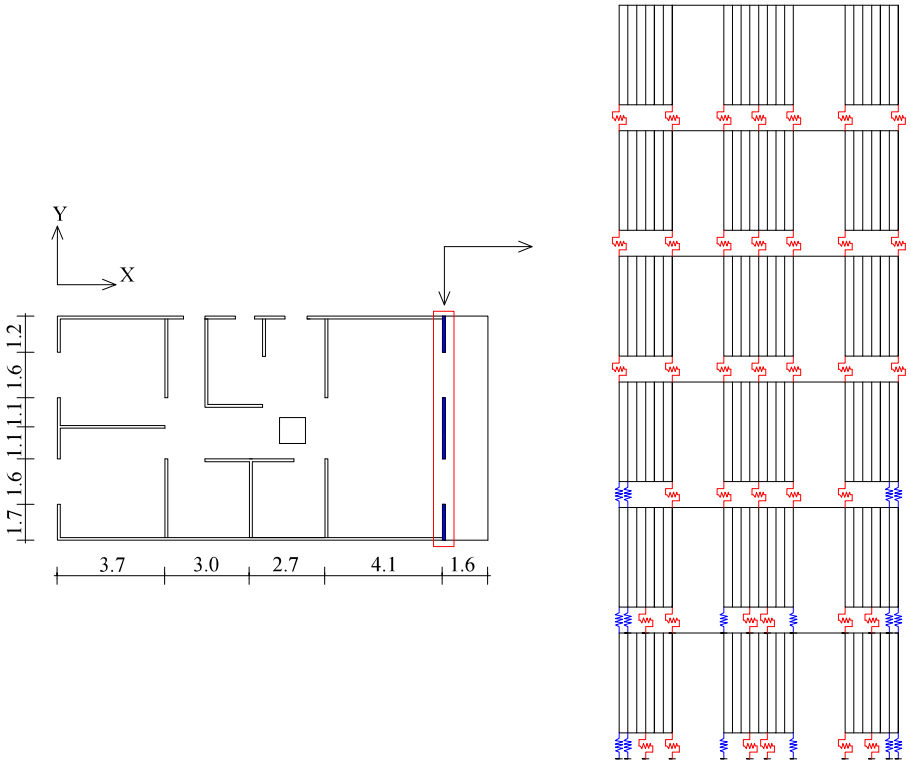
(e) Third floor.

(f) Fourth floor.

(g) Fifth floor.

Figure 4.15: Placement of structural joinery elements at each floor level [25].

Figure 4.17, while the acceleration response history plotted corresponds to the top floor level. While 3D excitations had been applied to the 7-storey full-scale building on a shake table, only Y-direction [76] was considered for numerical modelling purposes as depicted in Figure 4.16. However, a good representation of the lateral response of the building is evident in Figure 4.17. It is also important to note that despite the simplifications, a good match in the evolution of cumulative energy dissipation with a maximum difference of 7% was obtained.



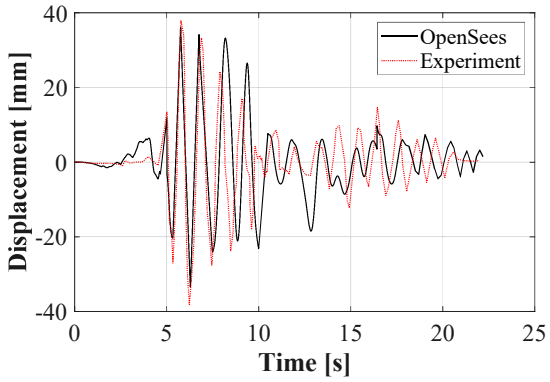
(a) Typical floor plan. (b) Building elevation.

Figure 4.16: Plan view and the elevation of SOFIE building.

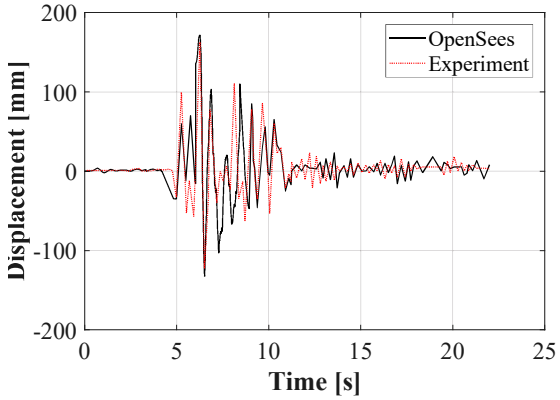
4.4 Non-linear response history analyses and parameters investigated

Extensive non-linear response history analyses were performed using the high performance research computing facility at Imperial College London. An array function PBS -J 1-1656 was employed to run with a total of 1656 ground-motion input files for a single model in parallel.

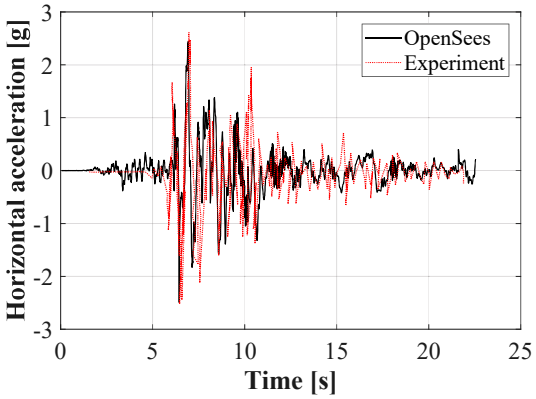
The catalogue of earthquakes employed in the study is summarized in Table 4.7. A total of 1656 real ground-motion records from 51 seismic events with moment magnitude varying between 5.1 and 7.9 with an average acceleration (PGA) of 1 g were employed. The PEER-NGA database was used to procure the acceleration records which involve different site classes and fault types. Detailed information on the selected ground-motion records can be found in [41].



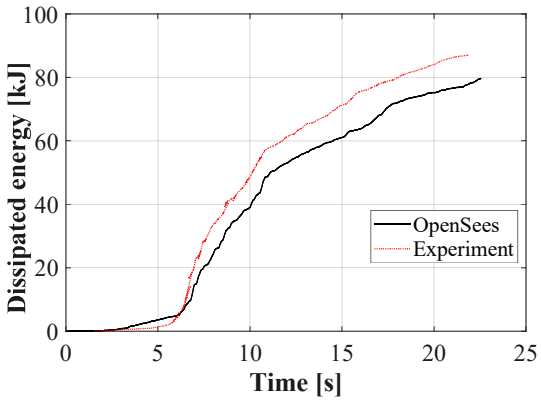
(a) Displacement response histories at the first level.



(b) Displacement response histories at the top level.



(c) Acceleration response histories at the top level.



(d) Evolution of cumulative energy dissipation.

Figure 4.17: Experimental [76] and numerical response comparison of 7-storey SOFIE building.

4.4.1 Ground-motion characteristics

Frequency content index

The ground-motion mean period (T_m) was selected as the frequency content indicator. The mean period was initially proposed by Rathje et al. [73, 74]. It is determined as the weighted mean of the periods of the Fourier Spectrum over a pre-defined frequency range and can be calculated as:

$$T_m = \frac{\Sigma_i C_i^2 \cdot \frac{1}{f_i}}{\Sigma_i C_i^2} \quad \text{for} \quad 0.25\ \text{Hz} \leq f_i \leq 20\ \text{Hz} \quad \text{with} \quad \Delta f \leq 0.05\ \text{Hz} \tag{4.11}$$

where C_i is the Fourier amplitude corresponding to the i^{th} frequency, f_i; and Δf is the spacing

between frequencies. The distribution of mean periods employed in the study can be seen in Figure 4.18.

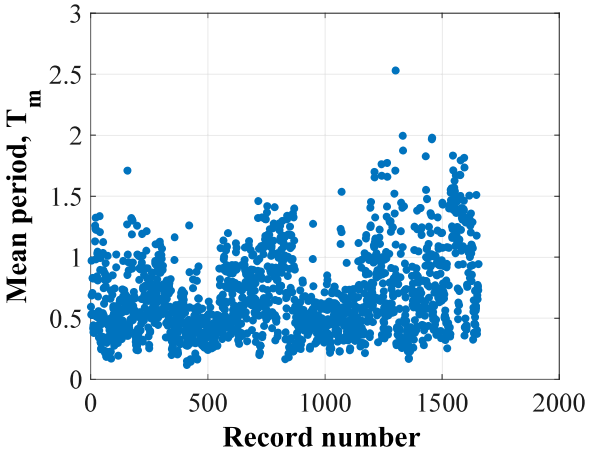


Figure 4.18: Distribution of mean periods (T_m) employed in the study.

4.4.2 Structural parameters

In order to investigate the influence of salient structural characteristics on the seismic response of multi-storey CLT buildings, numerous parameters are considered. They are summarised in this section.

Fundamental period

An Eigen Value analysis was performed for each building configuration to estimate the structural periods associated with the first natural mode of vibration T_1. Figure 4.19a shows the distribution of fundamental periods of all building configurations studied herein. The fundamental periods for the multi-storey CLT buildings under study range from 0.3 s to 1.0 s.

Building aspect ratio

The building aspect ratio, λ, also called slenderness, is calculated as the ratio between the height and the width of the building facade (H/B). Figure 4.19b depicts the distribution of building aspect ratios for all building configurations studied. The slenderness of the buildings analysed range from 2.56 to 8.33.

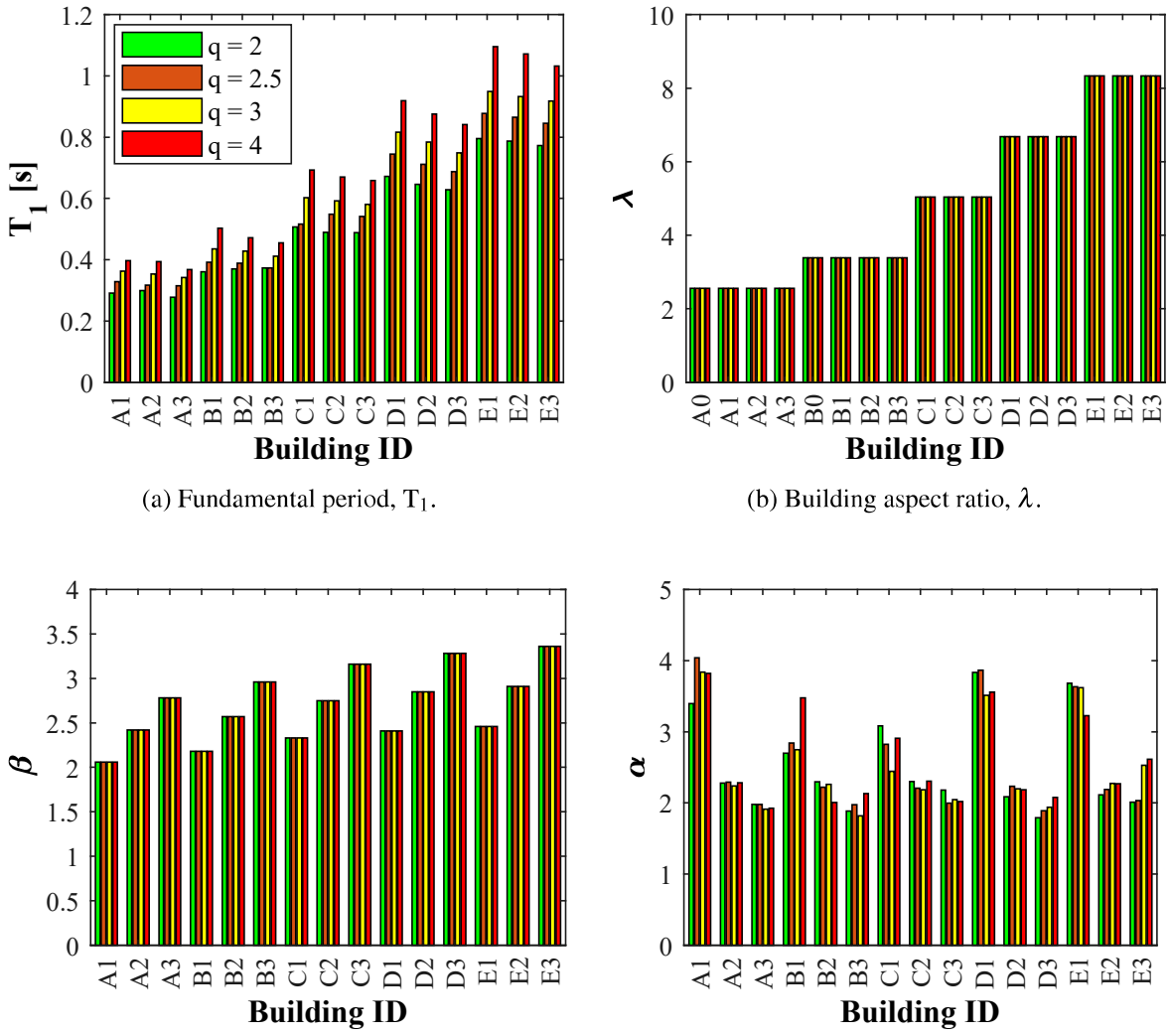
Joint density parameter

The joint density parameter, β, is determined as the ratio between all fastening lines in the wall (P_0) and the perimeter of the wall (P). This parameter was initially defined in [71] to quantify

the degree of panel fragmentation in CLT buildings. The distribution of joint density parameter of the buildings ranges between 2.06 and 3.36 and is presented in Figure 4.19c.

Plasticity resistance ratio

Plasticity resistance ratio, α is calculated as the ratio between the ultimate base shear, V_u, when a plastic mechanism is developed in the structure, and the yield base shear, V_1. The distribution of the plasticity resistance ratio within the database of buildings considered is shown in Figure 4.19d and ranges from α = 1.8 to α = 3.8.



(a) Fundamental period, T_1.

(b) Building aspect ratio, λ.

(c) Joint density parameter, β.

(d) Plasticity resistance ratio, α.

Figure 4.19: Distribution of key structural parameters.

It is important to understand the correlation among the structural characteristics of the building

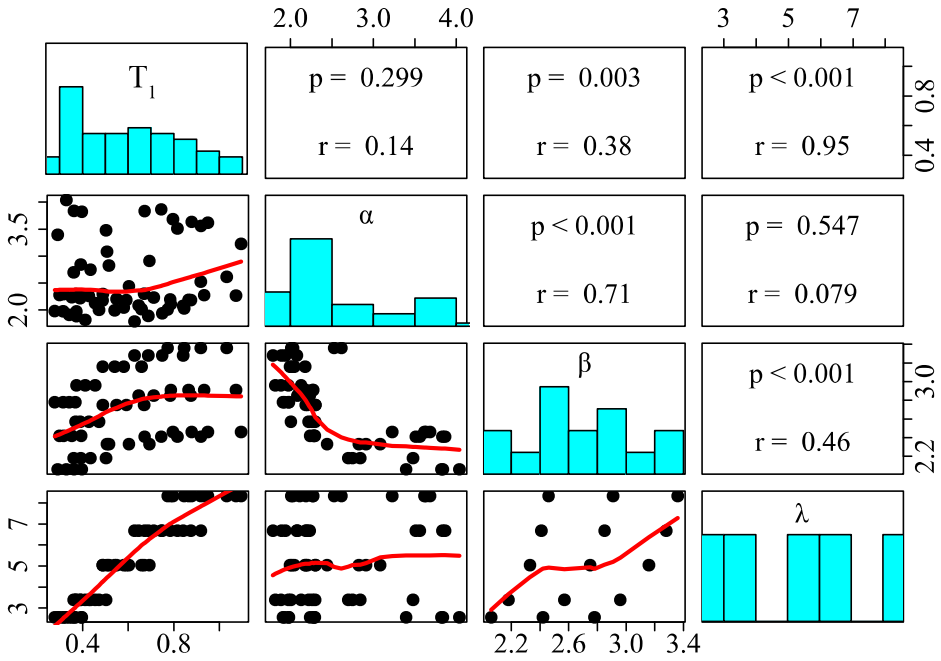


Figure 4.20: Scatterplot matrix of the key structural characteristics.

dataset created. For this purpose, Figure 4.20 presents a scatter plot matrix of the fundamental period (T_1), the plasticity resistance ratio (α), the joint density parameter (β), and the building aspect ratio (λ). The lower panels in this figure show the distribution of the key structural parameters shown in the diagonal with a trend line obtained by means of a locally weighted regression. The associated histograms are presented in the diagonal boxes while the upper panels present the p-values and correlation coefficients for each trendline identified. The scatter plot presented in Figure 4.20 informed the development of the predictive models presented later in this thesis.

4.5 Concluding remarks

This chapter has presented a detail description of the numerical modelling strategy adopted to construct finite element models of multi-storey CLT buildings in the research oriented FE framework OpenSees [59]. These models are validated in the light of available experimental data, and a good level of approximation was observed by means of comparative studies. The key structural and ground-motion parameters of interest considered in the numerical study were described. Having gained confidence in the numerical model performance, the next chapter will employ the building database to perform extensive non-linear static and dynamic analyses, and analyse their response in terms of deformation, force and acceleration demands.

Table 4.7: Ground motion catalogue employed for non-linear response history analysis of buildings.

EQ No	EQ Name	Year	Moment magnitude (Mw)	Number of records
1	Imperial Valley-02	1940	6.95	2
2	Kern County	1952	7.36	4
3	Parkfield	1966	6.19	11
4	Borrego Mtn	1968	6.63	8
5	San Fernando	1971	6.61	54
6	Managua, Nicaragua-01	1972	6.24	2
7	Friuli, Italy-01	1976	6.5	8
8	Gazli, USSR	1976	6.8	2
9	Friuli, Italy-02	1976	5.91	4
10	Santa Barbara	1978	5.92	4
11	Tabas, Iran	1978	7.35	14
12	Coyote Lake	1979	5.74	18
13	Imperial Valley-06	1979	6.53	68
14	Mammoth Lakes-01	1980	6.06	4
15	Victoria, Mexico	1980	6.33	9
16	Irpina, Italy-01	1980	6.9	20
17	Irpina, Italy-02	1980	6.2	14
18	Corinth, Greece	1981	6.6	2
19	Westmorland	1981	5.9	8
20	Coalinga-01	1983	6.36	86
21	Borah Peak, ID-01	1983	6.88	12
22	Morgan Hill	1984	6.19	49
23	Lazio-Abruzzo, Italy	1984	5.8	2
24	Nahanni, Canada	1985	6.76	6
25	N. Palm Springs	1986	6.06	22
26	Chalfant Valley-01	1986	5.77	8
27	Chalfant Valley-02	1986	6.19	16
28	San Salvador	1986	5.8	4
29	Whittier Narrows-01	1987	5.99	81
30	Superstition Hills-01	1987	6.22	2
31	Superstition Hills-02	1987	6.54	22
32	Loma Prieta	1989	6.93	163
33	Erzincan, Turkey	1992	6.69	2
34	Cape Mendocino	1992	7.01	10
35	Landers	1992	7.28	130
36	Northridge-01	1994	6.69	296
37	Kobe, Japan	1995	6.9	44
38	Kozani, Greece-01	1995	6.4	2
39	Dinar, Turkey	1995	6.4	8
40	Gulf of Aqaba	1995	7.2	4
41	Kocaeli, Turkey	1999	7.51	55
42	Duzce, Turkey	1999	7.14	44
43	Sitka, Alaska	1972	7.68	4
44	Caldiran, Turkey	1976	7.21	2
45	St Elias, Alaska	1979	7.54	4
46	Manjil, Iran	1990	7.37	15
47	Sierra, Madre	1991	5.61	4
48	Little Skull Mtn, NV	1994	5.65	16
49	Hector Mine	1999	7.13	167
50	Nenana Mountain, Alaska	2002	6.7	72
51	Denali, Alaska	2002	7.9	48
Sum				**1656**

Chapter 5

Assessment of Seismic Drift Demands

5.1 Introduction

The literature survey presented in Chapter 2 has shown that, there is a lack of consensus on the influence of key structural parameters and ground-motion frequency content in drift demands of multi-storey CLT buildings and that the ground-motion frequency content is often neglected in research studies of CLT buildings. Therefore, this chapter aims to provide a detailed assessment on the influence of key structural parameters on seismic drift demands in multi-storey CLT buildings. To this end, global and maximum inter-storey drifts and a number of structural parameters are taken into account. These structural parameters correspond to the building aspect ratio λ, the fundamental period T_1, the joint density (panel fragmentation) β, and the response modification factor q whose meaning has been specified in Chapter 4.

A total of 60 prototype CLT building configurations described in Chapter 4 are employed to study the influence of above-mentioned parameters and frequency content of ground-motion by means of extensive non-linear response history analyses. The mean period of the ground motion, (T_m) is adopted as a frequency content measure.

This chapter is divided into 6 sections. The first section provides a description of the adopted procedure to perform extensive non-linear response history analyses on the building models described before and presents the key structural parameters investigated. The second section offers a detailed parametric assessment carried out to investigate the influence of parameters on the inelastic deformation demands. Predictive models developed by means of non-linear regression analyses are presented in the third section. Even though it is difficult to fully compare the findings of this research with the previous research studies, a restrictive yet illustrative comparative study is outlined in the fourth section. Finally, concluding remarks are highlighted in the last section of this chapter.

5.2 Assessment of seismic drift demands

5.2.1 Assessment procedure

A total of 99360 non-linear response history analyses were performed on the high-performance research computing service at Imperial College London by means of an array mode of input data. The results were then post-processed to obtain maximum roof displacement (Δ_{max}), and maximum storey drifts (θ_{max}) for each analysis. These values were finally used to calculate the global and maximum drift modification factors. The two quantities of interests are:

- Global drift modification factor (δ_{mod}) is the ratio between maximum inelastic roof displacement (Δ_{max}) as obtained from the non-linear response history analysis and the product of roof yield displacement ($\Delta_{1,roof}$) times the corresponding behaviour factor (q) employed for the design of a structure. A non-linear static analysis with monotonically increasing lateral loads adopting a first mode distribution along the building's height was performed to obtain the roof yield displacement. δ_{mod} can be expressed as:

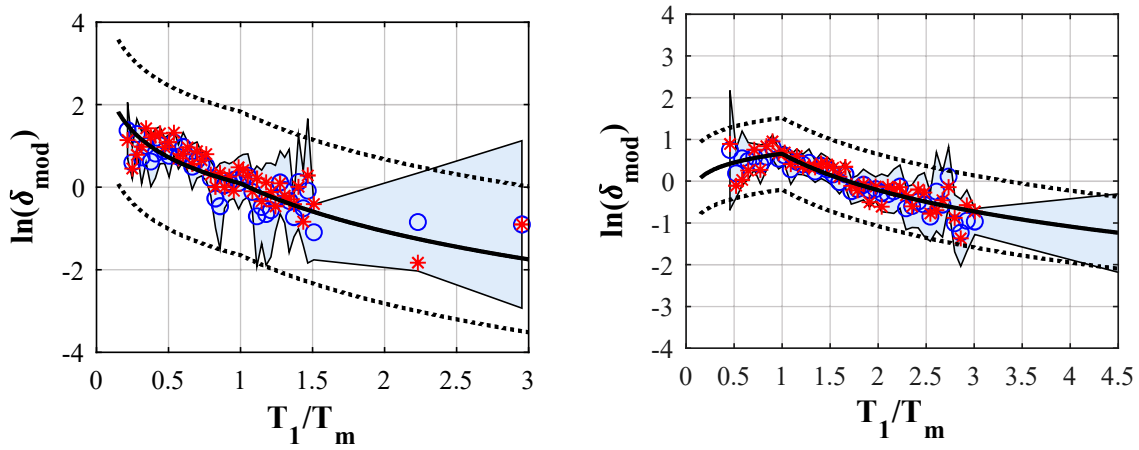
$$\delta_{mod} = \frac{\Delta_{max}}{q \cdot \Delta_{1,roof}} \tag{5.1}$$

- Maximum drift modification factor (θ_{mod}) is the ratio between the maximum inter-storey drift along the height of a building (θ_{max}) obtained from non-linear response history analysis and the maximum inter-storey drift at first yield ($\theta_{1,max}$) obtained from non-linear static analyses. θ_{mod} can be determined from:

$$\theta_{mod} = \frac{\theta_{max}}{q \cdot \theta_{1,max}} \tag{5.2}$$

5.2.2 Global drift demands

The variation in δ_{mod} for 8-storey (B1) and 20-storey (E3) buildings as a function of the period ratio (T_1/T_m) for a design behaviour factor of q = 3 are presented in Figure 5.1. The period ratio (T_1/T_m) is defined as the ratio between the structural period which is associated with the first elastic mode of the structure and the mean period of the ground-motion adopted as the frequency content indicator described before. The (o) open and (*) symbols in Figure 5.1 denote the mean and median values within each data bin, respectively. The shaded regions indicate the 95% confidence interval in the estimate of the mean logarithmic drift modification factor. Finally, the dashed lines show the ± one standard deviation of the mean logarithmic global drift modification factor for the best-fit model represented by the solid line.



(a) 8 storey B1 building (n = 8, m = 1).

(b) 20 storey E3 building (n = 20, m = 3).

Figure 5.1: Mean logarithmic global drift modification factor ($\ln(\delta_{mod})$), against period ratio (T_1/T_m) for a response modification factor of q = 3.

A non-linear relationship is observed in Figure 5.1 between structural deformations and frequency content of the ground-motion along the full range of period ratios in both building configurations. Most design codes assume that drift estimations, particularly in long period structures are linear, based on the results of generalized SDoF systems [78, 53], therefore these non-linear scaling is important. The analysis of drift estimations presented in Figure 5.1 can be divided into two ranges, namely short (ie. $T_1/T_m < 1$) and long (ie. $T_1/T_m > 1$) period ratios. Figure 5.1a shows that higher global drift modification factors (δ_{mod}) are expected with lower period ratios for the 8-storey B1 building in the short period range (ie. $T_1/T_m < 1$). Previous studies on SDoF systems with and without pinching [78, 53] have also identified this trend. The scaling of global drift modification factor (δ_{mod}) shown in Figure 5.1a can be explained by the period elongation whereby the secant structural period approaches to the mean period (T_m) of the ground-motion leading to higher drift demands in this range. On the other hand, for the long period range (ie. $T_1/T_m > 1$) lower level of drift estimations are expected due to increasing difference between the structural period associated with the first elastic mode of the structure and the mean period of the ground-motion.

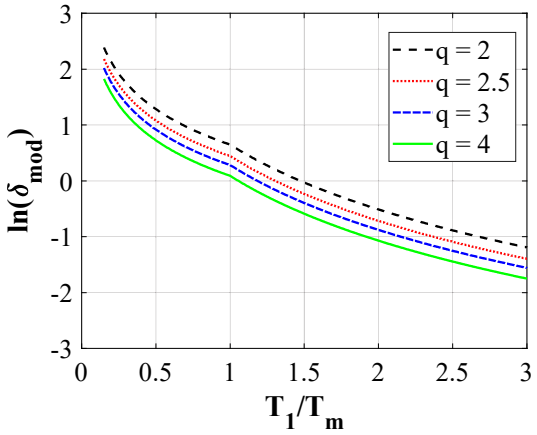
A different correlation between the global drift modification factor and period ratio can be seen in Figure 5.1b for the 20-storey E3 building configuration. Contrary to the 8-storey building, the global drift modification factor (δ_{mod}) increases with increasing period ratios (T_1/T_m) in the short period range in this figure. Furthermore, the highest δ_{mod} is observed when the structural period is equal to mean period of the ground-motion. This can be attributed to the distinctive resonant response expected in taller CLT buildings due to lower level of inelastic deformation demands compared to shorter buildings where earthquake is the governing design considera-

tion. The corresponding variation for other building heights can be seen in Appendix D.

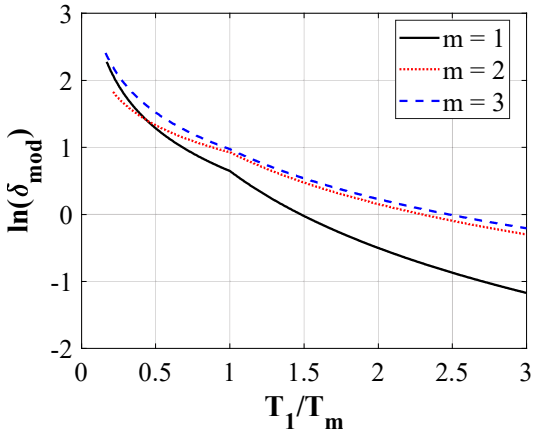
The influence of key structural parameters such as design response modification factor (q), building height (n), and the level of panel fragmentation (m) on the inelastic deformation demands in multi-storey CLT buildings was also investigated. Figure 5.2a presents the relationship between global drift modification factor (δ_{mod}) and the period ratio (T_1/T_m) in the 8-storey B1 building configuration with the lowest level of panel fragmentation (i.e. m = 1) for the range of response modification factors q = {2, 2.5, 3, 4} considered in this study. It can be appreciated from this figure that non-linear scaling of global drift demands (δ_{mod}) is a function of the expected level of inelastic response indicated herein by the behaviour factor, q. In other words, the higher the value of response modification factor, the lower the corresponding value of global drift demands (δ_{mod}), and the higher the energy dissipation capacity of the structure.

The variation in global drift modification factor (δ_{mod}) and period ratio (T_1/T_m) for various levels of panel fragmentation (β) is shown in Figure 5.2b. It is clear from Figure 5.2b that the increase in the number of panels per wall results in larger global drift modification factor. This suggests that, at least initially, panel modularization in CLT structures leads to higher drift demands. This can be attributed to the additional multiple rocking segments in modularized configurations associated with a more flexible response. Furthermore, the influence of increasing the number of vertical joint lines from m = 1 to m = 2 shows higher drift increments for period ratios longer than 0.5 (i.e. $T_1/T_m > 0.5$) compared to increasing the number of intermediate joint lines from m = 2 to m = 3. Therefore, the corresponding loss in stiffness in comparison with the benefits of enhanced energy dissipation capacity as a result of higher level of panel fragmentation is important for individual panel lengths of 2.85 m or less.

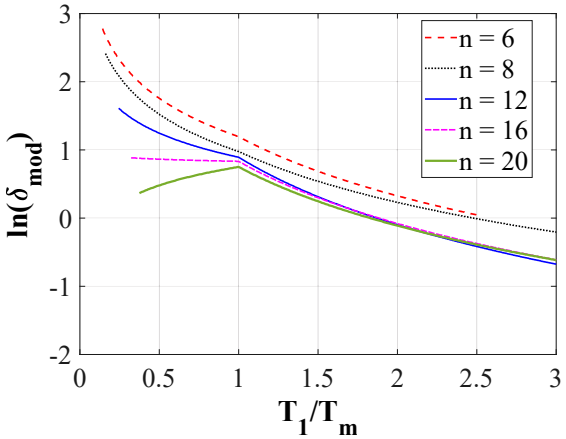
Similarly, the correlation between the global drift modification factor (δ_{mod}) and the period ratio (T_1/T_m) for various building heights (n) is presented in Figure 5.2c. This figure shows a comparison of evolution of drift demands in multi-storey CLT buildings of different heights, all designed for a response modification factor of q = 3 while keeping the level of panel fragmentation the same (i.e. m = 1). It is clear from Figure 5.2c that the global drift modification factor (δ_{mod}) decreases non-linearly irrespective of the building height while the period ratio (T_1/T_m) increases in the long period range ($T_1/T_m > 1$). In addition, it can be appreciated from this figure that a higher global drift modification factor is expected in shorter buildings (i.e. 6- and 8-storey) along the full range of period ratios. Importantly, the evolution of global drift demands with period ratio shows different behavioural trends depending on the number of storeys in the short period range ($T_1/T_m < 1$). While the global drift modification factor decreases with increasing period ratios in the case of 6-, 8-, and 12-storey CLT buildings, this correlation is



(a) $\ln(\delta_{mod})$ and T_1/T_m relationship for various response modification (q) factors in 8-storey B1 building.



(b) $\ln(\delta_{mod})$ and T_1/T_m relationship for various level of panel fragmentation (m) in 8-storey building, for a response modification (q) factor of q = 3.



(c) $\ln(\delta_{mod})$ and T_1/T_m relationship for various building heights (n), for a response modification (q) factor of q = 3.

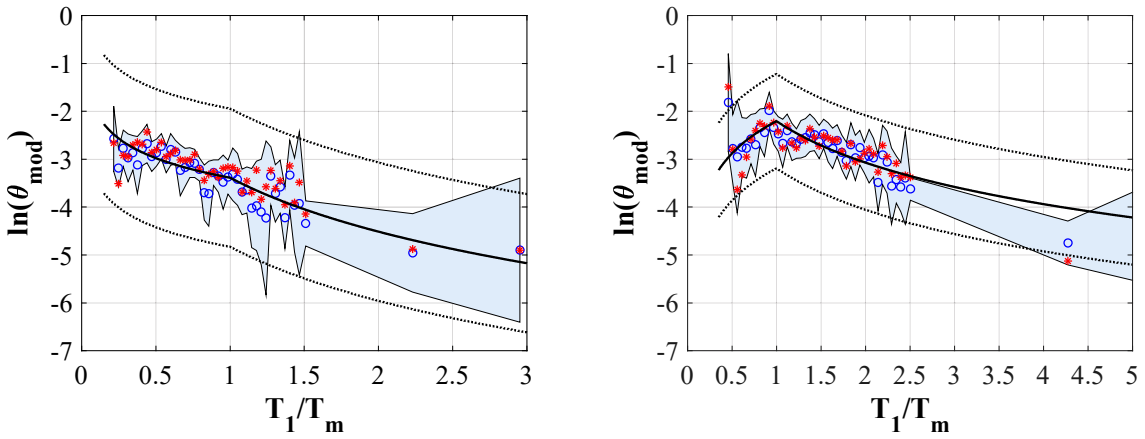
Figure 5.2: Relationship between $\ln(\delta_{mod})$ and T_1/T_m for various response modification (q) factors, level of panel fragmentation (m), and number of storeys (n).

negligible in the case of 16-storey CLT building, and fully-opposite in 20-storey CLT building. This difference highlights the relative importance of the level of inelastic deformations in low- and mid-rise CLT buildings.

5.2.3 Maximum inter-storey drift demands

To investigate the correlation between the maximum drift modification factor (θ_{mod}) and various salient structural parameters of interest, the same procedure performed for global drift modification factor (δ_{mod}) was followed. The variation in maximum drift modification factor (θ_{mod}) as a function of the period ratio (T_1/T_m) for a response modification factor of q =

3 is presented in Figure 5.3. While Figure 5.3a shows the variation in θ_{mod} for the 8-storey B1 building configuration, Figure 5.3b shows the corresponding variation for the 20-storey E3 building configuration. The corresponding variation for other building heights can be seen in Appendix D. As described before, the shaded regions indicate the 95% confidence interval in the estimate of mean logarithmic maximum drift modification factor ($\ln(\theta_{mod})$) whereas open (o) and asterisk (*) symbols denote the mean and median values within each data bin, respectively. The dotted lines in these figures represent the ± 1 standard deviation of the mean drift modification factor illustrated by the solid line. It is clear from these figures that the maximum drift modification factor, θ_{mod}, shows similar trends as those obtained for the global drift modification factor, δ_{mod}.



(a) 8 storey B1 building (n = 8, m = 1).

(b) 20 storey E3 building (n = 20, m = 3).

Figure 5.3: Mean logarithmic maximum drift modification factor ($\ln(\theta_{mod})$), against period ratio (T_1/T_m) for a response modification factor of q = 3.

The influence of key structural parameters namely response modification factor (q), number of storeys (n), and the level of panel fragmentation (m) on the maximum drift modification factor is presented in Figure 5.4. As seen for the global drift modification factor, lower maximum drift demands are associated with larger behaviour factors (q = {2, 2.5, 3, 4}), as shown in Figure 5.4a.

On the other hand, Figure 5.4b depicts the correlation between maximum drift modification factor θ_{mod}, and the period ratio T_1/T_m, for a range of joint density parameters (level of panel modularization, m = {1, 2, 3}). This figure shows a comparison between building models of different panel arrangements, namely 8-storey B1, B2 and B3 building configurations which indicates the influence of panel subdivision on the inelastic seismic demands in multi-storey CLT buildings. The maximum drift modification factor, θ_{mod}, increases with increasing number of intermediate joint lines due to the influence of overall stiffness reduction brought about

by the increasing number of vertical joints. These results are found to be consistent with the observations for global drift modification factor, δ_{mod}.

Finally, Figure 5.4c presents the variation in maximum drift modification factor for a range of building heights (n). It is clear from this figure that, in the short period range $T_1/T_m < 0.5$, where higher maximum drift demands are expected for the 6- and 8-storey CLT buildings, the main scaling features observed in the global drift modification factor (δ_{mod}) can also be seen for the maximum drift modification factor (θ_{mod}). However, in the long period range $T_1/T_m > 1$, higher inter-storey drift demands are expected in taller CLT buildings. This highlights that even though taller CLT buildings show smaller global inelastic deformation demands overall, higher normalized local seismic demands become more prominent due to the influence of higher mode effects in tall buildings.

5.3 Regression analyses

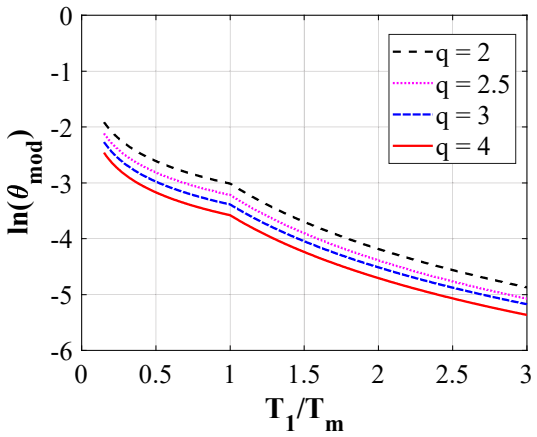
This section discusses the development of non-linear regression models put forward to predict global and maximum drift modification factors. These models are based on the extensive numerical analyses discussed in the previous sections. Standard regression procedures using a least squares algorithm were followed to identify the most appropriate functional forms. The most effective forms are presented on the basis of a preliminary study on a number of potential expressions and a detailed analysis of residuals. All regression analyses are performed in Matlab [56].

5.3.1 Global drift modification factor

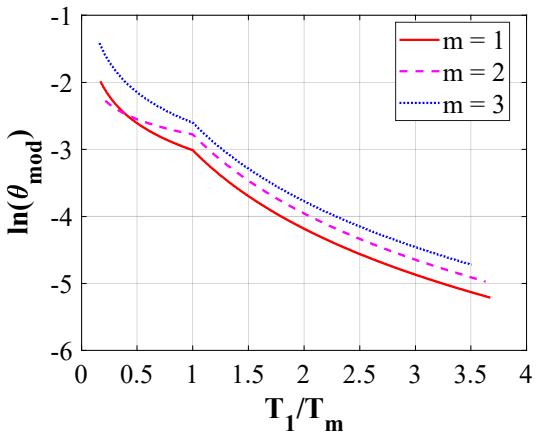
The following prediction model is proposed based on statistical investigations on the parameters which are found to have the greatest influence on the global drift modification factor:

$$\ln\delta_{mod} = a + b\cdot\beta + c\cdot\lambda + (d + e\cdot q)\cdot\ln\left[\min\left(\frac{T_1}{T_m}, 1\right)\right] + f\cdot\ln\left[\max\left(\frac{T_1}{T_m}, 1\right)\right] \tag{5.3}$$

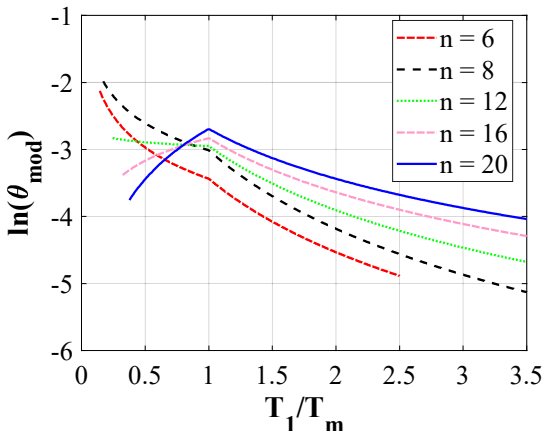
where δ_{mod} is the global drift modification factor; β is the joint density parameter; λ is the building aspect ratio; q is the design behaviour factor; T_1/T_m is the period ratio; and a, b, c, d, e, f are regression coefficients. λ is calculated as the quotient between height and width of the building facade. To this end, β is calculated as the ratio between all fastening lines (P_o) in the



(a) $\ln(\theta_{mod})$ and T_1/T_m relationship for various response modification (q) factors in 8-storey B1 building.



(b) $\ln(\theta_{mod})$ and T_1/T_m relationship for various level of panel fragmentation (m) in 8-storey building, for a response modification (q) factor of q = 3.



(c) $\ln(\theta_{mod})$ and T_1/T_m relationship for various building heights (n), for a response modification (q) factor of q = 3.

Figure 5.4: Relationship between $\ln(\theta_{mod})$ and T_1/T_m for various response modification (q) factors, level of panel fragmentation (m), and number of storeys (n).

wall and its perimeter (P).

The assumption of log-normality for the global drift modification factors fits well within a performance-based design framework. The statistically significant regression coefficients associated with Equation 5.3 are presented in Table 5.1. They were obtained by means of generalized non-linear least squares algorithm. The standard deviation of the dataset employed in this model is calculated as $\sigma = 1.29$. A residual plot of the parameters used in the global drift modification factor prediction model is presented in Figure 5.5. It can be appreciated from Figure 5.5 that there is no significant trend observed in residuals and not accounted for in the

model suggested.

Table 5.1: Regression coefficients for the global drift modification factor (δ_{mod}).

a	b	c	d	e	f
0.1652	0.2307	-0.0468	-2.0700	0.05007	-1.1443

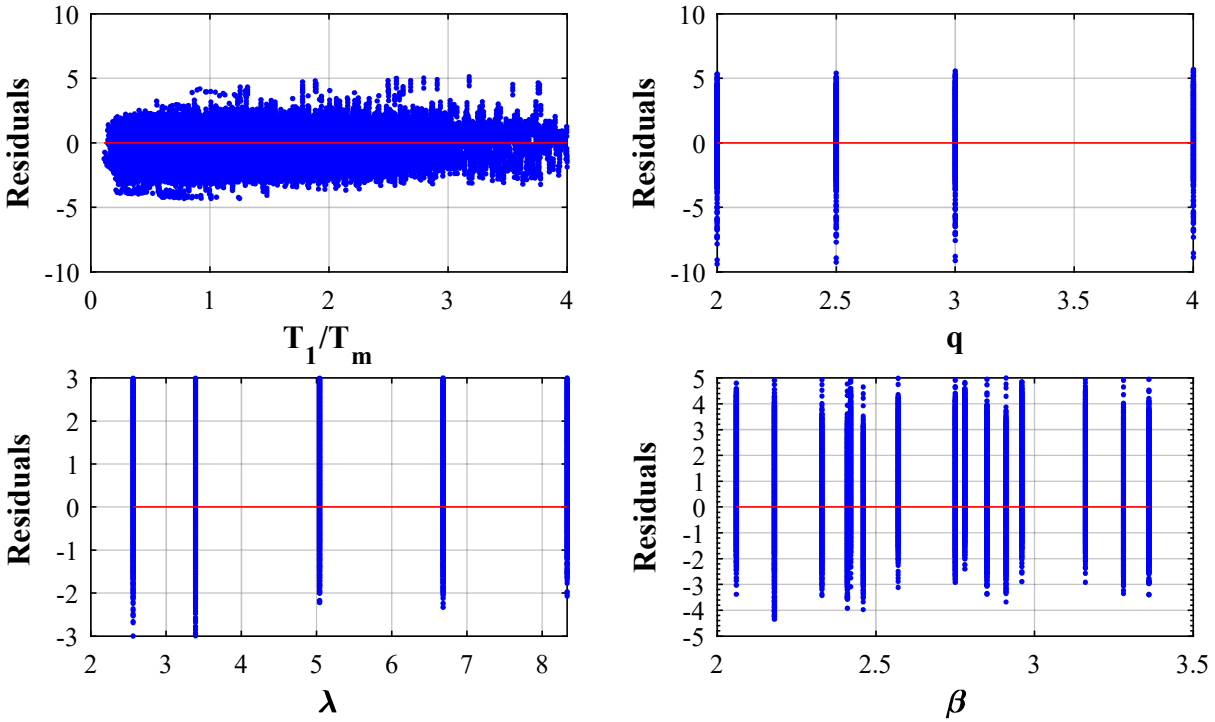


Figure 5.5: Residual plots for the global drift modification factor (δ_{mod}) prediction model.

5.3.2 Maximum drift modification factor

A functional form similar to that employed for the global drift modification factor is adopted herein for modelling the maximum drift modification factor taking into account the parameters β, λ, q and T_1/T_m. Equation 5.4 indicates this relationship:

$$\ln\theta_{mod} = a + b\cdot\beta + c\cdot\ln\lambda + (d + e\cdot q)\cdot\ln\left[\min\left(\frac{T_1}{T_m}, 1\right)\right] + f\cdot\ln\left[\max\left(\frac{T_1}{T_m}, 1\right)\right] \tag{5.4}$$

The corresponding regression coefficients for the maximum drift modification factor are summarized in Table 5.2. As with global drift demands, all regression terms were found to be statistically significant for the maximum inter-storey drift modification factor. The standard deviation of the dataset employed in this model is determined as $\sigma = 1.20$. Finally, a residual plot of the parameters used in the regression model is presented in Figure 5.6. It is clear from this figure that there is no significant residual trend.

Table 5.2: Regression coefficients for the maximum drift modification factor (θ_{mod}).

a	b	c	d	e	f
-4.3548	0.2421	0.5228	-1.7093	0.4027	-1.0708

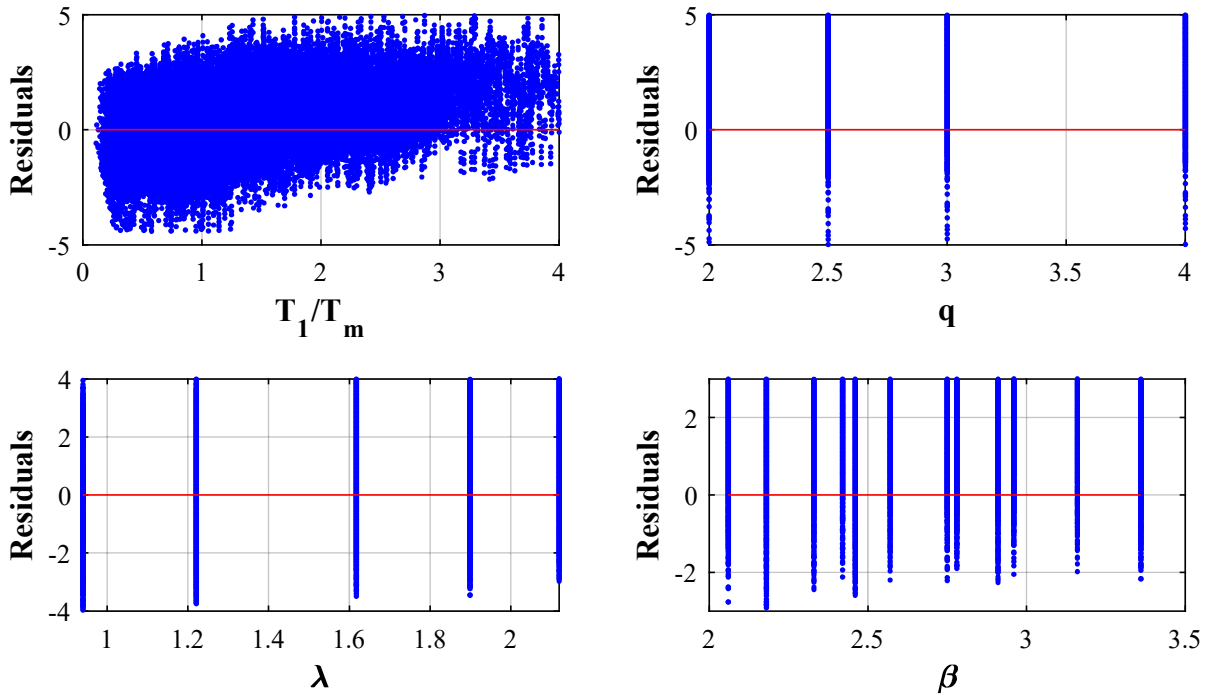


Figure 5.6: Residual plots for the maximum drift modification factor (θ_{mod}) prediction model.

5.4 Comparative studies

As discussed in Chapter 2, previous research conducted on the inelastic displacement demands of multi-storey CLT buildings has been framed within a force-based design framework and has been limited to the identification of an appropriate response modification (q) factors by neglecting frequency-dependency. In contrast, the preceding results and discussion have revealed

the significant influence of the ground-motion frequency content characterized by the scalar parameter, T_m on the building response. Although it is not possible to fully compare the results obtained above with the findings of previous investigations, a restricted comparison can still be made particularly with the most recent investigations by Pozza and Trutalli [71], and the well-known equal displacement rule adopted in Eurocode 8 [29].

Building characteristics

Based on the previous results of this thesis, a strong correlation was found between the dissipative capacity and a number of building characteristics. More precisely, the density of vertical and horizontal panel-to-panel joints and the ratio between the height and the width of the building facade have significant influence on the actual dissipative capacity of CLT structures. Pozza and Trutalli [71] proposed a new relationship for the q factor as a function of the wall joint density (β) and building aspect ratio (λ).

An index, α, is defined as the ratio between the area of the building facade, A, and the total length of the fastening line, P. Furthermore, a reference configuration of a hypothetical facade with no intermediate joints is defined as α_0 which is the ratio between the wall area, A, and the perimeter, P_0. The process for the computation of these indexes is depicted in Figure 5.7.

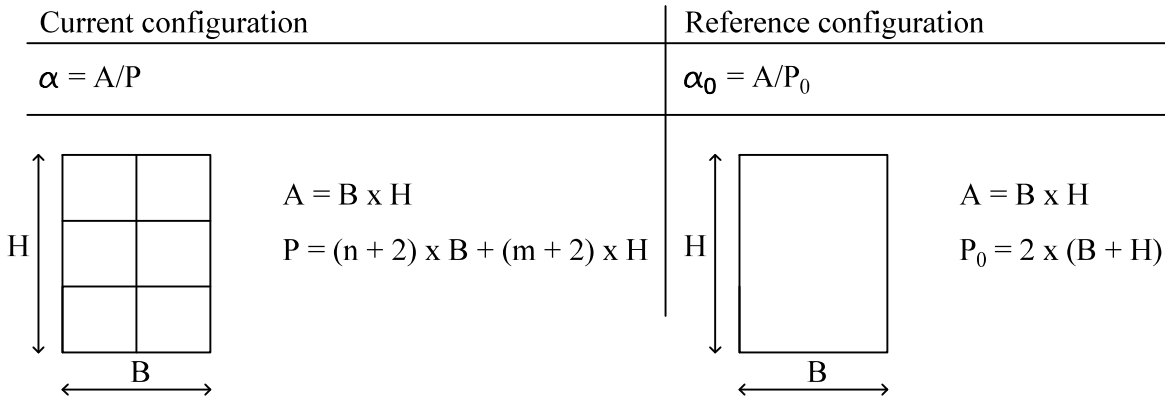


Figure 5.7: Computation of indexes for the actual and reference configurations.

Where B is the width of building facade; H is the building height; m is the number of vertical joint lines per storey; and n is the number of horizontal joint lines along the building height.

A dimensional joint density parameter, β is defined as the ratio of the indexes described above, accounting for all fastening lines both in vertical and horizontal directions. The joint density

parameter is calculated as:

$$\beta = \frac{\alpha}{\alpha_0} = \frac{P}{P_0} \tag{5.5}$$

Finally, the second parameter that has influence on the dissipative capacity of the building is the building aspect ratio, which can be determined as the ratio of the building height and the width of the building facade as shown in Equation 5.6:

$$\lambda = \frac{H}{B} \tag{5.6}$$

Table 5.3 presents the list of building configurations along with the associated building aspect ratios and joint density parameters.

Table 5.3: Computation of building aspect ratio (λ) and joint density parameter ($\beta = P_o/P$).

Building	Model	Height H	Width B	Slenderness λ	Length of fastening lines (m) P_o	Perimeter (m) P	β
6 Storey	A1	21.8	8.5	2.56	124.90	60.60	2.06
	A2	21.8	8.5	2.56	146.70	60.60	2.42
	A3	21.8	8.5	2.56	168.50	60.60	2.78
8 Storey	B1	28.8	8.5	3.39	162.90	74.60	2.18
	B2	28.8	8.5	3.39	191.70	74.60	2.57
	B3	28.8	8.5	3.39	220.50	74.60	2.96
12 Storey	C1	42.8	8.5	5.04	238.90	102.60	2.33
	C2	42.8	8.5	5.04	281.70	102.60	2.75
	C3	42.8	8.5	5.04	324.50	102.60	3.16
16 Storey	D1	56.8	8.5	6.68	314.90	130.60	2.41
	D2	56.8	8.5	6.68	371.70	130.60	2.85
	D3	56.8	8.5	6.68	428.50	130.60	3.28
20 Storey	E1	70.8	8.5	8.33	390.90	158.60	2.46
	E2	70.8	8.5	8.33	461.70	158.60	2.91
	E3	70.8	8.5	8.33	532.50	158.60	3.36

Proposed correlation

Once the building characteristics that have a significant influence on the dissipative capacity of CLT buildings are determined, the proposed correlation [71] for the q factor can be calculated as shown in Equation 5.7:

$$q_0(\beta, \lambda) = (q_{0,ref} + \lambda^k)\beta^k \leq 5.0 \tag{5.7}$$

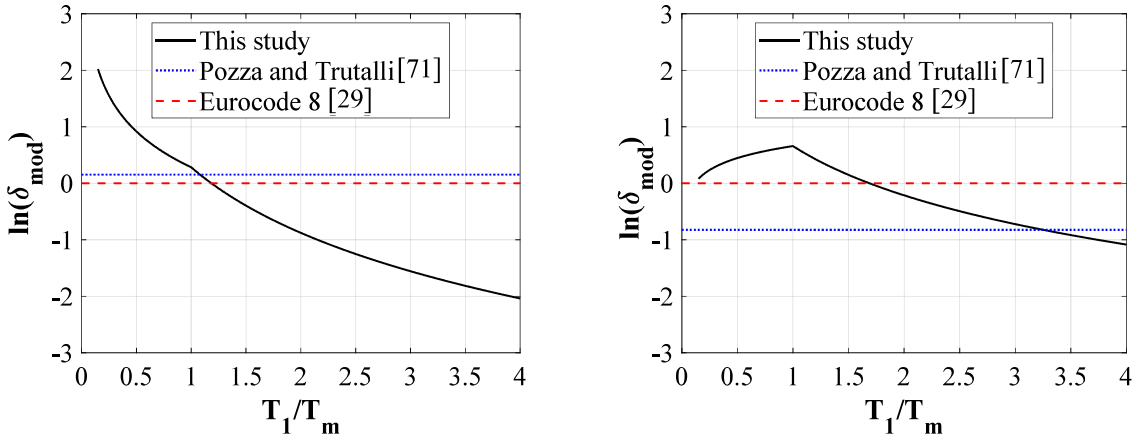
A value of $q_{o,ref}$ = 1.5 was recommended by Pozza and Trutalli [71] in accordance with current suggested levels of energy dissipation in low-ductility and non-dissipative buildings in Eurocode 8 [29]. Furthermore, a coefficient k = 0.458 was found to provide the best fit and minimize the sum of square difference between the analytical values and the numerical mean q_0 factor values. It is important to note that the q_0 factor was limited to 5.00, which is the highest value proposed by Eurocode 8 [29] for timber structures. Using Equation 5.7, new response modification factors (q) for the developed building configurations were determined and summarized in Table 5.4. Subsequently, global drift modification factors associated with the corresponding behaviour (q) factors in accordance with Equation 5.7 were estimated and compared to previous results as well as Eurocode 8 [29] approximations. To this end, a comparison of mean global drift modification factors obtained by means of the prediction model developed by Pozza and Trutalli [71] as well as Eurocode 8 [29] well-known equal displacement rule is presented in Figure 5.8. The results of an 8-storey and a 20-storey CLT buildings are shown as representative of short and tall CLT buildings.

Table 5.4: Computation of q values using the proposed Equation 5.7 for building configurations.

Building	Model	λ	β	q
6 Storey	A1	2.56	2.06	4.13
	A2	2.56	2.42	4.43
	A3	2.56	2.78	4.71
8 Storey	B1	3.39	2.18	4.51
	B2	3.39	2.57	4.85
	B3	3.39	2.96	5.15*
12 Storey	C1	5.04	2.33	5.11*
	C2	5.04	2.75	5.49*
	C3	5.04	3.16	5.85*
16 Storey	D1	6.68	2.41	5.58*
	D2	6.68	2.85	6.00*
	D3	6.68	3.28	6.39*
20 Storey	E1	8.33	2.46	5.98*
	E2	8.33	2.91	6.44*
	E3	8.33	3.36	6.85*

*Values of q capped to 5 according to [29, 71]

It can be appreciated from Figure 5.8 that the proposal by Pozza and Trutalli [71] shows a general improvement compared to Eurocode 8 [29], as it takes into account the level of panel fragmentation and approximates the overall mean of the dataset. However, it neglects the period dependency while estimating the inelastic deformation demands which can lead to significant



(a) 8 storey B1 building (n = 8, m = 1).

(b) 20 storey E3 building (n = 20, m = 3).

Figure 5.8: Comparison of mean logarithmic global drift modification factors ($\ln(\delta_{mod})$) obtained using the prediction model developed in this study with the proposal by Pozza and Trutalli [71] as well as Eurocode 8 [29] approximations.

mis-estimations except for very limited period ranges, namely $T_1/T_m \approx 1$ for B1 building and $T_1/T_m \approx 3$ for E3. This neglection can lead up to 80% over-estimations in the case of B1 building when the ground-motion has a strong short period component and important under-estimations of up to 70% for more distant (long-period dominated) earthquakes.

In the case of taller CLT structures like the 20-storey E3 building configuration, the highest under-estimations are seen when $T_1/T_m \approx 1$ with inelastic drift estimations proposed by Pozza and Trutalli [71] giving even higher non-conservative results than the Eurocode 8 [29]. As this range of building heights was not considered during the development of Equation 5.7, this level of non-conservative results are not surprising. In short, these results highlight the importance of an explicit account of the frequency content of the ground-motion on the assessment of inelastic deformation demands in multi-storey CLT buildings.

5.5 Concluding remarks

This chapter has investigated the influence of key structural characteristics and the frequency content of the ground-motion on the inelastic deformation demands in multi-storey CLT buildings. Analyses were performed on two parameters, namely global (δ_{mod}) and maximum (θ_{mod}) drift modification factors. Based on the parametric investigations performed, both global and maximum inter-storey drift modification factors were found to be notably dependent on the ground-motion frequency content characterised by the mean period (T_m) along the full range

of period ratios (T_1/T_m) for all building heights studied.

Observations on the inelastic seismic demands in multi-storey CLT structures showed different behavioural trends in short and tall CLT buildings. Global (δ_{mod}) and maximum (θ_{mod}) drift modification factors decrease with increasing period ratios (T_1/T_m) for the long period range, $T_1/T_m > 1$. On the other hand, while drift modification factors decrease in low- and mid-rise CLT buildings (n = {6, 8, and 12}), this relationship is neglected in the case of 16-storey building, and fully-reversed in the case of 20-storey building, for the short period range, $T_1/T_m < 1$. A distinct resonant response was also observed for taller CLT structures which was attributed to their overall lower relative inelastic deformation levels. Furthermore, relatively higher maximum inter-storey drift demands was observed in taller CLT structures explained by the influence of higher mode effects in tall buildings.

Based on the extensive parametric studies performed, a set of prediction models were proposed for the estimation of global (δ_{mod}) and maximum (θ_{mod}) drift modification factors as a function of design behaviour factor q, building aspect ratio λ, joint density β, and period ratio T_1/T_m. The simulation of prediction equations demonstrated that increasing the level of panel fragmentation can result in enhanced flexibility and inelastic deformations. Furthermore, individual panel lengths of 2.85 m or less showed an increased energy dissipation capacity brought about by a greater number of joints. The prediction models developed in this study showed a good agreement with the data over the range of structural properties and ground-motion characteristics.

Finally, a comparative study was conducted with the recent assessment proposals by Pozza and Trutalli [71] and the well-known equal displacement rule described in Eurocode 8 [29]. Comparisons were made on two building models as representatives of low- and high-rise CLT structures. On the basis of comparative assessment, it was found that despite the fact that correlation equation proposed in [71] showed an improved response over the Eurocode 8 equal displacement rule as the proposal approximates the overall mean of dataset, relatively higher mis-estimations were observed due to neglecting period dependency in the estimation of inelastic deformation demands. For instance, when the ground-motion has a strong short period component, up to 80% over-estimations were observed while up to 70% non-conservative results were seen when the ground-motion has a long period (more distant earthquakes) in the case of the 8-storey B1 building. On the other hand, the highest under-estimations were expected in the case of 20-storey E3 building configuration when the period ratio was $T_1/T_m \approx 1$ leading to even more non-conservative results than equal displacement rule approximation. Given that such higher buildings were not incorporated in the study by Pozza and Trutalli [71], this results

were not surprising. These comparisons confirm an urgent need for a comprehensive account for the frequency content of the ground-motion on the design and assessment of seismic drift demands in multi-storey CLT structures.

Chapter 6

Assessment of Seismic Force Demands

6.1 Introduction

As highlighted in the literature survey presented in Chapter 2, there is no study conducted to date focusing on seismic force demands in multi-storey CLT buildings as correlated with ground-motion characteristics. Therefore, there is a need to develop simple yet robust models incorporating frequency content descriptions of ground-motion and structural properties of interest to estimate seismic strength demands. To this end, the structural parameters considered in Chapter 5 (e.g. design behaviour factor q, building aspect ratio λ, and joint density parameter β) are also considered to evaluate force demands in the present chapter. In addition, a new parameter denominated plasticity resistance ratio α, is included in the estimation of seismic force demands. This is done in light of the importance that an accurate estimation of plastic strenghts has in ensuring the achievement of ductile failure modes and capacity design. Therefore, the present chapter aims to address the influence of key structural parameters as well as ground-motion frequency content on the seismic force demands in multi-storey CLT buildings.

The procedure described earlier for the assessment of seismic drift demands in Chapter 5 is followed to evaluate the influence of above mentioned parameters on the strength demands in multi-storey CLT structures. Furthermore, the same dataset of analyses developed above is used herein. Two seismic force demand parameters, base shear and inter-storey shear modification factors described later in this chapter are examined.

This chapter has been organized in the following way. The first section provides information on the structural response parameters of interest. The assessment of peak seismic forces is described in the second part. The third section is devoted to the presentation of the non-linear regression analyses conducted to estimate the evolution of seismic force demands. Simplified models are proposed and discussed in the fourth section. Finally, the concluding remarks are

outlined in the last part.

6.2 Structural response parameters

Extensive non-linear response history analyses were performed as defined in previous chapters and from each analysis, maximum base shear (V_{max}) and maximum inter-storey shear ($V_{i,max}$) forces were recorded. These parameters were defined as:

- V_{max} is defined as the sum of the shear forces at all the supports of the building.
- $V_{i,max}$ is the maximum shear force at the i^{th} storey, and can be determined as the sum of the shear forces in all shear wall elements.

Similarly, non-linear static pushover analyses were conducted on the CLT building models and the base shear (V_1) and storey shear ($V_{i,1}$) forces at the formation of first yield in the structure were determined together with plasticity resistance ratio (α). The definition of these parameters are given as follows:

- V_1 is the base shear at yield is calculated as the sum of the all reactions at all supports of the building at the point of first yield, obtained from a non-linear static analysis with monotonically increasing lateral loads adopting a first mode distribution along the building's height.
- $V_{i,1}$ is the total shear force at the i^{th} storey, which is calculated as the sum of shear forces in all shear wall elements at the formation of first yield in the structure.

6.3 Assessment of peak forces

Once the quantities described above are determined by means of dynamic as well as static analyses procedures, the seismic force demand modification factors can be computed as follows:

- Base shear modification factor (V_{mod}) is the ratio between the maximum base shear (V_{max}) obtained from the non-linear response history analysis and the product of the plasticity resistance ratio (α) and the base shear at first yield (V_1) as defined before. V_{mod} can be expressed as:

$$V_{mod} = \frac{V_{max}}{\alpha \cdot V_1} \tag{6.1}$$

- Inter-storey shear modification factor ($V_{st,mod}$) is the ratio between the maximum inter-storey shear at the i^{th} storey of the building ($V_{i,max}$) obtained from non-linear response history analysis and the product of the plasticity resistance ratio (α) and total inter-storey shear at the i^{th} storey at the first yield ($V_{i,1}$) defined before. $V_{st,mod}$ can be expressed as:

$$V_{st,mod} = \frac{V_{i,max}}{\alpha \cdot V_{i,1}} \tag{6.2}$$

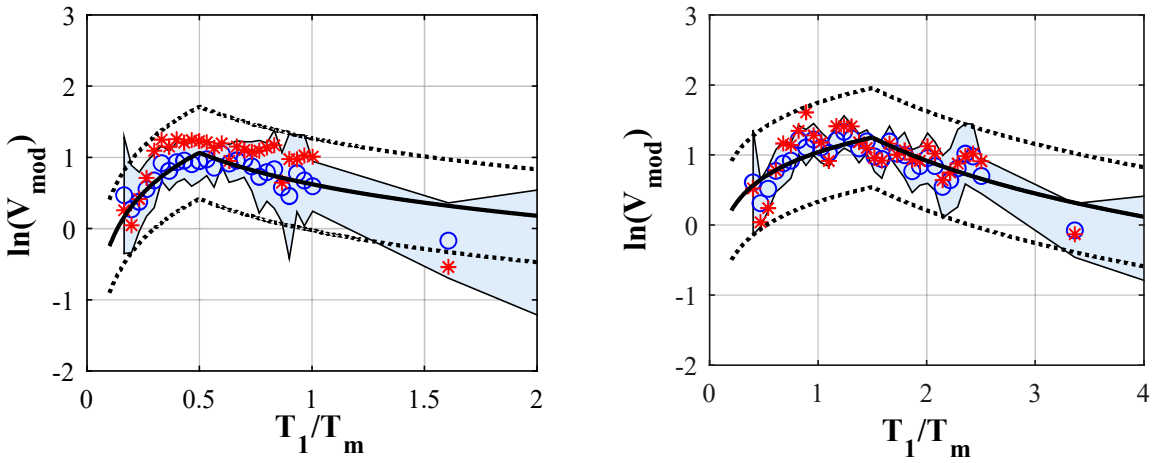
It should be noted that the definitions offered above follow widely accepted formulations for structures dimensioned according to ductile design approaches [29, 79]. In the following sections of this chapter, the results of the large dataset of non-linear static and dynamic analyses created are examined to investigate the influence of various structural characteristics on base and inter-storey shear modification factors.

6.3.1 Base shear demands

The variation of base shear modification factors, V_{mod}, for the A1 (n = 6) building configuration as a function of the period ratio, T_1/T_m, is presented in Figure 6.1a, whereas Figure 6.1b shows the corresponding results for the E1 (n = 20) building. The period ratio is defined as the ratio between the fundamental period of the structure (T_1) and the mean period of the ground-motion (T_m) while the base shear modification factor is defined as explained above. The open circles (o) and asterisks (*) symbols in Figure 6.1 denote the mean and median values within each data bin, respectively. The shaded regions show the 95% confidence interval in the estimate of the mean base shear and the dotted lines depict the ± one standard deviation limits of the base shear modification factor, $\ln V_{mod}$, for the best-fit prediction model described in latter parts of this paper. The mean estimate of the best-fit prediction model is depicted by the solid line in Figure 6.1.

It is clear from Figure 6.1 that the relationship between inelastic shear demands and ground-motion frequency content is non-linear along the full range of period ratios. Besides, Figure 6.1a shows that in the short period range the base shear modification factor, V_{mod}, of mid-rise CLT structures (6-storey building) tends to increase with increasing period ratios up until $T_1/T_m = 0.5$. An inverse relationship is observed thereafter with decreasing V_{mod} values for longer periods, $T_1/T_m > 0.5$. The same piece-wise non-linear relationship is observed for the 20-storey building in Figure 6.1b, but in this case V_{mod} peaks at $T_1/T_m = 1.5$. The corresponding variation for other building heights can be seen in Appendix D.

The influence of salient structural design parameters, namely, response modification factor, q, number of storeys, n, and the level of panel modularization, β, on the seismic strength demands



(a) 6-storey A1 building (n = 6, m = 1).

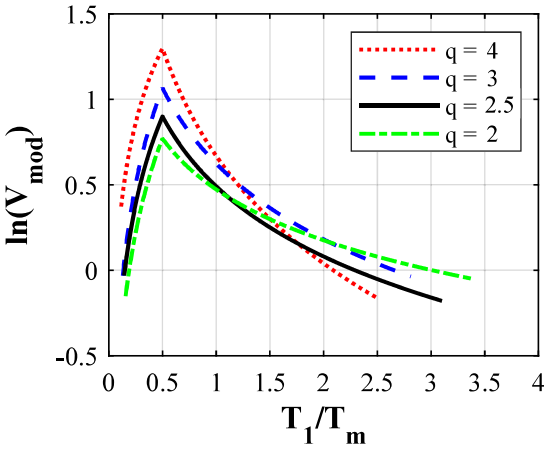
(b) 20-storey E1 building (n = 20, m = 1).

Figure 6.1: Mean logarithmic base shear modification factor ($\ln(V_{mod})$) against period ratio (T_1/T_m) for a response modification factor of q = 3.

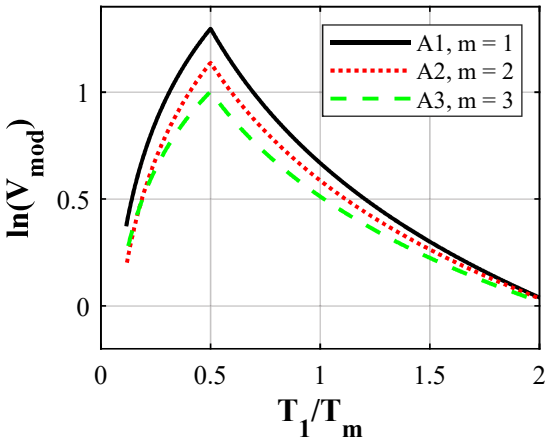
in multi-storey CLT buildings is investigated in Figure 6.2. For this purpose, the evolution of base shear demands attained in CLT structures as a function of the behaviour factor, q, is illustrated in Figure 6.2a with reference to the 6-storey A1 building. This figure shows that the different trends observed before for the short ($T_1/T_m < 0.5$) and long period ranges ($T_1/T_m > 0.5$) persist regardless of the q-factor employed in the design. Although the rate of decay in V_{mod} at longer periods increases with increasing levels of assumed energy dissipation, (q), the main feature of Figure 6.2a is that peak base shear ratios (V_{mod} at $T_1/T_m = 0.5$) increase in direct proportion to the q values, or what is the same, in direct proportion to the energy dissipation capacity of the building. This is reasonable as larger forces, relative to the corresponding yield values, are expected for higher ductility levels in strongly hardening structures like these.

The relationship between mean values of base shear demands, V_{mod}, and period ratios, T_1/T_m, for various joint density parameters, β, is presented in Figure 6.2b. It is clear from this figure that the mean base shear modification factor decreases with increasing levels of panel fragmentation, showing that a higher modularization level of CLT panels leads to lower shear demands. This is a reflection of the enhanced energy dissipation capacity associated with multiple rocking segments coupled with the more pronounced post-yield hardening effects of long CLT panels.

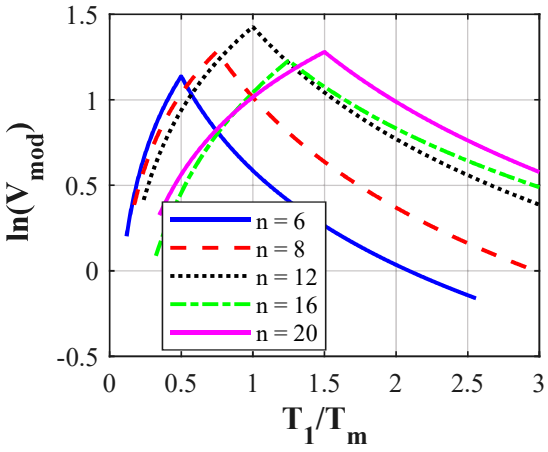
Finally, Figure 6.2c explores the relationship between base shear modification factor, V_{mod}, and the period ratio, T_1/T_m, for different building heights. The response of CLT building models of different number of storeys (i.e. n = {6,8,12,16,20}) but with a single line of vertical joinery



(a) Mean $\ln(V_{mod})$ and T_1/T_m relationship for various behaviour factors (q) in 6-storey (A1) buildings.



(b) Mean $\ln(V_{mod})$ and T_1/T_m relationship for various joint density parameters (β) in 6-storey (A1) buildings, q = 3.



(c) Mean $\ln(V_{mod})$ and T_1/T_m relationship for various building heights (n), q = 3.

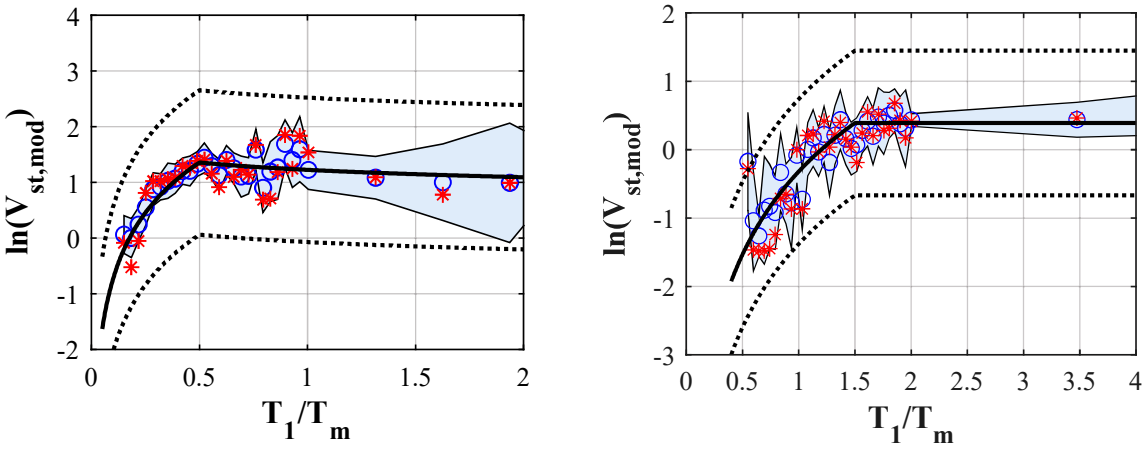
Figure 6.2: Relationship between $\ln(V_{mod})$ and T_1/T_m for various response modification (q) factors, level of panel fragmentation (m), and number of storeys (n).

(i.e. m = 1) designed with q = 3 is presented. It can be appreciated from Figure 6.2c that the mean base shear modification factor increases non-linearly with increasing period ratios irrespective of the building height in the short period range, peaking at increasingly longer periods as the structures become taller (i.e. $T_1/T_m = \{0.5, 0.75, 1, 1.25, 1.5\}$). This observation hints to the central role played by resonance (with the first building mode) in the evaluation of shear demands. Furthermore, the largest base shear modification factors take place in buildings of 12 storeys which fundamental period coincides with the mean period of the building (i.e. $T_1/T_m = 1$).

6.3.2 Inter-storey shear demands

A similar procedure as the one described above was followed to study the relationship between the inter-storey shear modification factors, $V_{st,mod}$, and the structural parameters of interest. Figure 6.3a shows the variation of $V_{st,mod}$ for the A1 (n = 6) building configuration as a function of the period ratio, T_1/T_m, while Figure 6.3b depicts the results corresponding to the E1 (n = 20) building. The corresponding variation for other building heights can be seen in Appendix D. As before, the shaded regions in these figures represent the 95% confidence interval in the estimate of the mean storey shear modification factor. The dashed lines indicate the ± one standard deviation of the mean logarithmic storey shear modification factor, represented by the solid line. And the open circles (o) and asterisk (*) symbols denote the mean and median values within data bins, respectively.

It is clear from Figure 6.3 that, unlike the base shear modification factor, milder variations of $V_{st,mod}$ are expected for the long period range, especially in taller CLT buildings. It should be noted that a complete lack of correlation between $V_{st,mod}$ and T_1/T_m at long periods is strictly valid only for taller building configurations (i.e. n = {16,20}) with the lowest number of vertical joints, m = 1. If more vertical joints are employed (e.g. m = 2 or 3 corresponding to β values in the order of 3 or 3.4), or shorter structures are considered, the evolution of storey shear modification factors is mildly non-linear, as discussed below with reference to Figure 6.4c.



(a) 6-storey A1 building (n = 6, m = 1).

(b) 20-storey E1 building (n = 20, m = 1).

Figure 6.3: Mean logarithmic storey shear modification factor ($\ln(V_{st,mod})$), against period ratio (T_1/T_m) for a response modification factor of q = 3.

The effect of key structural parameters such as behaviour factor, q, number of storeys, n, and panel fragmentation, β, on the inter-storey seismic shear demands in CLT buildings is presented in Figure 6.4. Figure 6.4a displays the variation in mean storey shear modification factor

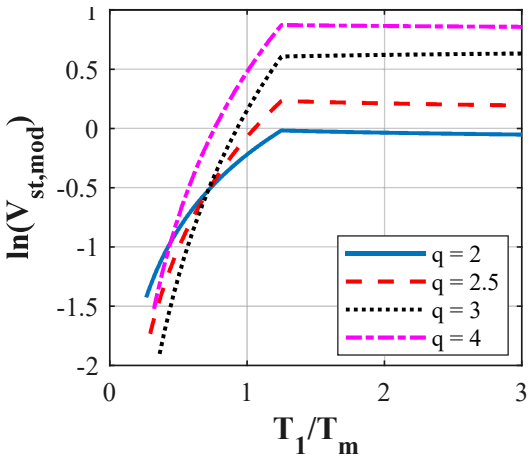
($V_{st,mod}$) as a function of the period ratio (T_1/T_m) for the D1 (n = 16) building configuration with the lowest panel fragmentation level and for various design response modification factors (i.e. q = {2,2.5,3,4}). It can be appreciated from this figure that larger response modification factors, q, are associated with correspondingly larger inter-storey shear demand ratios, $V_{st,mod}$, along the full period range. Again, the significant levels of post-yield hardening experienced by tied down CLT panels can explain these tendencies. In general, short period structures will experience inelastic inter-storey shear demands at or below the ultimate forces predicted from a pushover analysis. On the other hand, in the long period range, $T_1/T_m \geq 1.2$, the inter-storey shear demands from non-linear response history analyses will exceed the non-linear static predictions except when q-factors of 2 or less are employed.

The influence of panel fragmentation on the inter-storey shear demands is depicted in Figure 6.4b for A1, A2 and A3 (n = 6) building configurations. It can be observed from this figure that $V_{st,mod}$ decreases with increasing number of vertical joint lines, or higher β values. This can be attributed to the overall increment in energy dissipation capacity brought about by the larger number of ductile connectors. A change from β = 2.06 to β = 2.78, equivalent to going from a single vertical joint per wall to three vertical joints, reduces the shear demands in over 250% (note the logarithmic scale).

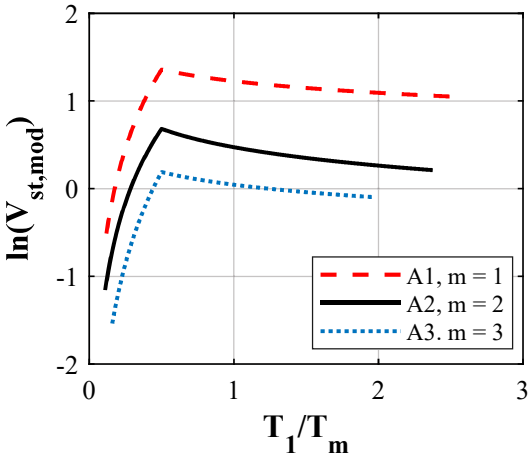
Finally, the relationship between the storey shear modification factor, $V_{st,mod}$, and the period ratio, T_1/T_m, for different building heights, n, is presented in Figure 6.4c. The buildings with the highest level of panel fragmentation studied (i.e. m = 3) are shown in this figure. It can be seen from Figure 6.4c that while lower shear demands are expected in the short period range for taller structures, larger shear demands will take place in the long period range in taller buildings. This can be attributed to the importance of higher mode-effects in the seismic response of buildings which becomes more prominent in taller, more slender, structures.

6.4 Regression analyses

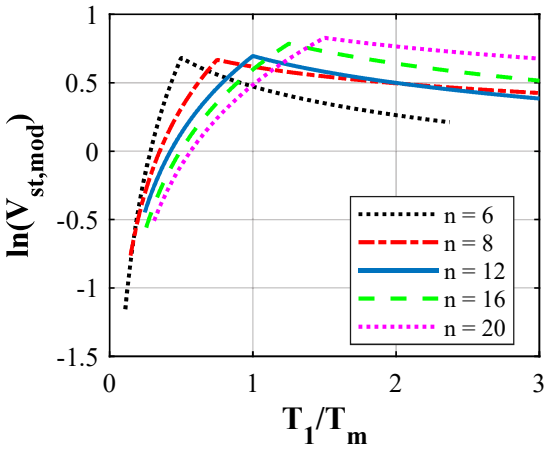
General statistical regression procedures are employed in this secton to develop prediction models that estimate the base (V_{mod}) and storey ($V_{st,mod}$) shear demands in multi-storey CLT buildings. Based on the extensive parametric investigations, the following parameters are found to have influence on the seismic force demands: building aspect ratio λ, design behaviour factor q, period ratio T_1/T_m, building height index ξ_1, joint density parameter β, and plasticity resistance ratio α. The most efficient expressions are presented below.



(a) Mean $\ln(V_{st,mod})$ and T_1/T_m relationship for various behaviour factors (q) in the 16-storey (D1) building.



(b) Mean $\ln(V_{st,mod})$ and T_1/T_m relationship for various joint density parameters (β) in the 6-storey building, q = 3.



(c) Mean $\ln(V_{st,mod})$ and T_1/T_m relationship for various building heights (n), q = 3.

Figure 6.4: Relationship between $\ln(V_{st,mod})$ and T_1/T_m for various response modification (q) factors, and level of panel fragmentation (m), and number of storeys (n).

6.4.1 Base shear modification factor

The following Equation 6.3 was developed by taking into consideration the parameters that have the greatest influence on the base shear modification factor (V_{mod}) as described above:

$$\begin{aligned} \ln V_{mod} = a + b\cdot\lambda + (c + d\cdot q)\cdot \ln\left[\min\left(\frac{T_1}{T_m}, \xi_1\right)\right] + \\ e\cdot\ln\left[\max\left(\frac{T_1}{T_m}, \xi_1\right)\right] + f\cdot\beta + g\cdot\alpha \end{aligned} \tag{6.3}$$

where V_{mod} is the base shear modification factor; λ is the building aspect ratio; q is the design behaviour factor; T_1/T_m is the period ratio; β is the joint density parameter; α is the plasticity resistance ratio; ξ_1 is the building height index; and a, b, c, d, e, f, g are regression coefficients. As a result of the primary investigations for the estimation of peak base shear demands, a new parameter, the building height index (ξ_1) is defined depending on the number of storey. This parameter can be expressed as:

$$\xi_1 = 3.42\times10^{-4}(n)^3 - 1.48\times10^{-2}(n)^2 + 2.65\times10^{-1}(n) - 6.23\times10^{-1} \tag{6.4}$$

Table 6.1 presents the computation of building height indexes obtained from Equation 6.4, and employed in the prediction models. To this end, Table 6.2 summarizes the regression coefficients that were found to be statistically significant associated with Equation 6.3 and obtained by means of a generalized non-linear least squares algorithm. The standard deviation for the dataset employed in the model is $\sigma = 0.77$. Finally, a residual plot is presented in Figure 6.5 for the parameters used in base shear modification factor prediction model. No significant trend was observed in residuals.

Table 6.1: Computation of building height indexes, ξ_1.

n	6	8	12	16	20
ξ_1	0.5	0.75	1.00	1.25	1.50

Table 6.2: Regression coefficients for the base shear modification factor (V_{mod}).

a	b	c	d	e	f	g
2.1169	0.1205	0.2150	0.1315	-0.7906	-0.2269	-0.3678

6.4.2 Inter-storey shear modification factor

A similar prediction model as the one presented in the previous section was employed to estimate the storey shear modification factor as a function of key structural parameters such as λ, q, T_1/T_m, β, and α. The functional form adopted is indicated in Equation 6.5:

$$\begin{aligned} \ln V_{st,mod} = a + b\cdot\lambda + (c + d\cdot q)\cdot\ln\left[\min\left(\frac{T_1}{T_m}, \xi_1\right)\right] + \\ e\cdot\ln\left[\max\left(\frac{T_1}{T_m}, \xi_1\right)\right] + f\cdot\beta + g\cdot\alpha \end{aligned} \tag{6.5}$$

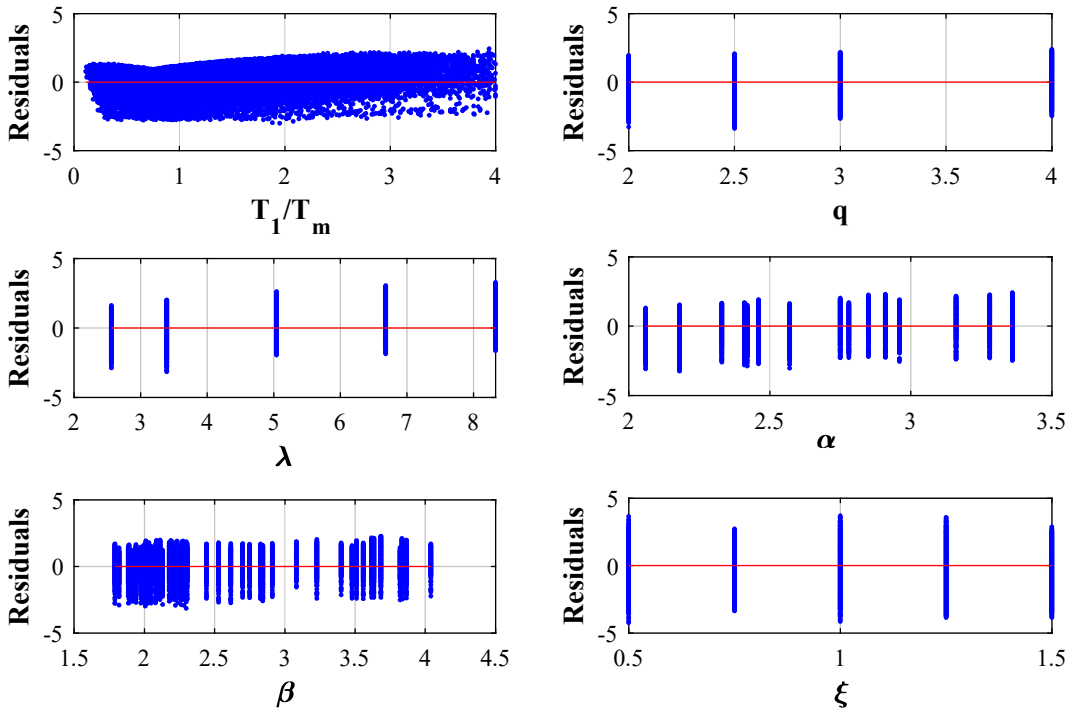


Figure 6.5: Residual plots of the parameters used in the base shear modification factor V_{mod} prediction model.

As per above, all regression terms were found to be statistically significant and are presented in Table 6.3. The standard deviation of the dataset employed in this model is calculated as $\sigma = 1.15$. To this end, Figure 6.6 presents a residual plot for the parameters used in storey shear modification factor prediction model. It is clear from this figure that no significant trend remains in the residuals.

Table 6.3: Regression coefficients for the storey shear modification factor ($V_{st,mod}$).

a	b	c	d	e	f	g
3.7369	-0.1567	0.7733	0.1410	-0.0339	-0.3317	-0.5105

6.5 Model simplification

Simplified functional forms for the building height index (ξ) and storey shear modification factor ($V_{st,mod}$) are developed and discussed in this section. This is done in attention to the need of striking a balance between predictive power and functional complexity.

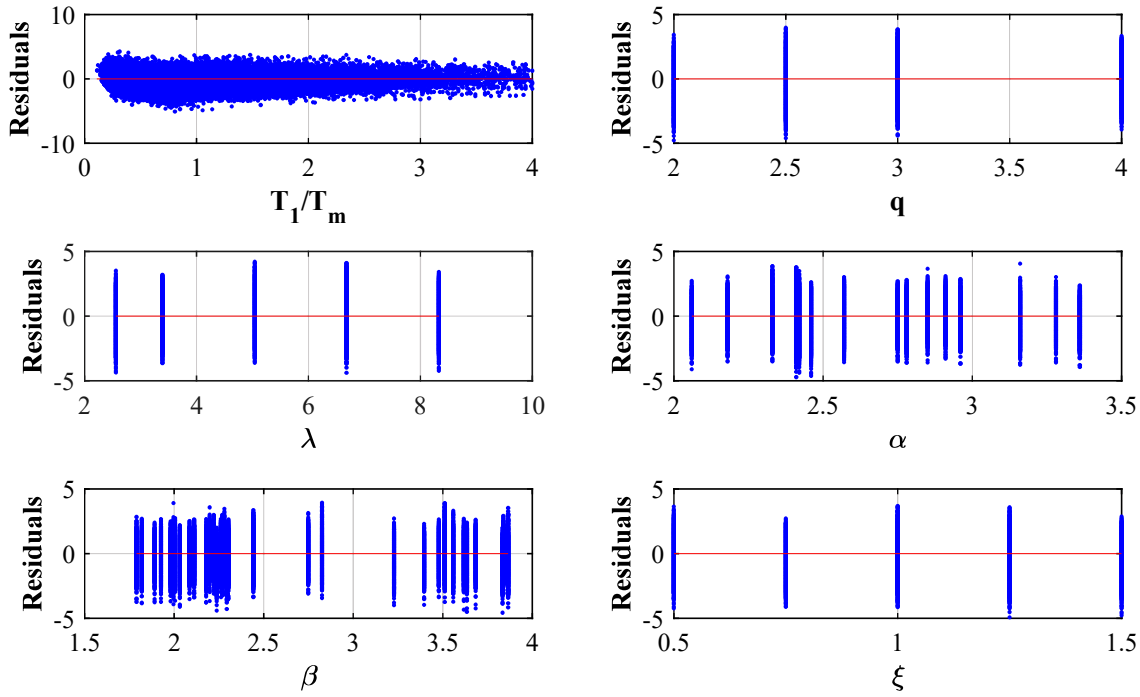


Figure 6.6: Residual plots for the storey shear modification factor $V_{st,mod}$ prediction model.

6.5.1 Building height index

On the basis of several functional forms considered to reduce the number of terms in the computation of building height index for each building height, the following Equation 6.6 is derived.

$$\xi_2 = 0.0686 \cdot n + 0.1494 \tag{6.6}$$

where n is the number of storey. Table 6.4 presents a comparison of the computed building height indexes (ξ_1 and ξ_2) associated with Equations 6.4 and 6.6, respectively. It can be appreciated from Table 6.4 that the simplified model is able to approximate the computed values by means of Equation 6.4 at a maximum level of %12 difference.

Table 6.4: Comparison of building height indexes, ξ.

n	6	8	12	16	20
ξ_1	0.5	0.75	1.00	1.25	1.50
ξ_2	0.56	0.70	0.97	1.25	1.52
Error %	12	6.7	3.0	0.0	1.3

6.5.2 Storey shear modification factor

Based on the non-linear regression analyses results, the correlation between the storey shear modification factor ($V_{st,mod}$) and period ratio (T_1/T_m) was found to be small or negligible in particular cases. Therefore, a new functional form with reduced number of terms is proposed and presented in Equation 6.7 for the estimation of inter-storey shear demands.

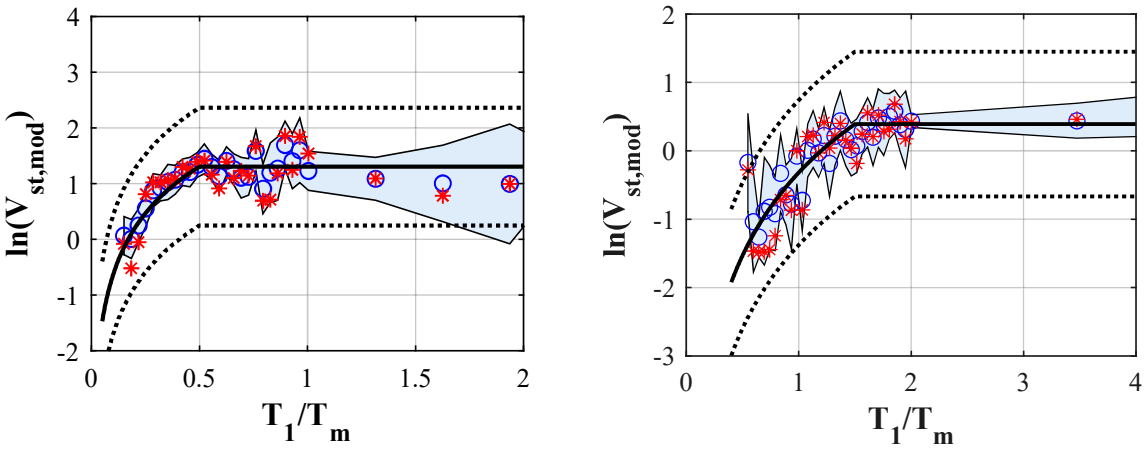
$$\ln V_{st,mod} = a + b \cdot \ln\left[\min\left(\frac{T_1}{T_m}, \xi_2\right)\right] \tag{6.7}$$

The regression coefficients for the simplified model is presented in Table 6.5 and the standard deviation of the dataset employed in this model is determined as $\sigma = 1.15$.

Table 6.5: Regression coefficients for the storey shear modification factor ($V_{st,mod}$), obtained using the simplified model.

a	b
-1.8110	0.4028

Figures 6.7a and 6.7b show the performance, against the observed response, of the new formulation for A1 (n = 6) and E1 (n = 20) building configurations, respectively. It is apparent from these figures that the plateau of the simplified model (Equation 6.7) is able to reproduce the tendency and variabilities of the building response to a reasonable degree.

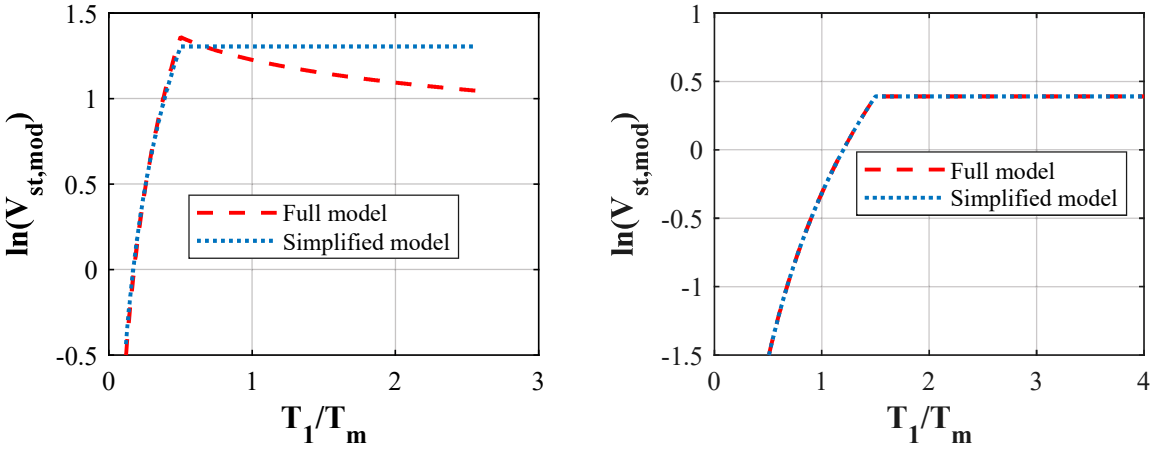


(a) 6 Storey A1 building (n = 6, m = 1).

(b) 20 Storey E1 building (n = 20, m = 1).

Figure 6.7: Mean storey shear modification ($V_{st,mod}$) against period ratios (T_1/T_m), obtained using the simplified prediction model of Equation 6.7, for a response modification factor of q = 3.

An alternative comparison between the median estimations of the full and simplified models associated with Equations 6.5 and 6.7 is offered in Figure 6.8. It can be appreciated from this figure that while an almost perfect match is observed for the 20-storey building, a maximum divergence in the $\ln(V_{st,mod})$ in the order of 10% is attained in the 6-storey building at the longest period ratio. The acceptance of this degree of over-conservativeness in storey shear estimations for low and medium-rise CLT buildings ought to be assessed in a case by case basis.



(a) 6 Storey (A1) building (n = 6, m = 1).

(b) 20 Storey E1 building (n = 20, m = 1).

Figure 6.8: Comparison between the results of mean storey shear modification ($V_{st,mod}$) against period ratios (T_1/T_m), obtained by means of the full and simplified models for a response modification factor of q = 3.

6.6 Concluding remarks

This chapter has investigated the influence of salient structural characteristics and ground-motion frequency content on the seismic shear force demands in multi-storey CLT buildings. Two parameters namely, base (V_{mod}) and storey ($V_{st,mod}$) shear modification factor were taken into account. Based on the extensive parametric investigations, the base shear modification factor (V_{mod}) was found explicitly dependent upon the ground-motion frequency content along the full range of period ratios (T_1/T_m) for all building configurations analysed. On the other hand, the evolution of inter-storey shear force demands ($V_{st,mod}$) against period ratio (T_1/T_m) for taller buildings of up to 16- and 20-storey, with the lowest level of panel fragmentation m = 1, was found to be ineffective in the long period range, $T_1/T_m > 1.25$.

The influence of key structural parameters, the level of panel fragmentation (m) and the building height (n) were also discussed. It was shown by means of developed prediction models

that a higher level of panel fragmentation was associated with a lower level of seismic shear demand (in both base and storey shear). This indicates that CLT panel modularization leads to a more resilient response by means of relative benefits of increased energy dissipation capacity of the building in seismic scenarios. Observations on the influence of building heights on the seismic shear demands in multi-storey CLT buildings showed that although taller buildings tend to have lower force demands in the short period range, larger demands were observed in the long period range. This is attributed to the increasing importance of higher mode effects with increasing structural height.

Finally, a range of regression models were developed to estimate the base (V_{mod}) and inter-storey ($V_{st,mod}$) shear modification factor as a function of the parameters that have the greatest influence on the seismic response of multi-storey CLT buildings. Furthermore, a set of simplified models with reduced number of terms was proposed that captures the general scaling features relatively well. In general, the proposed prediction models show a relatively good response on the data along the full range of ground-motion characteristics and salient structural parameters investigated.

Chapter 7

Assessment of Seismic Acceleration Demands

7.1 Introduction

A realistic assessment of seismic floor acceleration demands is fundamental for the appraisal of damage to non-structural elements and building contents. Besides, given the relative novelty of multi-storey tall timber buildings and their increasing popularity, a rigorous evaluation of their acceleration demands is all the more critical and timely. The review of past research presented in Chapter 2 has highlighted the proness of tall CLT buildings to high accelerations. Therefore, there is an urgent need to develop robust, yet simple, acceleration demand prediction procedures that can be incorporated into international standards and guidelines. To this end, this chapter investigates the evolution of seismic acceleration demands against ground-motion characteristics as well as the influence of a number of key structural parameters on floor acceleration demands in multi-storey CLT buildings.

The organization of this chapter is as follows: the first section describes the assessment of seismic acceleration demands and defines acceleration amplification factors employed and their relationship with ground-motion as well as key structural parameters. The non-linear regression models developed for the prediction of seismic acceleration demands are presented in the second section together with model simplifications where possible. Finally, a set of concluding remarks are summarised in the last part.

7.2 Assessment of peak floor accelerations

As with drift and force demands presented in the previous chapters, the extensive results from non-linear dynamic analyses carried out in this thesis were employed to identify the main scaling trends in the acceleration response of CLT buildings. To undertake these analyses, the acceleration amplification factor, γ, was calculated considering both spectral acceleration of ground-motion $S_a(T_1)$, and peak ground acceleration PGA. Although some previous research studies have investigated seismic acceleration demands using an amplification factor as a function of peak floor acceleration and peak ground acceleration (PGA), the use of spectral acceleration at the buildings fundamental period ($S_a(T_1)$) is also examined herein, since its favourable effects in reducing scatter of the response are well known. First, the amplification factor is derived as the ratio of the maximum floor acceleration, α_{max}, along the building height obtained from the non-linear response history analysis versus the spectral acceleration of the ground-motion corresponding to the fundamental vibration mode of the building, $S_a(T_1)$:

$$\gamma = \frac{\alpha_{max}}{S_a(T_1)} \tag{7.1}$$

The second amplification factor is derived as the ratio of the maximum floor acceleration, α_{max}, along the building height obtained from the non-linear response history analysis versus the peak ground acceleration of the original record applied at the base of the building:

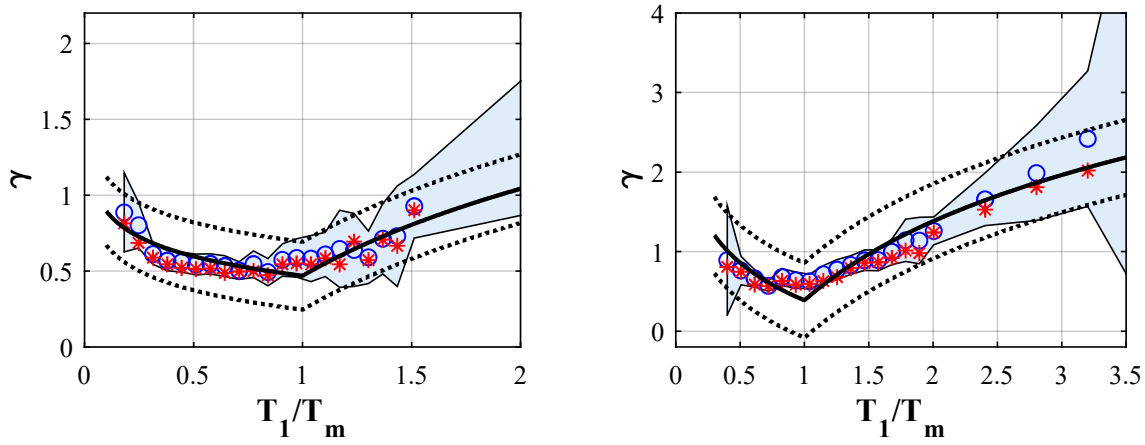
$$\gamma^{\circ} = \frac{\alpha_{max}}{PGA} \tag{7.2}$$

7.2.1 Peak floor accelerations

Amplification factor associated with $S_a(T_1)$, γ

The relationship between the acceleration amplification factor, γ, and the period ratio, T_1/T_m, is presented in Figure 7.1. Results are shown for two buildings, of 6 and 20 storeys, both designed with a single vertical joint per wall (i.e. m = 1). The shaded area in these figures shows the 95% confidence interval in the estimate of mean while open circles (o) and asterisk (*) symbols denote the individual bin mean and median values, respectively. Likewise, the dashed lines indicate ± 1 standard deviation of the mean amplification of peak acceleration demands for the non-linear model fitted to the data. The mean γ estimated by the fitted model is depicted as a solid line in Figure 7.1.

Figure 7.1 confirms the importance of taking into account the frequency content of the ground-motion, characterised herein by its mean period, T_m, when evaluating inelastic demands. Two clear behavioural regions are identified in Figure 7.1 depending on whether $T_1/T_m < 1$ or



(a) 6-storey A1 building.

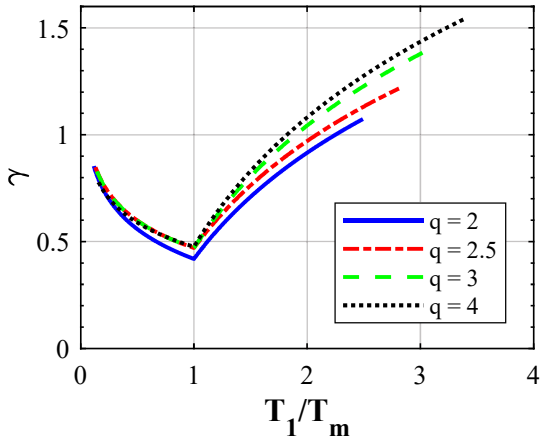
(b) 20-storey E1 building.

Figure 7.1: Mean peak floor acceleration amplification factor (γ) against period ratios (T_1/T_m), q = 3.

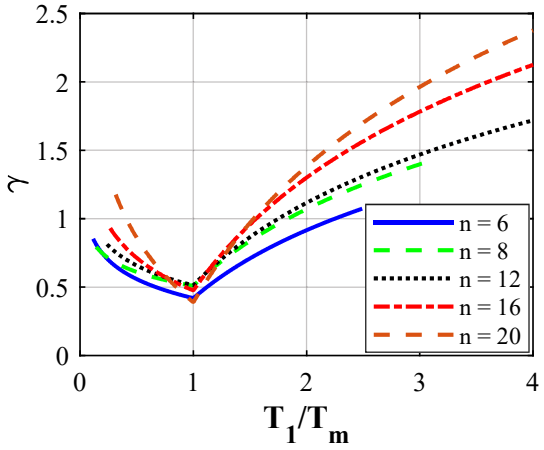
$T_1/T_m > 1$. Regardless of the building height, acceleration amplification demands decreases with increasing period ratios in the short period range ($T_1/T_m < 1$), reaching a minimum at $T_1 = T_m$, and increasing thereafter for longer periods. The response in the short period range, can be explained by the period lengthening associated with a plastic response coupled with the inherent scaling of the ground-motion spectral ordinates in this region. On the other hand, the increasing amplification of accelerations observed for $T_1 > T_m$ is a clear manifestation of the higher mode effects and it emphasizes the adequacy of T_m as a scalar frequency content indicator. The corresponding variation for other building heights can be seen in Appendix D.

The effect of the behaviour factor, q, on γ is investigated in Figure 7.2a. This figure shows the relationship between peak floor acceleration factors and period ratios, T_1/T_m, for various behaviour factors (i.e. $q = \{2, 2.5, 3, 4\}$). It is clear from Figure 7.2a that lower design behaviour factors are associated with lower acceleration levels when $T_1 > T_m$. Conversely, the effects of the behaviour factor are negligible for $T_1 < T_m$. This reinforces the previous observations regarding the importance of higher mode effects in the long period range and the mitigation of peak accelerations associated with the period lengthening which, as expected, is more pronounced when more inelastic behaviour takes place.

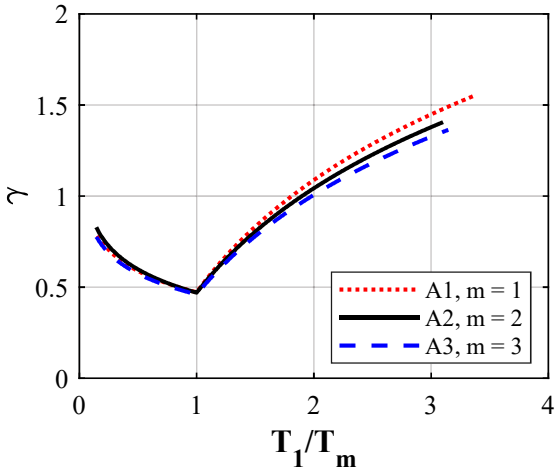
Likewise, Figure 7.2b offers an additional confirmation of the importance of higher mode effects on the determination of peak floor acceleration demands. The figure compares mean amplification factors of acceleration demands in buildings of different heights ($n = \{6, 8, 12, 16, 20\}$



(a) Mean γ and T_1/T_m relationship for various behaviour factors (q) in the 6-storey building.



(b) Mean γ and T_1/T_m relationship for various building heights (n), q = 3.



(c) Mean γ and T_1/T_m relationship for various joint density parameters (β) in the 6-storey building, q = 3.

Figure 7.2: Mean peak floor acceleration amplification factor (γ) against period ratios (T_1/T_m), for different key structural parameters.

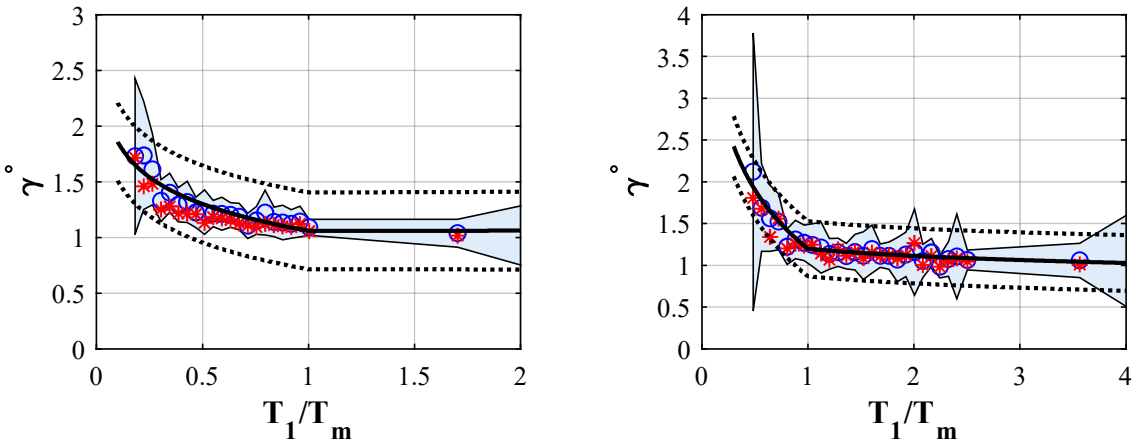
storeys) for a given number of vertical joint lines (m = 1). The same two spectral regions identified above are observed for all building heights in Figure 7.2a with higher mean accelerations occurring in taller buildings.

On the other hand, the level of panel fragmentation, characterized by β, is noticeable but less important. This can be appreciated in Figure 7.2c which summarizes the distribution of acceleration amplification factors, γ, in 6-storey building models with different wall arrangements conductive to β values of $\beta = \{2.1, 2.4, 2.8\}$ representing 1, 2 and 3 vertical joints per wall, re-

spectively (curves A1, A2, and A3). Again, the mitigating effects of higher levels of non-linear response in peak accelerations are evident from Figure 7.2c where higher β values (higher energy dissipation capacities) are associated with lower γ factors.

Amplification factor associated with PGA, γ°

The corresponding relationship between acceleration amplification factor associated with peak ground acceleration, γ°, and period ratio, T_1/T_m, is depicted in Figure 7.3. As before, 7.3a shows the correlation for 6-storey A1 building while 7.3b shows the correlation for 20-storey E1 building configuration. It is clear from Figure 7.3 that the acceleration amplification factor associated with peak ground acceleration decreases with increasing period ratios in the short period range, $T_1/T_m < 1$, as defined above. This correlation is also seen for the acceleration amplification factor (γ) determined as a function of spectral acceleration at the buildings' fundamental period, $S_a(T_1)$. On the other hand, in the long period range, $T_1/T_m > 1$, the change in the acceleration amplification factor (γ°) against period ratio (T_1/T_m) is found to be negligible in the case of 6-storey A1 building, while a minimal reduction in the amplification factor can be seen in the case of 20-storey E1 building in this range. The corresponding variation for other building heights can be seen in Appendix D.



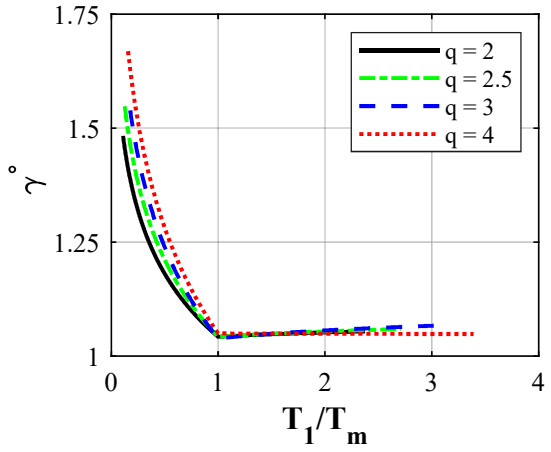
(a) 6-storey A1 building (n = 6, m = 1).

(b) 20-storey E1 building (n = 20, m = 1).

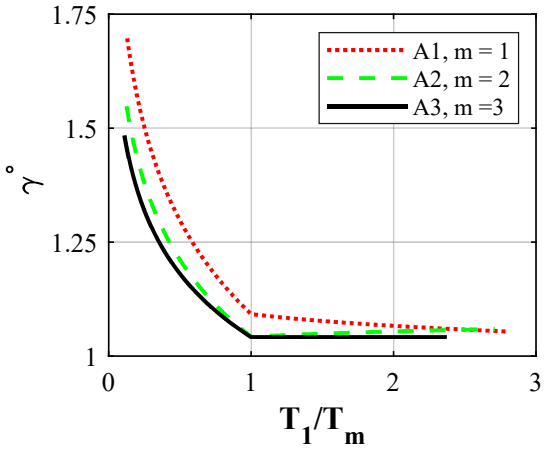
Figure 7.3: Mean peak floor acceleration amplification factor (γ°) against period ratios (T_1/T_m), q = 3.

The influence of structural parameters namely: the behaviour factor q, the number of storey n, and the level of intermediate vertical joint lines β is investigated for the acceleration amplification factor associated with peak ground acceleration, γ° can be studied with reference to Figure 7.4. Figure 7.4a presents a relationship between amplification factor and period ratio for

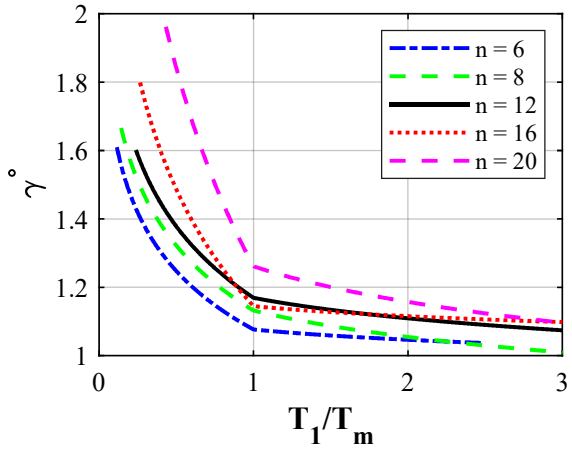
response modification factors considered in the design of the buildings. It can be appreciated from Figure 7.4a that higher acceleration demands (γ°) are expected with increasing design response modification factors in the short period range ($T_1/T_m < 1$). On the contrary, the effect of design behaviour factor becomes negligible in the long period range ($T_1/T_m > 1$).



(a) Mean γ° and T_1/T_m relationship for various behaviour factors (q) in the 6-storey building.



(b) Mean γ° and T_1/T_m relationship for various joint density parameters (β) in the 6-storey building, q = 3.



(c) Mean γ° and T_1/T_m relationship for various building heights (n), q = 3.

Figure 7.4: Mean peak floor acceleration amplification factor (γ°) against period ratios (T_1/T_m), for different key structural parameters.

Similarly, the correlation between acceleration amplification factor associated with peak ground acceleration γ°, and period ratio T_1/T_m for the level of intermediate vertical joint lines is demonstrated in Figure 7.4b. It is clear from Figure 7.4b that lower acceleration demands are

expected with higher joint density parameters suggesting that panel modularization improves the level of energy dissipation capacity in multi-storey CLT buildings. Besides, it can be seen that the difference on the acceleration demands between m = 1 and m = 2 is higher compared to corresponding demands between buildings designed for m = 2 and m = 3. More precisely, very minimal improvement in the structural response is seen from m = 2 to m = 3 along the full ranges of period ratio suggesting that panel lengths of 2.85 m or less provides best response in terms of energy dissipation in CLT wall structures. Finally, the influence of panel modularization becomes negligible for the period ratios higher than 2, ($T_1/T_m > 2$).

Finally, Figure 7.4c demonstrates the relationship between acceleration amplification factor γ°, and period ratio T_1/T_m for different building heights (n). It can be seen in Figure 7.4c that the amplification factor decreases with increasing period ratios in the short period range irrespective of the building height. On the other hand, the influence of building height is minimal or negligible in the long period range. All in all, high building storey numbers correspond to higher acceleration amplification factors along the full range of period ratios. This also confirms that taller CLT buildings are exposed to larger acceleration demands due to the higher mode effects.

7.3 Regression analysis

7.3.1 Prediction model for acceleration amplification factor γ

As with other demand parameters presented in previous chapters, a predictive model was developed in this chapter to estimate seismic acceleration demands associated with spectral acceleration at the buildings fundamental period (γ) in multi-storey CLT buildings by means of general statistical procedures. On the basis of preliminary parametric investigations, the joint density, β, the design behaviour factor, q, and the period ratio, T_1/T_m, were found to have non-negligible influence on the seismic acceleration demands experienced by CLT buildings. In line with this, the best-fit regression model described by Equation 7.3 is proposed herein.

$$\gamma = a \cdot \beta + b \cdot q \cdot \ln\left[\min\left(\frac{T_1}{T_m}, 1\right)\right] + c \cdot \ln\left[\max\left(\frac{T_1}{T_m}, 1\right)\right] \tag{7.3}$$

To this end, Table 7.1 summarizes the regression coefficients obtained by robust non-linear regression employing the functional form presented in Equation 7.3. The standard deviation of the dataset employed in this model is determined as $\sigma = 0.57$. All regression coefficients were tested for statistical significance and corresponding residual plots is presented in Figure 7.5.

It can be seen that no significant residual trend can be identified, suggesting that the model is able to explain the main trends of the acceleration response in CLT buildings, lending further support to the regression function employed.

Table 7.1: Regression coefficients for the peak floor acceleration (γ) in Equation 7.3.

a	b	c
0.4112	-0.0775	-0.0929

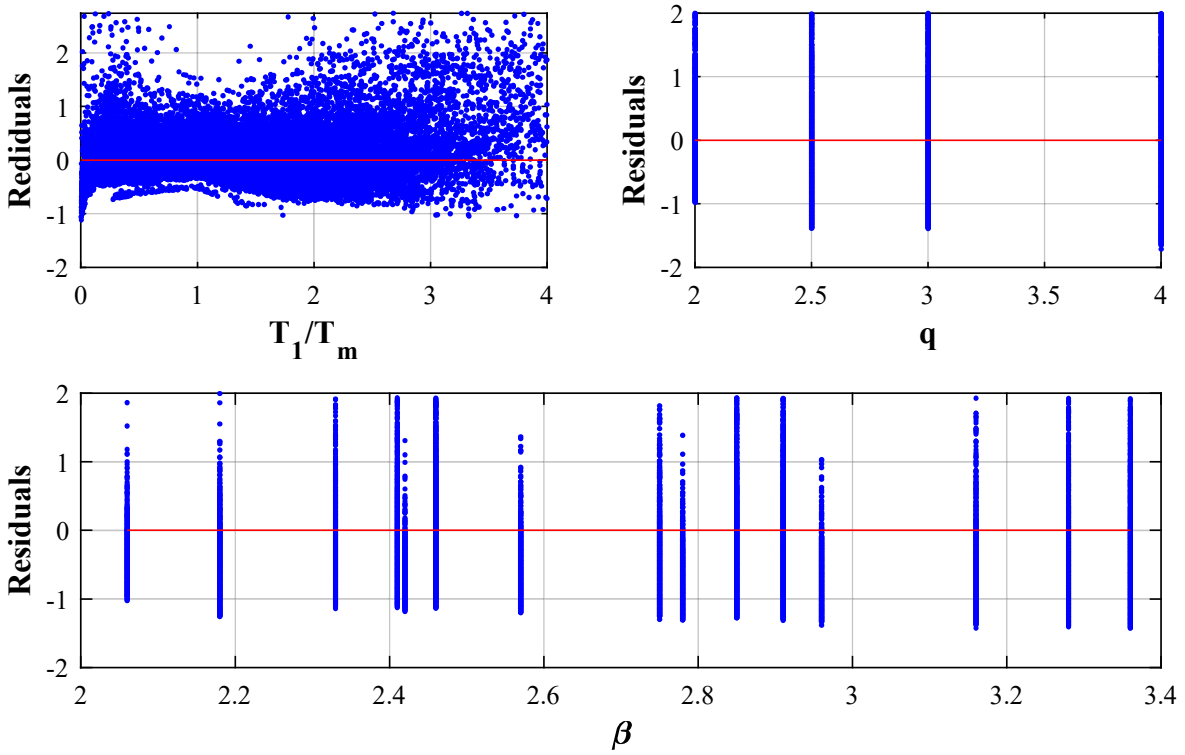


Figure 7.5: Residual plots for the amplification of peak floor acceleration (γ) prediction model.

7.3.2 Prediction model for acceleration amplification factor γ°

Based on parametric investigations, the same prediction model shown in Equation 7.4 is employed to investigate the evolution of acceleration demands associated with peak ground acceleration and period ratio. The standard deviation of the dataset employed in this model is calculated as $\sigma = 0.32$. The regression coefficients for this prediction model are presented in Table 7.2, whereas the residual plots for the most important parameters are shown in Figure

7.6. It is clear from residual plots that no significant trend is observed in residuals.

$$\gamma^{\circ} = a \cdot \beta + b \cdot q \cdot \ln\left[\min\left(\frac{T_1}{T_m}, 1\right)\right] + c \cdot \ln\left[\max\left(\frac{T_1}{T_m}, 1\right)\right] \tag{7.4}$$

Table 7.2: Regression coefficients for the peak floor acceleration (γ°) in Equation 7.4.

a	b	c
0.4365	-0.2568	-0.2064

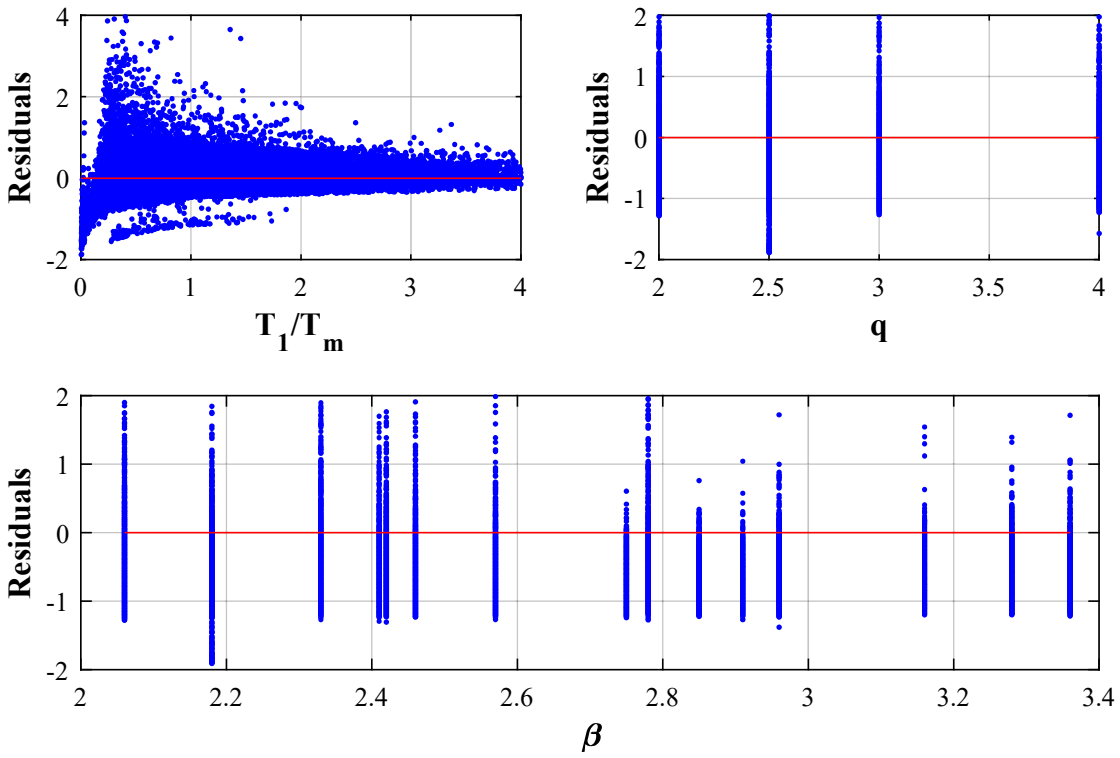


Figure 7.6: Residual plots for the amplification of peak floor acceleration (γ°) prediction model.

7.3.3 Model simplification

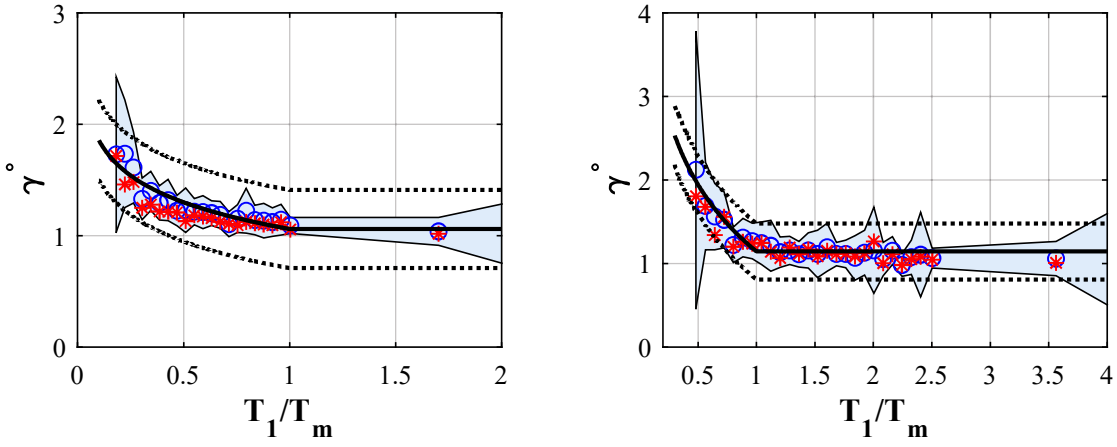
As discussed earlier, the non-linear evolution of acceleration amplification factor associated with the peak ground acceleration against period ratio is found to be minimal or negligible in some cases. A simplified model, therefore, incorporating reduced number of terms is proposed and examined in this section. The following functional form is derived for this purpose:

$$\gamma^{\circ} = a \cdot \beta + b \cdot q \cdot \ln\left[\min\left(\frac{T_1}{T_m}, 1\right)\right] \tag{7.5}$$

Table 7.3 presents corresponding regression coefficients for the simplified prediction model. Similarly, the standard deviation of the dataset employed in this model is determined as $\sigma = 0.32$. The performance of the simplified prediction model is shown in Figures 7.7a and 7.7b for building configurations A1 (n = 6) and E1 (n = 20), respectively. In these figures, it can be seen that the tendency along the period ratio is clearly obtained by means of the simplified model. A comparison between mean acceleration demands of initial and simplified models is presented for a short (6-storey) and a tall (20-storey) multi-storey CLT buildings in Figure 7.8. It is apparent from Figures 7.8a and 7.8b that the simplified model is able to capture all features of the full model prediction in the case of 6-storey A1 building. On the other hand, a maximum of 13% divergence is obtained in acceleration amplification factor for the 20-storey E1 building at the longest period ratio.

Table 7.3: Regression coefficients for the simplified peak floor acceleration amplification model (γ°).

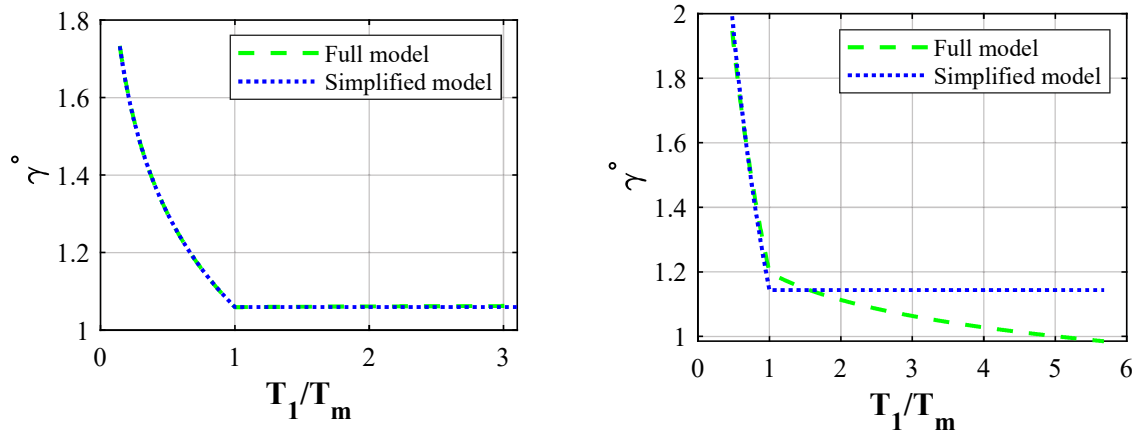
a	b
0.4256	-0.2711



(a) 6-storey A1 building (n = 6, m = 1).

(b) 20-storey E1 building (n = 20, m = 1).

Figure 7.7: Mean peak floor acceleration amplification factor (γ°) against period ratios (T_1/T_m), q = 3.



(a) 6-storey A1 building (n = 6, m = 1).

(b) 20-storey E1 building (n = 20, m = 1).

Figure 7.8: Comparison of full and simplified prediction models for mean peak floor acceleration amplification factor (γ°) against period ratios (T_1/T_m), q = 3.

7.4 Concluding remarks

The influence of ground-motion frequency content and key structural parameters on the seismic acceleration demands in multi-storey CLT buildings has been examined in this chapter. Two acceleration amplification factors were taken into account to identify the most accurate correlations between structural parameters and ground-motion characteristics. First, an amplification factor γ expressed as a function of maximum floor acceleration and spectral acceleration of the ground-motion at the buildings' fundamental period was employed. Second, an amplification factor γ° defined as the ratio of the peak floor acceleration obtained from non-linear response history analyses to the peak ground acceleration of ground-motion was considered. Based on the parametric investigations, the following conclusions can be offered:

While the acceleration amplification factor γ was found to be dependent upon the frequency content of the ground-motion along the full range of period ratios (T_1/T_m) for all building models examined, the evolution of acceleration demands for γ° was found to be very minimal or negligible in some cases in the long period range where $T_1/T_m > 1$. More precisely, acceleration amplification demands (γ) decreases with increasing period ratios in the short period range where it is less than 1, and it reaches its minimum at $T_1/T_m = 1$, and increasing thereafter in the long period range. On the other hand, while the same non-linear evolution of acceleration demands was observed in the short period range for γ°, different correlations can be identifiable in the long period range depending on the building configuration. This indicates the importance of ground-motion parameters selected for the estimation of seismic acceleration demands in multi-storey CLT buildings.

The influence of design response modification factor (q) on the acceleration demands (γ and γ°) showed that similar trends can be observed for different period ranges (T_1/T_m). For instance, lower acceleration demands are expected for lower design response modification factors in short period range ($T_1/T_m < 1$) for γ and in the long period range ($T_1/T_m > 1$) for γ°. Besides, the effects of the level of panel fragmentation (m) on the acceleration response were found to be that higher panel modularization leads to lower acceleration demands by the building and improved energy dissipation capacity for both acceleration demand parameters γ and γ°. Finally, observations on the evolution of acceleration demands for different building heights (n) demonstrated that taller buildings tend to experience higher acceleration demands along the full range of period ratios for both forms of amplification factors.

Regression models to estimate the evolution of seismic acceleration demands versus ground-motion characteristics were developed. Only the most significant parameters were considered while identifying the prediction equations. The developed regression models were examined for both p-values and residual plots and no p-value higher than 5% was obtained. Besides, no significant trend was observed in their residuals. Moreover, a simplified model was proposed for the acceleration amplification factor γ°, which still captures the main scaling features of full model with acceptable level of divergence in some cases. To this end, the proposed prediction models for acceleration amplification factors proved to be able to produce a relatively good response along the full range of ground-motion characteristics and the key structural parameters assessed.

Chapter 8

CLT Buildings Equipped with Flat Sliding Bearings

8.1 Introduction

Multi-storey cross-laminated timber (CLT) buildings are very efficient in resisting gravity loads, because their constituent CLT panels act as solid load-bearing components. The relative good seismic performance of low and mid-rise multi-storey CLT buildings has been proved by means of full-scale experimental shake table tests and multiple past numerical studies. On the other hand, the preceding chapters of this thesis have highlighted the potentially undesirable acceleration response of multi-storey CLT buildings exemplified by large values of peak floor accelerations. Therefore, there is a need to provide an economical and effective means of controlling these peak seismic forces and accelerations. To this end, this chapter investigates the potential benefits of providing seismic dislocation layers by means of flat sliding bearings, on the seismic response of buildings. With this purpose, the previously designed multi-storey CLT buildings are re-configured to incorporate flat sliding bearing elements at their base and at targeted levels along their height. Subsequently, a seismic demand assessment focused on peak shear forces and accelerations is conducted.

This chapter employs a selected sub-set of 10 CLT building configurations (all designed for a response modification factor of q = 3) taken from the building database described in Chapters 3 and 4. As before, the influence of key structural parameters and ground-motion frequency content on the seismic response of CLT buildings with multiple-sliding sections is evaluated by means of over 16000 non-linear response history analyses.

This chapter is composed of six sections. It starts by describing the design and numerical modelling approach followed to incorporate flat sliding bearing elements into the CLT cores.

A comparison between CLT buildings with and without flat slide bearings is presented in the second section. The third section assesses the non-linear seismic displacement demands in CLT buildings equipped with multiple-sliding section, whereas the fourth and fifth sections investigate their seismic force and acceleration demands, respectively. Finally, a comparison between conventional and multiple-sliding configurations is offered and the chapter ends by highlighting the conclusions of the investigation.

8.2 Design and numerical modelling formulation

8.2.1 PTFE slide bearing design

PTFE (Polytetrafluoroethylene) slide bearings have been commonly used in the past to accommodate movements brought about by thermal, pre-stressing, creep, and shrinkage effects in bridge structures. On the other hand, the use of seismic isolation systems employing PTFE slide bearings has been proposed nearly 10 years ago [22]. The low friction coefficient of PTFE makes it an ideal material to introduce sliding sections in buildings where their own self weight is not a major design constraint. PTFE slide bearings consist of two elements of PTFE layers, the upper and the lower element that work by sliding against each other. The size of the upper PTFE layer is typically smaller than the lower PTFE layer. The difference in size is employed to accommodate predicted/allowable movement for a given structure. Figure 8.1 depicts a typical configuration of a PTFE slide bearing element produced by Fluorotec [72]. In general, both the the top and the bottom sliding plates are made of 2.5 mm thick PTFE layers, bonded to 3 mm thick carbon or stainless steel plates. PTFE slide bearing pads were selected in this study due to their relative benefits in terms of the simplicity of bearing design, ease of fabrication and installation, cost effectiveness compared to alternative applications, low maintenance costs, and avoidance of fatigue failure [72].

Figure 8.2 depicts the new CLT building configurations equipped with multiple sliding sections. Two bearing elements (located at the edges of each wall panel) are found adequate to transfer all the vertical and overturning loads in general. A schematic of the PTFE slide bearing element is provided in Figure 8.1 for the 6-storey (A1) CLT building as an example. The main design variable of PTFE slide bearing is the bearing area. To calculate the required bearing area, the total vertical load applied on the bearing element and the load carrying capacity of the bearing element are required. The load carrying capacity of the bearing element shown in Figure 8.1, obtained from the manufacturer [72] for a reinforced PTFE is 184 kg/cm^2 [72]. As an example, vertical loads at the base of the structure and at its mid-height are calculated as 84.4 tonne-force and 57.0 tonne-force for the A1 building, respectively. Therefore, the correspond-

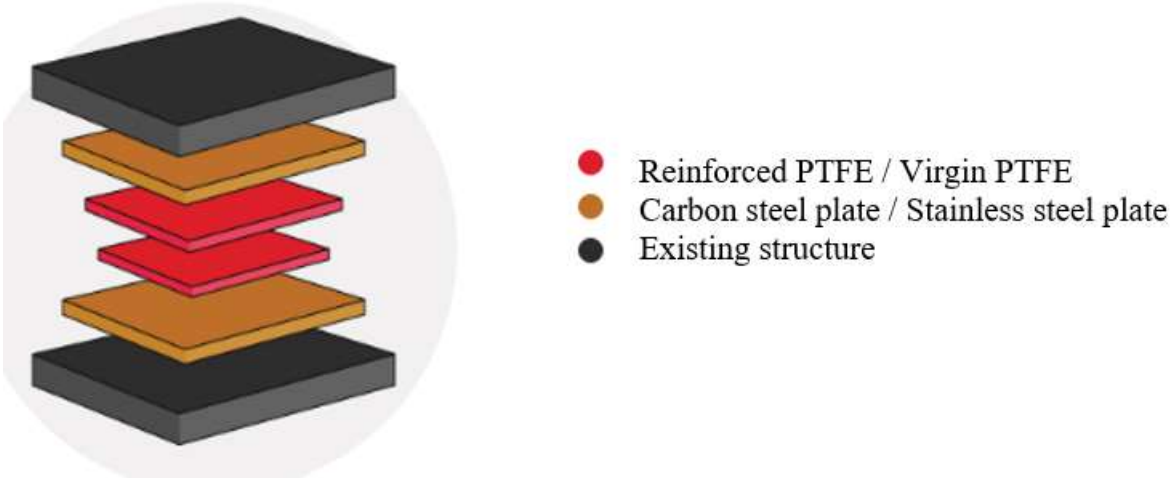


Figure 8.1: A typical configuration of PTFE Slide bearings [72].

ing bearing area for the third and ground floor levels in the A1 building were determined as 310 cm^2 and 460 cm^2, respectively. Since two PTFE slide bearing elements are placed at each corner of the CLT wall panels, each bearing element should have 77.5 cm^2 and 115 cm^2, at the mid-height and at the base of 6-storey A1 building configuration, respectively. This translates into bearings of 0.12 m by 0.10 m at the base of the structure. Additionally, a steel plate is employed to transfer the uplift forces while allowing the the wall panels to slide sideways by means of a slotted connection. A connection detail that can be potentially employed between the CLT panel and the bearing pad is shown in Figure 8.3.

8.2.2 Numerical modelling

A maximum drift of 0.5% which is consistent with the design of conventional buildings was considered for buildings equipped with PTFE sliding sections. The coefficient of friction of PTFE slide bearing has been reported to be between 0.02 and 0.2 in past experimental studies [22, 11, 84]. A friction coefficient of 0.1 was chosen herein as recommended in [12]. By considering a maximum drift of 0.5%, the maximum displacements at the third floor and roof of the 6-storey building are 0.05 m and 0.11 m, respectively. Also, the lateral load required for the bearing element to start sliding can be calculated with reference to the vertical load and the PTFE coefficient of friction. Based on these assumptions, the hysteretic behaviour properties of each bearing element were determined depending on the location of each PTFE slide bearing element as reported in Table A.19. With reference to the 6-storey A1 building, the hysteresis of the bearing element located at the base of the structure is presented in Figure 8.4. It can be appreciated from this figure that besides the PTFE plates, a stopper element is provided in

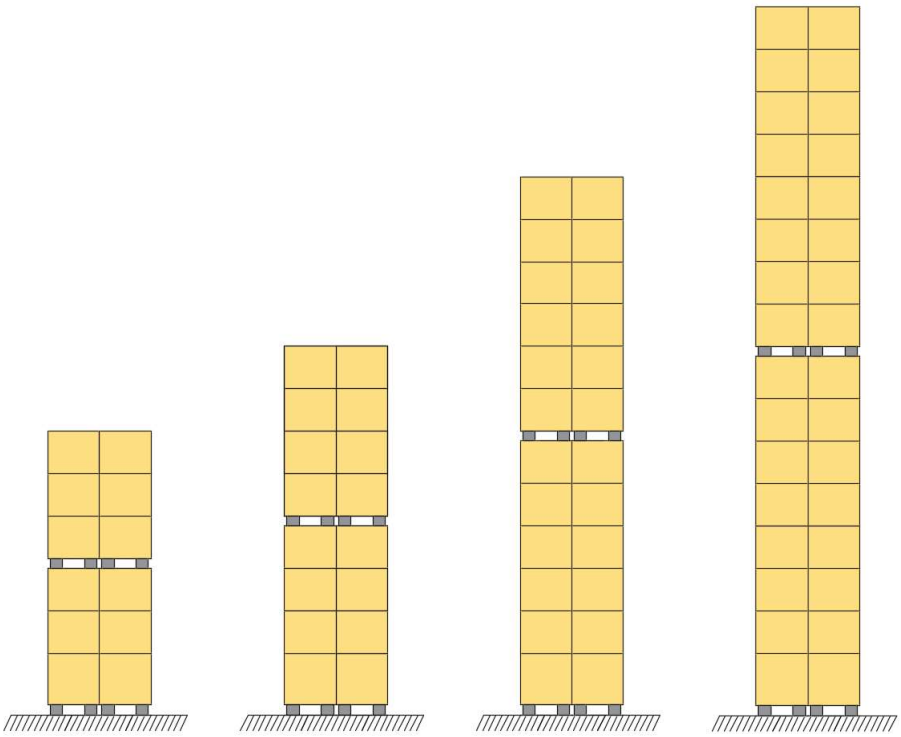


Figure 8.2: Location of flat sliding bearing elements in building models (6, 8, 12 and 16 storeys).

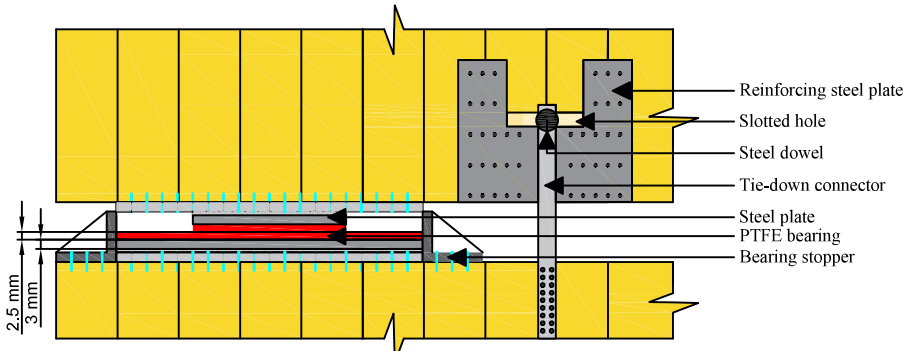


Figure 8.3: A possible connection detail of a PTFE slide bearing.

order to limit the probability of exceedance of allowable displacement as defined above. It is important to note that, the use of stoppers in base-isolated buildings is discouraged in Europe [8] but enforced in North American practice. In order to study these effects, two different cases were studied namely: i) bearing elements with stoppers and ii) when the stopper stroke is not exhausted or when there is no stopper in the sliding bearing.

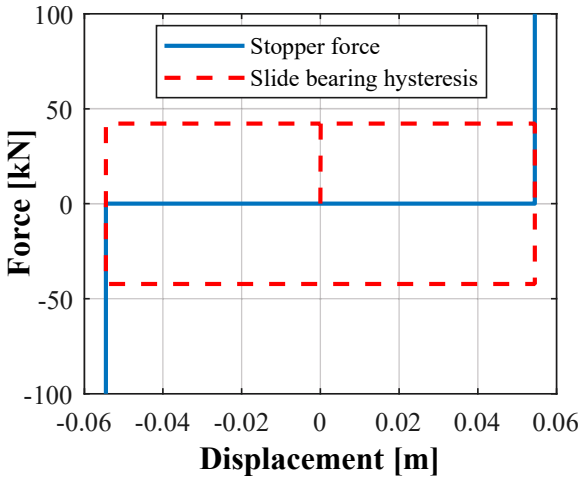


Figure 8.4: Hysteretic material behaviour of isolation bearing element and stopper in shear.

In order to simulate the response of the PTFE sliding bearings, a gap material model and a bi-linear material model were combined in series and implemented into a single two node element in OpenSees [59]. Figure 8.5 shows the results of non-linear static analyses on the conventional and isolated 6-storey A1 buildings. It is clear from this figure that the PTFE slide bearing incorporated into the 6-storey conventional structure, starts sliding after the design base shear of the conventional structure, and it slides until the predicted/allowable displacement is attained in the stopper, beyond this point, increased levels of lateral forces are resisted by the wall. A design wind load calculated on the basis of an average wind velocity of 25 m/s ($V_{b,map}$) and following general procedures outlined in Eurocode 1 [28] is also shown Figure 8.5 for comparison.

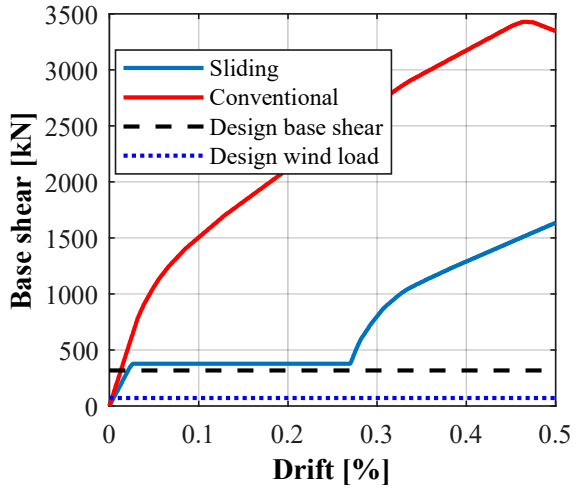


Figure 8.5: Non-linear pushover curves of 6-storey buildings with and without flat sliding bearing elements.

8.2.3 Static and Dynamic Response of CLT buildings with sliding sections

A comparative assessment between conventional and seismically isolated buildings is illustrated in this section. Figure 8.6 shows a comparison of structural periods associated with the first vibration mode of both type of structures. It is clear from this comparison that fundamental periods associated with multi-storey CLT buildings equipped with multiple sliding sections are elongated by factors between 1.25 and 1.5 in comparison with multi-storey CLT building configurations, as expected.

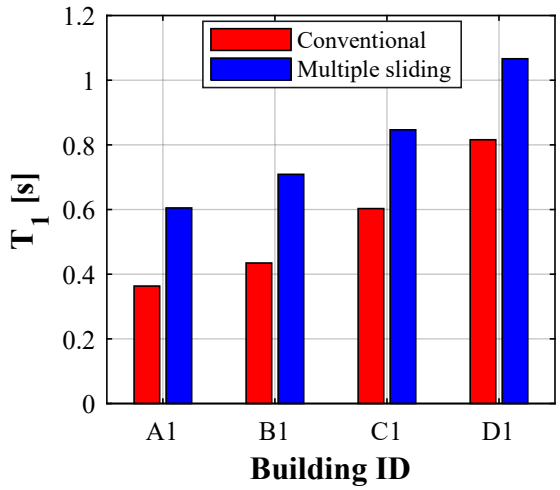
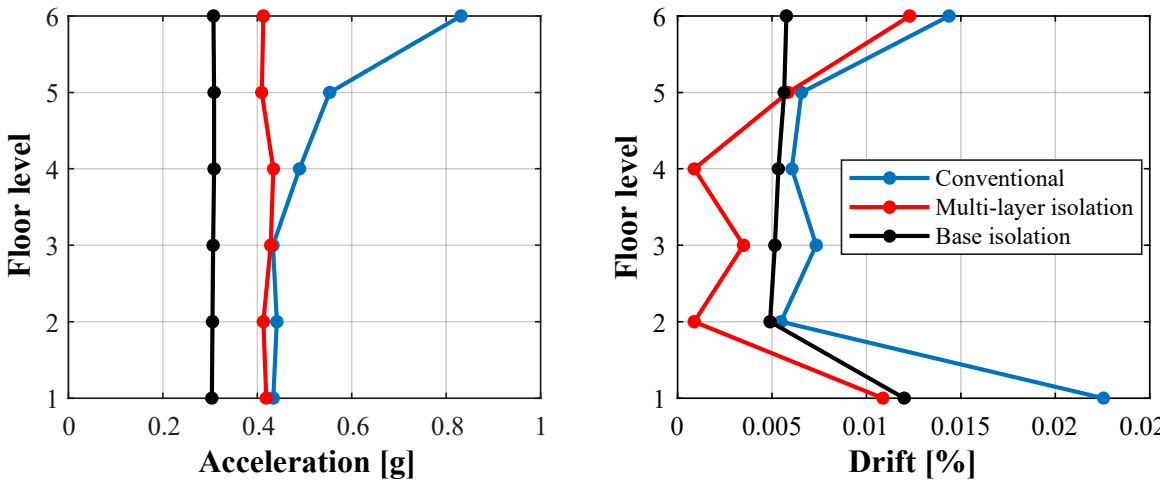


Figure 8.6: Fundamental period comparison of CLT buildings equipped with and without multiple sliding sections.

Likewise, a comparison between the response of the A1 CLT multi-storey buildings with and without multiple sliding sections in terms of peak floor accelerations, and inter-storey drifts is shown in Figure 8.7. Additionally, the influence of the more conventional base isolation only approach on the structural response is presented in this figure. The Imperial Valley-02 ground motion with 0.25 g PGA was employed for this illustrative purposes. It is clear from this figure that a more uniform distribution of floor accelerations along the building height is expected in the 6-storey CLT building equipped with multiple flat sliding bearing elements. Moreover, a maximum of 29% reduction in the acceleration response of this building is achieved between the conventional building response and the implementation of multi-level sliding.

Furthermore, Table 8.1 presents the structural response difference between conventional and isolated buildings in percentage. To this end, these corresponding results and comparisons prove that the incorporation of flat slide bearing elements within conventional CLT multi-storey buildings limits the drift, acceleration, and shear response of CLT buildings located in seismi-



(a) Comparison of peak floor accelerations, α_{max}

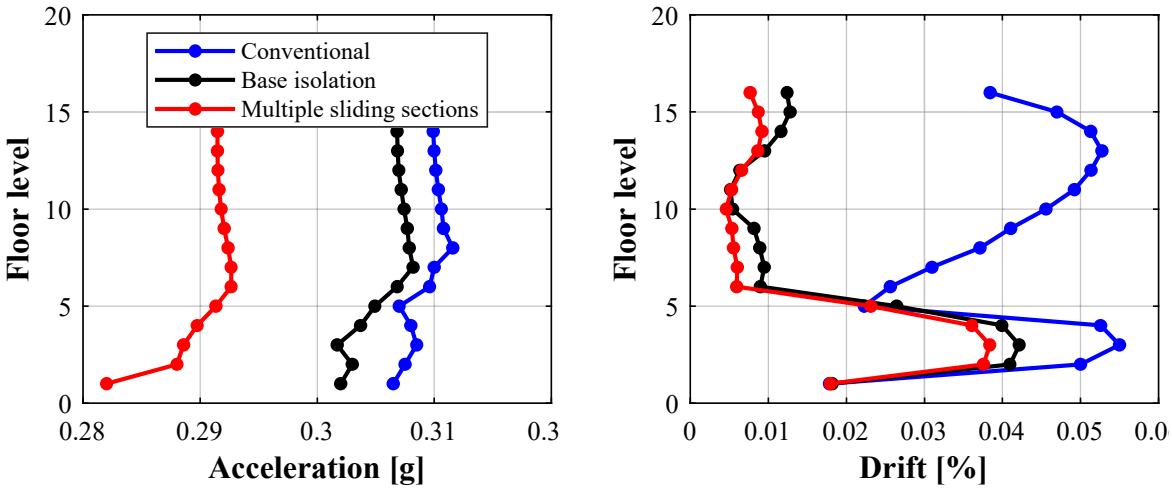
(b) Comparison of maximum inter-storey drifts, θ_{max}.

Figure 8.7: Seismic response comparison of 6-storey (A1) CLT buildings with and without flat sliding bearing elements.

cally prone areas. In addition, employing multi-layer sliding provides a better response in terms of inter-storey drifts in most floor levels compared to only base isolation, which plays a crucial role in modern seismic design and assessment.

Likewise, the influence of incorporating sliding sections into tall multi-storey CLT buildings can be seen in Figure 8.8. A comparison of the acceleration and drift responses of the 16-storey CLT buildings that are designed with base isolation, multiple sliding sections and monolithical without sliding. These comparisons give further evidence that incorporating multiple sliding sections, compared to only base isolation, improves the structural response in terms of peak floor accelerations and inter-storey displacement ratios. While a 2% improvement is observed by means of incorporating base isolation alone, a nearly 10% reduction is observed when a multiple sliding configuration is considered.

Finally, a preliminary comparison of peak floor accelerations and shear forces between conventional and isolated 6-storey CLT buildings subjected to a wider set of ground-motions is presented in Figure 8.9. This figure summarizes the results of 1656 non-linear response history analyses using the suite of records described in Chapter 4. A scatter plot of peak floor accelerations (α_{max}), base shear forces (V_b), and inter-storey displacement ratios (θ_{max}) with exponential trend lines obtained by means of least-square regression are presented. It is clear from Figure 8.9 that significantly less seismic acceleration, base shear and inelastic drift demands are expected in the CLT structure with sliding sections. These results provide preliminary ev-



(a) Comparison of peak floor acceleration, α_{max}.

(b) Comparison of inter-storey drifts, θ_{max}.

Figure 8.8: Seismic response comparison of 16-storey (D1) CLT buildings with and without flat sliding bearing elements.

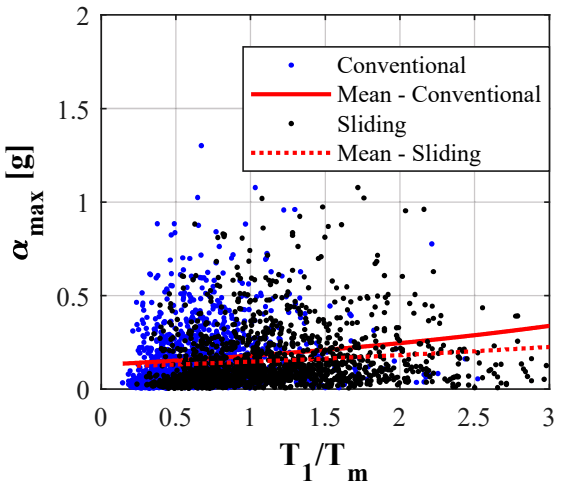
idence of the benefits of employing multiple-sliding sections and warrant the detailed studies presented in the following sections.

Table 8.1: Structural response comparison of multi-storey CLT buildings equipped with and without flat slide bearings.

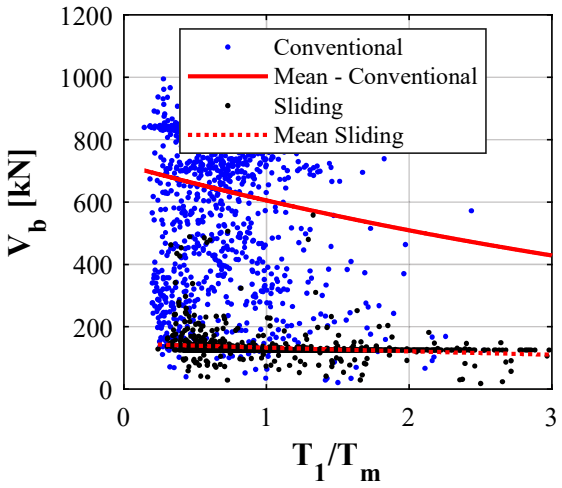
	Conventional	Multi-layer isolation	Difference [%]
Drift [%]	0.014	0.012	15
Acceleration [g]	0.254	0.182	29
Base shear [kN]	776.72	358.12	54

8.3 Assessment of seismic drift demands

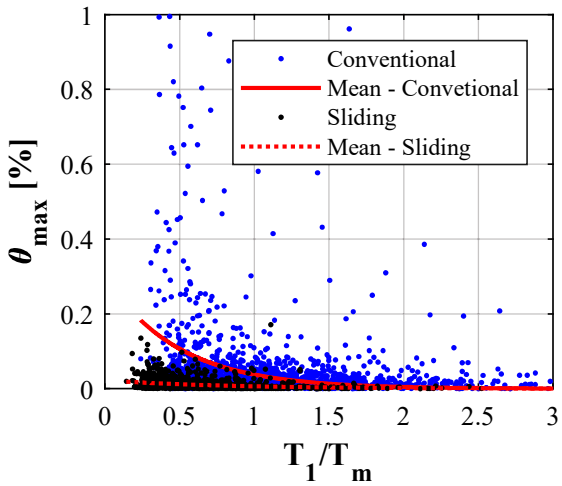
This section investigates the inelastic deformation demands (θ_{max}) in multi-storey CLT buildings equipped with multiple sliding sections. As before, the maximum inter-storey drifts (θ_{max}) were obtained by means of non-linear response history analyses, from which the correlations between the maximum drifts (θ_{max}) and period ratio (T_1/T_m) are identified. First of all, the results are distinguished between those cases where: i) no contact between the PTFE bearing element and the stopper takes place; and ii) contact between the PTFE bearing element and the stopper occurs. Then the corresponding drift response is examined in these two data bins with attention to the influence of the ground-motion frequency content and salient structural



(a) Distribution of peak floor accelerations (α_{max}) against period ratio (T_1/T_m).



(b) Distribution of maximum base shear forces (V_b) against period ratio (T_1/T_m).



(c) Distribution of maximum inter-storey drifts (θ_{max}) against period ratio (T_1/T_m).

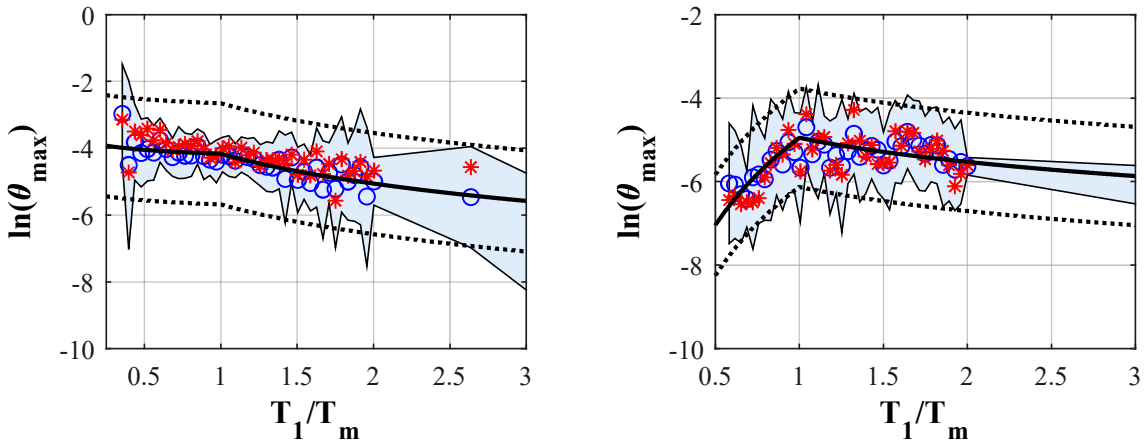
Figure 8.9: Comparison of peak floor accelerations (α_{max}), base shear forces (V_b), and inter-storey drifts (θ_{max}) obtained from extensive non-linear response history analyses on the 6-storey A1 buildings with and without slide bearings.

parameters.

8.3.1 Inter-storey drift demands

Figure 8.10 shows the variation in maximum inter-storey drift ($\ln(\theta_{max})$) as a function of the period ratio (T_1/T_m) for the 6-storey (A1) and 16-storey (D1) buildings designed with a response modification factor of q = 3. It is clear from this figure that the evolution of drift demands is non-linear along the full range of period ratios regardless of the building height, and that the

degree of this non-linearity is more pronounced for taller buildings. Figure 8.10a shows that the influence of the ground-motion frequency on the inelastic drift demands is small at lower period ratios (T_1/T_m) for the 6-storey A1 building. This can be attributed to the lower demand levels that are expected compared to conventional buildings due to sliding. On the other hand, lower level of drift estimations are expected because of increasing divergence between fundamental period and the mean period of ground-motion in the long period range where $T_1/T_m > 1$. Besides, the lower demands in the long period range are also a manifestation of the lower influence of higher modes in low-to-mid rise buildings. A different variation in $\ln(\theta_{max})$ can be seen in Figure 8.10b for the 16-storey (D1) building as a function of period ratio, T_1/T_m. Inter-storey drifts increase with increasing period ratio in the short period range, peaking at $T_1/T_m = 1$, and decreasing thereafter along the period ratios higher than 1 ($T_1/T_m > 1$).

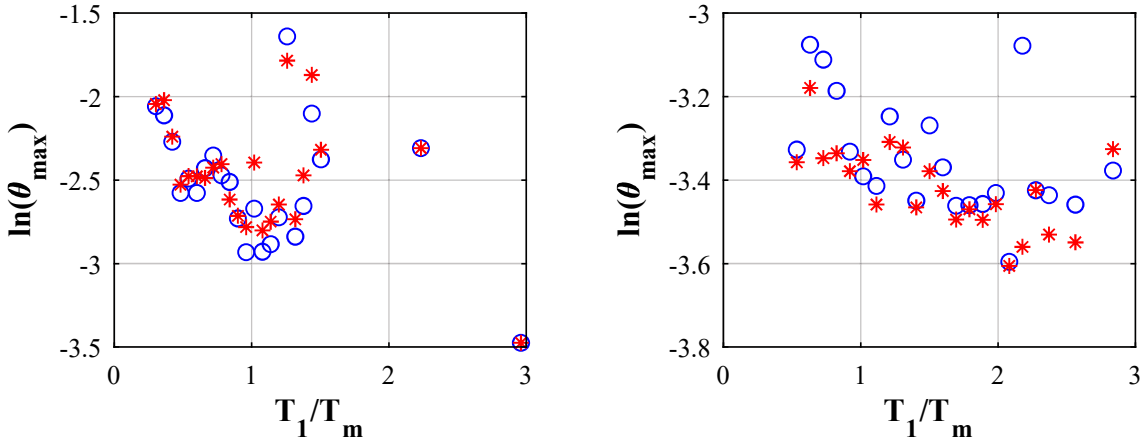


(a) 6-storey A1 building.

(b) 16-storey D1 building.

Figure 8.10: Maximum inter-storey drift ($\ln(\theta_{max})$) against period ratio (T_1/T_m) when there is no contact between the isolation bearing and the stopper.

On the other hand, Figure 8.11 presents the corresponding results associated with cases where there is contact between the PTFE slide bearing element and the stopper. No regression model is proposed for these cases since they constitute an undesirable response and represent less than 17% of the overall results. However, the mean and median values of each data bin are plotted. Figure 8.11a shows the results for 6-storey A1 building, whereas the results for 16-storey D1 building are shown in Figure 8.11b. Importantly, similar levels of inter-storey drift reductions are expected, even when the isolation bearing element hits the stopper at the maximum allowable displacement.



(a) 6-storey A1 building.

(b) 16-storey D1 building.

Figure 8.11: Maximum inter-storey drift ($\ln(\theta_{max})$) against period ratio (T_1/T_m) when there is contact between the isolation bearing and the stopper.

8.3.2 Regression analysis

Inter-storey drift prediction model

The following prediction model is proposed with the parameters that are found to have important influence on maximum inter-storey drifts:

$$\ln(\theta_{max}) = a + b \cdot \beta + c \cdot \lambda + d \cdot \ln\left[\min\left(\frac{T_1}{T_m}, 1.0\right)\right] + e \cdot \ln\left[\max\left(\frac{T_1}{T_m}, 1.0\right)\right] \tag{8.1}$$

where $\ln(\theta_{max})$ is the logarithmic maximum inter-storey drift associated with buildings with multiple sliding sections without stoppers; β is the joint density parameter defined in previous parts of this thesis; α is the building aspect ratio; T_1/T_m is the period ratio; and a, b, c, d, e are statistical regression coefficients. The statistically significant regression coefficients associated with Equation 8.1 are presented in Table 8.2. The standard deviation of the dataset employed in this model is σ = 1.43 %. Figure 8.12 shows the residual plot of the parameters used in the estimation of maximum inter-storey drifts together with the mean trend line (in red). It can be appreciated from this figure that no significant trend in residuals are observed.

Table 8.2: Regression coefficients for the non-linear displacement demands ($\ln(\theta_{max})$) in Equation 8.1.

a	b	c	d	e
-4.6784	0.6849	-0.287439	0.44668	-1.1602

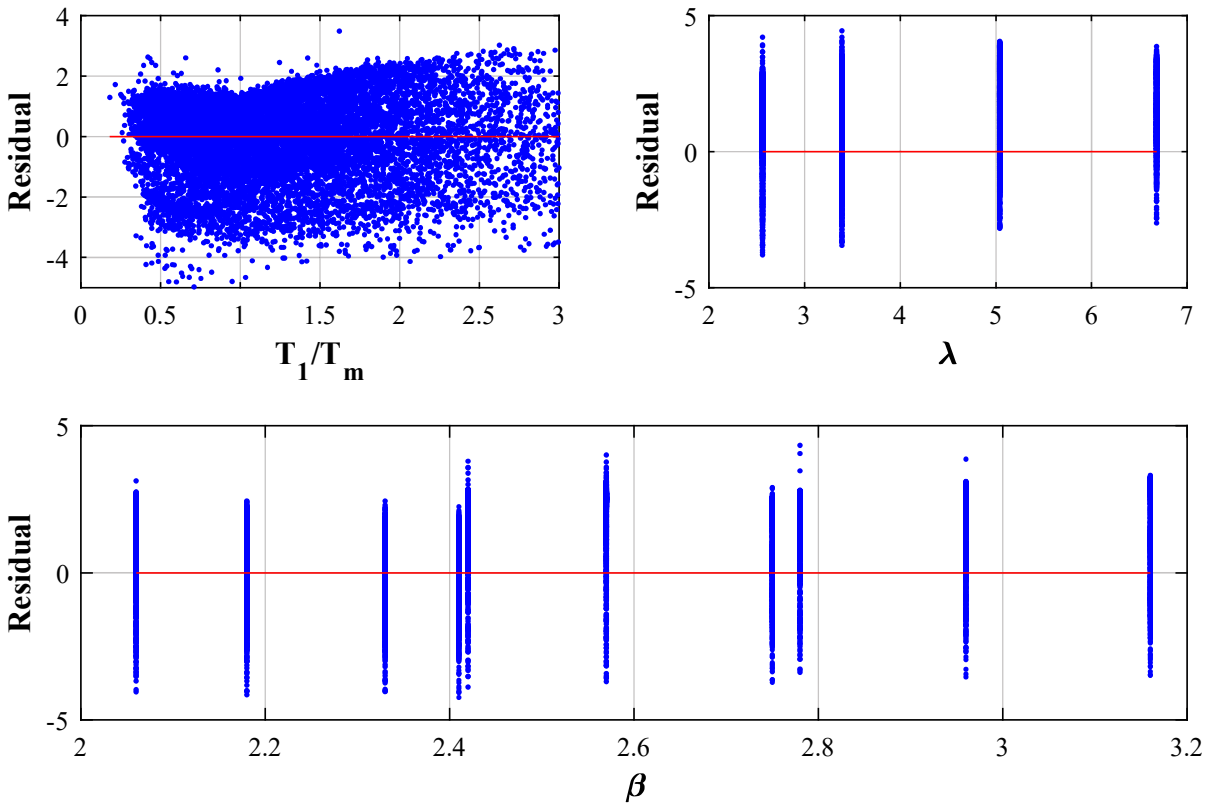


Figure 8.12: Residual plots for the maximum inter-storey drift ($\ln(\theta_{max})$) prediction model.

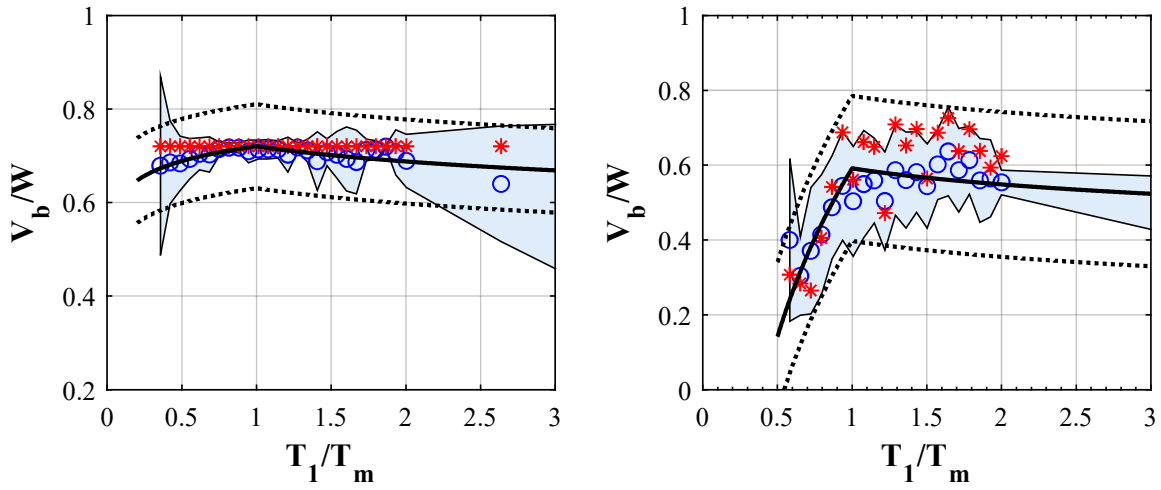
8.4 Assessment of seismic shear demands

The distribution of inelastic seismic force demands in multi-storey CLT buildings equipped with flat sliding bearing elements is investigated in this section. The normalized base shear, V_b/W, which is the ratio between the base shear and the corresponding building weight is considered as the seismic force demand parameter in this section. As with the maximum inter-storey drifts, the relationship between normalized base shear and period ratio (T_1/T_m) is evaluated in two categories, as defined before depending on whether stoppers are provided or not.

8.4.1 Base shear demands

The variation in normalized base shear (V_b/W) for the 6-storey (A1) and 16-storey (D1) buildings as a function of the period ratio (T_1/T_m) is shown in Figure 8.13. Figure 8.13a presents relationship between normalized base shear (V_b/W) and period ratio for the 6-storey A1 building, whereas the corresponding results for 16-storey D1 building are presented in Figure 8.13b. It is important to note that results employed in this parametric investigation are associated with

no contact between the PTFE slide bearing and the stopper. It can be appreciated from Figure 8.13a that higher seismic force demands are expected with increasing period ratio (T_1/T_m) in the short period range ($T_1/T_m < 1$). Besides, the largest shear force demands are expected at $T_1/T_m = 1$, and a very small decrease in force demands is seen in the long period range ($T_1/T_m > 1$). This relationship is found to be consistent with the seismic shear demand estimations in conventional multi-storey CLT buildings. On the other hand, a similar relationship is seen in the case of 16-storey D1 building in the short period range ($T_1/T_m < 1$), however the influence of ground-motion period ratio on the inelastic force demands are greater in the case of high-rise buildings. Besides, less shear demands are expected in the 16-storey building with decreasing period ratios in the short period range and force demands is almost negligibly influenced by the ground-motion period in the long period range ($T_1/T_m > 1$). It is important to note that these findings highlight the importance of inelastic demands in low-to-mid rise CLT buildings.



(a) 6-storey A1 building.

(b) 16-storey D1 building.

Figure 8.13: Mean normalized base shear forces (V_b/W) against period ratio (T_1/T_m) when there is no contact between the isolation bearing and the stopper.

Figure 8.14 presents the results associated with numerical predictions where the PTFE slide bearing elements hit to the stopper at the maximum allowable displacement employed in the design of slide bearing elements. Only mean and median values of each data bin are presented in these figures. It is important to note that, compared to results shown in Figure 8.13, very high seismic shear demands are observed in Figure 8.14. This is attributed to the influence of stoppers employed in the design of flat sliding bearing elements. More precisely, when seismically isolated multi-storey CLT buildings are subjected to very strong ground-motions, very high base shear forces are generated due to a contact between the structure and the stopper of

slide bearing elements. Because of this detrimental influence, the use of stoppers is prohibited in Europe [8].

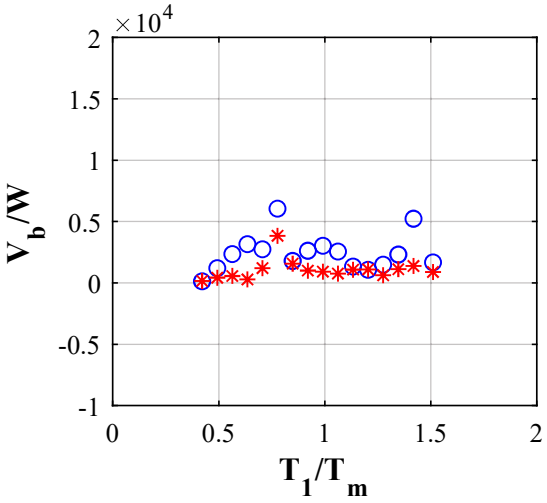


Figure 8.14: Mean normalized base shear forces (V_b/W) against period ratio (T_1/T_m) when there is contact between the isolation bearing and the stopper.

8.4.2 Regression analysis

Normalized base shear prediction model

On the basis of statistical investigations, the following prediction model is proposed for the estimation of seismic force demands associated with moderate seismic intensities in multi-storey CLT buildings with multiple sliding sections:

$$V_b/W = a + b \cdot \ln\left[\min\left(1.2 \cdot \frac{T_1}{T_m}, 1.0\right)\right] + c \cdot \ln\left[\max\left(1.2 \cdot \frac{T_1}{T_m}, 1.0\right)\right] \tag{8.2}$$

The statistically significant coefficients associated with Equation 8.2 are presented in Table 8.3. The standard deviation of the dataset employed in this model is $\sigma = 0.128$ kN/kN. To this end, residual plot of the parameters used in the prediction model can be seen in Figure 8.15. The central tendency of the residual plot confirms the suitability of the regression model developed.

Table 8.3: Regression coefficients for the non-linear shear demands (V_b/W) in Equation 8.2.

a	b	c
6.0515	-7.9297	-3.3497

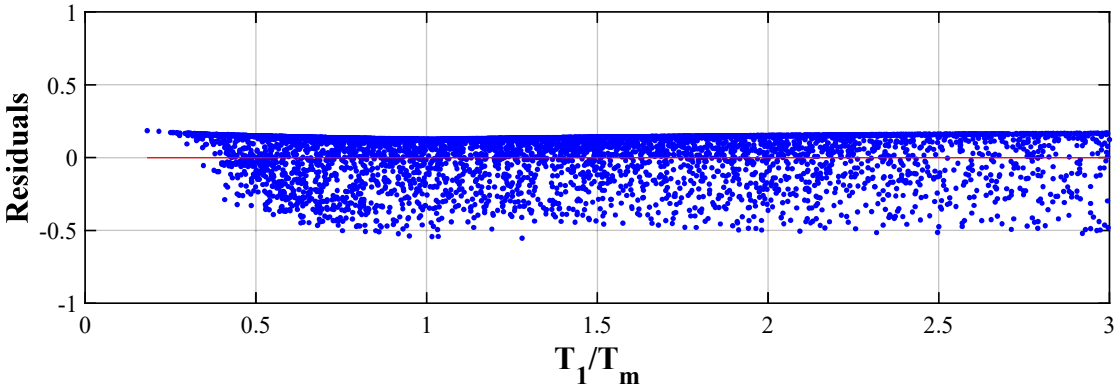


Figure 8.15: Residual plots for the normalized base shear (V_b/W) prediction model.

8.5 Assessment of acceleration demands

8.5.1 Acceleration amplification factor

The evolution of acceleration demands against structural characteristics in multi-storey CLT buildings equipped with flat sliding bearing elements is investigated in this section. An acceleration amplification factor associated with the peak ground acceleration of ground-motion at the base of the building (PGA) is selected for this purpose. The amplification factor is shown in the following expression:

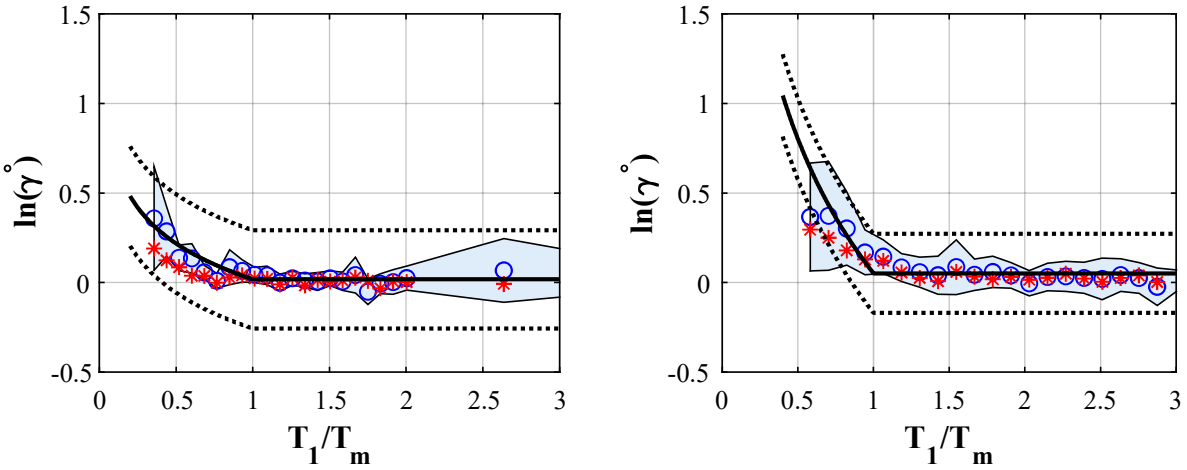
$$\gamma^{\circ} = \frac{\alpha_{max}}{PGA} \tag{8.3}$$

As with drift and force demands, the relationship between acceleration amplification factor and ground-motion mean period is evaluated.

8.5.2 Seismic acceleration demands

Figure 8.16 presents the evolution of acceleration demands ($\ln(\gamma^{\circ})$) against ground-motion characteristics for the 6- (A1)and 16-storey (D1) building configurations. It is clear from these figures that similar observations are obtained in comparison with conventional multi-storey CLT buildings. In both cases, the acceleration amplification factor decreases at larger ground-motion mean periods and no effect of amplification factor is evident in the very long period range ($T_1/T_m > 1$).

On the other hand, Figure 8.17 shows logarithmic mean values of acceleration amplification factor when there is a contact between the PTFE slide bearing and the stopper. It is important to highlight that as with seismic shear force demands, very high acceleration demands, γ_h°, are

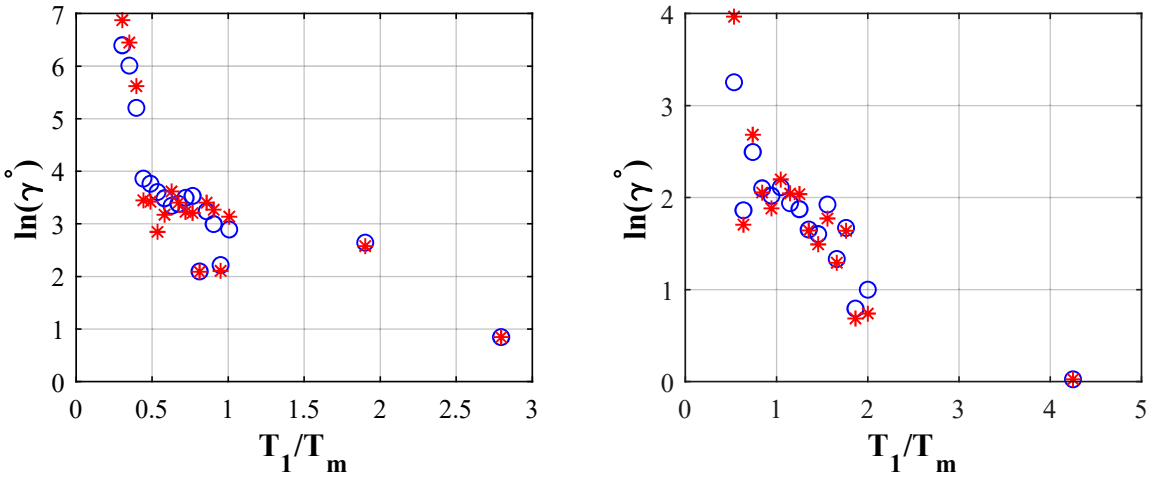


(a) 6-storey A1 building.

(b) 16-storey D1 building.

Figure 8.16: Relationship between acceleration amplification factor ($\ln(\gamma^{\circ})$) and period ratio (T_1/T_m) when there is no contact between the isolation bearing and the stopper.

also expected in comparison to Figure 8.16. This is a direct consequence of the influence of the stopper elements utilized in the seismic isolation. Additionally, it can be appreciated from Figure 8.17 that relatively higher peak floor accelerations are generated when the short CLT buildings enter into contact with the stopper of the isolation system. These observations stresses the further importance of inelastic demands in low-to-mid rise multi-storey CLT buildings and the need to avoid stoppers when sliding bearings are implemented.



(a) 6-storey A1 building.

(b) 16-storey D1 building.

Figure 8.17: Relationship between acceleration amplification factor ($\ln(\gamma^{\circ})$) and period ratio (T_1/T_m) when there is contact between the isolation bearing and the stopper.

8.5.3 Regression analysis

Acceleration amplification factor prediction model

A non-linear regression model is proposed on the basis of several functional forms with the most influential key structural as well as ground-motion parameters on the seismic acceleration demand of multi-storey CLT buildings. This relationship can be formulated as:

$$\ln(\gamma^{\circ}) = a + b \cdot \beta + c \cdot \lambda + d \cdot \ln\left[\min\left(\frac{T_1}{T_m}, 1.0\right)\right] \tag{8.4}$$

Table 8.4 summarizes the statistically significant regression coefficients, while Figure 8.18 shows the residual plot of the parameters employed in Equation 8.4. No significant trend is identifiable in the residual plots. The standard deviation of the dataset employed in this model is calculated as $\sigma = 0.41$ g/g.

Table 8.4: Regression coefficients for the non-linear acceleration demands ($\ln(\gamma^{\circ})$) associated with Equation 8.4.

a	b	c	d
0.1571	-0.0402	0.0050	-0.2826

8.6 Seismic demand comparison

A number of comparisons between inelastic seismic demand estimations of conventional CLT buildings and CLT buildings equipped with multi-layer flat sliding bearings are presented in this section. Two seismic demand parameters were considered for the comparison; i) acceleration amplification factor, γ°, and ii) inter-storey displacement ratio, θ_{max}. In order to make the comparisons fully consistent, the corresponding results associated with contact between the sliding layer and the stopper have been removed from the results of considered sub-set of conventional buildings employed in the previous chapters of this thesis.

Figure 8.19 shows the comparison of peak floor acceleration demands of low- and high-storey CLT buildings. It is clear from Figure 8.19 that the same non-linear tendency is expected in both conventional CLT buildings and CLT buildings equipped with multi-layer sliding elements in the short period range $T_1/T_m < 1$. On the other hand, the influence of ground-motion frequency content becomes negligible in the long period range $T_1/T_m > 1$ for both buildings. It is important to note that a level of 10% less seismic acceleration demands are expected in average in

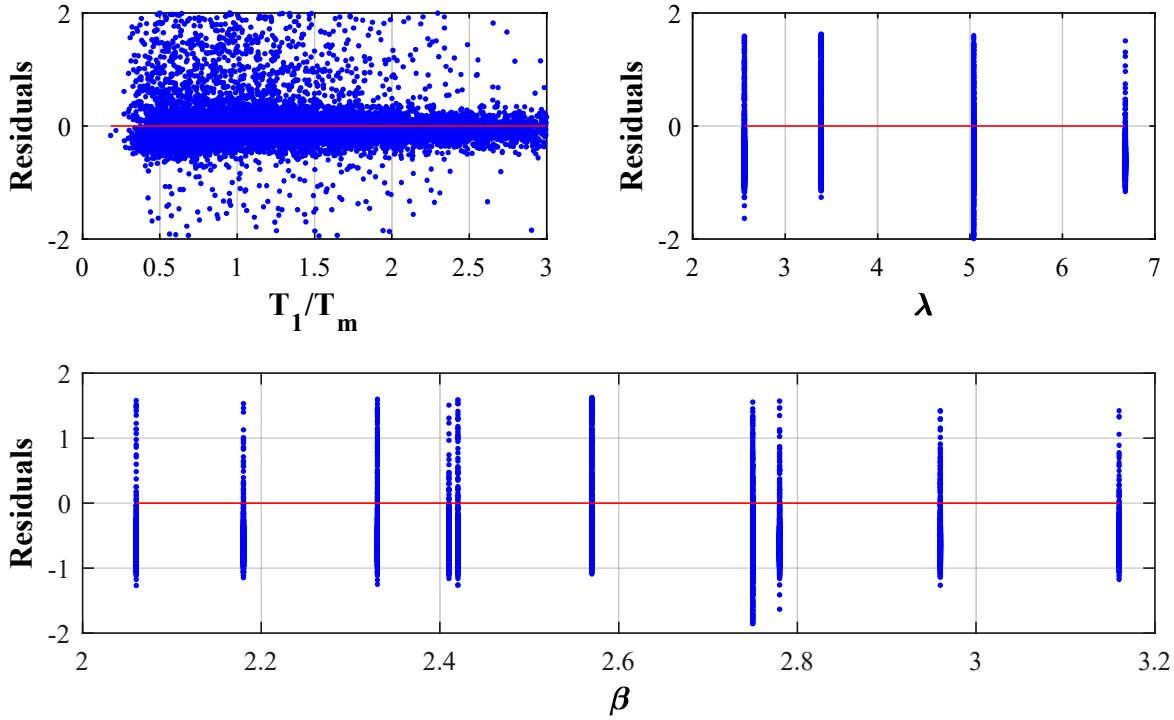
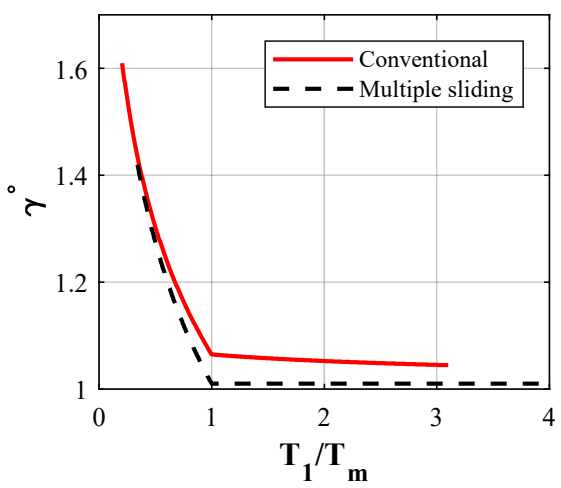


Figure 8.18: Residual plots for the acceleration amplification factor (γ°) prediction model.

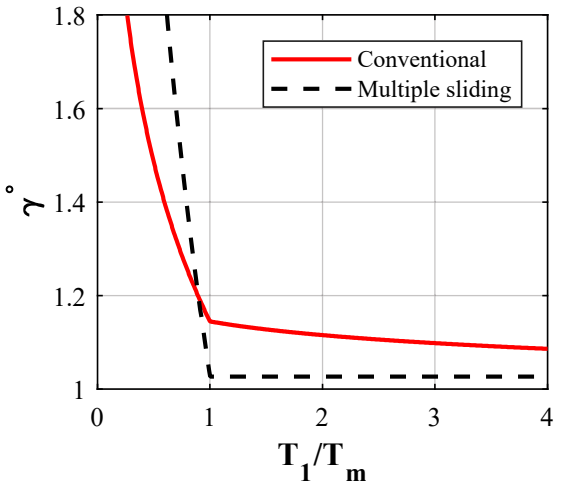
low-to-mid rise structures, while around 15% smaller demands are observed in high-rise buildings when incorporating multi-layer sliding sections into conventional CLT buildings. These results show that the use of sliding elements provides an improved acceleration response in taller CLT buildings.

Likewise, comparisons between the inter-storey drift response of CLT buildings equipped with and without multiple sliding sections are presented in Figure 8.20 for both building of 6 and 16 storeys. In this case, while at around 25% reductions are seen in mid-rise CLT buildings, a reductions of up to 50% are expected in the drift response of high-rise CLT buildings when multiple sliding sections are employed. These findings highlight the remarkable benefits of incorporating innovative isolation layers into conventional CLT buildings, and fuel further interest in innovative CLT building configurations.

Finally, it is important to note that some level of residual displacements are expected in the sliding sections of the buildings due to the absence of a restoring force in the flat sliding bearing elements. An alternative to re-centre the building after a seismic event would be incorporation of post-tension bars into sliding sections of a multi-storey building. Since this was not the scope of this thesis, this strategy has not been applied herein. However, it is recommended to study

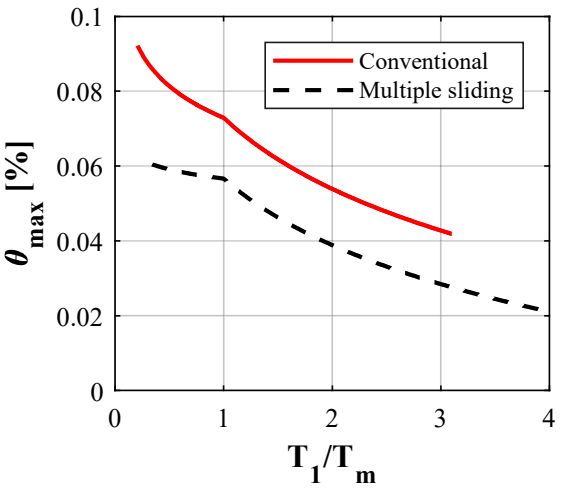


(a) 6-storey A1 building.

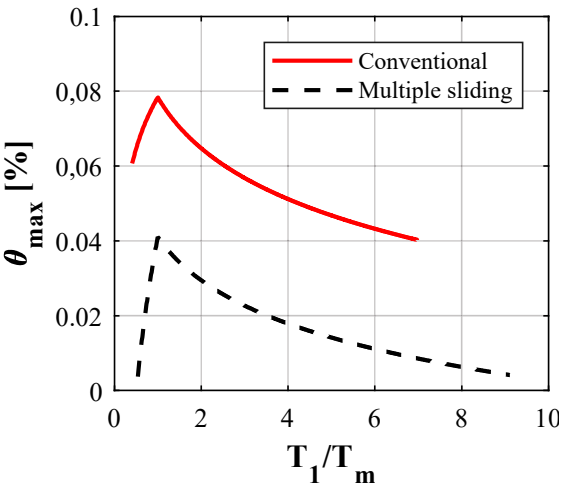


(b) 16-storey D1 building.

Figure 8.19: Acceleration amplification factor (γ°) comparison between the conventional and buildings with multiple sliding sections.



(a) 6-storey A1 building.



(b) 16-storey D1 building.

Figure 8.20: Inter-storey drift demand (θ_{max}) comparison between the conventional and buildings with multiple sliding sections.

the incorporation of post-tension bars into multi-storey CLT buildings equipped with flat slide bearing elements in future research studies.

8.7 Concluding remarks

The seismic response and demands of multi-storey cross-laminated timber buildings with multiple sliding sections employing flat sliding bearing elements was evaluated in this chapter. A numerical formulation of flat slide bearing elements was introduced and several comparative studies were performed to explore the effectiveness of the modelling approach adapted. The numerical models were then employed to conduct a thorough assessment of seismic displacement, shear force as well as acceleration demands on this innovative building configuration. On the basis of these assessments, the following conclusions can be drawn:

The comparisons between CLT buildings with multiple sliding sections and their conventional counterparts revealed the number of improvements in the seismic response brought about by the incorporation of multiple sliding bearings. As an example, when results of a conventional and new configurations of the 6-storey CLT buildings were compared, a reduction at around 15% was observed in the inter-storey displacement ratios, whereas reductions of 29% and 54% were experienced in the peak floor accelerations and base shear forces, respectively. These findings highlighted the need for a more robust exploration of the seismic demands on this innovative building configuration.

The parametric investigations performed were concerned with two distinct scenarios depending on whether sliding stoppers were provided or not. It was shown that the influence of ground-motion frequency on inelastic drift demands is almost negligible for the low-to-mid rise CLT multi-sliding buildings in the short period range, where $T_1/T_m < 1$. This can be attributed to the lower demands expected in comparison with conventional buildings due to sliding. On the other hand, lower levels of drift estimations are expected because of increasing divergence between fundamental period and the mean period of ground-motion in the long period range where $T_1/T_m > 1$. In the case of high-rise buildings, higher period ratios correspond to higher inter-storey drifts in the short period range, peaking at T_1/T_m, and lower inter-storey drift estimations were seen with increasing period ratios in the long period range.

The seismic shear force demand assessments showed that in the case of low-to-mid rise CLT buildings, minimal higher seismic force demands were observed with increasing period ratio in the short period range ($T_1/T_m < 1$), reaching a maximum value when the fundamental period of the structure and mean period of the ground motion are equal ($T_1/T_m = 1$). On the other hand, a similar relationship was observed in the short period range ($T_1/T_m < 1$), however the influence of ground-motion mean period on the inelastic force demands were greater in the case of high-rise CLT buildings. Besides, less shear demands were observed in taller buildings with

decreasing period ratios in the short period range ($T_1/T_m < 1$) and force demands were found to be almost negligible in the long period range ($T_1/T_m > 1$). Furthermore, the influence of stoppers incorporated in the design of flat slide bearing elements was clearly evidenced when the buildings were subjected to high-intensity ground-motions. More precisely, extremely large base shear forces were generated when the flat slide bearing elements hit the stopper at the maximum predicted/allowable displacement.

An assessment of seismic acceleration demands in seismically isolated multi-storey buildings was performed by means of a commonly defined acceleration amplification factor, which is the ratio of peak floor acceleration to the peak ground acceleration, $\gamma^{\circ} = \alpha_{max}/PGA$. Similar demand estimations that were seen in conventional multi-storey CLT buildings were also observed in sliding structures. However, when high displacement demands lead to contact between the PTFE slide bearing element and the stopper, very large floor accelerations were generated. These findings highlighted the adverse effects of stoppers that are incorporated to seismic isolation elements, and provided further support for their prohibition as is currently the case in Europe [8].

A comparative study was conducted on the inelastic seismic demands of conventional CLT buildings and CLT buildings equipped with multiple sliding sections. The observations showed that reductions at a level of 10% in the peak floor accelerations in mid-rise structures and 15% in high-rise structures. On the other hand at a level of 25% reductions were observed in the drift response of mid-rise buildings while reductions of up to 50% were documented in high-rise CLT buildings when a multiple sliding section was employed. These findings proved the relative benefits of innovative configurations and inspired more interest in these concepts.

Finally, regression models that help estimate the seismic drift, shear force, and accelerations demands in multi-storey CLT buildings equipped with flat slide bearing elements were proposed and examined. On the basis of statistical investigations and residual plots, all prediction models were proven to capture the features of the evolution of seismic demands very well. The findings outlined in this chapter constitute a fundamental step towards the understanding the seismic response of CLT buildings with multiple sliding sections and their benefits. They set the foundational stone over which more practically oriented studies could be performed in the future.

Chapter 9

Closure

9.1 Preamble

The main focus of this thesis was to understand the influence of ground-motion frequency content and key structural characteristics on the inelastic response of multi-storey CLT platform structures. For this purpose, a comprehensive building database including 60 CLT buildings with specific design practices, number of storeys, and panel fragmentation was developed. Subsequently, the salient structural characteristics were identified by means of modal analysis, non-linear static analysis and a careful consideration of the building configurations. These characteristics included: the structural period associated with the first elastic mode of vibration (T_1), the aspect ratio (λ), the joint density parameter (β), and the plasticity resistance ratio (α).

On the other hand, the Mean Period (T_m) of the ground-motion was adopted as its frequency-content indicator. Subsequently, the influence of ground-motion mean period on inelastic demands of multi-storey buildings was studied with particular attention to global and inter-storey drifts, base and inter-storey shear forces, and peak floor accelerations. Furthermore, the design and seismic response of multi-storey CLT buildings equipped with flat sliding bearing elements located at different levels of the buildings was investigated as an alternative innovative building option to limit inter-storey drifts, base shears, and peak floor accelerations.

9.2 Summary of main findings

This section provides a summary of the main findings discovered as part of this thesis.

9.2.1 Drift demands

As highlighted in Chapter 2, drift estimations have paramount importance in modern seismic design and assessment. Besides, the influence of frequency content of the ground-motion, which has been widely accepted as the determinant on the seismic response of buildings, has usually been neglected in past studies with multi-storey CLT buildings. Therefore, the influence of key structural characteristics and frequency content of the ground-motion on the inelastic deformation demands in multi-storey CLT buildings was investigated in Chapter 5. Analyses were performed on two parameters, namely global (δ_{mod}) and maximum (θ_{mod}) drift modification factors. Based on the extensive parametric investigations conducted, both global and maximum inter-storey drift modification factors were found to be notably dependent on the ground-motion frequency content characterised by the mean period (T_m) along the full range of period ratios (T_1/T_m) for all building heights studied.

A careful observation of the inelastic seismic demands in multi-storey CLT structures showed different behavioural trends for short and tall CLT buildings. Although, global (δ_{mod}) and maximum (θ_{mod}) drift modification factors decrease with increasing period ratios (T_1/T_m) for the long period range, $T_1/T_m > 1$, drift modification factors decrease in low- and mid-rise CLT buildings (n = {6, 8, and 12}). This relationship is negligible in the case of 16-storey building, and fully-reversed in the case of 20-storey building, for the short period range, $T_1/T_m < 1$. A distinct resonant response was also observed for taller CLT structures which was attributed to their overall lower relative inelastic deformation levels. Furthermore, relatively higher maximum inter-storey drift demands was observed in taller CLT structures, explained by the influence of higher mode effects in tall buildings.

Based on the rigorous parametric studies, a set of prediction models were proposed for the estimation of global (δ_{mod}) and maximum (θ_{mod}) drift modification factors as a function of design behaviour factor q, building aspect ratio λ, joint density β, and period ratio T_1/T_m. The simulation of prediction equations demonstrated that increasing the level of panel fragmentation can result in enhanced flexibility and inelastic deformations. Furthermore, individual panel lengths of 2.85 m or less showed an increased energy dissipation capacity brought about by a greater number of joints. The prediction models developed in this study showed a good agreement with the data over the range of structural properties and ground-motion characteristics.

Finally, a comparative study was conducted with the recent assessment proposals by Pozza and Trutalli [71] and the well-known equal displacement rule described in Eurocode 8 [29]. Comparisons were made on two building models as representatives of low- and high-rise CLT

structures. It was found that despite the proposed correlation equation showed an improved response over the Eurocode 8 equal displacement rule as the proposal approximates the overall mean of dataset, relatively higher mis-estimations were observed due to the neglection of the period dependency in the estimation of inelastic deformation demands. For instance, when the ground-motion has a strong short period component, up to 80% over-estimations was observed while up to 70% non-conservative results was seen when the ground-motion has a long period (more distant earthquakes) in the case of 8-storey B1 building. On the other hand, the highest under-estimations were expected in the case of 20-storey E3 building configuration when the period ratio was $T_1/T_m \approx 1$ leading to even more non-conservative results than the equal displacement rule approximation. Given that such higher buildings were not incorporated in the formation of the correlation equation proposed by Pozza and Trutalli [71], these results were not unexpected. More importantly, these comparisons highlight the urgent need for a realistic consideration of the frequency content of the ground-motion on the design and assessment of seismic drift demands in multi-storey CLT structures.

9.2.2 Shear force demands

Besides global and inter-storey drifts which have primary relevance in performance-based design philosophies due to their strong correlation with damage, it is also imperative that a structure meets capacity design requirements in order to ensure predictability of response and failure mode control. Therefore, it is important to investigate the evolution of strength demands and their correlation with frequency content of the ground-motion. To this end, the influence of salient structural characteristics and ground-motion frequency content on the seismic shear force demands in multi-storey CLT buildings was addressed in Chapter 6. Two parameters namely, base (V_{mod}) and storey ($V_{st,mod}$) shear modification factor were taken into account. Based on the extensive parametric investigations, the base shear modification factor (V_{mod}) was found explicitly be dependent upon the ground-motion frequency content along the full range of period ratios (T_1/T_m) for all building configurations analysed. On the other hand, the evolution of inter-storey shear force demands ($V_{st,mod}$) against period ratio (T_1/T_m) for taller buildings of up to 16- and 20-storey, with the lowest level of panel fragmentation m = 1, was found to be unaffected in the long period range, $T_1/T_m > 1.25$.

The influence of key structural parameters, the level of panel fragmentation (m) and the building height (n) was also investigated. It was shown that higher level of panel fragmentation are associated with lower level of seismic shear demands (in both base and storey shear). This indicates that CLT panel modularization leads to a more resilient response by means of relative benefits of increased energy dissipation capacity of the building in seismic scenarios. An

examination of the influence of building heights on the seismic shear demands in multi-storey CLT buildings showed that although taller buildings tend to have lower force demands in the short period range, larger demands are expected in the long period range. This is attributed to the importance of higher mode effects with increasing structural height.

Finally, a range of regression models were developed to estimate the base (V_{mod}) and inter-storey ($V_{st,mod}$) shear modification factor as a function of the parameters that have the greatest influence on the seismic response of multi-storey CLT buildings. Furthermore, a set of simplified models with reduced number of terms that captures the general scaling features relatively well were proposed and validated. The proposed prediction models show a relatively good response along the full range of ground-motion characteristics and salient structural parameters investigated.

9.2.3 Acceleration demands

A relatively good seismic performance of low- to mid-rise multi-storey CLT buildings has been documented by means of full-scale shaking table experiments as described in Chapter 2. However, these experimental studies have shown that multi-storey CLT buildings might experience high levels of floor accelerations which can affect building content and cause harm to its occupants leading to significant losses. Therefore, a detailed account of the influence of ground-motion frequency content and key structural parameters on the seismic acceleration demands in multi-storey CLT buildings was examined in Chapter 7. Two acceleration amplification factors were taken into account to identify the most accurate correlations between structural parameters and ground-motion characteristics. First, an amplification factor γ defined as a function of maximum floor acceleration and spectral acceleration of the ground-motion at the buildings' fundamental period was employed. Second, an amplification factor γ° defined as the ratio of the peak floor acceleration obtained from non-linear response history analyses to the peak ground acceleration of ground-motion.

While the acceleration amplification factor γ was found to be dependent upon the frequency content of the ground-motion along the full range of period ratios (T_1/T_m) for all building models examined, the evolution of acceleration demands for γ° was found to be very minimal or negligible in some cases in the long period range where $T_1/T_m > 1$. More precisely, acceleration amplification demands (γ) decreases with increasing period ratios in the short period range where it is less than 1, and reaches its minimum at $T_1/T_m = 1$, and increases thereafter in the long period range. On the other hand, while the same non-linear evolution of acceleration demands was observed in the short period range for γ°, different correlations can be identifiable

in the long period range depending on the building configuration. This stresses the importance of ground-motion parameters selected for the estimation of seismic acceleration demands in multi-storey CLT buildings.

The influence of design response modification factor (q) on the acceleration demands (γ and γ°) showed that similar trends can be observed for different period ranges (T_1/T_m). For instance, lower acceleration demands are expected for lower design response modification factors in short period range ($T_1/T_m < 1$) for γ and in the long period range ($T_1/T_m > 1$) for γ°. Besides, the effects of the level of panel fragmentation (m) on the acceleration response were found to be that higher panel modularization leads to lower acceleration demands by the building and improved energy dissipation capacity for both acceleration demand parameters γ and γ°. Finally, observations on the evolution of acceleration demands for different building heights (n) demonstrated that taller buildings tend to experience higher acceleration demands along the full range of period ratios for both amplification factors.

Regression models to estimate the evolution of seismic acceleration demands versus ground-motion characteristics were developed. Only the most significant parameters were considered while identifying the prediction equations. The developed regression models were examined for both p-values and residual plots and no p-value higher than 5% and no significant residual trend was observed. Moreover, a simplified model was proposed for the acceleration amplification factor γ° which still captures the main scaling features of full model with an acceptable level of divergence in some cases. To this end, the proposed prediction models for acceleration amplification factors proved to be able to produce a relatively good response along the full range of ground-motion characteristics and key structural parameters assessed.

9.2.4 Seismic demands in CLT buildings equipped with flat sliding bearings

A number of novel CLT systems with several innovative configurations aimed at increasing the resiliency of CLT buildings have been highlighted in Chapter 2. Among those, the provision of inter-storey isolation layers appears to be an attractive solution to limit inter-storey drifts and accelerations in tall CLT structures. However, previous assessments have relied on a limited number of ground-motions and neglected the effects of frequency variations. Therefore, the seismic response and demands of multi-storey cross-laminated timber buildings with multiple sliding sections employing flat sliding bearing elements was evaluated in Chapter 8. A numerical formulation of flat slide bearing elements was introduced and several comparative studies were performed to explore the reliability of the modelling approach adapted. The numerical

models were then employed to conduct a thorough assessment of seismic displacement, shear force as well as acceleration demands on this innovative building configuration.

The comparisons between CLT buildings with multiple sliding sections and their conventional counterparts evidenced the number of improvements in the seismic response brought about by the incorporation of multiple sliding bearings. As an example, when results of a conventional and new configurations of the 6-storey CLT buildings were compared, a reduction at around 15% was observed in the inter-storey displacement ratios whereas reductions of 29% and 54% were experienced in the peak floor accelerations and base shear forces, respectively. These findings highlighted the need for a more robust exploration of the seismic demands on this innovative building configuration.

The parametric investigations performed were concerned with two distinct scenarios depending on whether sliding stoppers were provided or not. It was shown that the influence of ground-motion frequency on inelastic drift demands is almost negligible for the low-to-mid rise CLT multi-sliding buildings in the short period range, where $T_1/T_m < 1$. This can be attributed to the lower demands expected in comparison with conventional buildings due to sliding. On the other hand, lower levels of drift estimations are expected because of increasing divergence between fundamental period and the mean period of ground-motion in the long period range where $T_1/T_m > 1$. In the case of high-rise buildings, higher period ratios correspond to higher inter-storey drifts in the short period range, peaking at T_1/T_m, and lower inter-storey drift estimations were seen with increasing period ratios in the long period range.

The seismic shear force demand assessments showed that in the case of low-to-mid rise CLT buildings, minimal higher seismic force demands were observed with increasing period ratio in the short period range ($T_1/T_m < 1$) reaching a maximum value when the fundamental period of the structure and mean period of the ground motion are equal ($T_1/T_m = 1$). On the other hand, a similar relationship was observed in the short period range ($T_1/T_m < 1$), however the influence of ground-motion mean period on the inelastic force demands were greater in the case of high-rise CLT buildings. Besides, lower shear demands were observed in taller buildings with decreasing period ratios in the short period range ($T_1/T_m < 1$) and force demands were found to be almost negligible in the long period range ($T_1/T_m > 1$). Furthermore, the influence of stoppers incorporated in the design of flat slide bearing elements was clearly evidenced when the buildings were subjected to high-intensity ground-motions. More precisely, extremely large base shear forces were generated when the flat slide bearing elements hit the stopper at the maximum predicted/allowable displacement.

An assessment of seismic acceleration demands in seismically isolated multi-storey buildings was performed by means of a commonly defined acceleration amplification factor which is the ratio of peak floor acceleration to the peak ground acceleration, $\gamma^{\circ} = \alpha_{\max}/\text{PGA}$. Modestly lower demand estimations that were seen in sliding structures. However, when high displacement demands lead to contact between the PTFE slide bearing element and the stopper, very large floor accelerations were generated. These findings highlight the adverse effects of stoppers, and provide further support for their prohibition as is currently the case in Europe [8].

A comparative study was conducted on the inelastic seismic demands of conventional CLT buildings and CLT buildings equipped with multiple sliding sections. The observations showed reductions at a level of 10% in the peak floor accelerations in mid-rise structures and 15% in high-rise structures. On the other hand at a level of 25% reductions were observed in the drift response of mid-rise buildings while reductions of up to 50% were documented in high-rise CLT buildings when a multiple sliding section was employed. These findings prove the relative benefits of innovative configurations and inspired more interest in these concepts.

Finally, regression models that help estimate the seismic drift, shear force, and accelerations demands in multi-storey CLT buildings equipped with flat slide bearing elements were proposed and examined. On the basis of statistical investigations and residual plots, all prediction models were proven to capture the features of seismic demand data very well. The findings outlined in this thesis constitute a fundamental step towards the understanding the seismic response of CLT buildings with multiple sliding sections and their benefits. They set the foundational stone over which more practically oriented future studies can be performed.

9.3 Future work

The primary focus of this thesis was to understand the influence of frequency content and structural characteristics on the drift, force, and acceleration demands in multi-storey CLT buildings, and CLT buildings equipped with multiple sliding sections. The findings of this thesis have also uncovered the need for further research in the following areas:

The assessment of seismic demands presented in this thesis was limited to the response of 2-dimensional numerical models. A similar study can be conducted taking into account 3-dimensional response of multi-storey CLT buildings.

A comprehensive assessment of inelastic demands in multi-storey CLT buildings has been investigated and presented in this thesis. However, the investigations on the influence of ground-

motion characteristics were limited to frequency content. It would be interesting to explore the influence of the duration of ground-motion on the inelastic demands in multi-storey CLT buildings.

A detailed characterization of inelastic demands in multi-storey CLT buildings equipped with flat sliding bearing elements was presented in Chapter 8. Although, a relatively good level of seismic demand predictions have been observed by means of proposed regression models, it is important to extend these investigations to a wider building database with many more characteristics and include the 3D seismic effects. Besides, these investigations were also limited to CLT buildings equipped with flat sliding bearings at only two levels (base and the mid-height) of the buildings. It might be important that incorporating more sliding sections and investigate the change in the response of buildings and compare to the results presented in this thesis.

Finally, the findings of this study and a number of prediction models for the estimation of inelastic demands in multi-storey CLT buildings constituted a simple tool which were proposed to be incorporated in current design and assessment procedures. Besides, all findings of this study were obtained from experimentally validated numerical models. To this end, these findings formed a basis on the inelastic demands in multi-storey CLT buildings; however, it might be interesting to perform more practically oriented future studies on multi-storey CLT buildings equipped with innovative response modification systems as the new era of construction has been becoming the era of tall timber buildings made of CLT.

9.4 Dissemination

As part of this thesis, a number of publications presented in national and international symposiums, and published in scientific journals are listed below.

1. C. DEMIRCI, C. MÁLAGA-CHUQUITAYPE, and L. MACORINI. An innovative material of construction of 21st century: Cross Laminated Timber. *Young Researchers Forum III, Innovation in Construction Materials*, Imperial College London, London, UK, 2016.

2. C. DEMIRCI, C. MÁLAGA-CHUQUITAYPE, and L. MACORINI. Seismic Behaviour and Design of Tall Cross-Laminated Timber Buildings. *Proceedings of the* 16^{th} *World Conference on Earthquake Engineering*, Santiago, Chile, Jan. 9-13, 2017, Paper No: 2096, 2017.

3. C. DEMIRCI, C. MÁLAGA-CHUQUITAYPE, and L. MACORINI. Seismic drift demands in multi-storey cross-laminated timber buildings. *Earthquake Engineering and*

Structural Dynamics, 47[4]:1014–1031, 10.1002/eqe.3003, 2018.

4. C. DEMIRCI, C. MÁLAGA-CHUQUITAYPE, and L. MACORINI. Recent findings on the assessment of seismic demands in CLT buildings. *Proceedings of the Young Researchers Forum IV*, Innovation in Construction Materials, Northumbria University, Newcastle, UK, 2018.

5. C. DEMIRCI. Seismic response of tall multi-storey cross-laminated timber buildings. *Proceedings of the* 20^{th} *Young Researchers Conference*, The Institution of Structural Engineers, London, UK, 2018.

6. C. DEMIRCI, C. MÁLAGA-CHUQUITAYPE, and L. MACORINI. Drift Response of Tall Cross-Laminated Timber Buildings Under Realistic Earthquake Loads. *Proceedings of the* 16^{th} *European Conference on Earthquake Engineering*, Thessaloniki, Greece, Jun. 18-21, 2018.

7. C. DEMIRCI, C. MÁLAGA-CHUQUITAYPE, and L. MACORINI. Seismic shear and acceleration demands in multi-storey cross-laminated (CLT) timber buildings. *Engineering Structures*, 2019.

8. C. DEMIRCI, C. MÁLAGA-CHUQUITAYPE, and L. MACORINI. Seismic demands in multi-storey cross-laminated timber (CLT) structures. *SECED 2019, Earthquake risk and engineering towards a resilient world*, 9-10th September 2019, University of Greenwich, London, 2019.

Bibliography

[1] ABAQUS 3DS [FE Framework]. Waltham, MA, Ansys. 45, 51

[2] I. ABEYSEKERA and C. MÁLAGA-CHUQUITAYPE. Dynamic Response of Tall Timber Buildings. *SECED 2015 Conference: Earthquake Risk and Engineering towards a Resilient World*, 9-10 July, Cambridge UK, 2015. 54

[3] T. AKBAS, R. SAUSE, J.M. RICLES, R. GANEY, J. BERMAN, S. LOFTUS, J.D. DOLAN, S. PEI, J.W. van de LINDT, and H.E. BLOMGREN. Analytical and experimental lateral load response of self-centering CLT walls. *Journal of Structural Engineering*, 10.1061/(ASCE)ST.1943-541X.0001733, 04017019, 2017. 46

[4] ANSYS Mechanical Workbench; R14; ANSYS, Inc.: Canonsburg, PA, USA. 51

[5] ARCHITECT, Timber on the rise, Part 1, Dowel-laminated timber, 2018. 41

[6] ASCE, Minimum design loads for buildings and other structures, *ASCE7*, Washington, DC, 2010. 50

[7] AxisVM Structural Analysis Software. InterCAD, Budapest, Hungary. 50

[8] Y. BAO, T.C. BECKER, T. SONE, and H. HAMAGUCHI. To limit forces or displacements: Collapse study of steel frames isolated by sliding bearings with and without restraining rims. *Soil Dynamics and Earthquake Engineering*. Volume 112, September 2018, Pages 203-214, https://doi.org/10.1016/j.soildyn.2018.05.006, 2018. 135, 145, 152, 159

[9] H.J. BLASS and P. FELLMOSER. Design of solid wood panels with cross layers, *Proceedings of the 8th World Conference on Timber Engineering*, Volume II, Lahti, Finnland, 2004. Available:http://holz.vaka.kit.edu/19.php 24, 72, 73, 75, 82

[10] V. BOLVARDI, S. PEI, J.W. van de LINDT, and J.D. DOLAN. Direct displacement design of tall cross laminated timber platform buildings with inter-story isolation. *Engineering Structures*, 167:740–749, 2017. 53, 54

[11] G. BONDONET and A. FILIATRAULT. Frictional response of PTFE Sliding Bearings at High Frequencies. *Journal of Bridge Engineering*, 2[4]: 139–148, 1997. 134

[12] Carpenter. http://www.cp-ltd.co.uk/wp-content/uploads/2011/09/PTFE-Sliders.pdf. 134

[13] A. CECCOTTI. New technologies for construction of medium-rise buildings in seismic regions: The XLAM case, *Structural Engineering International*, 18[2], 156–165, 2008. 47, 64, 65

[14] A. CECCOTTI, M.P. LAURIOLA, M. PINNA, and C. SANDHAAS. SOFIE project - Cyclic tests on cross-laminated wooden panels, *Proceedings of the 9th World Conference. on Timber Engineering*, Oregon State University, Corvallis, OR, 2006. 47

[15] A. CECCOTTI, C. SANDHAAS, M. OKABE, M. YASUMURA, C. MINOWA, and N. KAWAI. SOFIE project - 3D shaking table test on a seven-storey full-scale cross-laminated timber building. *Earthquake Engineering and Structural Dynamics*, 42[13]:2003–2021, 2006. 33, 47, 48, 50, 52, 54

[16] A. CECCOTTI. Seismic safety in seven-storey buildings - a practical test, 14 International Holzbau-Forum 08, 2006. 54

[17] A. CHOPRA and C. CHINTANAPAKDEE. Comparing response of SDF systems to near-fault and far-fault earthquake motions in the context of spectral regions. *Earthquake Engineering and Structural Dynamics*, 30[12]:1769–1798, 2001. 34

[18] CLT DESIGNER, Holz.Bau Forschungs Gmbh and Institute for Timber Engineering and Wood Technology of Graz University of Technology, 2009. 63, 64, 182

[19] E. DIMITRAKOPOULOS, A.J. KAPPOS and N. MAKRIS. Dimensional analysis of yielding and pounding structures for records without distinct pulses. *Soil Dynamics and Earthquake Engineering*, 29[7], 1170–1180, 2009. 34

[20] E. DIMITRAKOPOULOS and T.S. PARASKEVA. Dimensionless fragility curves for rocking response to near-fault excitations. *Earthquake Engineering and Structural Dynamics*, 44[12], 2015–2033, 2015. 34

[21] J.D. DOLAN, V. BORDRY, S. PEI, and J. van de LINDT. Tall cross-laminated timber building: Design and performance session WW300 experimental and modelling studies on wood frame buildings. Structures Congress, ASCE, Washington, DC, 2886–2893, 2014. 50

[22] M. DOLCE, D. CARDONE, and F. CROATTO. Frictional behaviour of Steel-PTFE Interfaces for Seismic Isolation. *Bulletin of Earthquake Engineering*, 3:75-99, 2005. 133, 134

[23] B. DUJIC, J. PUCELJ, and R. ZARNIC. Testing of racking behavior of massive wooden wall panels. *Proceedings of the 37th CIB-W18 Meeting, International Council for Building Research and Innovation*, Rotterdam, Netherlands, 2004. 44

[24] B. DUJIC and R. ZARNIC. Study of lateral resistance of massive X-Lam wooden wall system subjected to horizontal loads. *COST E29 Int. Workshop on Earthquake Engineering on Timber Structures*, Coimbra, Portugal, European Cooperation in Science and Technology, Brussels, Belgium, 97-104, 2006. 44

[25] B. DUJIC, K. STRUS, R. ZARNIC, and A. CECCOTTI. Prediction of dynamic response of a 7-storey massive XLam wooden building tested on a shaking table. *World Conference on Timber Engineering*, Italian National Research Council, Roma, Italia, 2024, 2010. 24, 34, 44, 47, 48, 81, 82, 83

[26] B. DUJIC, S. AICHER, and R. ZARNIC. Testing of wooden wall panels applying realistic boundary conditions. *Proc., 9th World Conference on Timber Engineering*, Oregon State University, Corvallis, OR, 2006. 46

[27] ECO-WALD, Glued laminated timber, 2017. 41

[28] COMITÉ EUROPÉEN NORMALISATION. EN 1991-1-1, Eurocode 1: Actions on structures. BS EN 1991-1-1. Brussels, Belgium, 2004. 56, 58, 136

[29] COMITÉ EUROPÉEN NORMALISATION. EN 1998-1, Eurocode 8: Design of structures for earthquake resistance, Part 1: General rules, seismic actions and rules for buildings, Brussels, Belgium, 2005. 20, 25, 47, 60, 61, 62, 63, 100, 102, 103, 104, 108, 154

[30] COMITÉ EUROPÉEN NORMALISATION. BS EN 12512: Timber structures - Test methods - Cyclic testing of joints made with mechanical fasteners. EN 12512:2001, Brussels, Belgium, 2001. 79

[31] M. FOLLESA, I.P. CHRISTOVASILIS, D. VASSALLO, M. FRAGIACOMO and A. CECCOTTI. Seismic design of multi-storey cross lamineted timber buildings according to Eurocode 8. *Ingegneria sismica*, 30[4]:27–53, 2013. 24, 74, 75

[32] R.M. FOSTER, T. REYNOLDS, and M.H. RAMAGE. Proposal for defining a tall timber building. *Journal of Structural Engineering*, 142[12], 10.1061/(ASCE)ST.1943-541X.0001615, 2016. 33

[33] M. FRAGIACOMO, B. DUJIC, and I. SUSTERSIC. Elastic and ductile design of multi-storey crosslam massive wooden buildings under seismic actions. *Engineering Structures*, 33[11], 3043–3053, 2011. 34, 48, 73

[34] I. GAVRIC, M. FRAGIACOMO, and A. CECCOTTI. Strength and deformation characteristics of typical XLam connections. *World Conference on Timber Engineering 2012*, New Zealand Timber Design Society, Auckland, New Zealand, 2012. 47

[35] I. GAVRIC and M. POPOVSKI. Design models for CLT shear-walls and assemblies based on connection properties. *International Network on Timber Engineering Research*, Bath, UK, September, 2014. 64

[36] I. GAVRIC, G. RINALDIN, C. AMADIO, M. FRAGIACOMO, and A. CECCOTTI. Experimental-numerical analyses of the seismic behaviour of cross-laminated wall systems. *15 World Conference of Earthquake Engineering*, Lisboa, 2012. 24, 45, 47, 63, 78, 79, 80, 81

[37] I. GAVRIC, A. CECCOTTI, and M. FRAGIACOMO. Experimental cyclic tests on cross-laminated timber panels and typical connections. *Proceedings of the 14th ANIDIS Conference*, Bari, Italy, September 18-22, 2011. 47, 79

[38] I. GAVRIC, M. FRAGIACOMO, and A. CECCOTTI. Cyclic behaviour of typical metal connectors for cross-laminated (CLT) structures. *Materials and Structures*, 48:1841–1857. 10.1617/s11527-014-0278-7, 2015. 24, 68, 78

[39] I. GAVRIC, M. FRAGIACOMO, and A. CECCOTTI. Cyclic behavior of typical screwed connections for cross-laminated (CLT) structures. *European Journal of Wood and Wood Products*, 73[2]:179–191. 10.1007/s00107-014-0877-6, 2015. 24, 68, 78

[40] M. GREEN. The case for tall wood buildings [Online] Available at: www.woodworks.org/download.php?file=152, 2012. 33

[41] J. HANCOCK, J. BOMMER and P. STAFFORD. Numbers of scaled and matched accelerograms required for inelastic dynamic analyses. *Earthquake Engineering and Structural Dynamics*, 37[14]:1585–1607, 10.1002/eqe.827, 2008. 84

[42] A. HASHEMI, W.Y. LOO, R. MASOUDNIA, P. ZARNANI, and P. QUENNEVILLE. Ductile Cross Laminated Timber (CLT) Platform Structures with Passive Damping. *World Conference on Timber Engineering*, August 22-25, Vienna, Austria, 2016. 51, 54

[43] A. HASHEMI, P. ZARNANI, R. MASOUDNIA, and P. QUENNEVILLE. Experimental Testing of Rocking Cross-Laminated Timber Walls with Resilient Slip Friction Joints. *Journal of Structural Engineering*, 10.1061/(ASCE)ST.1943-541X.0001931, 2018. 51, 54

[44] V. HRISTOVSKI, B. DUJIC, M. STOJMANOVSKA, and V. MIRCEVSKA. Full-scale shaking-table tests of XLam panel systems and numerical verification: Specimen 1. *Journal of Structural Engineering*, 10.1061/(ASCE)ST.1943 -541X.0000754, 2012. 46

[45] T. JOYCE, M. BALLERINI, and I. SMITH. Mechanical behaviour of in-plane shear connections between CLT wall panels. *Proceedings of* 44^{th} *CIB-W18 Meeting*, International Council for Building Research and Innovation, Rotterdam, Netherlands, 2011. 45

[46] E. KARACABEYLI and B. DOUGLAS. CLT handbook, FPInnovations, Pointe-Claire, QC, Canada, 2013. 50

[47] KLH UK LTD. http://www.klhuk.com/ 43, 60

[48] KVH, Structural Timber - A precision Building Material. Available online: http://www.kvh.eu/en/kvhr-structural-timber/. 2017. 41

[49] M. LATOUR, G. RIZZANO, and G. TORELLO. Seismic Performance of Cross Laminated Timber Panel Buildings with Dissipative Connections. 15^{th} *World Conference on Earthquake Engineering*, 2012. 33

[50] W.Y. LOO, C. KUN, P. QUENNEVILLE, and N. CHOUW. Experimental testing of a rocking timber shear wall with slip-friction connectors. *Earthquake Engineering and Structural Dynamics*, 43[11]:1621-1639, 10.1002/eqe.2413, 2014. 52, 54

[51] W.Y. LOO, P. QUENNEVILLE, and N. CHOUW. Rocking Timber Structure with Slip-Friction Connectors Conceptualized As a Plastically Deformable Hinge within a Multistory Shear Wall. *Journal of Structural Engineering*, 10.1061/(ASCE)ST.1943-541X.0001387, 2015. 52

[52] C. MÁLAGA-CHUQUITAYPE and A.Y. ELGHAZOULI. Chapter 8: Design of timber structures. In Seismic Design to Eurocode 8, 2016. 24, 56, 64, 65

[53] C. MÁLAGA-CHUQUITAYPE and A.Y. ELGHAZOULI. Inelastic displacement demands in steel structures and their relationship with earthquake frequency content parameters. *Earthquake Engineering and Structural Dynamics*, 2012;41[5]:831–852, 2012. 92

[54] C. MÁLAGA-CHUQUITAYPE. Estimation of peak displacements in steel structures through dimensional analysis and the efficiency of alternative ground-motion time and length scales. *Engineering Structures*, Vol. 101, 264–278, 2015. 34

[55] C. MÁLAGA-CHUQUITAYPE and K. BOUGATSAS. Vector-IM-based assessment of alternative framing systems under bi-directional ground-motion. *Engineering Structures*, Vol. 132, 188–204, 2017. 34

[56] MATLAB and Statistics Toolbox Release 2017b, The MathWorks, Inc., Natick, Massachusetts, United States. 96

[57] MIDROC PROPERTY DEVELOPMENT, Swedens largest newly constructed building made of wood!, Available online: http://mpd.midroc.se/en/about-mpd/references/limnologen, 2018. 43

[58] N.M. NEWMARK and W. HALL. Earthquake spectra and design. Technical Report, Oakland, California, Earthquake Engineering Research Institute; 1982. 34

[59] OpenSees (Open System for Earthquake Enginnering Simulations) FE Framework, Berkeley, CA, Univ. of California. 24, 67, 68, 69, 74, 79, 81, 82, 88, 136, 173

[60] S. PEI, J.W. van de LINDT and M. POPOVSKI. Approximate R-factor for cross-laminated timber walls in multistory buildings. *Journal of Architectural Engineering*, 10.1061/(ASCE)AE.1943-5568.0000117, 245–255, 2012. 34, 50, 54

[61] S. PEI, J.W. van de LINDT, M. POPOVSKI, J. BERMAN, J. DOLAN, J. RICLES, R. SAUSE, H. BLOMGREN, and D. RAMMER. Cross-Laminated Timber for Seismic Regions: Progress and Challenges for Research and Implementation. *Journal of Structural Engineering*, 142[4]:E2514001, 10.1061/(ASCE)ST.1943-541X.0001192, 2016. 54

[62] S. PEI, J.W. van de LINDT, M. POPOVSKI, J. BERMAN, J. DOLAN, J. RICLES, R. SAUSE, H. BLOMGREN, and D. RAMMER. Progress on the development of seismic resilient tall CLT buildings in the Pacific Northwest. *World Conference on Timber Engineering*, Canada, August 10-14, 2014. 54

[63] S. PEI, M. POPOVSKI and J.W. van de LINDT. Analytical study on seismic force modification factor for cross laminated timber buildings for NBCC. *Canadian Journal of Civil Engineering*, 40[9]:887–896, 2013. 54

[64] S. PEI, and J.W. van de LINDT. Users manual for SAPWood for windows, version 1.0, Colorado State Univ., Fort Collins, CO, 2007. 50, 53

[65] S. PEI, C. LENON, G. KINGSLEY, and P. DENG. Seismic Design of Cross-Laminated Timber Platform Buildings Using a Coupled Shearwall Concept. *Journal of Architectural Engineering*, 23[3]:06017001, 10.1061/(ASCE)AE.1943-5568.0000257, 2017. 50, 54

[66] G.H. POH'SIE, C. CHISARI, G. RINALDIN, C. AMADIO, and M. FRAGIACOMO. Optimal design of tuned mass dampers for a multi-storey cross laminated timber building against seismic loads. *Earthquake Engineering and Structural Dynamics*, 45[12]:1977–1995, 10.1002/eqe.2736, 2016. 52

[67] M. POPOVSKI, J. SCHNEIDER, and M. SCHWEINSTEIGER. Lateral load resistance of cross-laminated wood panels. *World Conference on Timber Engineering*, Italian National Research Council, Roma, Italia, 20-24, 2010. 45

[68] M. POPOVSKI and E. KARACABEYLI. Seismic behaviour of cross-laminated timber structures. *World Conf. on Timber Engineering 2012*, New Zealand Timber Design Society, Auckland, New Zealand, 2012. 46

[69] M. POPOVSKI, E. KARACABEYLI, and A. CECCOTTI. Seismic performance of cross-laminated timber buildings. *Chapter 4, Canadian design handbook on cross-laminated timber, FP Innovations Special Publication SP-528E*, 2011. 49

[70] M. POPOVSKI, S. PEI, J.W. van de LINDT, and E. KARACABEYLI. Force modification factors for CLT structures for NBCC. *Materials and Joints in Timber Structures*, RILEM Bookseries, vol 9. Springer, Dordrecht, 543–553, 10.1007/978-94-007-7811-5_50, 2014. 34

[71] L. POZZA and D. TRUTALLI. An analytical formulation of q-factor for mid-rise CLT buildings based on parametric numerical analyses. *Bulletin of Earthquake Engineering*, 15[5]:2015–2033, 10.1007/s10518-016-0047-9, 2016. 25, 34, 49, 86, 100, 101, 102, 103, 104, 154, 155

[72] PTFE Slide Bearing, https://www.fluorotec.com/products/ptfe-slide-bearings/typical-configurations/. 26, 133, 134

[73] E.M. RATHJE, N.A. ABRAHAMSON, and J.D. BRAY. Simplified frequency content estimates of earthquake ground motions. *Journal of Geotechnical and Geoenvironmental Engineering*, 124[2]:150–9, 1998. 85

[74] E.M. RATHJE, F. FARAJ, S. RUSSEL, and J.D. BRAY. Empirical relationships for frequency content parameters of earthquake ground motions. *Earthquake Spectra*, 20[1]:119–44, 2004. 34, 85

[75] G. RINALDIN, C. AMADIO, and M. FRAGIACOMO. A component approach for the hysteretic behaviour of connections in cross-laminated wooden structures. *Earthquake Engineering and Structural Dynamics*, 42[13], 2023–2042, 2013. 20, 49, 81, 82

[76] G. RINALDIN and M. FRAGIACOMO. Non-linear simulation of shaking-table tests on 3- and 7-storey X-Lam timber buildings. *Engineering Structures*, 113:133–148, 2016. 25, 34, 47, 54, 82, 83, 85

[77] ROTHOBLASS, https://www.rothoblaas.com 70

[78] J. RUIZ-GARCIA and E. MIRANDA. Inelastic displacement ratios for evaluation of existing structures. *Earthquake Engineering and Structural Dynamics*, 32[8]:1237–1258, 10.1002/eqe.271, 2003. 34, 92

[79] L. SANCHEZ-RICART and A. PLUMIER. Parametric study of ductile moment-resisting steel frames: A first step towards Eurocode 8 calibration. *Earthquake Engineering and Structural Dynamics*, 37[7]:1135–1155, 10.1002/eqe.809, 2008. 108

[80] SAP2000, [FE framework], *Computers & Structures*, Walnut Creek, CA. 44, 48, 49, 51

[81] M. SARKISIAN. Designing Tall Buildings - Structure as Architecture, Routledge, Taylor & Francis Group, New York and London, 2012. 33

[82] R. SCOTTA, L. MARCHI, D. TRUTALLI, and L. POZZA. A Dissipative Connector for CLT Buildings: Concept, Design and Testing. *Materials*, 9[3]:139, 10.3390/ma9030139, 2016. 51, 54

[83] Y.L. SHEN, J. SCHNEIDER, S. TESFAMARIAM, S.F. STIEMER, and Z.G. MU. Hysteresis behavior of bracket connection in cross-laminated timber shear walls. *Construction and Building Materials*, 48:980–991, 10.1016/j.conbuildmat.2013.07.050, 2013. 45

[84] J.S. STEELMAN, L.A. FAHNESTOCK, J.F. HAJJAR, and J.M. LaFAVE. Performance of Nonseismic PTFE Slide Bearings When Subjected to Seismic Demands. *Journal of Bridge Engineering*, 21[1]: 04015028, 10.1061/(ASCE)BE.1943-5592.0000777, 2016. 134

[85] I. SUSTERSIC, M. FRAGIACOMO, and B. DUJIC. Influence of the connection behaviour on the seismic resistance of multi-storey crosslam buildings. *World Conf. on Timber Engineering 2012*, New Zealand Timber Design Society, Auckland, New Zealand, 2012. 49

[86] The University of British Columbia, Brock Commons - Tallwood House, Available online: http://vancouver.housing.ubc.ca/residences/brock-commons/, 2018. 43

[87] TreeHugger, The old is new again with Nail Laminated Timber, Available online: https://www.treehugger.com/green-architecture/old-new-again-nail-laminated-timber.html, 2017. 41

[88] A. VELETSOS and N.M. NEWMARK. Effect of inelastic behaviour on the response of simple systems to earthquake motions. *Proceedings of the Second World Conference on Earthquake Engineering*, Vol. 2; 1960; Japan:895-912, 1960. 34

[89] Victoria Harbour, Forte, Available online: https://www.victoriaharbour.com.au/ Developments/AU/VH/Home/Live%20Here/Forte%20Living, 2018. 43

[90] Urban Hub, Des gratte-ciel en bois et en plastique ? Dcouvrez les nouveaux matriaux de construction, Available online: http://www.urban-hub.com/fr/ideas/des-materiaux-de-construction-innovants/, 2018. 43

[91] I. UTNE. Numerical Models for Dynamic Properties of a 14 Storey Timber Building. Department of Structural Engineering, Norwegian University of Science and Technology, 2012. 43

[92] Waugh Thistleton Architects, Dalston Lane The world's largest CLT building, Available online: http://waughthistleton.com/dalston-lane/, 2018. 43

[93] WoodProducts, Cross Laminated Timber, Available online: http://www.woodproducts.fi/content/cross-laminated-timber-clt, 2017. 41

Appendices

Appendix A

Summary of Design Values

This appendix shows the summary of design values of the seismic design of 6-storey CLT building. Besides, the lateral load distribution for taller buildings and design values for PTFE slide bearings employed in taller buildings are presented.

A.1 Design values for 6-storey CLT building

Table A.1: Floor-slab components.

Layer	Thickness [mm]
Glued parquet floor	10
Final screed	25
Insulation of impact of noise	12
Filling material	60
CLT panel	200
Suspended ceiling (gypsum plaster)	95
Total	**402**

The following command is used to construct a uniaxial bilinear hysteretic material object in OpenSees [59].

```
uniaxialMaterial Hysteretic $matTag $s1p $e1p $s2p $e2p <$s3p $e3p> $s1n $e1n
    $s2n $e2n <$s3n $e3n> $pinchX $pinchY $damage1 $damage2 <$beta>
```

Table A.2: Roof components.

Layer	Thickness [mm]
Mineral plant substrate (layer of vegetation)	90
Protective coat with filtering features	12
Roof Sheeting	10
Wooden formwork	20
Thermal insulation with timber slats in between	250
CLT panel	200
Suspended ceiling (gypsum plaster)	95
Total	**677**

Table A.3: External wall components.

Layer	Thickness [mm]
Facade Plate	15
Counter battens / ventilation zone	40
Concealed facade insulating board with timber slats in between	160
CLT panel	128
Gypsum plaster plate	15
Total	**358**

Table A.4: Internal wall components.

Layer	Thickness [mm]
Gypsum plaster plate	15
CLT panel	128
Gypsum plaster plate	15
Total	**158**

Table A.5: Permanent action due to ceiling.

Layer	Thickness [mm]	γ [kN/m^3]	d $*$ γ [kN/m^2]
Glued parquet floor	10	8.0	0.88
Final Screed	25	22.0	0.55
Insulation of impact noise	12	1.40	0.017
Filling material	60	20.0	1.20
CLT panel	200	5.0	1.00
Suspended ceiling (gypsum plaster)	95	3.47	0.33
Total	**402**		**3.177**

Table A.6: Permanent action due to flat roof.

Layer	Thickness [mm]	γ [kN/m^3]	d $*$ γ [kN/m^2]
Mineral plant substrate (layer of vegetation)	90	20.0	1.80
Protective coat with filtering features	12	25.0	0.30
Roof Sheeting	10	5.00	0.05
Wooden formwork	20	5.50	0.11
Thermal insulation with timber slats in between	250	1.20	0.30
CLT panel	200	5.00	1.00
Suspended ceiling (gypsum plaster)	95	3.47	0.33
Total	**677**		**3.89**

Table A.7: Permanent action due to external load bearing wall.

Layer	Thickness [mm]	γ [kN/m^3]	d $*$ γ [kN/m^2]
Facade Plate	15	8.00	0.12
Counter battens / ventilation zone	40	0.44	0.02
Concealed facade insulating board with timber slats in between	160	1.93	0.31
CLT panel	128	5.00	0.64
Gypsum plaster plate	15	10.0	0.15
Total	**358**		**1.24**

Table A.8: Permanent action due to internal load bearing wall.

Layer	Thickness [mm]	γ [kN/m^3]	d $*$ γ [kN/m^2]
Gypsum plaster plate	15	10.0	0.15
CLT panel	128	5.00	0.64
Gypsum plaster plate	15	10.0	0.15
Total	**158**		**0.94**

Table A.9: Calculation of permanent loads.

Level	Section	Calculation	Dead load per storey [kN]
6	Slab	(56 * 20) * 3.89	4,365.00
2-5	Slab	(56 * 20) * 3.17	3,558.20
	External wall	[(56 * 2) * 3.5 + 40 * 3.5] * 1.24	659.68
	Internal wall	[(56 * 2) * 3.5 + (8.5 * 26) * 3.5] * 0.94	1,095.67
Ground	Slab	(56 * 40) * 3.177	7,116.48
	External glazing	[2 * (56 * 40) * 4.3] * 0.4	330.00
	Internal wall	[(56 * 2) * 4.3 + (8.5 * 26) * 4.3] * 0.94	1,345.98
Total			**34,497.98**

Table A.10: Calculation of superimposed loads.

Level	Section	Calculation	Live load per storey [kN]
6	Roof	(56 * 20) * 2.0	2,240.00
2-5	Corridors	[(56 * 3.0) + (8.5 * 4) + (8.5 * 8)] * 4.0	1.080.00
	Bedrooms	[(56 * 20) - 270] * 2.0	1,700.00
Ground	Roof terrace	(56 * 20) * 4.0	4,480.00
	2-7		2,780.00
Total			**20,620.00**

Appendix A. Summary of Design Values

Table A.11: Calculation of superimposed loads for 6-storey CLT building

Level	Dead load G [kN]	Imposed load [kN]	Load combination $G + \lambda_{Ei} * Q$ [kN]	Mass [tonne]
Ground	8878.38	7260	11,056.38	1127.44
2	5313.45	2780	6147.45	626.86
3	5313.45	2780	6147.45	626.86
4	5313.45	2780	6147.45	626.86
5	5313.45	2780	6147.45	626.86
6	4365.80	2240	5037.80	513.71
Total	**34,497.98**	**20,620.00**	**40,683.98**	**4,148.59**

Table A.12: Lateral load distribution for the 6-storey CLT building

Floor	Height above ground (z_i) [m]	Mass (m_i) [t]	$z_i * m_i$ [t*m]	Force (F_i) [kN]	Moment ($F_i * z_i$) [kN*m]
1	4.3	1,127.44	4,847.99	1,007.80	4,333.54
2	7.8	626.86	4,889.51	1,016.44	7,928.23
3	11.3	626.86	7,083.52	1,472.53	16,639.59
4	14.8	626.86	9,277.53	1,928.62	28,543.58
5	18.3	626.86	11,471.54	2,384.72	43,640.38
6	21.8	513.71	11,198.88	2,328.03	50,751.05
Sum		4,148.59	48,768.96	10,138.14	151,836.37

Table A.13: Storey shear and bending moment distribution for the 6-storey CLT building

Floor	Height above ground (z_i) [m]	Base shear [kN]	Storey shear [kN]	Bending moment [kN*m]
6	21.8	2,328.03	2,328.03	50,751.05
5	18.3	2,384.72	4,712.75	94,391.43
4	14.8	1,928.62	6,641.37	122,935.00
3	11.3	1,472.53	8,113.90	139,574.60
2	7.8	1,016.44	9,130.34	147,502.82
1	4.3	1,007.80	10,138.14	151,836.36

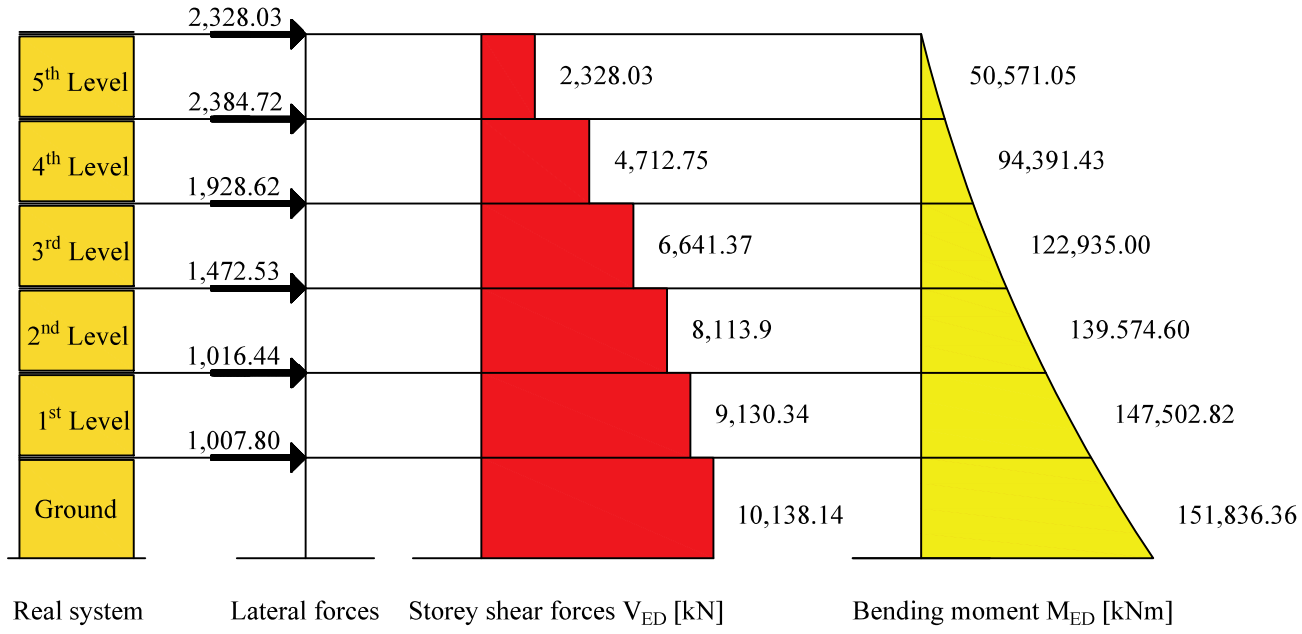


Figure A.1: Cantilever wall model with actions and internal forces.

Table A.14: Distributed lateral forces to each 8.5 m length walls for the 6-storey CLT building.

Floor	Number of walls in x- direction	Storey shear force [kN]	Lateral force at each wall [kN]	With additional torsional effects [kN]
6	30	2,328.03	77.60	97.00
5	30	4,712.75	139.09	173.86
4	30	6,641.37	221.38	276.72
3	30	8,113.90	270.46	338.08
2	30	9,130.34	304.34	380.43
1	30	10,138.14	337.94	422.42

Table A.15: Lateral load distribution for the 8-storey CLT building

Floor	Height above ground (z_i) [m]	Mass (m_i) [t]	$z_i * m_i$ [t*m]	Force (F_i) [kN]	Moment ($F_i * z_i$) [kN*m]
1	4.3	1,127.44	4,847.99	755.74	3,429.68
2	7.8	626.86	4,889.51	762.22	5,945.32
3	11.3	626.86	7,083.52	1,104.23	12,477.80
4	14.8	626.86	9,277.53	1,446.25	21,404.50
5	18.3	626.86	11,471.54	1,788.27	32,725.34
6	21.8	626.86	13,665.55	2,130.29	46,440.32
7	25.3	626.86	15,859.56	2,472.31	62,549.44
8	28.8	513.71	14,794.85	2,306.34	66,422.59
Total		5,402.31	81,890.05	12,765.65	317,817.58

Table A.16: Lateral load distribution for the 12-storey CLT building

Floor	Height above ground (z_i) [m]	Mass (m_i) [t]	$z_i * m_i$ [t*m]	Force (F_i) [kN]	Moment ($F_i * z_i$) [kN*m]
1	4.3	1127.44	4,847.99	397.95	1,711.17
2	7.8	626.86	4,889.51	401.36	3,130.62
3	11.3	626.86	7,083.52	581.46	6,570.49
4	14.8	626.86	9,277.53	761.56	11,271.04
5	18.3	626.86	11,471.54	941.66	17,232.29
6	21.8	626.86	13,665.55	1,121.75	24,454.22
7	25.3	626.86	15,859.56	1,301.85	32,936.83
8	28.8	626.86	18,053.86	1,481.95	42,680.13
9	32.3	626.86	20,247.90	1,662.05	53,684.11
10	35.8	626.86	22,441.95	1,842.14	65,948.79
11	39.3	626.86	24,635.99	2,022.24	79,474.14
12	42.8	513.71	21,986.79	1,804.78	77,244.72
Total		7,909.85	174,462.67	14,320.75	416,338.55

Table A.17: Lateral load distribution for the 16-storey CLT building

Floor	Height above ground (z_i) [m]	Mass (m_i) [t]	$z_i * m_i$ [t*m]	Force (F_i) [kN]	Moment ($F_i * z_i$) [kN*m]
1	4.3	1,127.44	4,847.99	245.09	1,053.87
2	7.8	626.86	4,889.51	247.19	1,928.07
3	11.3	626.86	7,083.52	358.11	4,046.60
4	14.8	626.86	9,277.53	469.02	6,941.56
5	18.3	626.86	11,471.54	579.94	10,612.94
6	21.8	626.86	13,665.55	690.86	15,060.74
7	25.3	626.86	15,859.56	801.78	20,284.97
8	28.8	626.86	18,053.86	912.70	26,285.63
9	32.3	626.86	20,247.90	1,023.61	33,062.71
10	35.8	626.86	22,441.95	1,134.53	40,616.22
11	39.3	626.86	24,635.99	1,245.45	48,946.15
12	42.8	626.86	26,830.04	1,356.37	58,052.50
13	46.3	626.86	29,024.08	1,467.28	67,935.28
14	49.8	626.86	31,218.13	1,578.20	78,594.49
15	53.3	626.86	33,412.17	1,689.12	90,030.12
16	56.8	513.71	29,178.73	1,475.10	83,785.84
Total		10,417.33	30,2139.02	15,274.35	587,237.68

Table A.18: Lateral load distribution for the 20-storey CLT building

Floor	Height above ground (z_i) [m]	Mass (m_i) [t]	$z_i * m_i$ [t*m]	Force (F_i) [kN]	Moment ($F_i * z_i$) [kN*m]
1	4.3	1127.44	4,847.99	167.25	719.19
2	7.8	626.86	4,889.51	168.69	1,315.78
3	11.3	626.86	7,083.52	244.38	2,761.53
4	14.8	626.86	9,277.53	320.08	4,737.15
5	18.3	626.86	11,471.54	395.77	7,242.62
6	21.8	626.86	13,665.55	471.47	10,277.95
7	25.3	626.86	15,859.56	547.16	13,843.14
8	28.8	626.86	18,053.86	622.85	17,938.18
9	32.3	626.86	20,247.90	698.55	22,563.09
10	35.8	626.86	22,441.95	774.24	27,717.85
11	39.3	626.86	24,635.99	849.94	33,402.47
12	42.8	626.86	26,830.04	925.63	39,616.95
13	46.3	626.86	29,024.08	1,001.32	46,361.29
14	49.8	626.86	31,218.13	1,077.02	53,635.48
15	53.3	626.86	33,412.17	1,152.71	61,439.54
16	56.8	626.86	35,606.22	1,228.41	69,773.45
17	60.3	626.86	37,800.26	1,304.10	78,637.22
18	63.8	626.86	39,994.31	1,379.79	88,030.85
19	67.3	626.86	42,188.35	1,455.49	97,954.33
20	70.8	513.71	36,370.67	1,254.78	88,838.37
Total		12,924.81	464,920.09	16,039.63	766,806.43

Table A.19: Design values for PTFE slide bearings in taller buildings

Building	Displacement at mid-height [m]	Displacement at base [m]	Force at mid-height [kN]	Force at base [kN]
6	0.054	0.109	21.65	42.2
8	0.072	0.144	28.5	55.9
12	0.107	0.214	42.2	83.3
16	0.142	0.284	55.9	110.7

Appendix B

Panel thickness verifications in CLT designer

This appendix illustrates the design of CLT floor and wall panel thickness obtained from one of the earliest research tool CLT Designer [18]. The floor panel verifications on 182 mm 5S and 200 mm 5S CLT panels, and a few examples of wall panel checks are presented.

Kompetenzzentrum
holz.bau forschungs gmbh
Inffeldgasse 24, A-8010 Graz
cltdesigner@tugraz.at

CLTdesigner
Version 3.5

Summary of results

Project number:	
Project:	182 mm Floor Slab verification test in CLT designer
Structural element:	
Cross section:	KLH: 5s 182mm DL
Description:	
Date:	Jan 26, 2015
Time:	11:11:53 AM
Author:	

Table of content

1 General 3

2 Structural system 3

2.1 Width of supports 3

3 Cross section 4

3.1 Layer composition 4
3.2 Material parameters 4
3.3 Cross-sectional values 5

4 Loads 5

5 Specification concerning structural fire design 6

6 Information concerning vibrations 6

7 Results 7

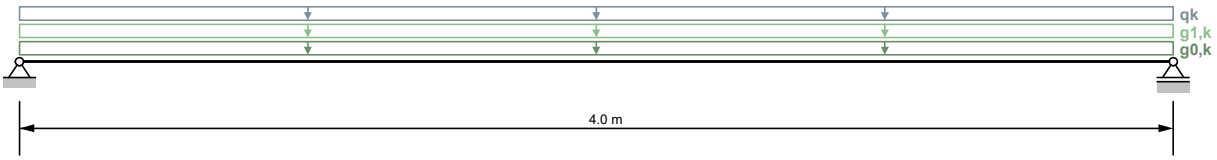
7.1 ULS 7
7.1.1 Bending 7
7.1.2 Shear 7
7.1.3 Bearing pressure 8
7.2 SLS 8
7.2.1 Deflection 8
7.2.2 Vibration 8
7.2.2.1 Verification corresponding to EN 1995-1-1 8
7.2.2.2 Verification corresponding to ON B 1995-1-1/NA:2009-07 9
7.2.2.3 Verification corresponding to DIN 1052 9
7.2.2.4 Verification according to Hamm/Richter 9
7.2.2.5 Verification according to modified Hamm/Richter 9

1 General

Service class 1

2 Structural system

Continuous beam with 1 spans

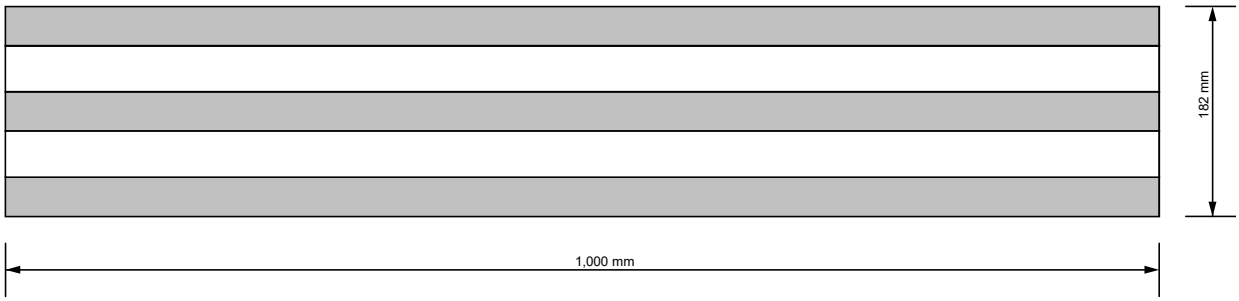


2.1 Width of supports

Support	x	Width
A	0.0 m	1.0 m
B	4.0 m	1.0 m

3 Cross section

CLT-Product with technical approval of the company KLH: 5s 182mm DL
5 layers (width: 1,000 mm / thickness: 182 mm)



3.1 Layer composition

Layer	Thickness	Orientation	Material
# 1	34 mm	0	C24-KLH
# 2	40 mm	90	C24-KLH
# 3	34 mm	0	C24-KLH
# 4	40 mm	90	C24-KLH
# 5	34 mm	0	C24-KLH

3.2 Material parameters

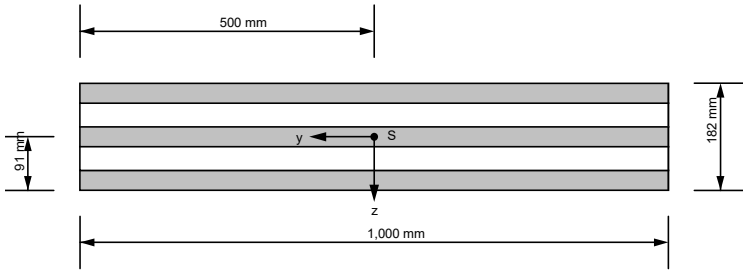
Partial safety factor γ_M = 1.25

Material parameters for C24-KLH	
bending strength	24.0 N/mm²
tensile strength parallel	16.5 N/mm²
tensile strength perpendicular	0.12 N/mm²
compressive strength parallel	21.0 N/mm²
compressive strength perpendicular	2.7 N/mm²
shear strength	2.7 N/mm²

Material parameters for C24-KLH	
rolling shear strength	1.2 N/mm²
Youngs modulus parallel	12,000.0 N/mm²
5%-quantile from Youngs modulus parallel	7,333.0 N/mm²
Youngs modulus perpendicular	0.0 N/mm²
shear modulus	690.0 N/mm²
rolling shear modulus	50.0 N/mm²
density	350.0 kg/m³
density mean value	420.0 kg/m³
in plane shear strength	5.2 N/mm²
torsional strength	2.5 N/mm²

3.3 Cross-sectional values

EA_{ef}	1.224E9 N
EI_{ef}	4.586E12 N·mm²
GA_{ef}	1.365E7 N



4 Loads

Field	$g_{0,k}$	$g_{1,k}$	q_k	Category	s_k	Altitude/Region	w_k
1	1.001 kN/m	2.97 kN/m²	2 kN/m²	A			

Partial safety factors:

γ_G = 1.35

γ_Q = 1.5

Load position:

Plate weight: Total
Permanent loads: Total
Imposed loads: Field-by-field
Snow: Field-by-field
Wind: Total

Combinations:
Combination factors: according to EN

5 Specification concerning structural fire design

No specifications are available

6 Information concerning vibrations

high requirements
Damping factor: 1.0 %
Width perpendicular to the main load bearing direction: 1.0 m

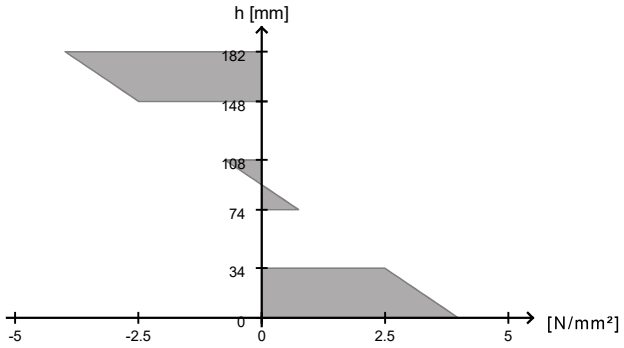
7 Results

Referenced standards: EN 1995-1-1:2009, ON B 1995-1-1/NA:2009-07
Underlying calculation method: Timoshenko

7.1 ULS

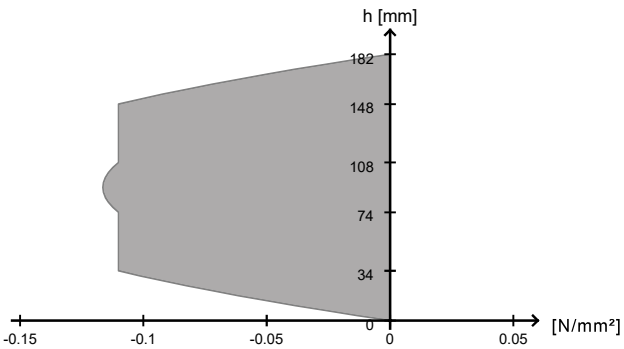
7.1.1 Bending

Utilisation ratio	23.6 %
k_{mod}	0.8
at x	2.0 m
Fundamental combination	$1.35*g_{0,k} + 1.35*g_{1,k} + 1.50*1.00*q_k$



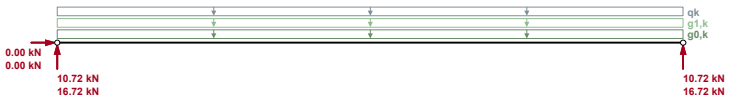
7.1.2 Shear

Utilisation ratio	14.3 %
k_{mod}	0.8
at x	4.0 m
Fundamental combination	$1.35*g_{0,k} + 1.35*g_{1,k} + 1.50*1.00*q_k$



7.1.3 Bearing pressure

Utilisation ratio	0.6 %
k_{mod}	0.8
at x	4.0 m
Fundamental combination	$1.35*g_{0,k} + 1.35*g_{1,k} + 1.50*1.00*q_k$



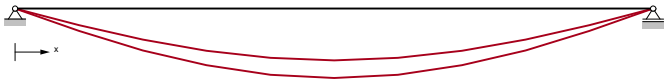
7.2 SLS

7.2.1 Deflection

Limit values according to EN 1995-1-1
Instantaneous deformation w_{inst} t = 0: l/300
Final deformation w_{fin} t = inf: l/150
Final deformation $w_{net,fin}$ t = inf: l/250

Limit values according to ON B 1995-1-1/NA:2009-07
Characteristic combination t = 0: l/300
Characteristic combination t = inf: l/200
Quasi-permanent combination: l/250

Utilisation ratio	53.8 %
w_{max}	8.6 mm
k_{def}	0.85
at x	2.0 m
Final deformation $w_{net,fin}$ t = inf (l/250)	



7.2.2 Vibration

The verification is only valid for residential ceilings!

7.2.2.1 Verification corresponding to EN 1995-1-1

Eigenfrequency: f_1 = 9.5 Hz > 8.0 Hz
Stiffness: w_{1kN} = 0.4 mm < 1.0 mm
Velocity/Unit impuls: v = 2.2 mm/s < 10.7 mm/s

---> Vibration verification fulfilled

7.2.2.2 Verification corresponding to ON B 1995-1-1/NA:2009-07

Eigenfrequency: f_1 = 8.9 Hz > 8.0 Hz
Stiffness: w_{1kN} = 0.4 mm < 1.0 mm
Velocity/Unit impuls: v = 1.9 mm/s < 10.4 mm/s
---> Vibration verification fulfilled

7.2.2.3 Verification corresponding to DIN 1052

w_{perm} = 4.0 mm <= 6,0 mm ---> Vibration verification fulfilled

7.2.2.4 Verification according to Hamm/Richter

Eigenfrequency: f_1 = 10.5 Hz > 8.0 Hz
Stiffness: w_{2kN} = 0.6 mm > 0.5 mm
---> Vibration verification not fulfilled

7.2.2.5 Verification according to modified Hamm/Richter

Eigenfrequency: f_1 = 10.4 Hz > 8.0 Hz
Stiffness: w_{2kN} = 0.6 mm > 0.5 mm
---> Vibration verification not fulfilled

Kompetenzzentrum
holz.bau forschungs gmbh
Inffeldgasse 24, A-8010 Graz
cltdesigner@tugraz.at

CLTdesigner
Version 3.5

Summary of results

Project number:	
Project:	200 mm Floor Slab verification test in CLT designer
Structural element:	
Cross section:	KLH: 5s 200mm DL
Description:	
Date:	Jan 26, 2015
Time:	11:06:20 AM
Author:	

Table of content

1 General **3**

2 Structural system **3**

2.1 Width of supports 3

3 Cross section **4**

3.1 Layer composition 4
3.2 Material parameters 4
3.3 Cross-sectional values 5

4 Loads **5**

5 Specification concerning structural fire design **6**

6 Information concerning vibrations **6**

7 Results **7**

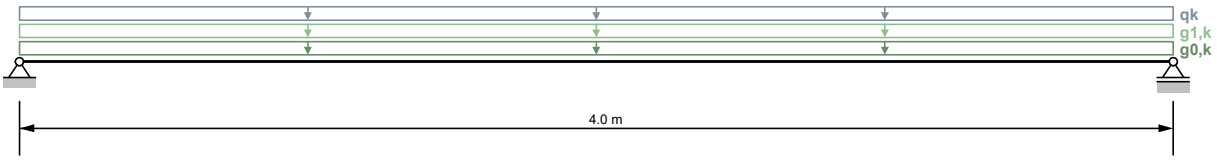
7.1 ULS 7
7.1.1 Bending 7
7.1.2 Shear 7
7.1.3 Bearing pressure 8
7.2 SLS 8
7.2.1 Deflection 8
7.2.2 Vibration 8
7.2.2.1 Verification corresponding to EN 1995-1-1 8
7.2.2.2 Verification corresponding to ON B 1995-1-1/NA:2009-07 9
7.2.2.3 Verification corresponding to DIN 1052 9
7.2.2.4 Verification according to Hamm/Richter 9
7.2.2.5 Verification according to modified Hamm/Richter 9

1 General

Service class 1

2 Structural system

Continuous beam with 1 spans

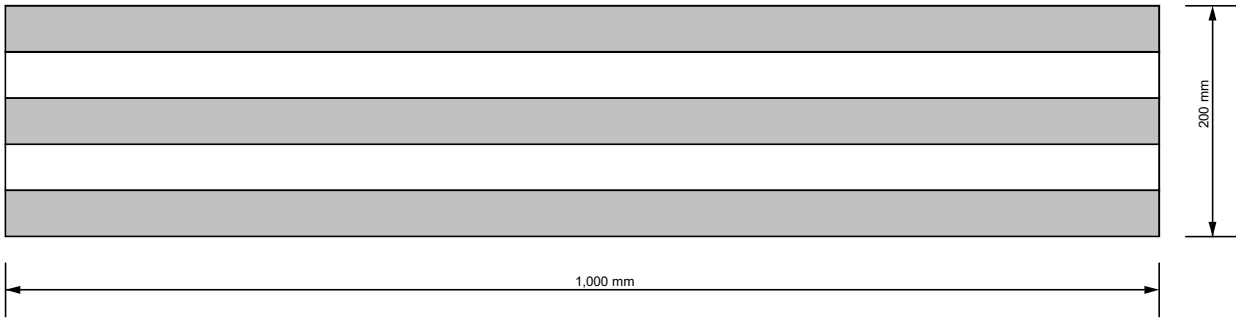


2.1 Width of supports

Support	x	Width
A	0.0 m	1.0 m
B	4.0 m	1.0 m

3 Cross section

CLT-Product with technical approval of the company KLH: 5s 200mm DL
5 layers (width: 1,000 mm / thickness: 200 mm)



3.1 Layer composition

Layer	Thickness	Orientation	Material
# 1	40 mm	0	C24-KLH
# 2	40 mm	90	C24-KLH
# 3	40 mm	0	C24-KLH
# 4	40 mm	90	C24-KLH
# 5	40 mm	0	C24-KLH

3.2 Material parameters

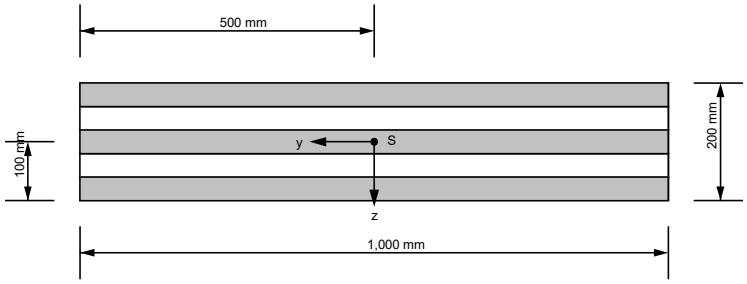
Partial safety factor γ_M = 1.25

Material parameters for C24-KLH	
bending strength	24.0 N/mm²
tensile strength parallel	16.5 N/mm²
tensile strength perpendicular	0.12 N/mm²
compressive strength parallel	21.0 N/mm²
compressive strength perpendicular	2.7 N/mm²
shear strength	2.7 N/mm²

Material parameters for C24-KLH	
rolling shear strength	1.2 N/mm²
Youngs modulus parallel	12,000.0 N/mm²
5%-quantile from Youngs modulus parallel	7,333.0 N/mm²
Youngs modulus perpendicular	0.0 N/mm²
shear modulus	690.0 N/mm²
rolling shear modulus	50.0 N/mm²
density	350.0 kg/m³
density mean value	420.0 kg/m³
in plane shear strength	5.2 N/mm²
torsional strength	2.5 N/mm²

3.3 Cross-sectional values

EA_{ef}	1.44E9 N
EI_{ef}	6.336E12 N·mm²
GA_{ef}	1.595E7 N



4 Loads

Field	$g_{0,k}$	$g_{1,k}$	q_k	Category	s_k	Altitude/Region	w_k
1	1.1 kN/m	2.97 kN/m²	2 kN/m²	A			

Partial safety factors:

γ_G = 1.35

γ_Q = 1.5

Load position:

Plate weight: Total
Permanent loads: Total
Imposed loads: Field-by-field
Snow: Field-by-field
Wind: Total

Combinations:
Combination factors: according to EN

5 Specification concerning structural fire design

No specifications are available

6 Information concerning vibrations

high requirements
Damping factor: 1.0 %
Width perpendicular to the main load bearing direction: 1.0 m

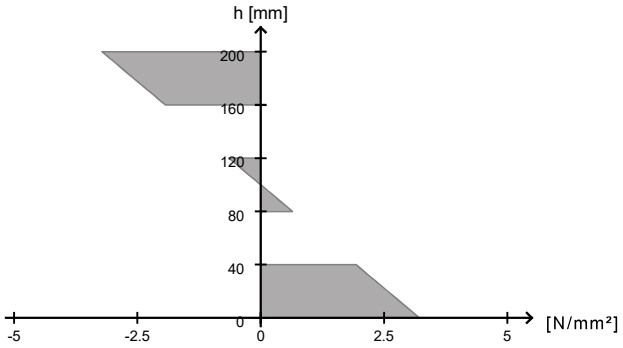
7 Results

Referenced standards: EN 1995-1-1:2009, ON B 1995-1-1/NA:2009-07
Underlying calculation method: Timoshenko

7.1 ULS

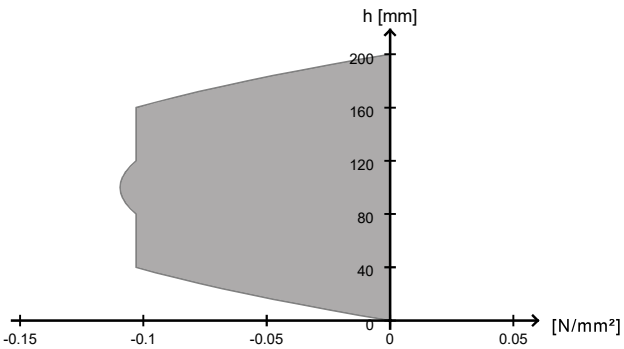
7.1.1 Bending

Utilisation ratio	19.0 %
k_{mod}	0.8
at x	2.0 m
Fundamental combination	$1.35*g_{0,k} + 1.35*g_{1,k} + 1.50*1.00*q_k$



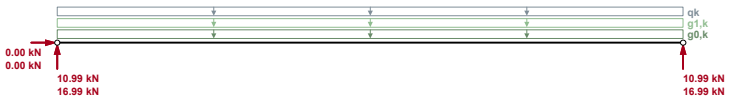
7.1.2 Shear

Utilisation ratio	13.4 %
k_{mod}	0.8
at x	4.0 m
Fundamental combination	$1.35*g_{0,k} + 1.35*g_{1,k} + 1.50*1.00*q_k$



7.1.3 Bearing pressure

Utilisation ratio	0.6 %
k_{mod}	0.8
at x	4.0 m
Fundamental combination	$1.35*g_{0,k} + 1.35*g_{1,k} + 1.50*1.00*q_k$



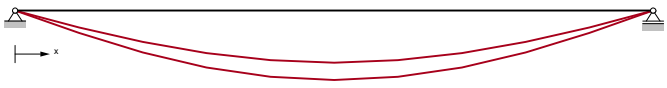
7.2 SLS

7.2.1 Deflection

Limit values according to EN 1995-1-1
Instantaneous deformation w_{inst} t = 0: l/300
Final deformation w_{fin} t = inf: l/150
Final deformation $w_{net,fin}$ t = inf: l/250

Limit values according to ON B 1995-1-1/NA:2009-07
Characteristic combination t = 0: l/300
Characteristic combination t = inf: l/200
Quasi-permanent combination: l/250

Utilisation ratio	40.9 %
w_{max}	6.5 mm
k_{def}	0.85
at x	2.0 m
Final deformation $w_{net,fin}$ t = inf (l/250)	



7.2.2 Vibration

The verification is only valid for residential ceilings!

7.2.2.1 Verification corresponding to EN 1995-1-1

Eigenfrequency: f_1 = 10.9 Hz > 8.0 Hz
Stiffness: w_{1kN} = 0.3 mm < 1.0 mm
Velocity/Unit impuls: v = 2.2 mm/s < 11.5 mm/s

---> Vibration verification fulfilled

7.2.2.2 Verification corresponding to ON B 1995-1-1/NA:2009-07

Eigenfrequency: f_1 = 10.2 Hz > 8.0 Hz
Stiffness: w_{1kN} = 0.3 mm < 1.0 mm
Velocity/Unit impuls: v = 1.9 mm/s < 11.1 mm/s
---> Vibration verification fulfilled

7.2.2.3 Verification corresponding to DIN 1052

w_{perm} = 3.0 mm <= 6,0 mm ---> Vibration verification fulfilled

7.2.2.4 Verification according to Hamm/Richter

Eigenfrequency: f_1 = 12.1 Hz > 8.0 Hz
Stiffness: w_{2kN} = 0.4 mm < 0.5 mm
---> Vibration verification fulfilled

7.2.2.5 Verification according to modified Hamm/Richter

Eigenfrequency: f_1 = 12.1 Hz > 8.0 Hz
Stiffness: w_{2kN} = 0.4 mm < 0.5 mm
---> Vibration verification fulfilled

Kompetenzzentrum
holz.bau forschungs gmbh
Inffeldgasse 24, A-8010 Graz
cltdesigner@tugraz.at

CLTdesigner
Version 6.10.5

Summary of results

Project number:	
Project:	6-Storey Building Ground FLoor
Structural element:	
Cross section:	KLH: 120mm 5s DL
Description:	
Date:	Jan 2, 2019
Time:	10:13:30 PM
Author:	

Table of content

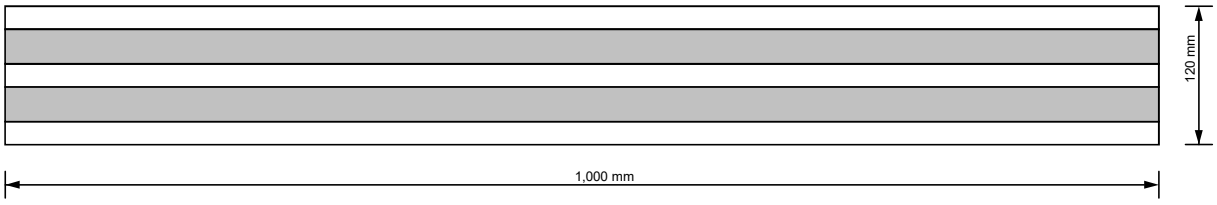
1 Cross section **3**
1.1 Layer composition 3
1.2 Material parameters 3
1.3 Cross-sectional values 4

2 Specification concerning structural fire design **4**

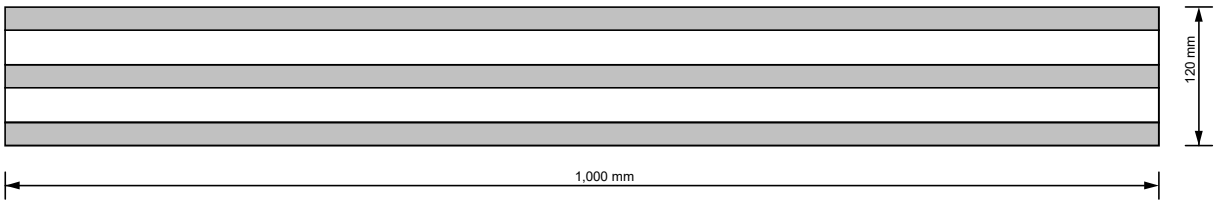
3 Internal forces, design values and results **4**

1 Cross section

CLT-Product with technical approval of the company KLH: 120mm 5s DL
5 layers (width: 1,000 mm / thickness: 120 mm)
Horizontal cross section



Vertical cross section



1.1 Layer composition

Layer	Thickness	Orientation	Material
# 1	20 mm	0	C24-KLH
# 2	30 mm	90	C24-KLH
# 3	20 mm	0	C24-KLH
# 4	30 mm	90	C24-KLH
# 5	20 mm	0	C24-KLH

1.2 Material parameters

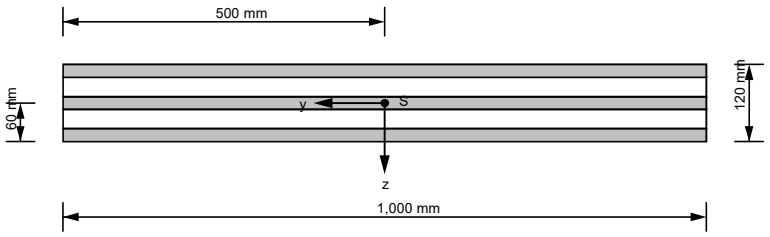
Partial safety factor γ_M = 1.25

Material parameters for	C24-KLH
bending strength [N/mm²]	24.0
tensile strength parallel [N/mm²]	16.5

Material parameters for	C24-KLH
tensile strength perpendicular [N/mm²]	0.12
compressive strength parallel [N/mm²]	21.0
compressive strength perpendicular [N/mm²]	2.7
shear strength [N/mm²]	2.7
rolling shear strength [N/mm²]	1.2
Youngs modulus parallel [N/mm²]	12,000.0
5%-quantile from Youngs modulus parallel [N/mm²]	7,333.0
Youngs modulus perpendicular [N/mm²]	0.0
shear modulus [N/mm²]	690.0
rolling shear modulus [N/mm²]	50.0
density [kg/m³]	350.0
density mean value [kg/m³]	420.0

1.3 Cross-sectional values

D_x	7.2E8 N/m
D_y	7.2E8 N/m
D_{xy}	5.587E7 N/m



2 Specification concerning structural fire design

No specifications are available

3 Internal forces, design values and results

Shear force per unit length	$n_{xy,d}$ = 80.0 kN/m
Modification factor	k_{mod} = 1.1
Partial safety factor	γ_M = 1.0

Mechanism I - shear	28.0 %
Mechanism II - torsion	32.7 %
Mechanism I - shear following ETA-09/0036	23.3 %
Mechanism II - torsion following ETA-08/0242	27.3 %

Kompetenzzentrum
holz.bau forschungs gmbh
Inffeldgasse 24, A-8010 Graz
cltdesigner@tugraz.at

CLTdesigner
Version 6.10.5

Summary of results

Project number:	
Project:	6-Storey Building Upper FLoors
Structural element:	
Cross section:	KLH: 100mm 5s DL
Description:	
Date:	Jan 2, 2019
Time:	10:16:59 PM
Author:	

Table of content

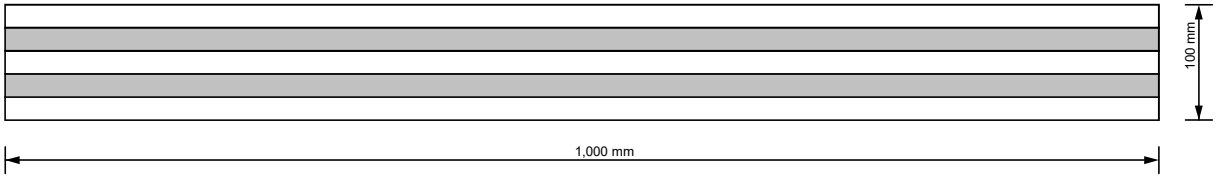
1 Cross section **3**
1.1 Layer composition 3
1.2 Material parameters 3
1.3 Cross-sectional values 4

2 Specification concerning structural fire design **4**

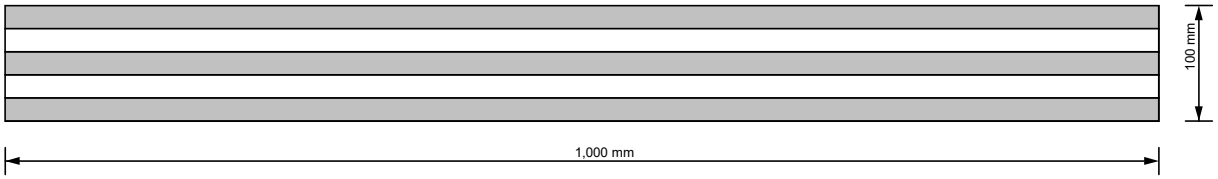
3 Internal forces, design values and results **4**

1 Cross section

CLT-Product with technical approval of the company KLH: 100mm 5s DL
5 layers (width: 1,000 mm / thickness: 100 mm)
Horizontal cross section



Vertical cross section



1.1 Layer composition

Layer	Thickness	Orientation	Material
# 1	20 mm	0	C24-KLH
# 2	20 mm	90	C24-KLH
# 3	20 mm	0	C24-KLH
# 4	20 mm	90	C24-KLH
# 5	20 mm	0	C24-KLH

1.2 Material parameters

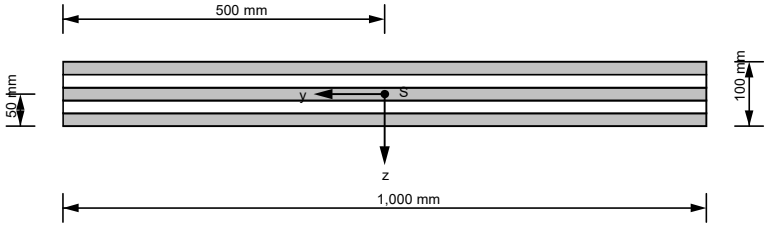
Partial safety factor γ_M = 1.25

Material parameters for	C24-KLH
bending strength [N/mm²]	24.0
tensile strength parallel [N/mm²]	16.5

Material parameters for	C24-KLH
tensile strength perpendicular [N/mm²]	0.12
compressive strength parallel [N/mm²]	21.0
compressive strength perpendicular [N/mm²]	2.7
shear strength [N/mm²]	2.7
rolling shear strength [N/mm²]	1.2
Youngs modulus parallel [N/mm²]	12,000.0
5%-quantile from Youngs modulus parallel [N/mm²]	7,333.0
Youngs modulus perpendicular [N/mm²]	0.0
shear modulus [N/mm²]	690.0
rolling shear modulus [N/mm²]	50.0
density [kg/m³]	350.0
density mean value [kg/m³]	420.0

1.3 Cross-sectional values

D_x	4.8E8 N/m
D_y	7.2E8 N/m
D_{xy}	4.656E7 N/m



2 Specification concerning structural fire design

No specifications are available

3 Internal forces, design values and results

Shear force per unit length	$n_{xy,d}$ = 64.0 kN/m
Modification factor	k_{mod} = 1.1
Partial safety factor	γ_M = 1.0

Mechanism I - shear	28.0 %
Mechanism II - torsion	21.8 %
Mechanism I - shear following ETA-09/0036	28.0 %
Mechanism II - torsion following ETA-08/0242	21.8 %

Appendix C

Design of Connections

This appendix illustrates the number of CLT connection elements employed in the design of buildings. The following tables present corresponding type and number of metal connectors in multi-storey CLT buildings of different heights, covering different design practices characterised by the behaviour factor, q = 2, 2.5, 3, 4.

Table C.1: Number of connections for 6-storey A2 building.

Level	q = 2	q = 2.5	q = 3	q = 4
1	6 TTF 200 3 WHT 620	5 TTF 200 2 WHT 620	4 TTF 200 2 WHT 620	3 TTF 200 2 WHT 620
2	6 TTF 200 2 WHT 620	5 TTF 200 2 WHT 620	4 TTF 200 2 WHT 620	3 TTF 200 2 WHT 620
3	5 TTF 200 2 WHT 540	4 TTF 200 2 WHT 540	4 TTF 200 2 WHT 540	3 TTF 200 2 WHT 540
4	4 TTF 200 2 WHT 440	4 TTF 200 2 WHT 440	3 TTF 200 2 WHT 440	2 TTF 200 2 WHT 440
5	3 TTF 200 2 WHT 440	3 TTF 200 2 WHT 440	2 TTF 200 2 WHT 440	2 TTF 200 2 WHT 440
6	2 TTF 200 2 WHT 340	2 TTF 200 2 WHT 340	1 TTF 200 2 WHT 340	1 TTF 200 2 WHT 340

Table C.2: Number of connectors for 6-storey A3 building.

Level	q = 2	q = 2.5	q = 3	q = 4
1	5 TTF 200 4 WHT 620	4 TTF 200 2 WHT 620	3 TTF 200 2 WHT 620	3 TTF 200 2 WHT 620
2	5 TTF 200 2 WHT 620	4 TTF 200 2 WHT 620	3 TTF 200 2 WHT 620	3 TTF 200 2 WHT 620
3	4 TTF 200 2 WHT 540	3 TTF 200 2 WHT 540	3 TTF 200 2 WHT 540	2 TTF 200 2 WHT 540
4	3 TTF 200 2 WHT 440	3 TTF 200 2 WHT 440	2 TTF 200 2 WHT 440	2 TTF 200 2 WHT 440
5	3 TTF 200 2 WHT 440	2 TTF 200 2 WHT 440	2 TTF 200 2 WHT 440	2 TTF 200 2 WHT 440
6	2 TTF 200 2 WHT 340	1 TTF 200 2 WHT 340	1 TTF 200 2 WHT 340	1 TTF 200 2 WHT 340

Table C.3: Number of connectors for 8-storey B1 building.

Level	q = 2	q = 2.5	q = 3	q = 4
1	12 TTF 200 4 WHT 620	9 TTF 200 4 WHT 620	8 TTF 200 4 WHT 620	6 TTF 200 2 WHT 620
2	11 TTF 200 4 WHT 620	9 TTF 200 4 WHT 620	7 TTF 200 2 WHT 620	6 TTF 200 2 WHT 620
3	10 TTF 200 4 WHT 620	8 TTF 200 4 WHT 620	7 TTF 200 2 WHT 620	5 TTF 200 2 WHT 620
4	9 TTF 200 4 WHT 620	8 TTF 200 4 WHT 540	6 TTF 200 4 WHT 540	5 TTF 200 2 WHT 540
5	8 TTF 200 4 WHT 540	7 TTF 200 4 WHT 540	6 TTF 200 2 WHT 540	4 TTF 200 2 WHT 540
6	6 TTF 200 4 WHT 540	5 TTF 200 4 WHT 440	4 TTF 200 2 WHT 440	3 TTF 200 2 WHT 440
7	5 TTF 200 4 WHT 440	4 TTF 200 2 WHT 440	3 TTF 200 2 WHT 440	2 TTF 200 2 WHT 440
8	2 TTF 200 2 WHT 340	2 TTF 200 2 WHT 340	2 TTF 200 2 WHT 340	1 TTF 200 2 WHT 340

Table C.4: Number of metal connectors determined for 8-storey B2 building.

Level	q = 2	q = 2.5	q = 3	q = 4
1	8 TTF 200 4 WHT 620	6 TTF 200 4 WHT 620	5 TTF 200 4 WHT 620	4 TTF 200 2 WHT 620
2	7 TTF 200 4 WHT 620	6 TTF 200 4 WHT 620	5 TTF 200 4 WHT 620	4 TTF 200 2 WHT 620
3	7 TTF 200 4 WHT 620	6 TTF 200 4 WHT 620	5 TTF 200 2 WHT 620	4 TTF 200 2 WHT 620
4	6 TTF 200 4 WHT 620	5 TTF 200 2 WHT 620	4 TTF 200 4 WHT 540	3 TTF 200 2 WHT 620
5	4 TTF 200 4 WHT 540	4 TTF 200 4 WHT 540	4 TTF 200 2 WHT 540	3 TTF 200 2 WHT 540
6	4 TTF 200 4 WHT 540	4 TTF 200 2 WHT 540	3 TTF 200 2 WHT 540	3 TTF 200 2 WHT 540
7	3 TTF 200 4 WHT 440	3 TTF 200 2 WHT 440	2 TTF 200 2 WHT 440	2 TTF 200 2 WHT 440
8	3 TTF 200 2 WHT 340	2 TTF 200 2 WHT 340	1 TTF 200 2 WHT 340	1 TTF 200 2 WHT 340

Table C.5: Number of metal connectors for 8-storey B3 building.

Level	q = 2	q = 2.5	q = 3	q = 4
1	6 TTF 200 4 WHT 620	5 TTF 200 4 WHT 620	4 TTF 200 4 WHT 620	3 TTF 200 2 WHT 620
2	6 TTF 200 4 WHT 620	5 TTF 200 4 WHT 620	4 TTF 200 4 WHT 620	3 TTF 200 2 WHT 620
3	5 TTF 200 4 WHT 620	4 TTF 200 4 WHT 620	4 TTF 200 2 WHT 620	3 TTF 200 2 WHT 620
4	5 TTF 200 4 WHT 620	4 TTF 200 4 WHT 540	3 TTF 200 4 WHT 540	3 TTF 200 2 WHT 540
5	4 TTF 200 4 WHT 540	4 TTF 200 4 WHT 540	3 TTF 200 2 WHT 540	2 TTF 200 2 WHT 540
6	4 TTF 200 4 WHT 440	3 TTF 200 4 WHT 440	2 TTF 200 2 WHT 440	2 TTF 200 2 WHT 440
7	3 TTF 200 4 WHT 440	2 TTF 200 2 WHT 440	2 TTF 200 2 WHT 440	2 TTF 200 2 WHT 440
8	2 TTF 200 2 WHT 340	1 TTF 200 2 WHT 340	1 TTF 200 2 WHT 340	1 TTF 200 2 WHT 340

Table C.6: Number of metal connectors for 12-storey C1 building.

Level	q = 2	q = 2.5	q = 3	q = 4
1	13 TTF 200 6 WHT 620	10 TTF 200 4 WHT 620	9 TTF 200 4 WHT 620	7 TTF 200 4 WHT 620
2	13 TTF 200 4 WHT 620	10 TTF 200 4 WHT 620	9 TTF 200 4 WHT 620	7 TTF 200 2 WHT 620
3	12 TTF 200 4 WHT 620	10 TTF 200 4 WHT 620	8 TTF 200 4 WHT 620	6 TTF 200 2 WHT 620
4	12 TTF 200 4 WHT 620	9 TTF 200 4 WHT 620	8 TTF 200 4 WHT 620	6 TTF 200 2 WHT 620
5	11 TTF 200 4 WHT 620	9 TTF 200 4 WHT 620	8 TTF 200 4 WHT 620	6 TTF 200 2 WHT 540
6	10 TTF 200 4 WHT 620	8 TTF 200 4 WHT 620	7 TTF 200 4 WHT 540	5 TTF 200 2 WHT 540
7	9 TTF 200 4 WHT 620	8 TTF 200 4 WHT 620	6 TTF 200 4 WHT 540	5 TTF 200 2 WHT 540
8	8 TTF 200 4 WHT 540	7 TTF 200 4 WHT 540	6 TTF 200 2 WHT 540	4 TTF 200 2 WHT 440
9	7 TTF 200 4 WHT 540	6 TTF 200 2 WHT 540	5 TTF 200 2 WHT 540	4 TTF 200 2 WHT 440
10	5 TTF 200 2 WHT 540	4 TTF 200 2 WHT 540	4 TTF 200 2 WHT 540	3 TTF 200 2 WHT 440
11	4 TTF 200 2 WHT 440	3 TTF 200 2 WHT 440	3 TTF 200 2 WHT 440	2 TTF 200 2 WHT 340
12	2 TTF 200 2 WHT 340	2 TTF 200 2 WHT 340	2 TTF 200 2 WHT 340	1 TTF 200 2 WHT 340

Table C.7: Number of metal connectors for 12-storey C2 building.

Level	q = 2	q = 2.5	q = 3	q = 4
1	9 TTF 200 6 WHT 620	7 TTF 200 4 WHT 620	6 TTF 200 4 WHT 620	5 TTF 200 4 WHT 620
2	9 TTF 200 4 WHT 620	7 TTF 200 4 WHT 620	6 TTF 200 4 WHT 620	5 TTF 200 2 WHT 620
3	8 TTF 200 4 WHT 620	7 TTF 200 4 WHT 620	6 TTF 200 4 WHT 620	4 TTF 200 2 WHT 620
4	8 TTF 200 4 WHT 620	6 TTF 200 4 WHT 620	6 TTF 200 4 WHT 620	4 TTF 200 4 WHT 540
5	8 TTF 200 4 WHT 540	6 TTF 200 4 WHT 540	5 TTF 200 4 WHT 540	4 TTF 200 2 WHT 540
6	7 TTF 200 4 WHT 540	6 TTF 200 4 WHT 540	5 TTF 200 4 WHT 540	4 TTF 200 2 WHT 540
7	6 TTF 200 4 WHT 540	5 TTF 200 4 WHT 540	4 TTF 200 4 WHT 540	3 TTF 200 2 WHT 540
8	6 TTF 200 4 WHT 540	5 TTF 200 4 WHT 540	4 TTF 200 2 WHT 540	3 TTF 200 2 WHT 440
9	5 TTF 200 4 WHT 540	4 TTF 200 4 WHT 440	3 TTF 200 4 WHT 440	3 TTF 200 2 WHT 440
10	4 TTF 200 4 WHT 440	3 TTF 200 2 WHT 440	3 TTF 200 2 WHT 440	2 TTF 200 2 WHT 440
11	3 TTF 200 2 WHT 440	2 TTF 200 2 WHT 440	2 TTF 200 2 WHT 340	2 TTF 200 2 WHT 340
12	2 TTF 200 2 WHT 340	1 TTF 200 2 WHT 340	1 TTF 200 2 WHT 340	1 TTF 200 2 WHT 340

Table C.8: Number of metal connectors for 12-storey C3 building.

Level	q = 2	q = 2.5	q = 3	q = 4
1	7 TTF 200 6 WHT 620	5 TTF 200 4 WHT 620	5 TTF 200 4 WHT 620	4 TTF 200 4 WHT 620
2	7 TTF 200 4 WHT 620	5 TTF 200 4 WHT 620	5 TTF 200 4 WHT 620	4 TTF 200 2 WHT 620
3	6 TTF 200 4 WHT 620	5 TTF 200 4 WHT 620	4 TTF 200 4 WHT 620	3 TTF 200 2 WHT 620
4	6 TTF 200 4 WHT 620	5 TTF 200 4 WHT 620	4 TTF 200 4 WHT 620	3 TTF 200 2 WHT 620
5	6 TTF 200 4 WHT 620	5 TTF 200 4 WHT 620	4 TTF 200 4 WHT 620	3 TTF 200 2 WHT 620
6	5 TTF 200 4 WHT 620	4 TTF 200 4 WHT 620	4 TTF 200 2 WHT 620	3 TTF 200 2 WHT 620
7	5 TTF 200 4 WHT 620	4 TTF 200 4 WHT 620	3 TTF 200 2 WHT 620	3 TTF 200 2 WHT 620
8	4 TTF 200 3 WHT 540	4 TTF 200 4 WHT 540	3 TTF 200 2 WHT 540	2 TTF 200 2 WHT 540
9	4 TTF 200 4 WHT 540	3 TTF 200 2 WHT 540	3 TTF 200 2 WHT 540	2 TTF 200 2 WHT 540
10	3 TTF 200 2 WHT 540	2 TTF 200 2 WHT 540	2 TTF 200 2 WHT 540	2 TTF 200 2 WHT 540
11	2 TTF 200 2 WHT 440	2 TTF 200 2 WHT 440	2 TTF 200 2 WHT 440	1 TTF 200 2 WHT 440
12	1 TTF 200 2 WHT 340	1 TTF 200 2 WHT 340	1 TTF 200 2 WHT 340	1 TTF 200 2 WHT 340

Table C.9: Number of metal connectors for 16-storey D1 building.

Level	q = 2	q = 2.5	q = 3	q = 4
1	14 TTF 200 6 WHT 620	11 TTF 200 4 WHT 620	10 TTF 200 4 WHT 620	7 TTF 200 4 WHT 620
2	14 TTF 200 4 WHT 620	11 TTF 200 4 WHT 620	9 TTF 200 4 WHT 620	7 TTF 200 2 WHT 620
3	14 TTF 200 4 WHT 620	11 TTF 200 4 WHT 620	9 TTF 200 4 WHT 620	7 TTF 200 2 WHT 620
4	13 TTF 200 4 WHT 620	11 TTF 200 4 WHT 620	9 TTF 200 4 WHT 620	7 TTF 200 2 WHT 620
5	13 TTF 200 4 WHT 620	10 TTF 200 4 WHT 620	9 TTF 200 4 WHT 620	7 TTF 200 2 WHT 620
6	12 TTF 200 4 WHT 620	10 TTF 200 4 WHT 620	8 TTF 200 4 WHT 620	6 TTF 200 2 WHT 620
7	12 TTF 200 4 WHT 620	9 TTF 200 4 WHT 620	8 TTF 200 4 WHT 620	6 TTF 200 4 WHT 540
8	11 TTF 200 4 WHT 620	9 TTF 200 4 WHT 620	7 TTF 200 4 WHT 620	6 TTF 200 2 WHT 540
9	10 TTF 200 4 WHT 620	8 TTF 200 4 WHT 620	7 TTF 200 2 WHT 620	5 TTF 200 2 WHT 540
10	9 TTF 200 4 WHT 620	7 TTF 200 4 WHT 540	6 TTF 200 4 WHT 540	5 TTF 200 2 WHT 540
11	8 TTF 200 4 WHT 540	7 TTF 200 4 WHT 540	6 TTF 200 2 WHT 540	4 TTF 200 2 WHT 440
12	7 TTF 200 4 WHT 540	6 TTF 200 4 WHT 540	5 TTF 200 2 WHT 540	4 TTF 200 2 WHT 440
13	6 TTF 200 4 WHT 540	5 TTF 200 2 WHT 540	4 TTF 200 2 WHT 540	3 TTF 200 2 WHT 440
14	5 TTF 200 2 WHT 540	4 TTF 200 2 WHT 440	3 TTF 200 2 WHT 440	3 TTF 200 2 WHT 340
15	3 TTF 200 2 WHT 440	3 TTF 200 2 WHT 440	2 TTF 200 2 WHT 340	3 TTF 200 2 WHT 340
16	2 TTF 200 2 WHT 340	2 TTF 200 2 WHT 340	1 TTF 200 2 WHT 340	1 TTF 200 2 WHT 340

Table C.10: Number of metal connectors for 16-storey D2 building.

Level	q = 2	q = 2.5	q = 3	q = 4
1	10 TTF 200 6 WHT 620	8 TTF 200 4 WHT 620	7 TTF 200 4 WHT 620	5 TTF 200 4 WHT 620
2	9 TTF 200 4 WHT 620	8 TTF 200 4 WHT 620	6 TTF 200 4 WHT 620	5 TTF 200 2 WHT 620
3	9 TTF 200 4 WHT 620	7 TTF 200 4 WHT 620	6 TTF 200 4 WHT 620	5 TTF 200 2 WHT 620
4	9 TTF 200 4 WHT 620	7 TTF 200 4 WHT 620	6 TTF 200 4 WHT 620	5 TTF 200 2 WHT 620
5	9 TTF 200 4 WHT 620	7 TTF 200 4 WHT 620	6 TTF 200 4 WHT 620	5 TTF 200 2 WHT 620
6	8 TTF 200 4 WHT 620	7 TTF 200 4 WHT 620	6 TTF 200 4 WHT 620	4 TTF 200 2 WHT 620
7	8 TTF 200 4 WHT 620	6 TTF 200 4 WHT 620	5 TTF 200 4 WHT 620	4 TTF 200 4 WHT 540
8	7 TTF 200 4 WHT 620	6 TTF 200 4 WHT 620	5 TTF 200 4 WHT 620	4 TTF 200 2 WHT 540
9	7 TTF 200 4 WHT 620	6 TTF 200 4 WHT 620	5 TTF 200 2 WHT 620	4 TTF 200 2 WHT 540
10	6 TTF 200 4 WHT 620	5 TTF 200 4 WHT 540	4 TTF 200 4 WHT 540	3 TTF 200 2 WHT 540
11	6 TTF 200 4 WHT 540	5 TTF 200 4 WHT 540	4 TTF 200 2 WHT 540	3 TTF 200 2 WHT 440
12	5 TTF 200 4 WHT 540	4 TTF 200 4 WHT 540	3 TTF 200 2 WHT 540	3 TTF 200 2 WHT 440
13	4 TTF 200 4 WHT 540	3 TTF 200 2 WHT 540	3 TTF 200 2 WHT 540	2 TTF 200 2 WHT 440
14	3 TTF 200 2 WHT 540	3 TTF 200 2 WHT 440	2 TTF 200 2 WHT 440	2 TTF 200 2 WHT 340
15	2 TTF 200 2 WHT 440	2 TTF 200 2 WHT 440	2 TTF 200 2 WHT 340	1 TTF 200 2 WHT 340
16	1 TTF 200 2 WHT 340	1 TTF 200 2 WHT 340	1 TTF 200 2 WHT 340	1 TTF 200 2 WHT 340

Table C.11: Number of metal connectors for 16-storey D3 building.

Level	q = 2	q = 2.5	q = 3	q = 4
1	7 TTF 200 6 WHT 620	6 TTF 200 4 WHT 620	5 TTF 200 4 WHT 620	4 TTF 200 4 WHT 620
2	7 TTF 200 4 WHT 620	6 TTF 200 4 WHT 620	5 TTF 200 4 WHT 620	4 TTF 200 2 WHT 620
3	7 TTF 200 4 WHT 620	6 TTF 200 4 WHT 620	5 TTF 200 4 WHT 620	4 TTF 200 2 WHT 620
4	7 TTF 200 4 WHT 620	6 TTF 200 4 WHT 620	5 TTF 200 4 WHT 620	4 TTF 200 2 WHT 620
5	7 TTF 200 4 WHT 620	5 TTF 200 4 WHT 620	5 TTF 200 4 WHT 620	4 TTF 200 2 WHT 620
6	6 TTF 200 4 WHT 620	5 TTF 200 4 WHT 620	4 TTF 200 4 WHT 620	3 TTF 200 2 WHT 620
7	6 TTF 200 4 WHT 620	5 TTF 200 4 WHT 620	4 TTF 200 4 WHT 620	3 TTF 200 4 WHT 540
8	6 TTF 200 4 WHT 620	5 TTF 200 4 WHT 620	4 TTF 200 4 WHT 620	3 TTF 200 2 WHT 540
9	5 TTF 200 4 WHT 620	4 TTF 200 4 WHT 620	4 TTF 200 2 WHT 620	3 TTF 200 2 WHT 540
10	5 TTF 200 4 WHT 620	4 TTF 200 4 WHT 540	3 TTF 200 4 WHT 540	3 TTF 200 2 WHT 540
11	4 TTF 200 4 WHT 540	4 TTF 200 4 WHT 540	3 TTF 200 2 WHT 540	2 TTF 200 2 WHT 440
12	4 TTF 200 4 WHT 540	3 TTF 200 4 WHT 540	3 TTF 200 2 WHT 540	2 TTF 200 2 WHT 440
13	3 TTF 200 4 WHT 540	3 TTF 200 2 WHT 540	2 TTF 200 2 WHT 540	2 TTF 200 2 WHT 440
14	3 TTF 200 2 WHT 540	2 TTF 200 2 WHT 440	2 TTF 200 2 WHT 440	2 TTF 200 2 WHT 340
15	2 TTF 200 2 WHT 440	2 TTF 200 2 WHT 440	1 TTF 200 2 WHT 340	1 TTF 200 2 WHT 340
16	1 TTF 200 2 WHT 340	1 TTF 200 2 WHT 340	1 TTF 200 2 WHT 340	1 TTF 200 2 WHT 340

Table C.12: Number of metal connectors for 20-storey E1 building.

Level	q = 2	q = 2.5	q = 3	q = 4
1	15 TTF 200 6 WHT 620	12 TTF 200 6 WHT 620	10 TTF 200 4 WHT 620	8 TTF 200 4 WHT 620
2	14 TTF 200 6 WHT 620	12 TTF 200 4 WHT 620	10 TTF 200 4 WHT 620	7 TTF 200 4 WHT 620
3	14 TTF 200 6 WHT 620	12 TTF 200 4 WHT 620	10 TTF 200 4 WHT 620	7 TTF 200 4 WHT 620
4	14 TTF 200 4 WHT 620	11 TTF 200 4 WHT 620	10 TTF 200 4 WHT 620	7 TTF 200 2 WHT 620
5	14 TTF 200 4 WHT 620	11 TTF 200 4 WHT 620	9 TTF 200 4 WHT 620	7 TTF 200 2 WHT 620
6	13 TTF 200 4 WHT 620	11 TTF 200 4 WHT 620	9 TTF 200 4 WHT 620	7 TTF 200 2 WHT 620
7	13 TTF 200 4 WHT 620	11 TTF 200 4 WHT 620	9 TTF 200 4 WHT 620	7 TTF 200 2 WHT 620
8	13 TTF 200 4 WHT 620	10 TTF 200 4 WHT 620	9 TTF 200 4 WHT 620	7 TTF 200 2 WHT 620
9	12 TTF 200 4 WHT 620	10 TTF 200 4 WHT 620	8 TTF 200 4 WHT 620	6 TTF 200 2 WHT 620
10	11 TTF 200 4 WHT 620	9 TTF 200 4 WHT 620	8 TTF 200 4 WHT 620	6 TTF 200 2 WHT 620
11	11 TTF 200 4 WHT 620	9 TTF 200 4 WHT 620	7 TTF 200 4 WHT 540	6 TTF 200 2 WHT 540
12	10 TTF 200 4 WHT 620	8 TTF 200 4 WHT 540	7 TTF 200 4 WHT 540	5 TTF 200 2 WHT 540
13	9 TTF 200 4 WHT 620	7 TTF 200 4 WHT 540	6 TTF 200 4 WHT 540	5 TTF 200 2 WHT 540
14	8 TTF 200 4 WHT 540	7 TTF 200 4 WHT 540	6 TTF 200 2 WHT 540	4 TTF 200 2 WHT 540
15	7 TTF 200 4 WHT 540	6 TTF 200 4 WHT 540	5 TTF 200 2 WHT 540	4 TTF 200 2 WHT 440

16	6 TTF 200 4 WHT 540	5 TTF 200 2 WHT 540	4 TTF 200 2 WHT 440	3 TTF 200 2 WHT 440
17	5 TTF 200 2 WHT 540	4 TTF 200 2 WHT 440	4 TTF 200 2 WHT 440	3 TTF 200 2 WHT 440
18	4 TTF 200 2 WHT 440	3 TTF 200 2 WHT 440	3 TTF 200 2 WHT 340	2 TTF 200 2 WHT 440
19	3 TTF 200 2 WHT 340	2 TTF 200 2 WHT 340	2 TTF 200 2 WHT 340	2 TTF 200 2 WHT 340
20	2 TTF 200 2 WHT 340	1 TTF 200 2 WHT 340	1 TTF 200 2 WHT 340	1 TTF 200 2 WHT 340

Table C.13: Number of metal connectors for 20-storey E2 building.

Level	q = 2	q = 2.5	q = 3	q = 4
1	10 TTF 200 6 WHT 620	8 TTF 200 6 WHT 620	7 TTF 200 4 WHT 620	5 TTF 200 4 WHT 620
2	10 TTF 200 6 WHT 620	8 TTF 200 4 WHT 620	7 TTF 200 4 WHT 620	5 TTF 200 4 WHT 620
3	10 TTF 200 6 WHT 620	8 TTF 200 4 WHT 620	7 TTF 200 4 WHT 620	5 TTF 200 4 WHT 620
4	10 TTF 200 4 WHT 620	8 TTF 200 4 WHT 620	7 TTF 200 4 WHT 620	5 TTF 200 2 WHT 620
5	9 TTF 200 4 WHT 620	8 TTF 200 4 WHT 620	6 TTF 200 4 WHT 620	5 TTF 200 2 WHT 620
6	9 TTF 200 4 WHT 620	7 TTF 200 4 WHT 620	6 TTF 200 4 WHT 620	5 TTF 200 2 WHT 620
7	9 TTF 200 4 WHT 620	7 TTF 200 4 WHT 620	6 TTF 200 4 WHT 620	5 TTF 200 2 WHT 620
8	9 TTF 200 4 WHT 620	7 TTF 200 4 WHT 620	6 TTF 200 4 WHT 620	5 TTF 200 2 WHT 620
9	8 TTF 200 4 WHT 620	7 TTF 200 4 WHT 620	6 TTF 200 4 WHT 620	4 TTF 200 2 WHT 620

10	8 TTF 200 4 WHT 620	6 TTF 200 4 WHT 620	5 TTF 200 4 WHT 620	4 TTF 200 2 WHT 620
11	7 TTF 200 4 WHT 620	6 TTF 200 4 WHT 620	5 TTF 200 4 WHT 540	4 TTF 200 2 WHT 540
12	7 TTF 200 4 WHT 620	6 TTF 200 4 WHT 540	5 TTF 200 4 WHT 540	4 TTF 200 2 WHT 540
13	6 TTF 200 4 WHT 620	5 TTF 200 4 WHT 540	4 TTF 200 4 WHT 540	3 TTF 200 2 WHT 540
14	6 TTF 200 4 WHT 540	5 TTF 200 4 WHT 540	4 TTF 200 2 WHT 540	3 TTF 200 2 WHT 540
15	5 TTF 200 4 WHT 540	4 TTF 200 4 WHT 540	4 TTF 200 2 WHT 540	3 TTF 200 2 WHT 440
16	4 TTF 200 4 WHT 540	4 TTF 200 2 WHT 540	3 TTF 200 2 WHT 440	2 TTF 200 2 WHT 440
17	4 TTF 200 2 WHT 540	3 TTF 200 2 WHT 440	3 TTF 200 2 WHT 440	2 TTF 200 2 WHT 440
18	3 TTF 200 2 WHT 440	2 TTF 200 2 WHT 440	2 TTF 200 2 WHT 440	2 TTF 200 2 WHT 440
19	2 TTF 200 2 WHT 340	2 TTF 200 2 WHT 340	2 TTF 200 2 WHT 340	1 TTF 200 2 WHT 340
20	1 TTF 200 2 WHT 340	1 TTF 200 2 WHT 340	1 TTF 200 2 WHT 340	1 TTF 200 2 WHT 340

Table C.14: Number of metal connectors for 20-storey E3 building.

Level	q = 2	q = 2.5	q = 3	q = 4
1	8 TTF 200 6 WHT 620	6 TTF 200 6 WHT 620	5 TTF 200 4 WHT 620	4 TTF 200 4 WHT 620
2	7 TTF 200 6 WHT 620	6 TTF 200 4 WHT 620	5 TTF 200 4 WHT 620	4 TTF 200 4 WHT 620
3	7 TTF 200 6 WHT 620	6 TTF 200 4 WHT 620	5 TTF 200 4 WHT 620	4 TTF 200 4 WHT 620

4	7 TTF 200 4 WHT 620	6 TTF 200 4 WHT 620	5 TTF 200 4 WHT 620	4 TTF 200 2 WHT 620
5	7 TTF 200 4 WHT 620	6 TTF 200 4 WHT 620	5 TTF 200 4 WHT 620	4 TTF 200 2 WHT 620
6	7 TTF 200 4 WHT 620	6 TTF 200 4 WHT 620	5 TTF 200 4 WHT 620	4 TTF 200 2 WHT 620
7	7 TTF 200 4 WHT 620	6 TTF 200 4 WHT 620	5 TTF 200 4 WHT 620	4 TTF 200 2 WHT 620
8	7 TTF 200 4 WHT 620	5 TTF 200 4 WHT 620	5 TTF 200 4 WHT 620	4 TTF 200 2 WHT 620
9	6 TTF 200 4 WHT 620	5 TTF 200 4 WHT 620	4 TTF 200 4 WHT 620	3 TTF 200 2 WHT 620
10	6 TTF 200 4 WHT 620	5 TTF 200 4 WHT 620	4 TTF 200 4 WHT 620	3 TTF 200 2 WHT 620
11	6 TTF 200 4 WHT 620	5 TTF 200 4 WHT 620	4 TTF 200 4 WHT 540	3 TTF 200 2 WHT 540
12	5 TTF 200 4 WHT 620	4 TTF 200 4 WHT 540	4 TTF 200 4 WHT 540	3 TTF 200 2 WHT 540
13	5 TTF 200 4 WHT 620	4 TTF 200 4 WHT 540	3 TTF 200 4 WHT 540	3 TTF 200 2 WHT 540
14	4 TTF 200 4 WHT 540	4 TTF 200 4 WHT 540	3 TTF 200 2 WHT 540	2 TTF 200 2 WHT 540
15	4 TTF 200 4 WHT 540	3 TTF 200 4 WHT 540	3 TTF 200 2 WHT 540	2 TTF 200 2 WHT 440
16	3 TTF 200 4 WHT 540	3 TTF 200 2 WHT 540	2 TTF 200 2 WHT 440	2 TTF 200 2 WHT 440
17	3 TTF 200 2 WHT 540	2 TTF 200 2 WHT 440	2 TTF 200 2 WHT 440	2 TTF 200 2 WHT 440
18	2 TTF 200 2 WHT 440	2 TTF 200 2 WHT 440	2 TTF 200 2 WHT 440	1 TTF 200 2 WHT 440
19	2 TTF 200 2 WHT 340	1 TTF 200 2 WHT 340	1 TTF 200 2 WHT 340	1 TTF 200 2 WHT 340

20	1 TTF 200 2 WHT 340	1 TTF 200 2 WHT 340	1 TTF 200 2 WHT 340	1 TTF 200 2 WHT 340

Appendix D

Response of other building heights

This appendix illustrates the corresponding inelastic drift, force and acceleration demands for other building heights which are not presented in the main body of the thesis.

D.1 Drift response

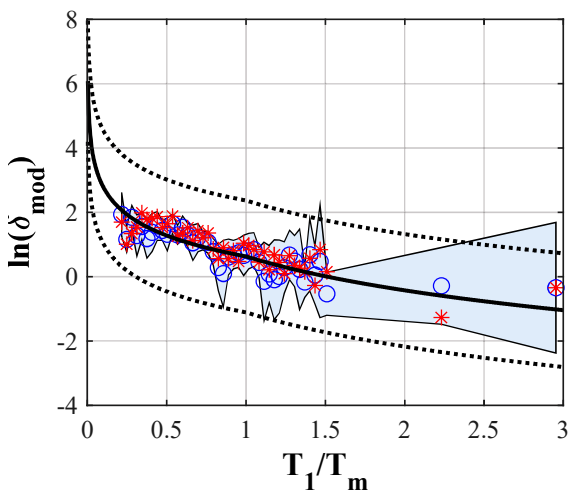
The corresponding seismic drift demands for different structural heights are presented in this section. To this end, Figure D.1 demonstrates global drift demands in 6-, 12-, and 16-storey CLT buildings, whereas Figure D.2 show maximum drift demands for the same building heights.

D.2 Shear response

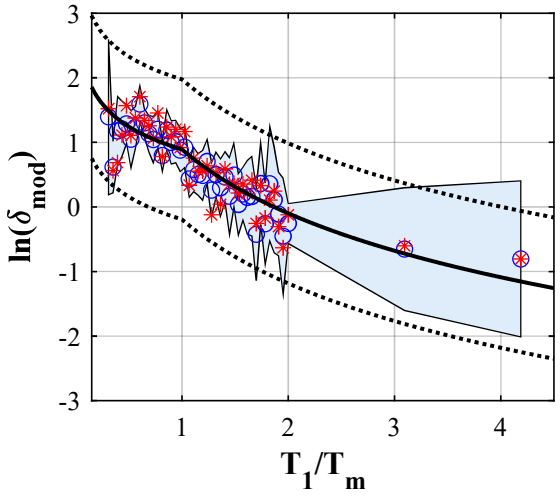
The corresponding seismic shear demands for different structural heights are presented in this section. To this end, Figure D.3 demonstrates base shear demands in 8-, 12-, and 16-storey CLT buildings, whereas Figure D.4 show storey shear force demands for the same building heights.

D.3 Acceleration response

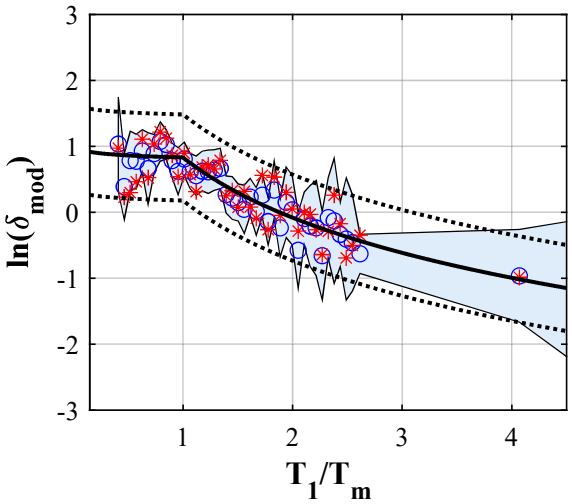
The corresponding peak floor acceleration demands for different structural heights are presented in this section. To this end, Figure D.5 demonstrates acceleration demands associated with $S_a(T_1)$ in 8-, 12-, and 16-storey CLT buildings, whereas Figure D.6 show acceleration demands associated with peak ground acceleration (PGA) for the same building heights.



(a) 6-storey A1 building.

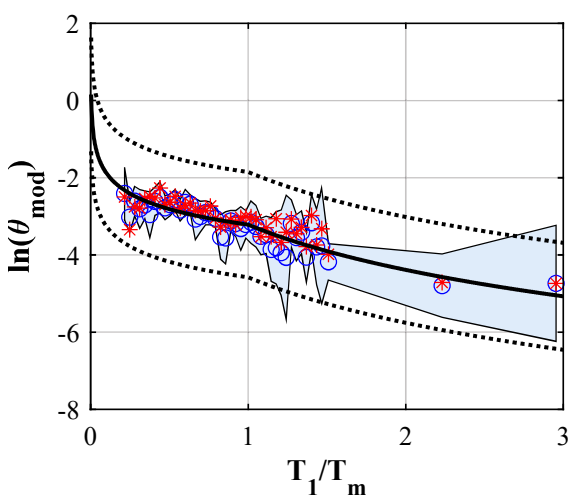


(b) 12-storey C1 building.

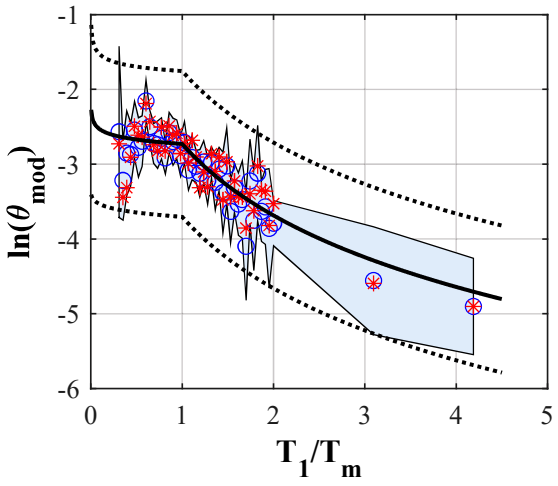


(c) 16-Storey D1 building.

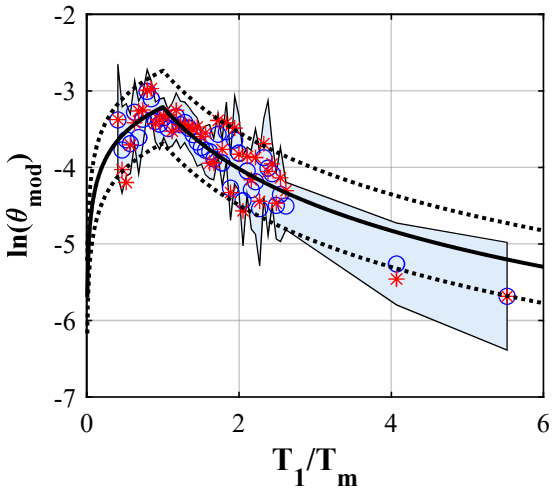
Figure D.1: Mean global drift modification factor ($\ln(\delta_{mod})$) against period ratios (T_1/T_m), for different structural heights.



(a) 6-storey A1 building.

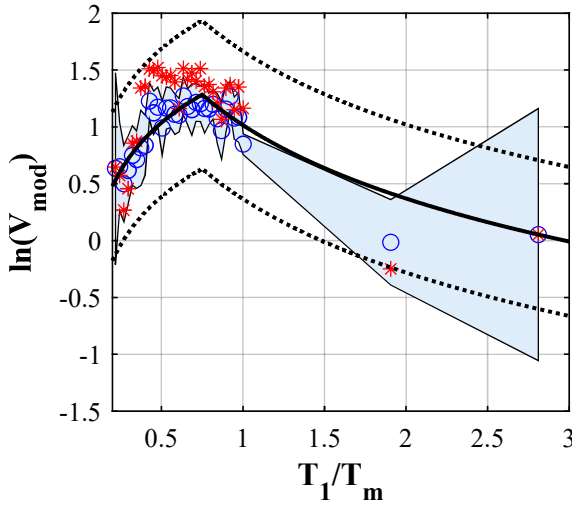


(b) 12-storey C1 building.

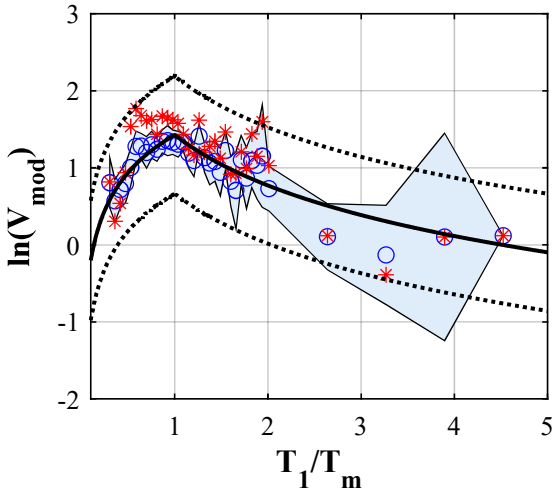


(c) 16-Storey D1 building.

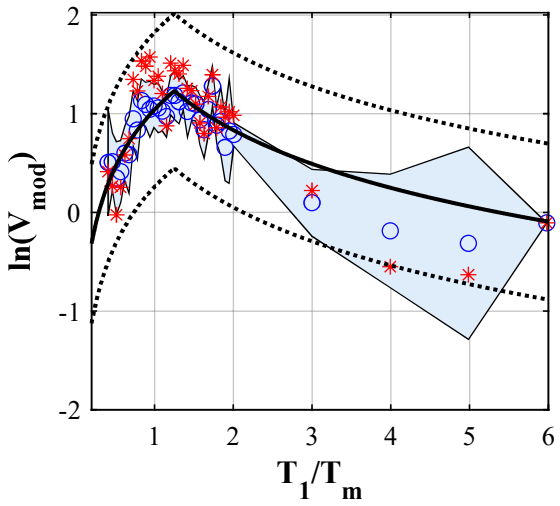
Figure D.2: Mean maximum drift modification factor ($\ln(\theta_{mod})$) against period ratios (T_1/T_m), for different structural heights.



(a) 8-storey B1 building.

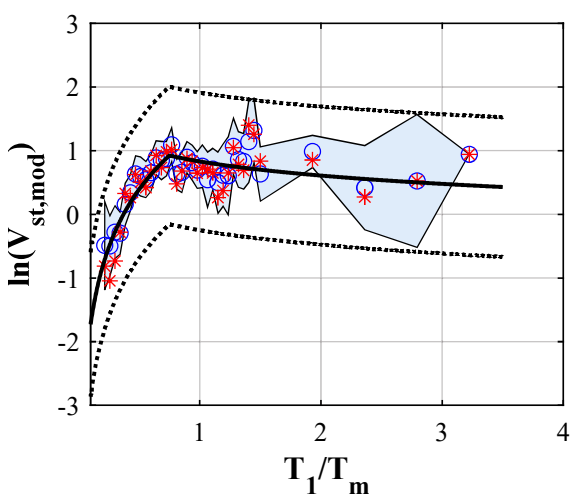


(b) 12-storey C1 building.

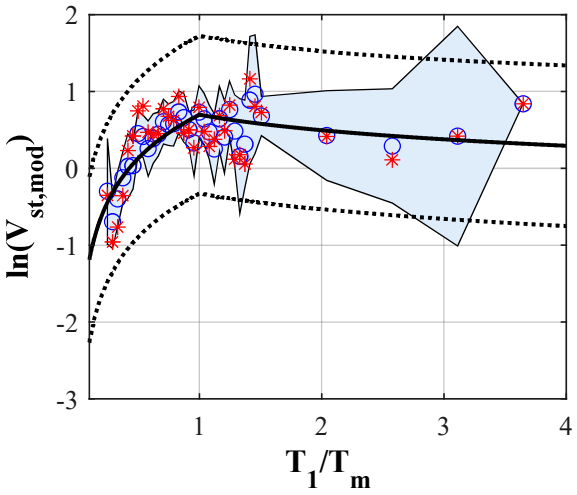


(c) 16-Storey D1 building.

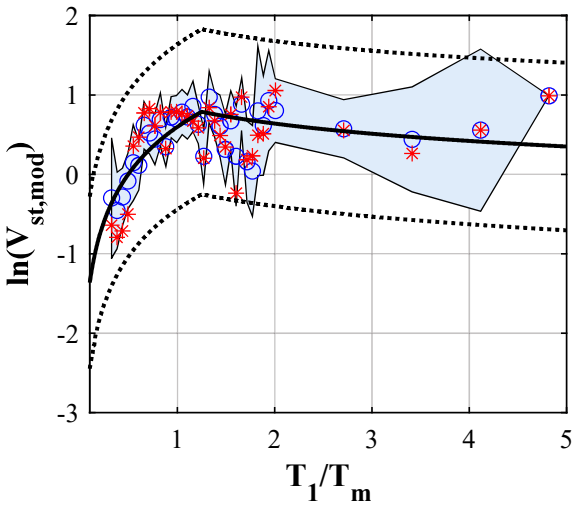
Figure D.3: Mean base shear modification factor ($\ln(V_{mod})$) against period ratios (T_1/T_m), for different structural heights.



(a) 8-storey B1 building.

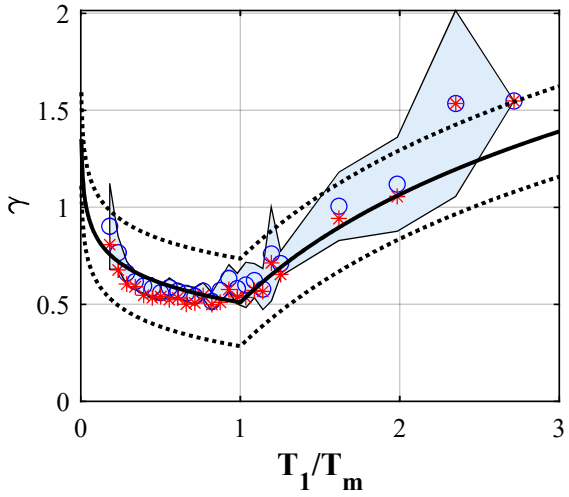


(b) 12-storey C1 building.

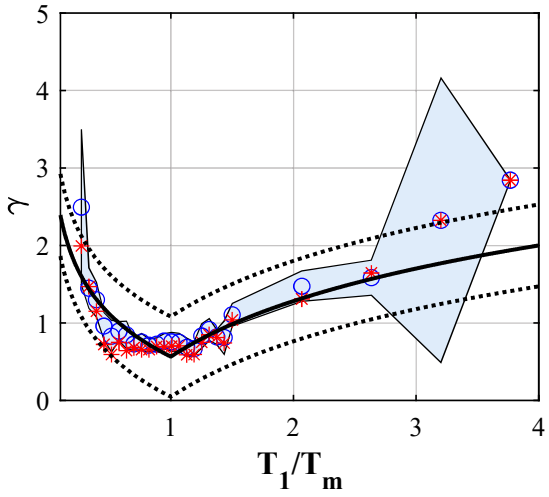


(c) 16-Storey D1 building.

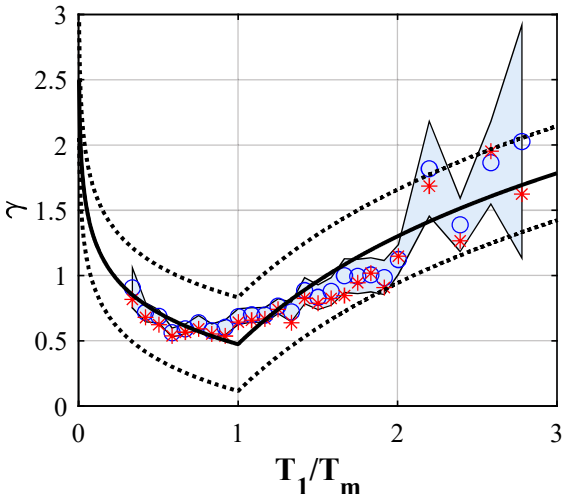
Figure D.4: Mean storey shear modification factor ($\ln(V_{st,mod})$) against period ratios (T_1/T_m), for different structural heights.



(a) 8-storey B1 building.

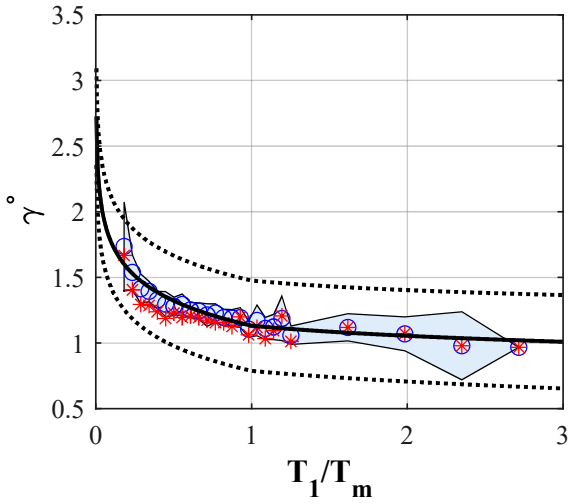


(b) 12-storey C1 building.

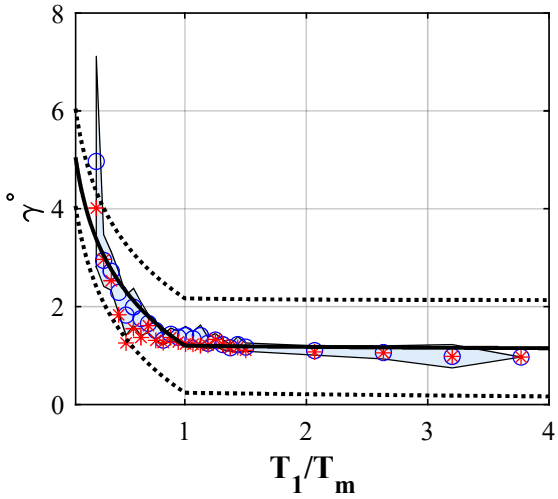


(c) 16-Storey D1 building.

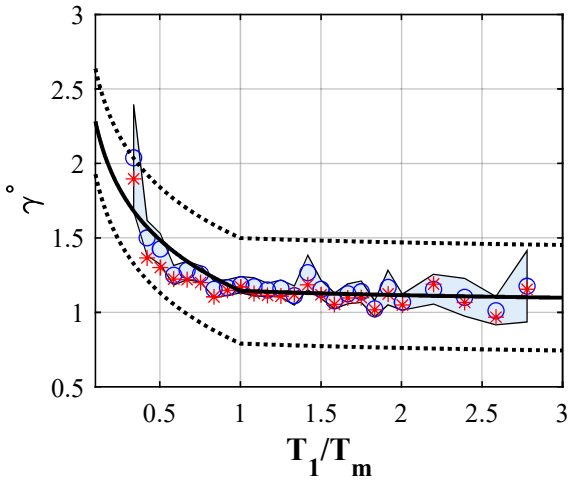
Figure D.5: Mean acceleration amplification factor (γ) associated with $S_a(T_1)$ against period ratios (T_1/T_m), for different structural heights.



(a) 8-storey B1 building.



(b) 12-storey C1 building.



(c) 16-Storey D1 building.

Figure D.6: Mean acceleration amplification factor (γ°) associated with PGA against period ratios (T_1/T_m), for different structural heights.